

**Experimental and Numerical Modelling of Gasket  
Materials and Property Correlation**

**Hongyi Zhao**

**A thesis submitted in partial fulfilment of the  
requirements of Liverpool John Moores University  
for the degree of Doctor of Philosophy**

**March 2015**

## ACKNOWLEDGEMENTS

I would like to express my sincere gratitude and special thanks to my supervisors, Prof. James Ren and Dr. Dave Allanson, who has provided guidance, advice and encouragement during this research study.

Many other academic, secretarial and technical members of staff have facilitated the realisation of this thesis and I express them all my gratitude. I would like to thank Mr. Clive Eyre and Mr. Anthony Dunmore for their invaluable technical support with material testing and sample manufacturing process.

I would like to take this opportunity to thank my group mates, Mr. Jensen Aw, Dr. Budiarsa Nyoman and Mr. Andrew Norbury for their friendship and sharing their experience. I am also grateful of the help from my friends, who gave me help in many ways and shared a great time in my studies and life at Liverpool John Moores University.

Finally, my sincere thanks go to my family for sustained encouragement, continuous and unselfish love and support during my Ph.D. study.

Hongyi Zhao

## ABSTRACT

In this work, a detailed combined numerical-experimental program has been developed to study the shore hardness testing of rubber materials principally used for gasket applications. The correlation between shore hardness and linear elastic and hyperelastic properties has been systematically investigated. A detailed FE model of the shore A hardness test has been developed with re-meshing functions in order to cope with the large deformation during simulation of shore hardness tests over a range of E values. The model is used in modelling shore A hardness on samples with standard thickness (over 6mm) and the result is validated against published experimental data. FE indentation models of thin samples are then developed and successfully used to predict the shore hardness of thinner samples over a property range relevant to gasket applications. A chart linking shore hardness, Young's modulus and samples thickness is established and used to analyse shore hardness of three cases including silicone rubber made in the lab with different thicknesses, thin silicone rubber gasket and an EPDM (Ethylene Propylene Diene Monomer) gasket for plate heat exchangers. In all of the cases, the estimated E values based on shore hardness tests are able to predict the deformation of the material under different loading conditions including tensile and compression tests on samples of different shapes. In shore OO hardness modelling, the numerical results show a good agreement with analytical solution for spherical indenters. The shore hardness, thickness and E value chart predicted is used to evaluate the properties (Young's modulus) of a soft silicone rubber and a latex rubber, in both cases, the E values predicted from hardness tests are able to predict the deformation of the material under tension and compression. In the case of latex rubber, the results also agree with hyperelastic properties from combined tensile and planar tests.

Based on the FE model developed, extensive data over a larger spectrum of material properties are developed and used in developing an Artificial Neural Network (ANN) program for inverse estimation of material properties from shore hardness and direct prediction of shore hardness for the cases when the material properties are known. The results show that the E values can be predicted from shore hardness tests with accuracy within 10% for both shore A and shore OO hardness tests. In the direct analysis, the ANN is able to predict the shore hardness values accurately from the linear elastic properties and sample thickness or a combination of hyperelastic parameters and sample thickness. The effect of indenter shape, testing condition, and

choice of linear or hyperelastic material models on shore hardness tests are established and discussed, which would provide a detailed understanding to further enhance the use of shore hardness tests as a quick and effective way to test rubber materials.

# Contents

**Acknowledgements**

**Abstract**

**Contents**

**Symbols (In order of appearance)**

**List of Figures**

**List of Tables**

<b>Chapter 1 Introduction</b> .....	1
1.1 Introduction.....	2
1.2 Aims and objectives.....	5
1.3 Outline of the thesis.....	5
<b>Chapter 2 Literature review</b> .....	8
2.1 Introduction.....	9
2.2 Indentation tests and applications.....	10
2.2.1 Different types of indentation testing and their applications.....	10
2.2.2 Shore hardness tests, mechanism and applications.....	14
2.3 Structures of rubber materials and properties.....	18
2.4 Gaskets and rubber materials.....	21
2.4.1 Application of rubber based materials in gasket and seal materials.....	21
2.4.2 Classifications of gasket material and developments.....	27
2.4.3 Manufacturing process & material selections of gasket.....	31
2.5 Indentation test of rubber and rubber like materials.....	33
2.5.1 Properties of rubbers.....	33
2.5.2 Test Method for compressibility and recovery of gasket materials.....	36

2.6 Deformation of materials and strain energy for nonlinear materials behaviours.....	41
2.7 Combined numerical and experimental methods and its application in material properties prediction.....	47
2.8 Artificial Neural Network (ANN).....	56
<b>Chapter 3 Research plan and Experiments.....</b>	<b>62</b>
3.1 Introduction.....	63
3.2 Testing facilities.....	66
3.3 Materials.....	69
3.4 FE modelling program.....	72
<b>Chapter 4 FE Modelling, Results and Analysis.....</b>	<b>73</b>
4.1 Introduction.....	74
4.2 FE modelling of shore A hardness test of linear elastic materials with standard sample thicknesses (over 6mm).....	77
4.2.1 FE Model.....	77
4.2.2 Re-meshing method used in the FE model of shore A hardness test.....	81
4.2.3 Shore A hardness ( $S_A$ ) for samples with standard thickness (t) over different Young's modulus (E) and comparison with published data on rubbers.....	84
4.3 FE modelling of shore A hardness tests of thinner samples (finite thickness samples).....	89
4.4 Use of the relationship of elastic modulus, thickness and shore A hardness in the testing and modelling of rubber and gaskets.....	98
4.4.1 Case 1: Testing and modelling of cast silicone rubber samples with different thicknesses.....	99
4.4.2 Case 2: Testing and modelling of thin silicone rubber gasket sheet.....	105
4.4.3 Case 3: Testing and modelling of an EPDM plate heat exchanger gasket.....	112

4.5 FE modelling of shore OO hardness tests with a spherical indenter on soft rubber materials.....	120
4.5.1 FE modelling of shore OO hardness ( $S_{OO}$ ) tests.....	120
4.5.2 Application of $S_{OO}$ -E relationship on silicone rubber.....	129
4.5.3 Shore OO hardness tests of latex rubber and properties estimation.....	134
4.6 Use of ANN to estimate material properties in inverse analysis and predict shore hardness through direct analysis .....	140
4.7 Prediction of shore hardness using ANN for thick and thin samples.....	151
<b>Chapter 5 Discussion.....</b>	<b>159</b>
5.1 Applications of indentation and characterize the material properties.....	160
5.2 Effect of different indenter shape and sample thickness on the indentation resistance and deformation of the material.....	165
5.3 Factors affect the indentation process.....	170
5.4 Effects of choice of linear and nonlinear hyper elastic properties on shore hardness prediction.....	172
<b>Chapter 6 Conclusions and Future works.....</b>	<b>176</b>
6.1 Summary and conclusions.....	177
6.2 Recommendations for future works.....	179
<b>References.....</b>	<b>180</b>

## Symbols (In Order of Appearance)

### Alphabet Symbols

$A$  Physical creep rate

$A_0$  Original specimen cross-sectional area ( $\text{mm}^2$ )

$ABS$  the absolute value function

$B$  Chemical creep rates  $h$  indentation depth at an indentation force

$B$  Cauchy-Green strain tensor in Ogden model

$b_1, b_2, b_3$  Principle values of  $B$

$C$  Curvature of indentation loading curve

$C_{10}, C_{01}$ , Temperature-dependent material parameters in Mooney Rivlin model

$C_{ij}$  Material parameters in Polynomial form

$D_1$  Temperature-dependent material parameters in Mooney Reviling model

$D_i$  Temperature-dependent material parameters in Ogden model

$E$  Young's modulus (MPa)

$E^*$  Reduced Young's modulus (MPa)

$E_{Predict}$  ANN predicted data of Young's Modulus (MPa)

$E_{Target}$  The corresponding original target data (MPa)

$h$  Indentation depth at an indentation force

$\bar{I}_1, \bar{I}_2$  The first and second deviatoric strain invariants

$J$  Total volume ratio

$J^{el}$  The elastic volume ratio

$K$  Strength coefficient

$K_0$  Bulk modulus (MPa)

$L_0$  Original specimen length (mm)

$M$  Thickness under total load (inch)

$N$  The order of the polynomial

$n$  The strain hardening exponent



$P$	Thickness under preload (inch) in a creep set test
$R$	Recovered thickness (inch) in a creep set test
$S_A$	Shore A hardness
$S_{OO}$	Shore OO hardness
$t$	Sample thickness (mm)
$\nu$	Poisson's ratio
$W_R$	Remaining work done (J)
$W_t$	Total work done (J)

### **Greek Symbols**

$\alpha_i$	Temperature-dependent material parameter in Ogden model
$\alpha_n$	Constants in Ogden model
$\delta$	Material deformation
$\varepsilon$	The plastic strain
$\varepsilon_e$	Engineering strain
$\sigma_e$	Engineering stress (MPa)
$\sigma_y$	The yield stress (MPa)
$\bar{\lambda}_i$	The deviator stretches
$\lambda_i$	The principal stretches
$\mu_0$	Initial shear modulus (MPa)
$\mu_n$	Constants in Ogden model
$\mu_i$	Temperature-dependent material parameter in Ogden model

### **Abbreviation**

ABI	Automated Ball Indentation
ANN	Artificial Neural Network
ASTM	American Society for Testing and Materials
BR	Butadiene Rubber
BS	Butadiene Styrene

CAE Computer Aided Engineering  
CR Chloroprene Rubber  
DMTA Dynamic Mechanical Thermal Analyser  
EMI Electromagnetic Interference  
EPDM Ethylene Propylene Diene Monomer  
EVA Ethylene Vinyl Acetate  
FE Finite Element  
FEA Finite Element Analysis  
FIP Form In Place  
HAZ Heat Affect Zone  
IIR Butyl Rubber  
LEFM Linear Elastic Fracture Mechanics  
LR Latex rubber  
NBR Acrylonitrile Butadiene Rubber  
NR Natural Rubber  
PHE Plate Heat Exchanger  
PSR Polysulfide Butadiene Rubber  
PTFE Polytetrafluoroethylene  
PU Polyurethanes  
SBR Styrene Butadiene Rubber  
SiCps Silicon Carbide Particles  
SR Silicone Rubber

# List of Figures

## Chapter 1

<b>Figure 1.1</b> Schematic to show an indentation process.....	3
---	---

## Chapter 2

<b>Figure 2.1</b> Schematic to show an indentation process and the representation of indentation resistance based on the size of the residual impression and force displacement data.....	12
<b>Figure 2.2</b> Diagrams showing different types of indenter tips.....	13
<b>Figure 2.3</b> Principle of rubber hardness tests and structure of a Shore Durometer.....	16
<b>Figure 2.4</b> Correlation between shore A and the other hardness systems.....	17
<b>Figure 2.5</b> The molecular structure of rubbers.....	24
<b>Figure 2.6</b> Force-displacement relations for a rubber vulcanizate exposed to cyclic loading showing its ability to recovery its original shape.....	25
<b>Figure 2.7</b> Different types of gaskets for different applications.....	26
<b>Figure 2.8</b> Classification of gasket materials.....	29
<b>Figure 2.9</b> Development of rubber based materials for gasket applications.....	30
<b>Figure 2.10</b> Compressibility and recovery of gasket materials.....	39
<b>Figure 2.11</b> Testing of rubber materials used in rubber gaskets.....	40
<b>Figure 2.12</b> Different stress strain curves for elastic-plastic materials (metal and plastics) and hyperelastic materials behaviours.....	46
<b>Figure 2.13</b> Different stress stain conditions and equivalent stress state by combining different testing modes.....	51
<b>Figure 2.14</b> Combined experimental and numerical method to estimate material properties or predict material behaviour.....	52
<b>Figure 2.15</b> Flow chart showing typical procedures in forward (a) and reverse (b) method.....	53

<b>Figure 2.16</b> Block diagram of the mixed numerical-experimental method ( $u$ denotes the observation of experiments, $h$ the output of the numerical/finite-element modelling).....	54
<b>Figure 2.17</b> Use of parametric studies in inverse materials properties identification of rubber block based on surface tension tests.....	55
<b>Figure 2.18 (a)</b> A single ANN system used in predicting plastic properties based on conical indentation and the equations.....	60
<b>Figure 2.18 (b)</b> Feed-forward neural network with back propagation algorithm for predicting the indentation force-displacement data based on material parameters ( $\mu$ and $\alpha$ ).....	61

### Chapter 3

<b>Figure 3.1</b> Flow chart to show the main research work in FE modelling and testing.....	65
<b>Figure 3.2</b> Durometer shore hardness indentation test machine and the indenters (shore A and shore OO).....	67
<b>Figure 3.3</b> Tensile and compression test machine.....	68
<b>Figure 3.4</b> Equipment and tools used in Silicone rubber casting and curing.....	70
<b>Figure 3.5</b> Different types of rubber samples used in the work.....	71

### Chapter 4

<b>Figure 4.1</b> Flow chart showing the main research work in developing the FE modelling program and its applications in testing rubbers .....	76
<b>Figure 4.2</b> FE model of shore A hardness test: Structure of the model and meshes (a & b), typical displacement field (c) and force-displacement curve (d) showing the procedure to determine the shore A hardness point by using the displacement at a force of 8.06N.....	79
<b>Figure 4.3</b> Effect of mesh density on the indentation curves with different Young's modulus. (Sample thickness=6mm). The mesh size for the square region underneath the indenter is set at 0.05, 0.1 and 0.15 for mesh 1, 2 and 3, respectively).....	80
<b>Figure 4.4</b> Re-meshing points and deformation fields illustrating the working process of the re-meshing program. ( $E=4.4\text{MPa}$ ).....	82

<b>Figure 4.5</b> FE force displacement data ( $E=11\text{MPa}$ ) with re-meshing point to show that for higher Young's modulus, less/no re-meshing is required as the depth are much lower to reach the force for shore A hardness.....	83
<b>Figure 4.6</b> Comparison between FE predicted shore A hardness values with different Young's modulus and experimental data from published paper on rubbers (Johannes et al, 2006). (The error bar represents maximum difference in depicting the data from the paper).....	86
<b>Figure 4.7</b> Correlations between shore A hardness values and Young's modulus. (Sample thickness=6mm).....	87
<b>Figure 4.8</b> Vertical displacement ( $U_2$ ) distributions with a low Young's modulus ( $E=4.4\text{MPa}$ ) and a higher Young's modulus in shore A hardness on sample of standard thickness.....	88
<b>Figure 4.9</b> Typical FE model of the shore A hardness test of a thinner (non-standard thickness) sample.....	89
<b>Figure 4.10</b> Typical P-h curve and re-meshing stages for thinner samples ( $t=2\text{mm}$ ) with different E values. The point in the red circled represents the displacement point used to calculate the shore hardness values for the corresponding E values and thicknesses.....	92
<b>Figure 4.11</b> Simulation domains showing the range of thicknesses and properties varied in the FE model to produce data for establishing the correlation between shore A hardness and Young's modulus for thinners samples. ....	93
<b>Figure 4.12</b> Main data processing procedures to determine the shore A hardness value ( $S_A$ ) for different combination of sample thickness ( $t$ ) and materials properties ( $E$ ).....	94
<b>Figure 4.13</b> Indentation P-h curves of samples with different thicknesses ( $E=11\text{MPa}$ ).....	95
<b>Figure 4.14</b> Bar chart to show the change of apparent shore A hardness ( $S_A$ ) with the sample thickness.....	96
<b>Figure 4.15</b> Correlations of shore A hardness values with Young's modulus and sample thicknesses.....	97
<b>Figure 4.16</b> Case one: silicone rubber samples of different thickness made in the lab.....	101
<b>Figure 4.17 (a)</b> Comparison of shore A hardness values tested on the three planes of the thick silicone rubber sample. <b>(b)</b> Shore A hardness test data of silicone rubber sample with different thicknesses.....	102

<b>Figure 4.18</b> Bar chart showing the predicted elastic modulus from shore hardness tests of sample with different thickness based on the E-thickness-Shore A hardness chart .....	103
<b>Figure 4.19</b> The experimental setup and FE modelling results of compression test of the thick silicone rubber sample .....	104
<b>Figure 4.20</b> Silicone rubber samples cut into different shapes from a commercially available gasket sheet and the shore hardness test procedure (Case two).....	107
<b>Figure 4.21</b> Bar chart showing the shore A hardness of silicone rubber sheet measured with different sample shapes and lubricant conditions.....	108
<b>Figure 4.22</b> Uniaxial compression tests of the round (a) and the ring silicone rubber gasket sample (b) and FE models simulating the tests (c & d).....	109
<b>Figure 4.23</b> Comparison of the experimental data and the FE modelling results of the round and ring samples of the silicone rubber gasket sample under different loading conditions.....	111
<b>Figure 4.24</b> EPDM plate heat exchanger gasket samples and the cross-section shape. The cross section shape is the same at different locations.....	114
<b>Figure 4.25</b> Shore A hardness tests conducted on different planes of the EPDM plate heat exchanger gasket.....	115
<b>Figure 4.26</b> Uniaxial tensile test, uniaxial unconstrained compression test and uniaxial constrained compression test of the EPDM gasket sample.....	116
<b>Figure 4.27</b> FE models of the uniaxial unconstrained compression test and uniaxial constrained compression test of the EPDM plate heat exchanger gasket sample.....	117
<b>Figure 4.28</b> Comparison of the experimental test and FE modelling results of EPDM gasket under different loading conditions.....	119
<b>Figure 4.29</b> FE model of the shore OO hardness test on samples of standard thickness.....	124
<b>Figure 4.30</b> Comparison between P-h curves for shore OO indentation from FE modelling and the analytical solutions.....	125
<b>Figure 4.31</b> Typical force-displacement curve with a shore OO indenter and the procedure to determine the displacement point corresponding to the load for shore OO hardness ( $E=5\text{MPa}$ ).....	126
<b>Figure 4.32</b> Correlation of shore OO hardness values and Young's modulus based on FE data and analytical solution for spherical indentation of thick samples (Johnson, 1985) ( $t=6\text{mm}$ ).....	127

<b>Figure 4.33</b> Correlation of shore OO hardness values and Young’s modulus based on FE data on samples of different thicknesses.....	128
<b>Figure 3.34</b> Soft silicone rubber samples with different thicknesses.....	130
<b>Figure 4.35 (a)</b> Measured hardness values of silicone rubber of different thickness.....	131
<b>Figure 4.35 (b)</b> Measured hardness values of soft silicone rubber when tested on different planes of the thick sample.....	131
<b>Figure 4.36</b> Predicted E values based on the shore hardness of silicone rubber with different thickness.....	132
<b>Figure 4.37</b> Comparison of the experimental compression test and FE modelling results based on the elastic properties predicted from shore OO hardness tests. (E=1.6MPa, averaged based on the data in Figure 4.36).....	133
<b>Figure 4.38</b> Photos of the latex rubber samples of different thickness for the shore OO hardness tests .....	136
<b>Figure 4.39</b> Measured hardness values of latex samples of different thicknesses.....	137
<b>Figure 4.40</b> Predicted E values for latex samples of different thicknesses.....	138
<b>Figure 4.41</b> Comparison between the FE predicted hardness values of different thickness samples with the estimated E values, testing data and FE prediction based on nonlinear hyperelastic properties from combination of shear (planar) and tension tests (Ogden model).....	139
<b>Figure 4.42</b> Proposed feed-forward neural network with back propagation Algorithm for estimating the elastic material properties (E) based on shore hardness data.....	145
<b>Figure 4.43</b> Effects of the number of neuron on the relative error of predicted E values in ANN training.....	146
<b>Figure 4.44 (a)</b> The relative error of ANN predicted E values using training data as target. (Shore A). (Detailed properties for each data points could be found in Table 4.1).....	147
<b>Figure 4.44 (b)</b> The relative error of ANN predicted E values based on data not used in the training. (Shore A). (Detailed properties for each data point could be found in Table 4.1).....	147
<b>Figure 4.45</b> Predicted E values of different rubbers based on the shore hardness for case 1, 2 and 3. (Shore A) .....	148
<b>Figure 4.46</b> The relative error of ANN predicted E values based on shore OO hardness data.....	149

<b>Figure 4.47</b> Comparison of predicted E values based on experimental data (shore OO) through different approaches.....	150
<b>Figure 4.48</b> Proposed feed-forward neural network with back propagation Algorithm for estimating the Shore hardness from known material properties and sample dimensions.....	154
<b>Figure 4.49</b> Effects of the number of neuron on the relative error predicted shore A hardness (Direct ANN program).....	155
<b>Figure 4.50 (a)</b> Relative error in predicted shore A hardness using the training data as input (direct predict shore A hardness) (neuron number =10).....	156
<b>Figure 4.50 (b)</b> Relative error in predicted shore A hardness using data not used in the training as input (direct predict shore A hardness) (neuron number =10).....	156
<b>Figure 4.51</b> Typical results showing the accuracy of the ANN in predicting Shore OO hardness from E values and sample thicknesses.....	157
<b>Figure 4.52</b> Typical ANN results showing the accuracy in predicting Shore OO hardness from nonlinear hyperelastic parameters (Ogden strain energy function) and thicknesses.....	158

## Chapter 5

<b>Figure 5.1</b> FE modelling results of gasket contact pressure in a plate heat exchanger plate and effects of material properties on the sealing pressure.....	163
<b>Figure 5.2</b> Effects of hardness and Elastic modulus on the sealing force.....	164
<b>Figure 5.3</b> Change of shore hardness with sample thickness (E=10MPa).....	167
<b>Figure 5.4 (a)</b> Stress distributions for shore OO indenter on samples of different thicknesses.....	168
<b>Figure 5.4 (b)</b> Stress distributions for shore A indentation on samples of different thicknesses.....	169
<b>Figure 5.5</b> Evaluation of the effect of friction on the predicted shore A values (E=11MPa) using FE model.....	171
<b>Figure 5.6</b> Typical force–displacement curves with same Ogden parameter ‘ $\mu$ ’ but different parameter ‘ $\alpha$ ’. This material property result in the same shore OO hardness as labelled at the force point for shore OO hardness .....	174



**Figure 5.7** FE modelling results of shore A hardness with different strain energy functions and models based on the testing data set on the same material. It shows the shore A hardness is the same when using linear or hyperelastic models.....175

## List of Tables

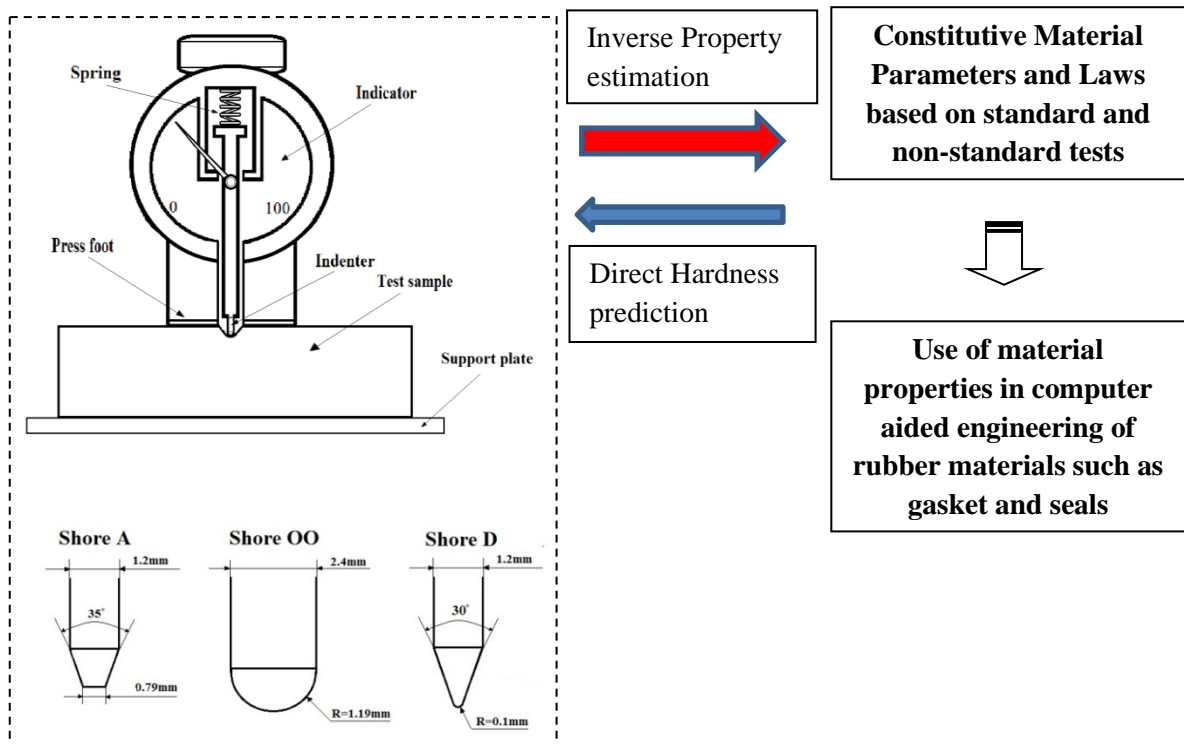
<b>Table 2.1</b> General characteristics of different types of shore durometer hardness.....	14
<b>Table 2.2</b> Structure of different rubbers.....	18
<b>Table 2.3</b> Relative properties of various elastomers.....	33
<b>Table 2.4</b> Comparison of the predicted material properties obtained from ANNs algorithm with inputs for various combinations of three-sided pyramidal indenter tips.....	59
<b>Table 3.1</b> List of main tests and materials.....	64
<b>Table 4.1</b> Training and output data used in the ANN program for shore A hardness tests.....	141
<b>Table 4.2</b> Training and output data used in the ANN program for shore OO hardness tests.....	143

**CHAPTER ONE**  
**INTRODUCTION**

## 1.1 Introduction

The shore hardness test is one form of indentation tests, which are widely used in testing materials such as rubbers, foam and plastics (*Morgans, 1999*). During an indentation test, an indenter is pressed onto the sample surface and the resistance of the material is represented by the size of the residual impression on the surface or the force-indentation depth data. The main reason for its ubiquitous use is its intrinsic experimental simplicity in terms of facilities and sample requirements. Indentation tests can be performed with minimal specimen preparation and/or mounting and can be conducted several times on a single specimen at different locations. In addition, indentation tests can also be performed in different environments (e.g. temperatures or humidities) with complicated loading histories (*Ren et al., 2002; Petre et al., 2007*). Different from hardness tests on metal materials such as Vickers or Knoop tests (*Rahul et al., 2006*), where the hardness is determined by measuring the size of the residual impressions left on the surface of the materials, shore hardness is defined by estimating the indentation depth from the deformation of a spring under a fixed load as illustrated in Figure 1.1. For material with different hardness, there is a range of hardnesses employing indenters of different shapes, load and preload. Shore hardness is a cheap, quick and easy way of material testing, however, comparing with micro hardness tests, it requires much larger sample size in particular material with sufficient thickness (minimum 6mm thick according to ASTM D2240-05), which makes it difficult to be conclusive when dealing with thin samples. Different from the case of compression, tension or shear tests, where the stress and strain can be calculated directly from the deformation or applied load, shore hardness values are not based on well-defined boundaries, the hardness values cannot be directly used in computer aided engineering (CAE) based product development and characterization when dealing with rubber based materials. In addition, many materials such as rubbers are used as thin layers/sheets (e.g. in sealing application), while the shore hardness is designed to be performed on a thicker sample typically, 6mm. So, a methodology to estimate the properties based on thinner samples is of significant importance for a wide spread of products. It is also essential to develop a program to inversely estimate the materials properties (such as Young's Modulus) from shore hardness tests of thick or thin samples. On the other side, the shore hardness to a certain extent, represents the indentation resistance of the materials, which can also be linked with the function such as perception of comfort, etc. A

direct analysis program to predict shore hardness from known material properties will aid the material development, comparison and selection process. Given the complexity of the shore hardness system over different scales (such as shore A, C, D, B, OO, etc.), it is difficult or impossible to link all the shore hardness scales to the constitutive material properties universally. This work is going to focus on rubber material for gasket and seals, where the suitability of hardness and property range and loading condition of the material is better defined.



**Figure 1.1** Schematic to show an indentation process.

Rubbers are widely used in making gaskets and seals for different industries such as chemical, food and energy sectors (*Chandrasekaran, 2009*). Shore hardness (shore A hardness for hard rubbers and shore OO hardness for soft rubbers) is used as the main material properties of rubber gaskets used by the suppliers and end users. However, as the link between the shore hardness and Young's modulus is not quantitatively established, this made it difficult to use the data in computer aided engineering. In addition, rubber gaskets are supplied in the form of thin sheets for maximum sealing performance, thus making it difficult to test the material as the standard thickness for shore hardness is 6 mm normally. Sometimes, a coupon testing sample has to be made purely to satisfy the requirement of the international

standards. A quantitative understanding of the effect of thickness on the shore tests will provide a tool to extend the use of shore hardness in thin gasket/seals design, comparison and selection. It will also provide a quick tool to estimate the material properties in material development; a thinner material or small volume would use much less materials which brings cost saving when dealing with expensive materials. For example, in developing conductive particle based materials some expensive particles (e.g. silver) are used (*Chung, 2001*).

Direct and inverse analyses are the two general forms of combined numerical and experimental approaches in materials characterisation (*Ren et al., 2009*), which have proven to be a very powerful analysis approach for nonstandard tests or for complex material behaviour (*Dao et al., 2001*). In an inverse analysis, the material properties are estimated by combining experimental tests and numerical modelling (e.g. finite element (FE) analysis). This is often achieved with the aid of interactive FE modelling or based on a relationship chart, dimensionless parameters, searchable database or other tools such as artificial neural network (ANN). A detailed study applying this approach to the shore hardness testing of rubbers would further enhance the understanding of shore hardness tests and establish the link between shore hardness and constitutive materials properties, which can aid the design process of gaskets and seals or in further materials developments. Direct hardness prediction is also of importance to the use and development of gasket materials. Rubber gasket based sealing is becoming more and more important and many new materials are being developed including different grade of rubbers. In some cases, the supplier is able to provide the material data from standard tests such as tensile, compression or shear tests, so the material properties are known to the end users. A direct link between the properties such as Young's modulus (E) or nonlinear hyperelastic parameters and the shore hardness will help the comparison of materials. In addition, the hardness is better linked to human perception of comfort/softness than material properties, such as E values. Therefore both inverse material property estimation from shore hardnesses and prediction of shore hardness with known material properties are important. However, there are many challenges on both the modelling approach and interpretation of the data driven by the complication of the tests and materials models. A detailed study is required to systematically establish the issues such as the suitability of the materials models (elastic or hyperelastic), the effect of thickness and other conditions, level of accuracy for particular applications.

## **1.2 Aims and Objectives**

This work aims to develop a combined numerical and experimental method to estimate the material parameters from shore hardness tests of rubber material used in gaskets and seals of different thicknesses and predict the shore hardness values from known constitutive material parameters.

### **Main objectives are:**

- To develop FE models of shore A hardness on hard rubbers of different thickness and establish the link between shore hardness and material properties;
- To develop FE models of shore OO hardness tests and use the results to characterise soft rubber materials for gaskets;
- To apply the program and data established to study the compression tests and modelling of different gasket rubbers;
- To explore the feasibility of ANN approach based on the data established for inverse properties estimation and direct shore hardness prediction
- To establish the effect of material properties/models on shores hardness testing and influence of testing conditions on the accuracy and robustness of the inverse and direct analysis.

## **1.3 Outline of the thesis**

In Chapter 2, different types of indentation methods and their applications in material characterisation are reviewed. The durometer shore hardness indentation method is reviewed including the instrument, mechanical process, different types of shore hardness methods, and the applications of shore hardness used in rubbers and gasket selections. A summary of current gasket types, their applications in different industries and structure of rubber materials are presented. The basic theories of nonlinear mechanics and strain energy functions are reviewed with key controlling material parameters critically discussed. The theoretical framework of different inverse FE modelling methods and optimisation programs are compared. The

challenges and significances of shore hardness modelling and correlations between shore A hardness and constitutive material properties are reviewed and discussed.

In Chapter 3, the research setup and details of some key experimental facilities and materials are presented. The facilities for shore hardness, compression and tension tests for different gasket samples are presented. The facilities used to make silicone rubbers and latex rubbers of different thicknesses are also presented. The main materials samples, including silicone rubber, EPDM and latex rubber, either made in laboratory or from commercial suppliers, used for shore hardness and other tests are also presented.

In Chapter 4, a FE model of shore A hardness indentation test is developed. Different modelling approaches are compared such as standard model, explicit model with adaptive mesh and re-meshing approach. A re-meshing program is developed in order to cope with the large element distortion when a softer material is being simulated. FE modelling of shore A hardness tests on thick samples (with standard sample thickness) is firstly generated and the results are compared with the published experimental data. The FE model is then transferred to modelling thinner samples. The correlation between shore A hardness, the effective Young's modulus and sample thickness (standard and non-standard thickness) is established. The accuracy of the data is assessed by correlating shore hardness tests and Young's modulus on silicone rubber and EPDM gaskets. Three different cases were studied to evaluate the results including hard silicone rubber specimens with different thickness, silicone rubber gasket samples and EPDM plate heat exchanger gasket samples. In the second part, an FE model of shore OO hardness indentation test with adaptive meshing is developed. The shore OO hardness predicted by the FE modelling of the standard sample thickness is compared with the prediction of analytical solution for spherical indenter. The correlations of shore OO hardness, Young's modulus and sample thickness (standard and non-standard thickness) are established. Two cases are studied to evaluate the results including soft silicone rubber specimens with different thicknesses and latex rubber specimens. In the third part, the Artificial Neural Network (ANN) method is developed using the FE data produced. The accuracy and feasibility of using ANN to predict material properties are evaluated. In the final part, an ANN program is developed to predict shore hardness from linear elastic and hyperelastic material parameters.



Chapter 5 discusses the applications of indentations tests and characterisation of material properties based on the relationship between the shore A hardness and Young's modulus. A typical case is presented, where the effect of shore hardness and E values are used to predicted the sealing pressure in a plate heat exchanger gasket. This concept and usage of the data could provide important information for material selections for gasketed plate heat exchanger or other similar situations. Effect of different hardness systems and indenter shapes is discussed focusing on the choice of shore A hardness for harder rubber material and shore OO hardness for softer rubber materials. Some key material or operation factors on shore hardness tests when testing rubber materials are discussed with a particular focus on friction at the lower boundary of the samples. Typical FE data is presented to show the influence of friction on the shore hardness values and the results are correlated to some tests with lubricated lower sample boundaries. The effect of thickness on the deformation during an indentation process is also presented. The suitability and effects of linear elastic (represented by E values) and nonlinear hyperelastic material properties in predicting shore hardness are compared and discussed.

In Chapter 6, overall conclusions are given and future works is recommended.

CHAPTER TWO  
LITERATURE REVIEW

## **2.1 Introduction**

In this chapter, the main types of indentation tests and their applications in testing a wide range of materials are reported. Different types of durometer shore hardness tests and the applications of shore A hardness in testing of elastomers and gaskets are critically reviewed. The structure and properties of rubber gasket materials in different industrial areas are presented. Manufacturing process, test methods and the material selections of rubber gasket materials are highlighted. The nonlinear mechanics and strain energy functions of materials are presented. The theoretical frame and current researches on combined numerical and experimental approaches are critically reviewed and potential improvement is discussed. Challenges and significance of simulating shores hardness tests and the correlation between shore A hardness and material properties in rubber materials are reviewed and discussed.

## 2.2 Indentation tests and Applications

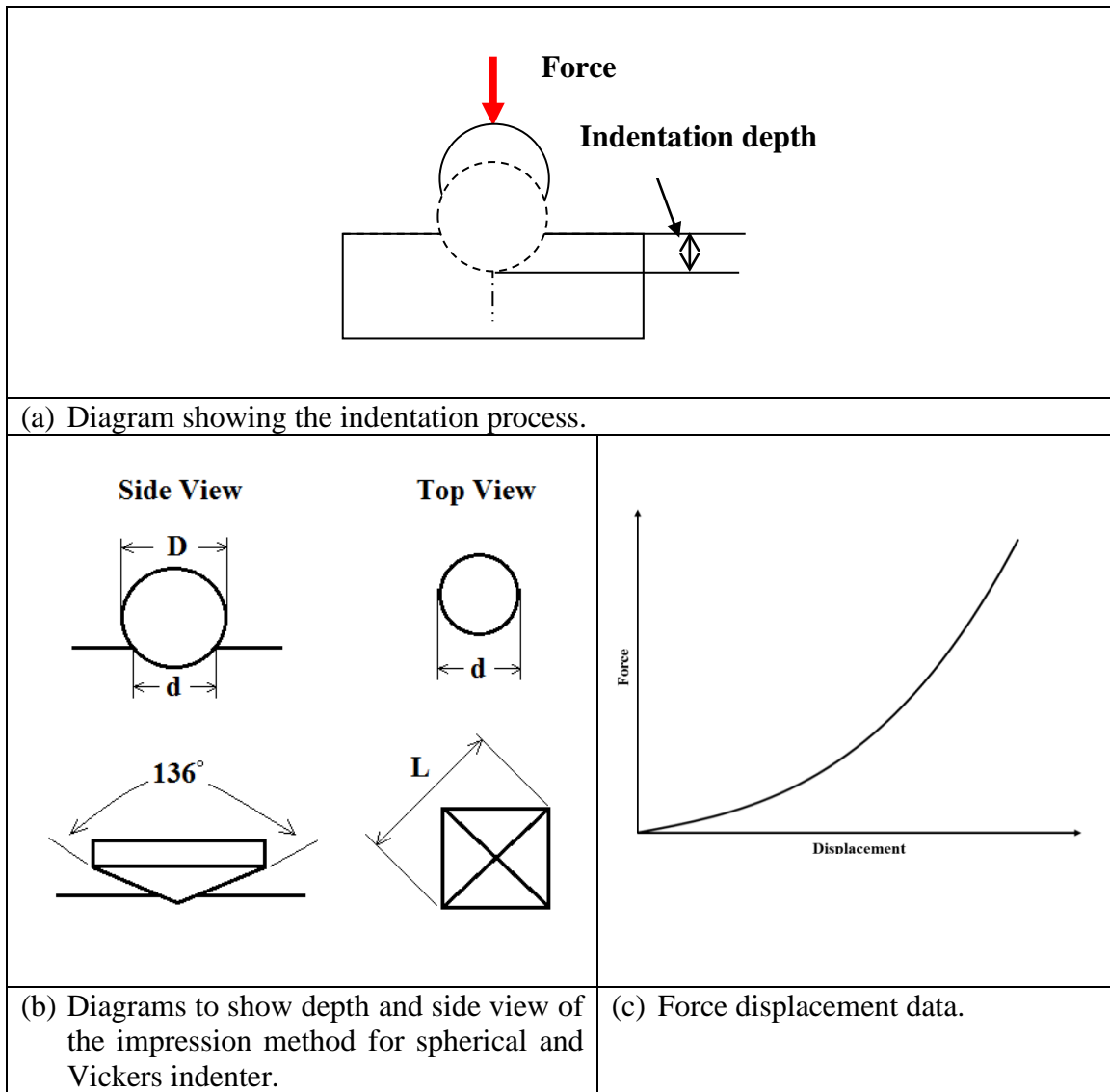
### 2.2.1 Different types of indentation testing and their applications

In an indentation test, an indenter is pressed onto the sample surface as illustrated in Figure 2.1 (a). The indentation resistance of the materials can be represented by the impression left on the materials surface (Figure 2.1(b)) or by the full force displacement curve ((Figure 2.1(c)) in the case of continuous indentation tests. Both approaches are widely used in metals, ceramics, polymers and composites (*Dao et al., 2001, Ren et al., 2003, Petr et al., 2010*). The indentation method has many advantages, it is convenient to use, and requires only a small amount of volume of materials. The indentation test has been employed to probe the mechanical behavior of materials for a wide range of engineering/medical applications (*Ren et al., 2002; Gérard et al., 2005*). In general, traditional hardness tests are based on the impression based approach, in which the application of a single static force and corresponding dwell time with a specified tip shape and tip material, results in a hardness impression in the order of micrometres (such as Vickers or Knoop hardness). The output of these hardness testers is typically a single indentation hardness value that is a measure of the penetration depth of the indentation tip into the sample surface (*Vanlandingham, 2003; Tobolski et al., 2007*). In continuous indentation, the resistance is monitored by the depth of penetration and load simultaneously. It can be used on much smaller scales (e.g. in nanometres) or in situations where no impression is measurable (such as foams or rubbers) but the test requires more complex facilities than static hardness approaches.

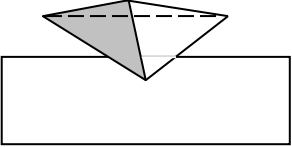
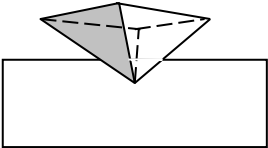
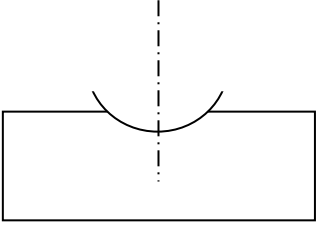
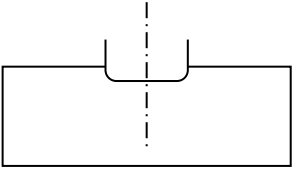
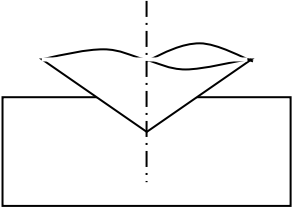
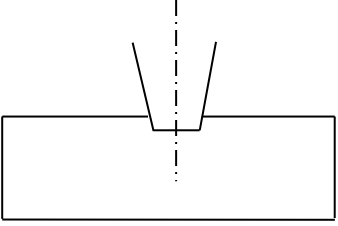
Many types of indenters with various shapes have been developed as schematically shown in Figure 2.2. Sharp indenters such as cone, sharp pyramidal tip indenter (trilateral or quadrilateral) and spherical indenter are normally used for harder materials such as metal, ceramic or plastics (*Dimitriadis et al., 2007, Hay, 2009 and Zhao et al., 2011*). Many hardness systems have been developed based on the average pressure underneath the indenters (*Dao et al., 2001, Armstrong et al., 2013*). For tests such as Vickers, the impression is in a scale of micrometers so it can be used to test very small volumes or areas. For example, it can be used to characterise the welded structure to work out the hardness profile of the HAZ zones (*Kong et al.,*

2008). It can also be used to test very thin structures such as the wire and nugget of thermocouples (*Zhao et al., 2011*).

Softer materials such as foams and biological tissues are normally tested using flat indenters and spherical indenters (*Farine, 2013*). In some cases, a combined conical and flat indenter is used, such as the shore A hardness test. All of these indenters can be classified as blunt indenters in comparison to sharp indenters. The advantages of these less sharp indenters lie in the fact that it is less damaging to the material and applicable to a wide range of materials. This method is particular useful for rubber like materials. Details of shore hardness tests and their applications are to be detailed in the next section.



**Figure 2.1** Schematic to show an indentation process (a) and the representation of indentation resistance based on the size of the residual impression (b) and force displacement data (c).

	
<p>(a) Pyramidal tip (trilateral) indenter. Berchvich</p>	<p>(b) Pyramidal tip (quadrilateral) indenter (Vickers)</p>
	
<p>(c) Spherical indenter. (Rockwell, shore OO)</p>	<p>(d) Flat indenter.</p>
	
<p>(e) Conical indenter.</p>	<p>(f) Conical+flat indenter (Shore A)</p>

**Figure 2.2** Diagrams showing different types of indenter tips.

## 2.2.2 Shore hardness tests, mechanism and applications

Figure 2.3(a) shows the basic structure of rubber testing machines. The load could be in the form of a dead load or loaded springs. The indenter used is normally a blunt one. Some harder rubbers may need to use a shore indenter such a conical indenter. Shore durometers are widely used in the testing of elastomers and plastics. They conform to all ASTM and international standards (*Serope et al., 2006*) and are easy to use. The shore hardness test uses a hardened indenter, an accurately calibrated spring, a depth indicator, and a flat presser foot as shown in Figure 2.3 (b). The indenter protrudes from the middle of the presser foot and extends a distance of 2.5 mm from the surface of the foot. The hardness is defined as zero when the indenter is in the fully extended position. When the indenter is depressed flat, i.e. in the same position as the surface of the presser foot, the hardness is defined as '100'. Therefore, every shore point is equal to 0.0025 mm penetration (*Durometer Hardness Handbook, Instron Company*). To perform a test, the unit is placed on the sample so that the presser foot is held firmly against the test surface. The spring pushes the indenter into the sample and the indicator displays the depth of penetration. The deeper the indentation is impressed, the softer the material with lower hardness value is achieved.

**Table 2.1** General characteristics of different types of shore durometer hardness (*DuroMeters, CCSI Inc.*).

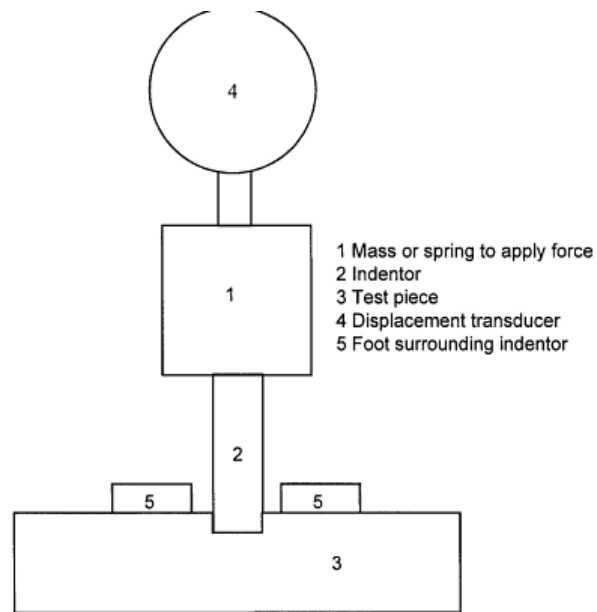
Durometer Type	Configuration	Diameter	Spring force
A	35° truncated cone	1.4mm (0.055in)	822gf (8.06N)
C	35° truncated cone	1.4mm (0.055in)	4536gf (44.48N)
D	30° cone	1.4mm (0.055in)	4536gf (44.48N)
B	30° cone	1.4mm (0.055in)	822gf (8.06N)
O	1.2mm (0.047in) spherical radius	2.4mm (0.094in)	822gf (8.06N)
OO	1.2mm (0.047in) spherical radius	2.4mm (0.094in)	113gf (1.11N)

Table 2.1 lists different Durometer systems with different shaped indenters and applied loads, which cover the entire spectrum of indentation hardness testing of rubber-like materials. Each durometer type is made to a specific scale (i.e. A, B, C,

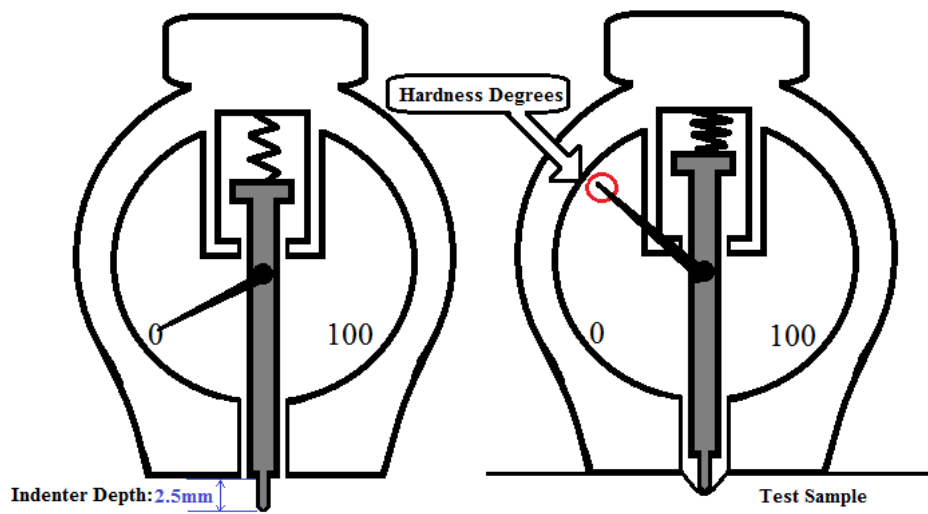


and D) and is capable of producing a value between 0 and 100. Each of the shore hardness scales is used for different situations and materials systems (*Kim et al., 2012, Obidiegwu and Ogbobe, 2012*). Different materials respond to the test scales in different ways which made it difficult to establish a direct quantitative correlation between different durometer scales. Most of the data available in the open literature is based on some specific material groups. Figure 2.4 (a) shows the correlation between shore A and shore D hardness of plastics. There is a general trend but the correlation is not very strong. Figure 2.4(b) plots the data for seal materials. It shows a much better trend, however, it is not very clear what materials the data is based on. (*Shore Hardness Testing of Plastics, MatWeb; Durometer Hardness Scales – General Reference Guide, Seal & Design Inc.*)

Shore hardness based data is effective in distinguishing the differences between materials. But for computer aided design, constitutive material properties (such as Young's modulus or hyperelastic parameters) are required in order to be able to predict the material behaviour. However, in most cases of the published literature or reports, the properties of elastomers are often conveniently quoted by specifying the shore A hardness, and less often via the modulus of elasticity. There is no well-established link between shore hardness and Young's modulus. This is partially due to the complex nature of the indenter shape and the definition of shore hardness in different scales. In addition, given that the material being tested by different shore hardness tests may have totally different structure and deformation mechanisms, a unified link between the shore hardness and properties such as Young's modulus is difficult. However, it is probably feasible when the research is focused on a particular group with similar behaviour and loading conditions, such as rubbers. Some experimental work has showed that there is a general form of trend of agreement between shore A hardness values and Young's modulus. For example, the work by *Johannes et al. (2006)* showed that there is general correlation between the modulus of elasticity in compression and the shore A hardness values of several rubber samples. This suggests that it is important to investigate the hardness and other properties in either standard size or non-standard size through detailed FE modelling and experimental tests. This is particularly important for situations such as gaskets or seals where the main loading condition of the material in service is principally in compression within the range of the linear elastic deformation.

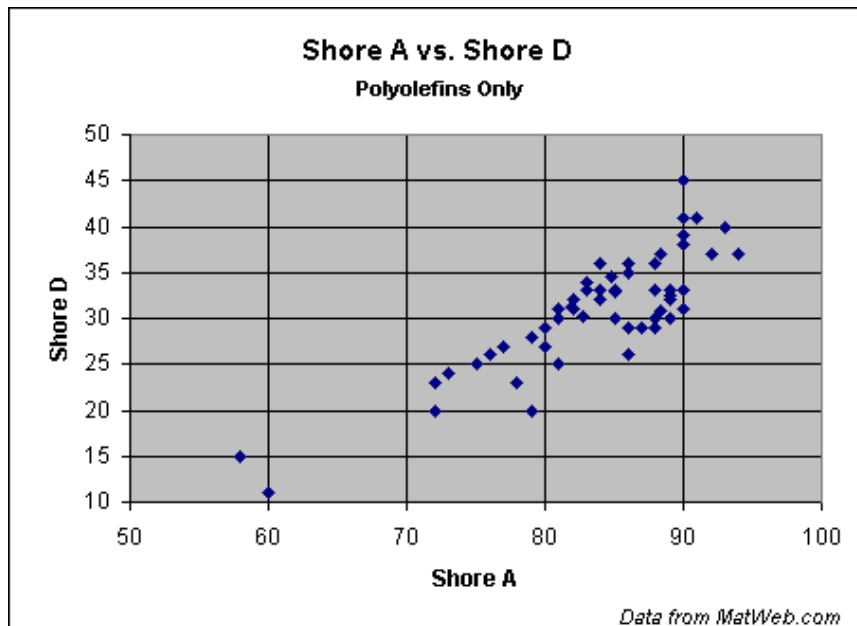


(a) Principle of hardness test of rubber (*Brown, 2005*).

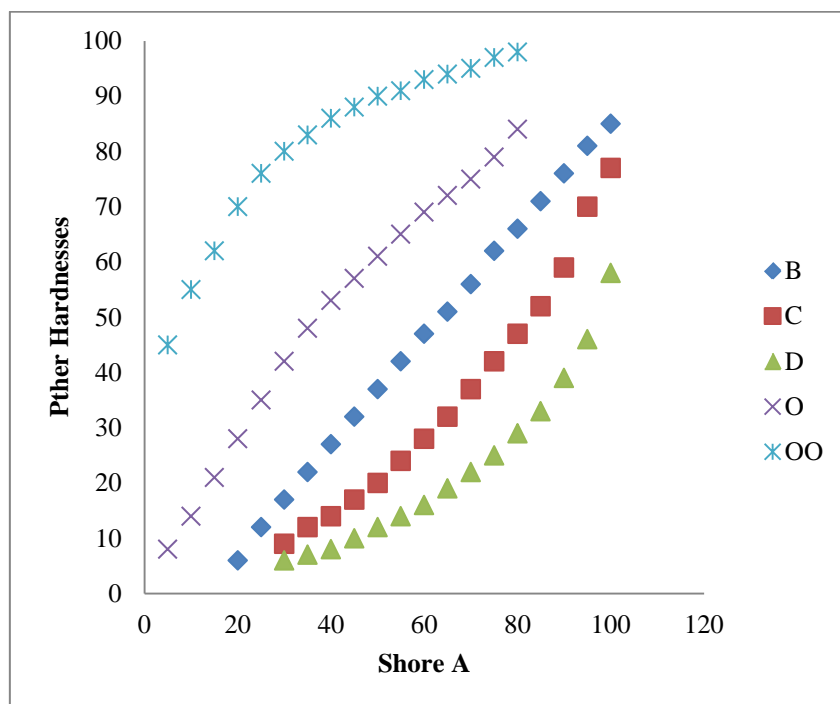


(b) Schematic to show the design of a Shore hardness tester.

**Figure 2.3** Principle of rubber hardness tests and structure of a Shore Durometer.



(a) Shore A and Shore D hardness data of plastics (polyolefin) showing it is difficult to compare different hardness (“*Shore (Durometer) Hardness Testing of Plastics*”. MatWeb).



(b) Correlation between shore A and other hardness tests (*Data taken from “Shore Durometer Conversion Chart”, Seal & Design Inc.*).

**Figure 2.4** Correlation between shore A and other hardness systems.

### 2.3 Structures of rubber materials and properties

Figure 2.5 illustrates the molecular structure of an elastomer consisting of random coils connected by crosslinks. There are many different types of rubbers/elastomers, the formula of the molecules of some key examples are listed in Table 2.2 (Shanks, 2013). Most of these rubber materials are used as gasket or seals materials.

**Table 2.2** Structure of different rubbers (Shanks, 2013).

Common name	Abbreviation	Structure of repeat unit
1, 2-polybutadiene	BR	$\text{H} \left[ \begin{array}{c} \text{CH}_2 - \text{CH} \\   \\ \text{CH} \\    \\ \text{CH}_2 \end{array} \right]_n \text{H}$
Ethylene propylene diene rubbers	EPDM	$\left[ \text{CH}_2 - \text{CH}_2 \right]_x \left[ \text{CH}_2 - \overset{\text{CH}_3}{\underset{ }{\text{CH}}} \right]_y$
Epichlorohydrin rubber	ECO	$\left[ \text{CH}_2 - \underset{\text{CH}_2\text{Cl}}{\underset{ }{\text{CH}}} - \text{O} \right]_n \left[ \text{CH}_2 - \text{CH}_2 - \text{O} \right]_m$
Polyurethanes	PU	$\left[ \text{C}(=\text{O}) - \text{NH} - \text{C}_6\text{H}_4 - \text{CH}_2 - \text{C}_6\text{H}_4 - \text{NH} - \text{C}(=\text{O}) - \text{O} - \text{CH}_2 - \text{CH}_2 - \text{O} \right]_n$
Latex rubber	LR	$\left[ \begin{array}{c} \text{CH}_2 \qquad \text{CH}_2 \\ \diagdown \quad / \\ \text{C} = \text{C} \\ / \quad \diagdown \\ \text{H} \qquad \text{CH}_3 \end{array} \right]_n$

Natural rubber (NR) is an elastomer with a basic monomer of cis-1, 4-isoprene. It is made by processing the stems of the rubber tree (i.e., *Hevea brasiliensis*) with steam, and compounding it with vulcanizing agents, antioxidants, and fillers (Sun, 2007). Natural rubber is widely used for applications requiring abrasion or wear resistance, electric resistance and damping or shock absorbing properties such as large truck tyres and aircraft tyres. It is chemically resistant to acids, alkalis and alcohol.

However, it does not do well with oxidizing chemicals, atmospheric oxygen, ozone, oils, petroleum, benzene, and ketones. Styrene-butadiene rubber (SBR) is a synthetic rubber copolymer consisting of styrene and butadiene. Its chemical resistance is similar to that of natural rubbers; however, it exhibits more abrasion resistance than polybutadiene and natural rubber that makes styrene-butadiene rubber a suitable material for automobile tyres. Ethylene propylene diene monomer (EPDM) is a synthetic rubber consisting of ethylene and propylene (*Modan et al., 2013*). It has outstanding heat, ozone and weather resistance due to its stable, saturated polymer backbone structure. As non-polar elastomers, EPDM rubbers have good electrical resistivity, as well as resistance to polar solvents, such as water, acids, alkalis, phosphate esters and many ketones and alcohols. It is mainly used as a standard lining material for steam hoses, automotive weather-stripping and seals, radiator, electrical insulation and roofing membrane.

Crosslinking or curing, i.e., forming covalent, hydrogen or other bonds between polymer molecules, is a technique used very widely to alter polymer/rubber properties (*Datta et al., 2002*). The typical process to change the properties of rubber is the vulcanisation process, in which sulphur is added to the raw material and the mixture is heated up to a certain temperature to enhance the cross linking process. This will transfer the rubber material from a soft plastic state to a more stable and solid molecular structure. Vulcanization forms chemical bonds between adjacent elastomer chains and subsequently imparts dimensional stability, strength, and resilience of the finished material. The properties of rubber materials can also be modified by adding small particles, fillers, to the raw material before the vulcanization process (*Austrell, 1997*). A typical example of reinforcing materials is carbon particles with a size of 20nm – 50µm, called carbon black. A molecular structure of a carbon black filled rubber is shown in Figure 2.5 (b) the polymer chains are shown as solid lines and cross links are shown as dashed lines. Under the vulcanization process, carbon black can increase the stiffness of the material by creating cross-links between the filler particles and the long molecular chains.

Rubber is highly elastic, nonlinear and viscous. Rubber has a low modulus of elasticity and is capable of sustaining a deformation of as much as 1000 % (*Schaefer,*

2009). After such deformation, it quickly and forcibly retracts to its original dimensions. It is very resilient and exhibits strong internal damping. When an unstrained rubber specimen undergoes a cyclic loading to a specific stretch, the force required will gradually decrease and reach a steady state after three to five cycles. Under cyclic loading the rubber network changes and the cross-links collapse, which causes the described phenomenon called Mullins effect as illustrated in Fig. 2.6. With these characteristics, rubber parts can therefore be used as shock and vibration isolators and/or as dampers (*Johansson et al., 2006; Nelson et al., 2015*). In addition, rubber will not corrode and normally requires no lubrication, which also makes it suitable for gasket applications. For application such as gaskets, rubber is a very good candidate material as it has a good compressibility and recovery ability.

Typical manufacturing process of rubber materials includes four operations: compounding, mixing, shaping, and vulcanizing (*Johnson, 2001*). Compounding aims to add chemicals (sulphur) for vulcanization to the rubber materials. Other additives are filled in the material to enhance the mechanical properties (carbon black), antioxidants, ozone protective chemicals and colouring pigments. Mixing is for mixing the additives with the base material. Vulcanization is a treatment for rubber to become stiffer and stronger. The process normally involves the use of sulphur at a temperature of 140 °C for about 5 hours; enough time to accomplish cross-linking of elastomers molecules (*Valery, 2013*). In a shaping process, extrusion and calendaring can be combined in a roller die process. Calendaring is a process for producing sheet and film stocks out of rubber materials (*Groober, 2010*). Another special process for rubber is so-called dip casting, in which a mould is submersed in a liquid polymer for a certain duration.

## 2.4. Gaskets and rubber materials

### 2.4.1 Application of rubber based material in Gasket and seal Materials

Gaskets are mechanical seals used to stop leakage in situations with two or more surfaces where leaks of fluid or air need to be enclosed. Materials for gaskets can typically be divided into three main categories based on the materials groups: Non-metallic types (e.g. rubbers, plastics), Semi-metallic types (e.g. stainless steel, carbon steel for inner and outer ring, polytetrafluoroethylene (PTFE), ceramic for fillers) and Metallic types (e.g. stainless steels, carbon steels, coppers) (*Shah, 2008*). Soft gaskets are typically made of deformable materials such as rubber, silicone, soft metal, cork, felt, neoprene, nitrile rubber or a plastic polymer (*Curtis, 2011*). Gaskets are extensively used in different types of equipment/structures in many industries, such as aerospace industries, general machinery, energy, food, etc. Some typical/representative structures with gaskets are shown in Figure 2.7, including flange, pump, valve, car engine and heat exchanger.

Figure 2.7 (a) shows a flange gasket for pipes. Flange gaskets are used to create a static seal between two flange faces, at various operating conditions, with different pressures and temperatures. The gasket material needs to fill the microscopic spaces and irregularities of the flange faces (*Lorenz, 2006*) to form a seal so that liquids and gases would be kept from escaping. The main property/performance requirements when selecting the design and materials for a gasket to be used for flanges includes fugitive emissions, chemical compatibility with the fluid, temperature, internal pressure. The main mechanical properties are compressibility, compress set and sealing force, these are important for the assembling, time dependent deformation, vibration and response of the seal to potential pressure or temperature changes (*Flanges, Gaskets & Bolts, Flowstar Inc.; Sealing Technology-BAT guidance notes, ESA Sealing Technology*). To achieve these functional requirements, the material properties (e.g. corrosion resistance) and the mechanical properties (e.g. stiffness and strengths) are very important. Rubber is widely used for the role as it yields slightly; this is an ideal feature as it allows the gasket to fill any small gaps around what it is fixed to. Rubber is also a less expensive option, but is still highly reliable and can often re-seal itself if it was to become dislodged (*Curtis, 2011*). In addition, rubber is known to be elastic over a large strain range, so that it will maintain the sealing

pressure when the position of the clamping joint deforms/displaces with changing temperature or pressure (*Guan et al., 2011*).

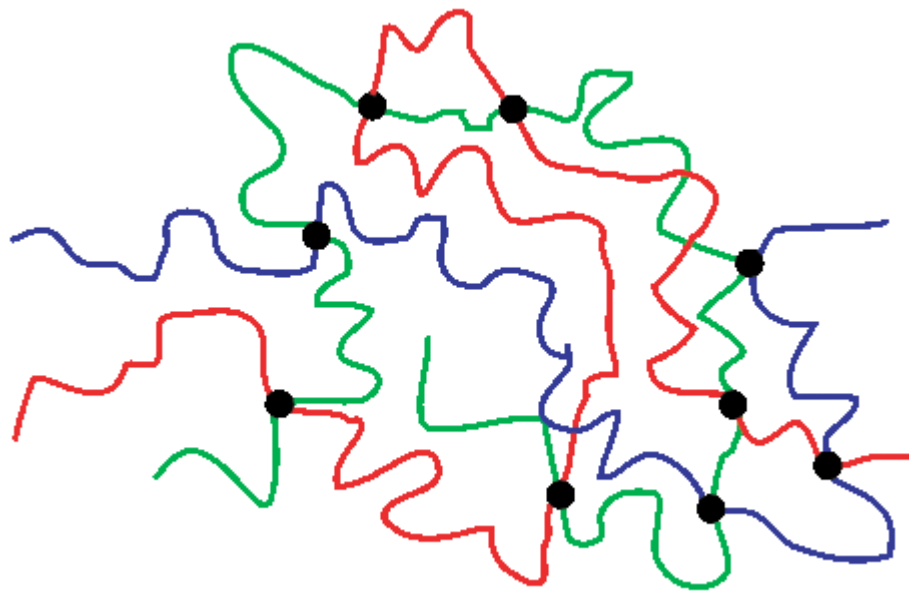
Figure 2.7 (b) shows a typical head gasket, which is used to seal an engine block. A head gasket, in service, sits between the engine block and cylinder heads in an internal combustion engine to seal the cylinders and avoid leakage of coolant or engine oil into the cylinders. It is the most critical sealing application in any engine and as part of the combustion chamber; it shares the same strength requirements as the other combustion chamber components (such as tubing, compressor, etc.). The main property/service requirements include gas, coolant and oil-tight, chemical influences resistance (combustion gas, lubricant/coolant), reduction in component stiffness. Typical materials used for head gaskets include stainless steels, coppers, graphite and polymers.

Figure 2.7 (c) shows a typical gasket for a plate heat exchanger (PHE), which is used for preventing leakage of the media from the channels between the plates to the surrounding atmosphere. Heat exchangers are widely used to transfer heat energy from warmer medium to the thin wall, which instantly loses it again to the colder medium on the other side. The warmer medium drops in temperature, while the colder one is heated up (*Sadik, 2003*). A PHE consists of a pack of thin corrugated metal plates with portholes for the passage of the fluids. There is a bordering gasket between each plate, which seals the channels formed when the plate pack is assembled together. The hot and cold fluids flow in alternate channels and the heat transfer takes place between adjacent channels. A heat exchanger gasket is used to stop the leakage from the channels between the plates to the surrounding atmosphere. The design and properties of gasket is very important as it has direct influence on the assembly, operation and maintenance of the heat exchangers. Figure 2.7 (d) & (e) shows the typical gasket for bolted structure and butterfly valve gasket. For these structures, the gasket material needs to have a good combination of compressibility and recovery ability. Figure 2.7 (f) shows a typical silicone rubber gasket which is used to seal the food media leakage from the flange joint in the pipeline. Most of the silicone rubbers used in the food industry are based on polydimethyl vinyl siloxane. Conventional silicone rubber has a very good thermal stability. It is the ability to

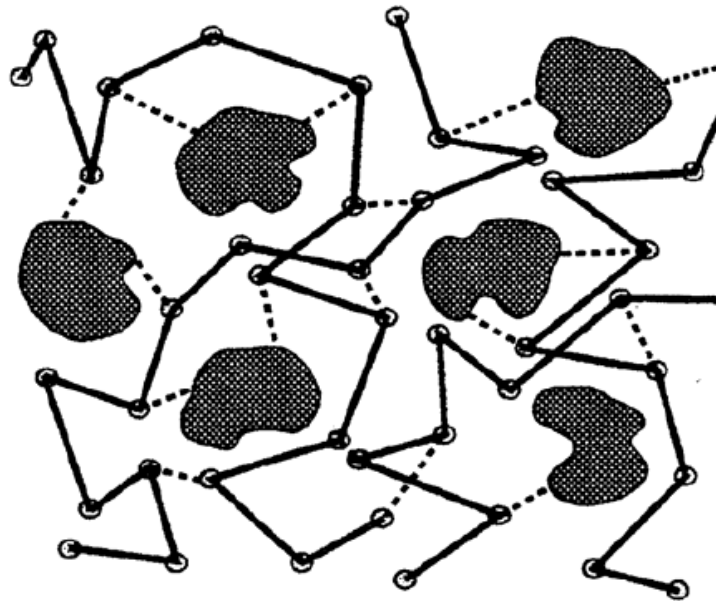


withstand high temperatures that makes it useful for seals and tubing, for example in drinks vending machine up to 100°C. Cold cured silicone is used as coatings to improve the release of adhering foods from surfaces, e.g. transportation belts, and it finds extensive use as sweet moulds (*Sidwell et al., 2000*).

Depending on the nature of the structure where the gasket is used, the function requirement may be significantly different including thermal, chemical and mechanical properties. To achieve these functional requirements, an in-depth understanding of the material properties and the mechanical behaviour of the gasket is very important and requires an integrated research by combining materials, testing and computer aided modelling.

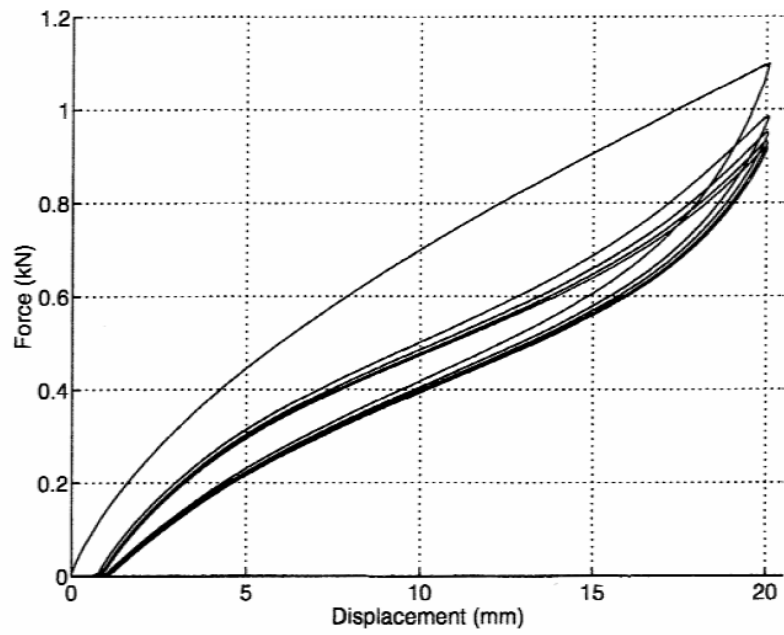


(a) Unloaded coil chains (*“The Stiffness of Rubber”*, University of Cambridge).



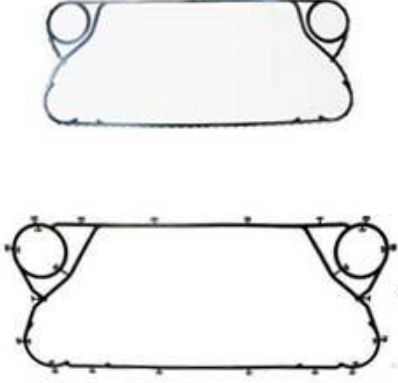

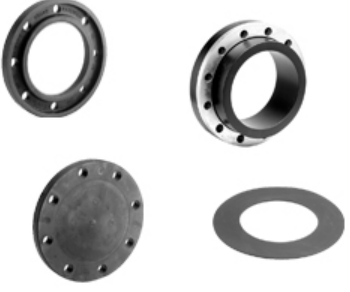



(b) The molecular structure for a carbon black filled rubber vulcanizate. Dashed lines are cross links and solid lines are the polymer chains (*Johansson et al., 2006*).

**Figure 2.5** The molecular structure of rubbers.



**Figure 2.6** Force-displacement relations for a rubber vulcanizate exposed to cyclic loading showing its ability to recover its original shape (*Johansson et al., 2006*).

	
<p><b>(a)</b> Pipe flange gasket</p>	<p><b>(b)</b> Engine valve cover gasket.</p>
	
<p><b>(c)</b> Heat exchanger gasket</p>	<p><b>(d)</b> Butterfly valve gasket for pipelines</p>
	
<p><b>(e)</b> Bolted joint gasket</p>	<p><b>(f)</b> Silicone gasket in food industry</p>

**Figure 2.7** Different types of gaskets for different applications.

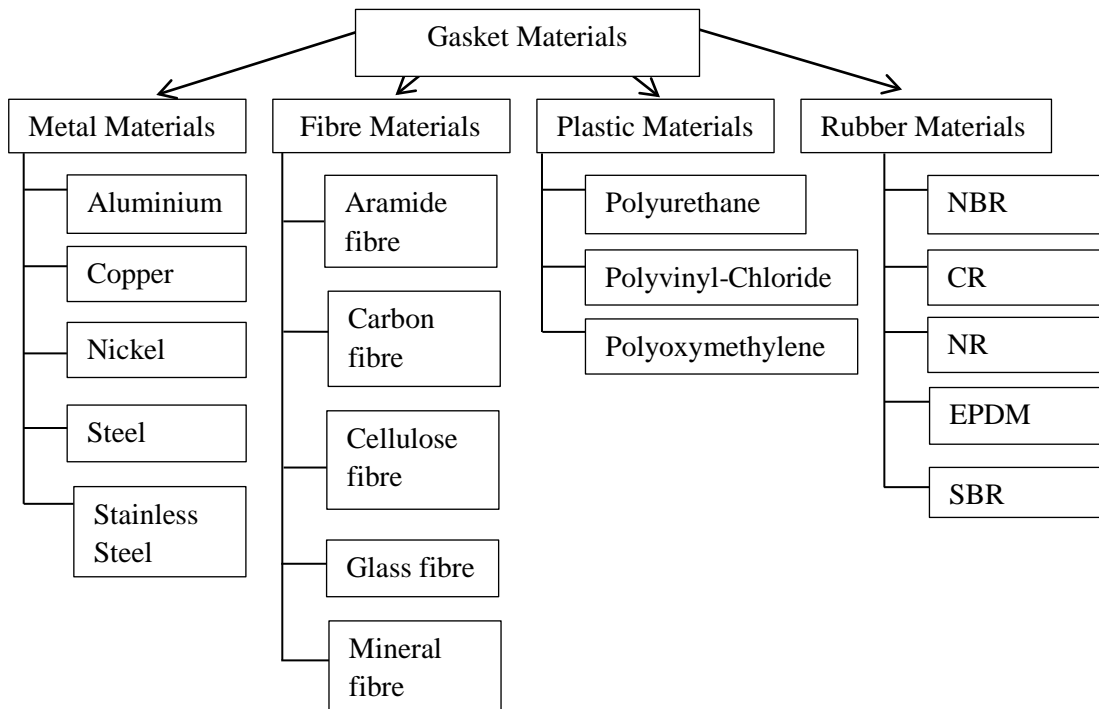
## 2.4.2 Classifications of gasket material and developments

Figure 2.8 (a) summarises different materials used in making gasket including metals, plastics and rubber like materials (*Steinetz, 2006*). Metal based gaskets have good mechanical, thermal and pressure resistance and are widely used in offshore and refining petrochemical applications. Metal gaskets are normally made through punching and machining operations. Fibres have good chemical and elasticity properties and are used for medium to high temperature applications (such as chemical processing, aerospace, automotive and water applications). Asbestos is traditionally used in the heat exchanger gaskets in particular when these heat exchangers are used for the systems of higher pressure steam. It is known to be of risks to the human health, hence its use should be avoided where possible. Increasingly, new materials are being developed to replace asbestos based gasket materials by using other fibres (*Currie, 2002*).

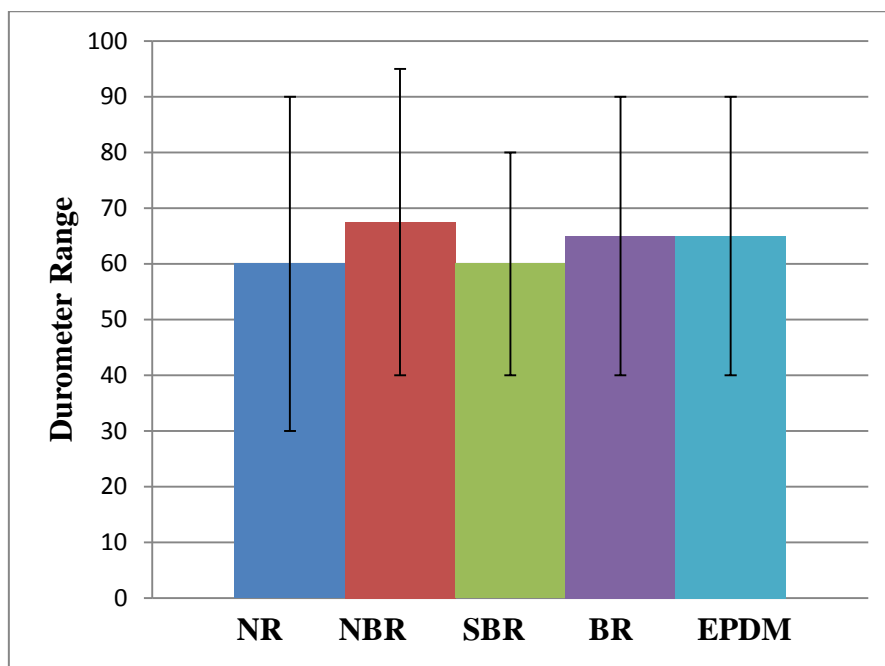
Selection of gasket is an important issue in engineering design and development as it influence the assembly and operation performance. The mechanical properties, shape and thickness of the gasket directly influences the performance. The performance of certain gasket material is subject to thickness dependency – as thickness increases sealing performance is reduced (*Lattimer, 2012*). A thinner gasket makes it easier to achieve a higher strain and sealing forces. However, it also requires high dimension surface finish of the joint, such as flatness etc. This is one of the reasons why most rubber based gasket is supplied in the form of a thin sheet, which can then be cut into different shapes accordingly. This to a certain extent has made testing rubber gasket in compression difficult, as normal compression tests require a sample of certain thickness (e.g. 25% strain according to the standard). While shore hardness offers a potential method which can be performed easily, the main question is if the constitutive material properties such as the Young's modulus can be estimated from the shore hardness values.

Rubber gaskets are based on various rubbers such as natural rubber (NR), acrylonitrile-butadiene rubber (NBR), ethylene propylene diene monomer rubber (EPDM), and so on. The shore hardness of some of the rubber materials is shown in Figure 2.8(b). These rubbers have a shore hardness range between 60 and 70. Many

research works have been conducted to develop rubber materials in order to enhance their performances, such as increasing the rubber's life time, temperature resistance, chemical resistance and so on (*Sohn et al., 2002; Suzuki et al., 2005; González et al., 2005; Mahaling et al., 2007; Rajasekar et al., 2009*). All these development works require a quick way of mechanical tests. In Sohn's research (2002), the dynamic mechanical property of particle-reinforced ethylene-propylene-diene monomer (EPDM) matrix composites has been studied by using a dynamic mechanical thermal analyser (DMTA) as shown in Figure 2.9 (a). The composites were strengthened with the various reinforcing particles including: silicon carbide particles (SiCps), copper (Cu) and aluminium (Al) particles. In this work, E values have been used as the main properties to represent the effects of the particles. Figure 2.9(b) gives a typical data showing temperature dependency of E. with different particle size and types. Traditionally, testing is an important part of development of gaskets; FE modelling is increasingly being used in material and product developments. However, due to the complex nature of rubber materials, the materials properties are much more complex than those for metals and plastics. A more rapid testing method is required, which requires further studies.

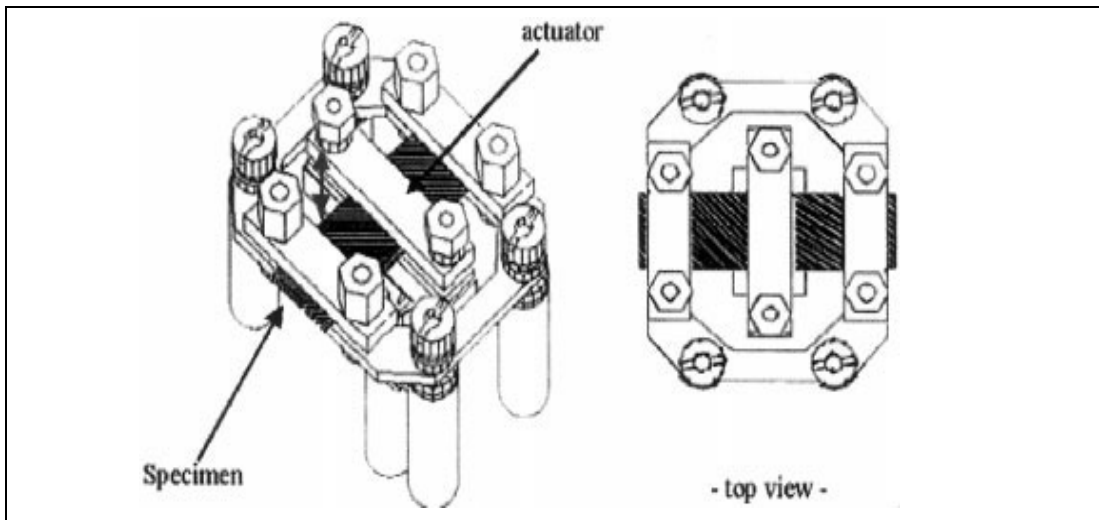


(a) Classification of gasket materials (*This table is based on the information from Shah, 2008*).

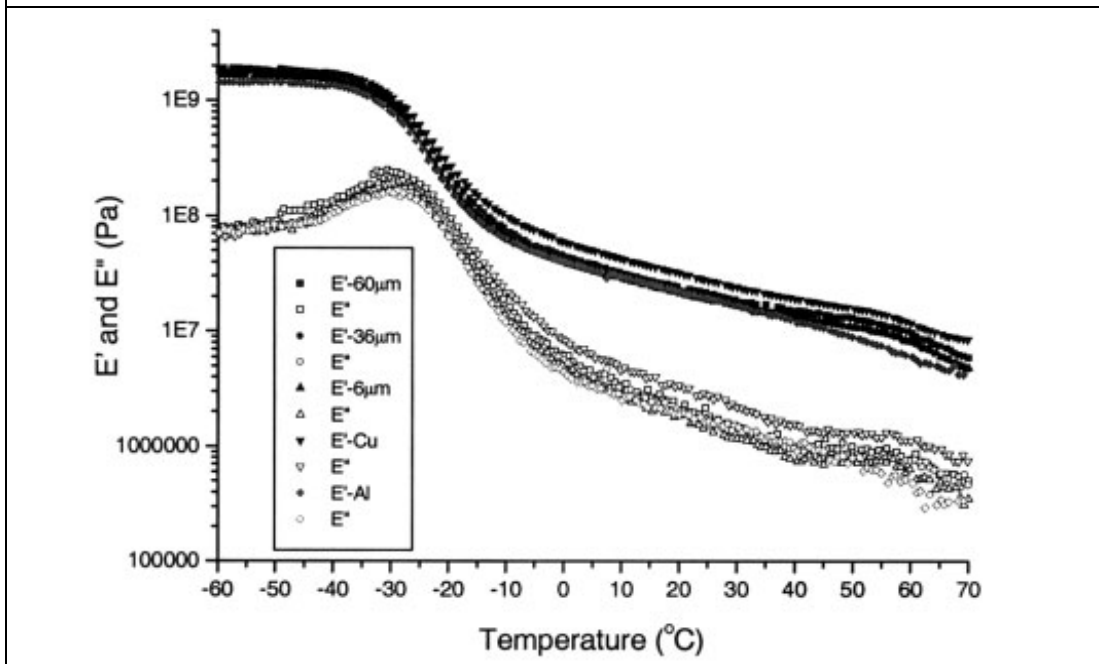


(b) A bar chart of shore hardness values in various rubbers (*Vishal and Matawala, 2003*).

**Figure 2.8** Classification of gasket materials.



(a) Geometry of dynamic mechanical thermal analyser (DMTA) test setup.



(b) Temperature dependency of E of rubber with different particle size and particle type (*Sohn et al., 2002*).

**Figure 2.9** Development of rubber based materials for gasket applications.



### 2.4.3 Manufacturing process & material selections of gasket

The development of quick testing methods is also directly relevant to the manufacturing process of rubbers or gaskets. A quick material testing or characterisation method will make the materials development quicker and quality control easier. Due to the different manufacturing processes, rubber products have different shapes, thickness, and hardness. In addition, the manufacturing process may also affect the properties, which requires routine examination and quality checks. All of these require a systematic understanding about rubber testing, in particular shore hardness tests. Typical manufacturing processes of rubber include the casting, the dipping, spreading, foaming and so on.

Dipping of rubber is widely used, in particular for latex rubber. A variety of thin rubber articles e.g. toy balloon, teats, gloves etc. can be prepared from latex by a dipping process. The process consists essentially of dipping a former (original model) in the shape of the article to be made into the compounded latex. The former may be made from a variety of materials, including metal, glass, lacquered wood and porcelain. The deposited film is dried, vulcanized in circulating hot air, steam or hot water and then stripped from the former. This is known as 'straight' dipping as against coagulant dipping where the former is first coated by dipping into a chemical coagulating agent. The coagulants may be either salt coagulants or acid coagulants. (*Uptal, 2007; Coagulant dipping, Kraton Inc.*)

Another widely used form of rubber product production is casting and moulding: casting involves the use of a mould on the inside walls of which the rubber article is formed, the pattern on the inside of the mould determining the ultimate shape of the article. The basic principle of casting is to 'set' the compound in the mould followed by subsequent drying, removal from the mould and vulcanizing. Depending on the technique of 'setting' (gelling) inside the mould, two types of moulds are used: i) Plaster of Paris moulds, and ii) Metal moulds. Gelation in plaster mould is brought about by partial absorption of water by the mould material or in a metal mould by using a heat-sensitizing agent (*Uptal, 2007*). In the materials development stage, normally the wooden mould is used as it can be used to produce samples of different sizes and thickness.

In some case, rubber has to be applied on site to the surface of the target area in gasket or seal related applications, such as cure-in-place gasket. *Thibeau (2004)* researched the selection method of form-in-place (FIP) gaskets. In this research, it was realized that dispensing an electrically conductive paste or semiliquid material in the precise location where the gasket is needed is a cost-effective method of gasketing for either metal or plastic enclosures. FIP EMI gaskets are made by dispensing an uncured elastomeric material on the surface of a part and curing the material in place. As with the more common, nonconductive FIP or cure-in-place gaskets, the uncured material is dispensed through a needle by computer-controlled, three-axis robotic equipment so gaskets with very complex geometries can be formed, positioned, and reproduced accurately. The size of the gasket bead is set by the diameter of the needle and the material flow rate, with typical gasket heights ranging from approximately 0.3 mm to 5 mm. The gasket material usually is dispensed as a thixotropic paste cured with heat or atmospheric moisture to a relatively soft, rubbery gasket with shore A hardness of 35 to 75. The conductive fillers are typically metal particles or nonconductive materials like glass that are plated with a conductive metal. When cured, the gasket material could have a volume resistivity of 0.003 to 0.100 W/cm depending on the filler, the same resistivity range could be achieved as extruded or moulded conductive elastomers. These gaskets are used due to their functional requirements (in this case, conductivity) but they have to maintain the mechanical properties to achieve sufficient sealing. For situations like this onsite gasket making, hardness test is the most viable way of testing on site to assess the curing process and control the quality.

## 2.5 Indentation test of rubber and rubber like materials

### 2.5.1 Properties of rubbers

To correctly use rubber in design and applications, a range of material properties will be required. The properties of rubber materials commonly used are listed in Table 2.3. These data will provide important data for materials selection and manufacturing process, among which the Durometer range is one of the main mechanical properties. Many of the functional or time/temperature dependent properties are related to the linear and nonlinear properties as well as hardness. Some key mechanical properties are presented in the next sections including: tensile and compression tests, viscoelastic, creep and fatigue.

**Table 2.3** Relative properties of various elastomers (*Schaefer, 2009*).

ASTM designation	NR	BR	SBR	IIR CIIR	EPDM EPDM	CSM	CR	NBR	HNBR	ACM ANM	T	FKM	FVMQ	VMQ MQ, PMQ, PVMQ	AU EU	GPO	CO ECO
Durometer range	30-90	40-90	40-80	40-90	40-90	45-100	30-95	40-95	35-95	40-90	40-85	60-90	40-80	30-90	35-100	40-90	40-90
Tensile max, psi	4500	3000	3500	3000	2500	4000	4000	4000	4500	2500	1500	3000	1500	1500	5000	3000	2500
Elongation max., %	650	650	600	850	600	500	600	650	650	450	300	400	900	750	600	350	
Compression set	A	B	B	B	B-A	C-B	B	B	B-A	B	D	B-A	C-B	B-A	D	B-A	B-A
Creep	A	B	B	B	C-B	C	B	B	B	C	D	B	B	C-A	C-A	B	B
Resilience	High	High	Med.	Low	Med.	Low	High	Med.-Low	Med.	Med.	Low	Low	Low	High-Low	High-Low	High	Med.-Low
Abrasion resistance	A	A	A	C	B	A	A	A	A	C-B	D	B	D	B	A	B	C-B
Tear resistance	A	B	C	B	C	B	B	B	B	D-C	D	B	D	C-B	A	A	C-A
Heat aging at 212°F	C-B	C	B	A	B-A	B-A	B	B	A	A	C-B	A	A	A	B	B-A	B-A
T <sub>g</sub> , °C	-73	-102	-62	-73	-65	-17	-43	-26	-32	-24, -54	-59	-23	-69	-127, -86	-23, -34	-67	-25, -46
Weather resistance	D-B	D	D	A	A	A	B	D	A	A	B	A	A	A	A	A	B
Oxidation resistance	B	B	C	A	A	A	A	B	A	A	B	A	A	A	B	B	B
Ozone resistance	NR-C	NR	NR	A	A	A	A	C	A	B	A	A	A	A	A	A	A
Solvent resistance																	
Water	A	A	B-A	A	A	B	B	B-A	A	D	B	A	A	A	C-B	C-B	B
Ketones	B	B	B	A	B-A	B	C	D	D	D	A	NR	D	B-C	D	C-D	C-D
Chlorohydrocarbons	NR	NR	NR	NR	NR	D	D	C	C	B	C-A	A	B-A	NR	C-B	A-D	A-B
Kerosene	NR	NR	NR	NR	NR	B	B	A	A	A	A	A	A	D-C	B	A-C	A
Benzol	NR	NR	NR	NR	NR	C-D	C-D	B	B	C-B	C-B	A	B-A	NR	C-B	NR	B-A
Alcohols	B-A	B	B	B-A	B-A	A	A	C-B	C-B	D	B	C-A	C-B	C-B	B	C	A
Water glycol	B-A	B-A	B	B-A	A	B	B	B	A	C-B	A	A	A	A	C-B	B	C
Lubricating oils	NR	NR	NR	NR	NR	A-B	B-C	A	A	A	A	A	A	B-C	A-B	D	A

A = excellent, B = good, C = fair, D = use with caution, NR = not recommended

### Tensile or Compression Tests

Rubber is essentially an incompressible substance which deforms by changing shape rather than changing volume. It has a Poisson's ratio of approximately 0.5. At low strains, the ratio of the resulting stress to the applied strain is a constant (Young's modulus). This value could be close when the strain is applied either in tension or compression (*Schaefer, 2009*). Hooke's law is therefore valid within this proportionality limit. However, as the strain increases, this linearity ceases, and Hooke's law is no longer applicable. Also the compression and tension stresses to the samples strain level could become different (*Czernik, 1996*). The stress-strain

properties of rubber compounds are usually measured under tension as per ASTM procedures. Either moulded rings or die-cut “dumbbell-shaped” specimens are used in testing. Stress measurements are made at a specified percentage of elongation and reported as modulus values. For example, 300 % modulus is defined as the stress per unit cross-sectional area (in psi or MPa units) at an elongation of 300 %. Also the stress at failure (tensile) and maximum percentage elongation can be determined from tensile tests. Since rubber is incompressible, compression in one direction results in extension in the other two directions, the effect of which is a bulging of the free sides. In characterising gasket or seals, shape factor describes the role of the shape in determining how a part with parallel load faces will behave under compressive forces. The shape factor is calculated by dividing the loaded area by the total free area (*Pinarbasi, 2009*), which decreases with increasing thickness. Therefore, the gasket should be as thin as possible to reduce relaxation. It must be thick enough, however, to permit adequate conformity. The clamp area should be as large as possible, consistent with sealing stress requirements (*Czernik, 1996*).

### **Viscoelasticity of rubber materials**

Rubber has elastic properties similar to those of a metallic spring and has energy absorbing properties like those of a viscous liquid. These viscoelastic properties allow rubber to maintain a constant shape after deformation, while simultaneously absorbing mechanical energy, represented by the area between the loading and unloading curves. The elasticity follows Hooke’s law and increases with increased strain, while the viscosity follows Newton’s law and increases with increased strain rate (*Ciesielski, 1999*). Therefore, when applying a strain, the resultant stress will increase with increasing strain rate. Non-linear springs or linear dashpots are frequently used to make theoretical models which illustrate the interaction of the elastic and viscous components of rubber. The springs and dashpots can be combined in series or in parallel, representing the Maxwell or Voigt elements (*Mainardi, 2011*). Rubber actually consists of an infinite number of such models with a wide spectrum of spring constants and viscosities.

### **Creep and fatigue failure**

In many situations (such as shock and vibration isolators and dampers, gaskets, etc.) rubber fails in service due to either creep (excessive drift) or mechanical fracture as a

result of fatigue. Creep in rubber consists of both physical creep (due to molecular chain slippage) and chemical creep (due to molecular chain breaking) (*Gent, 2001*). Physical creep rate (A) decreases in time and is usually expressed as a percentage of the original deflection per decade (factor of 10 increase) of time. Chemical creep rates (B) at a constant temperature are approximately linear with time, thus the total creep is given by

$$\text{Creep (\%)} = A \log_{10} (t / t_0) + B (t - t_0) \quad (2.1)$$

where A is physical creep rate (%), B is chemical creep rate (%), t is original deflection per decade of time, and  $t_0$  is creep decreasing in time.

Creep tests can be carried out by applying a constant load to the test specimen, and measuring its deformation as a function of time (*Hu and Olusanya, 1997*). Mechanical fractures could occur when a rubber part is subjected to a cyclic stress or strain (*Schaefer, 2009*). In a failure process, the initial crack usually originates at an area of high stress concentration and grows until complete fracture occurs. Both the time of initial crack initiation and the growth rate increase with increasing temperature and increased stress or strain amplitudes. With a gasket, the inner edge/side is under high pressure, which may cause cracks to form in that area, and then propagate into the bulk of the gasket (*Lorenz et al., 2009*). Fatigue life is determined based on three methods: stress-life, strain-life or crack growth. Stress-life method is often called S-N approach for long life situations where the strength of the material and the nominal stress control the fatigue life. Stresses remain elastic even around stress concentrations. Strain-life method sometimes referred to as the N approach is used for finite fatigue lives in ductile materials where plasticity around stress concentrations is important. Linear Elastic Fracture Mechanics (LEFM) is used to determine how long it will take for a crack to grow and reach a critical size. It is reported that, at low-energy input, the SBR compound has better fatigue resistance than the NR compound. However, when the strain and resulting input energy is increased, the NR compound has the better fatigue resistance (*Santangelo et al., 2003*). Reinforcing fillers and vulcanization systems also have definite effects on fatigue properties. Smaller particle-size carbon black typically gives increased reinforcement and improved fatigue resistance. Vulcanisation systems that produce high levels of polysulfide crosslinks are also known to give optimum fatigue resistance (*Schaefer, 2009*).

## 2.5.2 Test Method for Compressibility and Recovery of Gasket Materials.

Compressibility and recovery tests are two main tests for gaskets (*ASTM F36*). Figure 2.10 shows diagrammatic presentation of compressibility and recovery. The short duration test is performed at room temperature. The major load is applied for 60 seconds before taking the measurement for compressibility and the measurement of recovery is taken 60 seconds after removal of the major load. In the test process, specific loads are applied to preconditioned specimens depending on the material type. The load is applied over an area defined by a penetrator to a gasket stress of 5,000 psi (pounds per square inch). The average of a minimum of three samples constitutes a test. The results are calculated as follows:

$$\text{Compressibility (\%)} = [(P - M)/P] \times 100 \quad (2.2)$$

$$\text{Recovery (\%)} = [(R - M)/(P - M)] \times 100 \quad (2.3)$$

where P = Thickness under preload, M = Thickness under total load, R = Recovered thickness.

There are two different testing methods commonly used with different machine designs as described in ASTM F38, Method A and Method B.

### **Method A**

This procedure is normally run at room temperature. The test device uses a calibrated strain gauged bolt as shown in Figure 2.11(a). During a controlled application, the load is applied at a uniform rate, strain readings are taken at defined intervals of time. These readings are then converted to a percentage of initial stress and plotted on a semi-log plot with the percentage of initial stress plotted against the log of time.

### **Method B**

Method B is a more common procedure which records loss of load over time, but uses a different relax meter (see Figure 2.11(b)). As a significant advantage, method B can be performed at elevated temperatures. The sample material is first compressed and then the dial indicator is removed and the loaded specimen placed in an oven at 212 °F for 22 hours. The specimen with the device is then removed from the oven and allowed to cool to room temperature. The dial indicator assembly is

then re-attached to take a reading. The difference in this reading and the initial reading is used to calculate the percentage relaxation as follows:

$$\text{Relaxation (\%)} = [(D_0 - D_f)/D_0] \times 100 \quad (2.4)$$

where  $D_0$  = Initial dial reading,  $D_f$  = Final dial reading.

This basic test allows for a relative comparison of a gasket material's ability to maintain a compressive stress over time.

### **Compression Set**

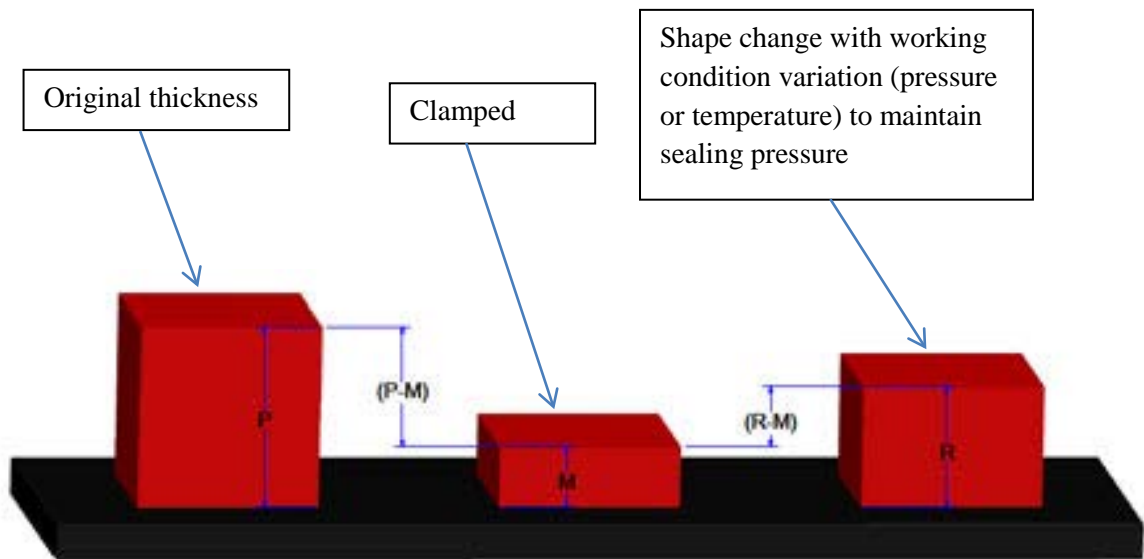
The compression set of a material is the permanent deformation remaining when a force (that was applied to it) is removed (*ASTM D395*). It is the end result of progressive stress relaxation. It means the sealing force can retain the decay when an elastomer is compressed over a period of time. Compression set is an easier way of quantifying of stress relaxation. According to ASTM D395, compression set testing for rubber should be conducted in air or liquid media. Figures 2.11 (c) and (d) illustrate the two methods, method A is a test with constant force and method B is a method applying constant deflection. In compression set test, it involves the cylindrical disk buttons taken from moulded slabs which are 0.49 inch in thick and 1.14 inch in diameter. In other forms, die-cut plied (stacked) samples can be used instead of the cylindrical disk buttons which are 0.07 inch thick and 1.14 inch in diameter. In the method A, the plates are forced together using either a calibrated spring or a pre-defined external force. In the method B, a bolt-tightened device and steel spacers are used. Normally 25 % of original thickness is compressed and then held for a given time (e.g. 22 hours) at a specific temperature (e.g. 100 °C), these two variables are determined based on prospective service conditions. After 30 minutes cooling period, the compression device is removed, and the specimens are measured by a dial micro-meter. Compression set can be calculated as a percentage of the original specimen thickness.

### **Durometer Measurements**

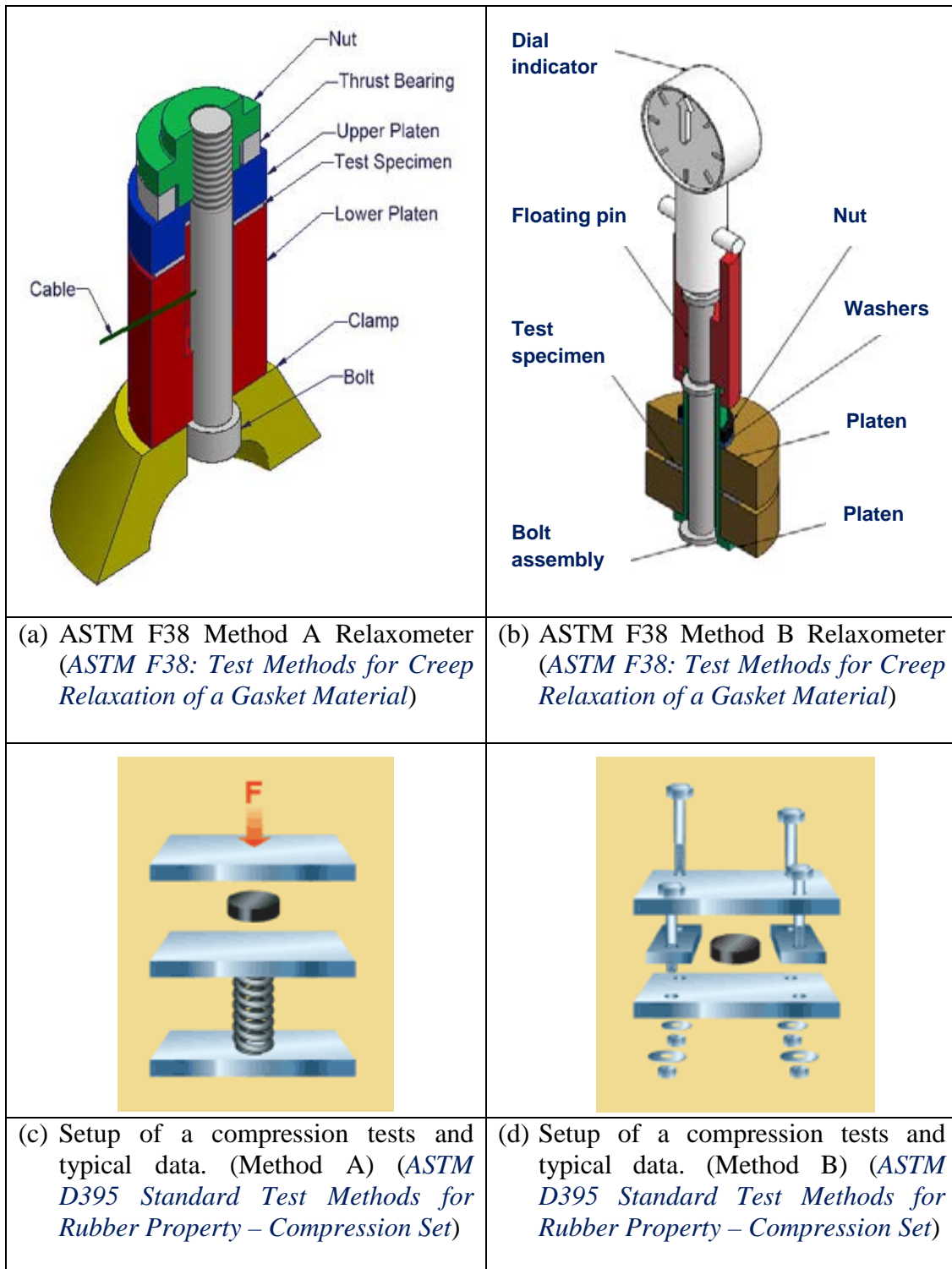
As shown in Table 2.3, for industrial application, durometer hardness is top of the property list of rubbers, reflecting its importance. As detailed in section 2.1 and 2.2, durometer measures the penetration of a metal sphere into the rubber material.

Hardness measurements in rubber are expressed in Shore A or Shore D units according to ASTM test procedures (*Sabrenal et al., 2010; ASTM D2240-05*). Because of the viscoelastic nature of rubber, a durometer reading reaches a maximum value as soon as the metal sphere reaches maximum penetration into the specimen and then decreases in the next 5 to 15 seconds. Hardness tests are routinely used in testing rubber gasket materials, in some cases, efforts have been made to correlate the hardness values to constitutive materials properties such as Young's modulus (*Alnawafleh et al., 2005*). It will provide valuable information for comparing materials, materials selection and CAE simulations gasketed structures. However, due to the complex nature of the durometer, it is difficult to link shore hardness to E values purely based on experimental works. A viable way is through combined FE modelling and experimental tests. There are many factors that need to be researched such as the suitability of the materials models, the effect of thickness, etc. This requires a detailed understanding of the mechanics of rubber and approaches to derive materials properties from nonstandard tests. Some basic theories and recent works are to be reviewed in the next two sections.





**Figure 2.10** Compressibility and recovery of gasket materials (*Hasha, 2010*) .



**Figure 2.11** Testing of rubber materials used in rubber gaskets.

## 2.6 Deformation of materials and Strain energy for nonlinear materials behaviours

### *Elastic–plastic behaviour of materials*

Figure 2.12 (a) shows a typical stress-strain curve of elastic–plastic materials (such as steel and plastics). Some gasket materials, such as PTFE (Polytetrafluoroethylene), follow such a deformation. The engineering stress and strain, denoted as  $\sigma_e$  and  $\epsilon_e$  respectively, are determined from the measured load and material deformation against the original specimen cross-sectional area  $A_0$  and length  $L_0$  :

$$\sigma_e = \frac{P}{A_0} ; \quad \epsilon_e = \frac{\delta}{L_0} \quad (2.5)$$

In the elastic portion of the curve, many materials obey Hooke's law; stress is proportional to strain with the constant of proportionality being the modulus of elasticity or Young's modulus, denoted 'E', is defined as the ratio of the stress over the strain.

$$\sigma_e = E \epsilon_e \quad (2.6)$$

The plastic behaviour is normally described by the three parameter power-hardening rule is commonly used as:

$$\sigma = \sigma_y + K \epsilon^n \quad (2.7)$$

where ' $\sigma_y$ ' represents the yield stress, ' $\epsilon$ ' represents the plastic strain, 'K' represents the strength coefficient and 'n' represents the strain hardening exponent. The Ludwig power equation is a simpler form which is used to describe isotropic elasto-plastic behaviour with isotropic work-hardening (*Swift, 1952*).

$$\sigma = K (\epsilon_0 + \epsilon)^n \quad (2.8)$$

### ***Hyperelastic material behaviour***

As shown in Figure 2.12 (b), rubber is a highly non-linear material, exhibiting different material behaviour at different strain levels/loading modes, which could not be fully represented by Young's modulus,  $E$ . Hyperelastic material models are developed/defined as a relation between the total stress and the total strain. Stresses are determined by derivatives of the strain energy function, giving the second Piola-Kirchhoff stresses (*Weiss et al., 2001*). Many strain energy function models have been developed to characterise various material systems which undergo large deformations, typically Mooney-Rivlin model, Neo-Hookean form and Ogden model (*Ogden, 1972; Petre et al., 2007*). They are generally used to describe incompressible materials (such as rubber and gel structures). These material models have been employed in several computational softwares including ABAQUS, which are briefly described below:

#### **Mooney-Rivlin model**

Mooney derived an expression for the strain energy function for rubber starting from several assumptions: (*Mooney, 1940*)

(1) The material is homogeneous and free from hysteresis; (2) The material is isotropic initially and throughout the deformation; (3) The deformations occur without a change in volume (i.e. incompressible); (4) The traction in simple shear in any isotropic plane is proportional to the shear.

The linear form of strain energy function Mooney initially proposed is:

$$W = C_{10}(\bar{I}_1 - 3) + C_{01}(\bar{I}_2 - 3) \quad (2.9)$$

where  $C_{10}$  and  $C_{01}$  are constants. It is the most general form admitting a linear relationship between stress and strain in simple shear, and has since been referred as the Mooney-Rivlin model. With suitable choices of the parameters, this equation gives a marginally better fit to some of the experimental data of rubber than pure elastic models (*Atkin and Fox, 1980*).

The strain energy  $W$  (Equation 2.9) can be split into two parts, the deviatoric and volumetric terms. Then the form of the Mooney-Rivlin strain energy density becomes (*ABAQUS Manual 6.11*).

$$U = C_{10}(\bar{I}_1 - 3) + C_{01}(\bar{I}_2 - 3) + \frac{1}{D_1}(J^{el} - 1)^2 \quad (2.10)$$

where  $U$  is the strain energy per unit of reference volume;  $C_{10}$ ,  $C_{01}$ , and  $D_1$  are temperature-dependent material parameters,  $\bar{I}_1, \bar{I}_2$  are the first and second deviatoric strain invariants defined as

$$\bar{I}_1 = \bar{\lambda}_1^2 + \bar{\lambda}_2^2 + \bar{\lambda}_3^2 \quad \text{and} \quad \bar{I}_2 = \bar{\lambda}_1^{(-2)} + \bar{\lambda}_2^{(-2)} + \bar{\lambda}_3^{(-2)} \quad (2.11)$$

$$\bar{\lambda}_i = J^{\frac{1}{3}}\lambda_i$$

where the deviator stretches  $\bar{\lambda}_i = J^{-\frac{1}{3}}\lambda_i$ ;  $J$  is total volume ratio;  $J^{el}$  is the elastic volume ratio.  $\lambda_i$  is the principal stretches. The initial shear modulus ( $\mu_0$ ) and bulk modulus ( $K_0$ ) are given by  $\lambda_i$ .

$$\mu_0 = 2(C_{10} + C_{01}) \quad (2.12)$$

$$K_0 = \frac{2}{D_1} \quad (2.13)$$

### **Neo-Hookean form model**

The form of the neo-Hookean strain energy potential is given by

$$U = C_{10}(\bar{I}_1 - 3) + \frac{1}{D_1}(J^{el} - 1)^2 \quad (2.14)$$

where  $C_{10}$  and  $D_1$  are temperature-dependent material parameters,  $\bar{I}_1$  is the first deviatoric strain invariants;  $J^{el}$  is the elastic volume ratio.

### **Ogden form models**

Another commonly used model is the Ogden model (*Ogden, 1972*). Instead of taking  $U$  as a function of  $I_1$  and  $I_2$ , the model is based on an assumption that  $U$  is a function of the principal values  $b_1, b_2, b_3$  of  $B$ .

$$U = \sum_n (\mu_n / \alpha_n) (b_1^{\alpha_n} + b_2^{\alpha_n} + b_3^{\alpha_n} - 3) \quad (2.15)$$

where  $\mu_n$  and  $\alpha_n$  are constants, and the  $\alpha_n$  is not necessarily integers and may be positive or negative.  $B$  is left Cauchy-Green strain tensor.  $b_1, b_2, b_3$  are principal values of  $B$ . The general form of the Ogden strain energy potential is

$$U = \sum_{i=1}^N \frac{2\mu_i}{\alpha_i^2} (\bar{\lambda}_1^{\alpha_i} + \bar{\lambda}_2^{\alpha_i} + \bar{\lambda}_3^{\alpha_i} - 3) + \sum_{i=1}^N \frac{1}{D_i} (J^{el} - 1)^{2i} \quad (2.16)$$

where  $\bar{\lambda}_i$  are the deviatoric principle stretches;  $\lambda_i$  are the principal stretches;  $N$  is the order of the polynomial;  $\mu_i, \alpha_i$  and  $D_i$  are temperature-dependent material parameters (*ABAQUS Manual 6.11*).

$$\mu_0 = \sum_{i=1}^N \mu_i, \quad K_0 = \frac{2}{D_1} \quad (2.17)$$

Following this form, the Mooney-Rivlin form can also be obtained from the general Ogden strain energy potential for special choices  $\mu_i, \alpha_i$ .

### **Polynomial form**

A common strain energy function used in FE-programs describing the hyperelastic material is the polynomial form as shown in Equation 2.18.

$$W = \sum_{i=0, j=0}^{\infty} C_{ij} (I_1 - 3)^i (I_2 - 3)^j \quad (2.18)$$

where  $C_{ij}$  are material parameters. The sum is normally just including a few terms and not written to infinity. As mentioned earlier, the strain energy density function has to fulfil some specific conditions. This is the reason for writing the series in terms of  $(I_1 - 3)(I_2 - 3)$ , as it gives  $W = 0$  in the un-deformed state, if  $C_{00} = 0$ .

Using index sum less than or equal to three, the equation can be written as

$$W = C_{10}(I_1 - 3) + C_{01}(I_2 - 3) + C_{20}(I_1 - 3)^2 + C_{11}(I_1 - 3)(I_2 - 3) + C_{02}(I_2 - 3)^2 + C_{30}(I_1 - 3)^3 + C_{21}(I_1 - 3)^2(I_2 - 3) + C_{12}(I_1 - 3)(I_2 - 3)^2 + C_{03}(I_2 - 3)^3 + \dots \quad (2.19)$$

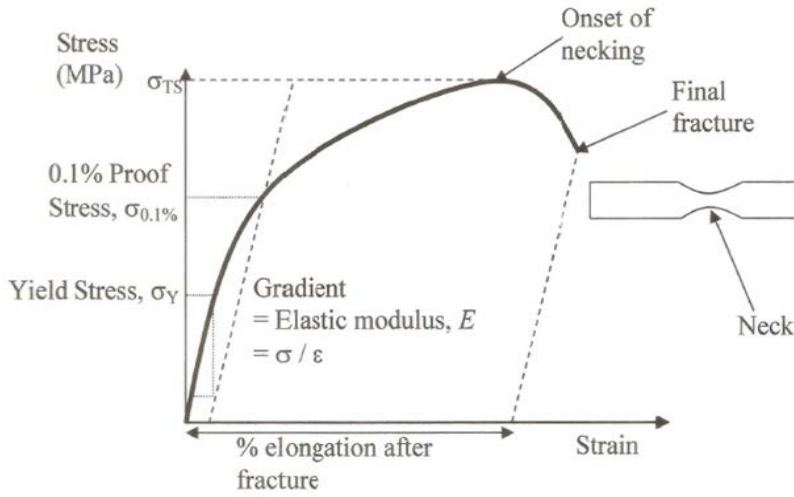
The Neo-Hooke strain energy function can be obtained from the polynomial form by only considering the first term, which yields,

$$W = C_{10}(I_1 - 3) \quad (2.20)$$

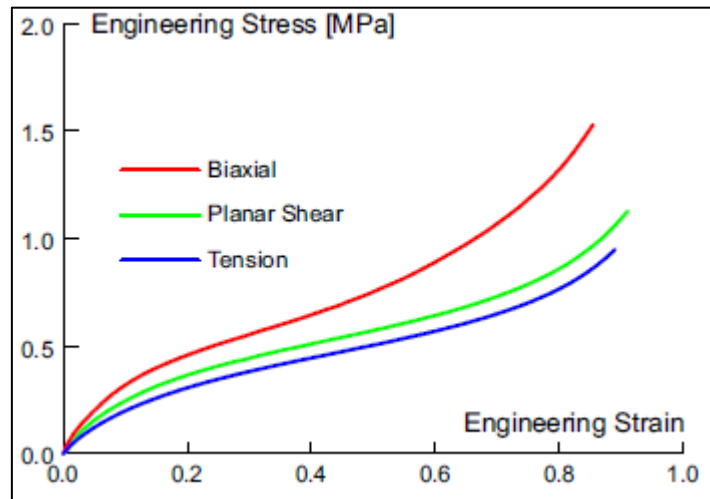
For experimental tests in compression and moderate shear, this Neo-Hooke model has shown a very good agreement. The first parameter,  $C_{10}$  is the most important parameter in the polynomial form. By excluding terms that contains the second invariant, Yeoh found a model that gives a good fit to experimental tests for carbon-black-filled rubbers. With the parameter  $I_2$  excluded, the following strain energy function was obtained called the Yeoh-model,

$$W = C_{10}(I_1 - 3) + C_{20}(I_1 - 3)^2 + C_{30}(I_1 - 3)^3 \quad (2.21)$$

The advantage of this model is that it is quite simple and the parameters can be found by only doing a shear test. But this is not possible for general choice of parameters.



(a) Typical elastic and plastic stress-strain curve (Wang, 2013)



(b) Typical one-dimensional stress strain curves of rubber materials (“White paper – Nonlinear finite element analysis of elastomers”, MSC Software Corporation.)

**Figure 2.12** Different stress strain curves for elastic-plastic materials (metal and plastics) and hyperelastic materials behaviours.



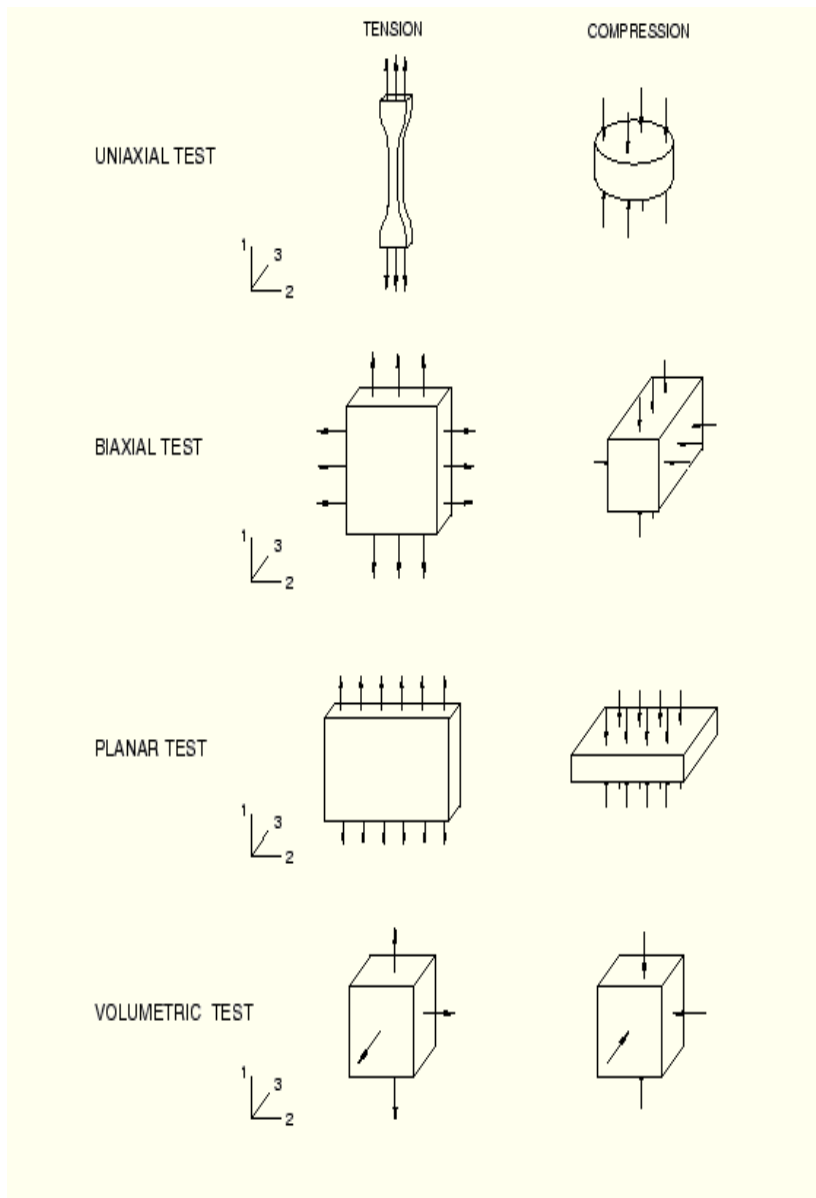
## 2.7 Combined numerical and experimental methods and its applications in material properties prediction

Material testing and parameter identification is very important for materials selection, manufacturing control, and new materials development. Increasingly, computer aided engineering is being used in gasket design as a major improvement from the empirical tradition based method (such as simple Y number (Gasket seating stress)) (Kelly, 2007). A successful CAE program requires detailed constitutive material parameters rather than indentation/hardness data. For metal materials, prediction of the key properties such as E values and yield stress, work hardening coefficients is relatively straightforward, through standard (e.g. tensile or compression) or nonstandard tests (e.g. Vickers hardness). But for rubber related materials with hyperelastic properties, it is much more difficult as most of the strain energy models have more than two parameters. In addition, the choice of linear elastic or hyperelastic is also much more difficult as the selection of modelling approach has to be based on the loading condition and the accuracy requirements. The determination of material parameters is based on the use of test samples with a standardised geometry and strain state as shown in Figure 2.13. The final parameters are determined through curve fitting data from different types of tests on the same material. These methods require testing of a combination of samples with standard shaped samples, which can be time consuming. In some cases, assembly of the sample can be very difficult (e.g. shear tests). Many efforts have been made to inverse predict material parameter from nonstandard tests such as indentation tests (Li et al., 2008; Ren et al., 2009). In material testing and characterisation, the most common inverse method is the combined experimental and numerical method. The method can be used in direct analysis or inverse analysis as shown in Figure 2.14. In a direct method, an FE model is developed and validated, then used to establish the link between material properties (e.g. E, hardness) or material behaviours (e.g. energy absorption, plastic work etc.) (Dao et al., 2001). In an inverse analysis, the material properties are estimated from material testing or deformation behaviours. In an inverse analysis, the properties can be predicted/estimated from experimental data. Dao et al., (2001) has used dimensionless functions and a forward and reverse analysis scheme based on extensive finite-element simulations. The frame of the direct and inverse process is shown in Figure 2.15 (a) and (b). Using dimensional analysis, a new set of dimensionless functions was constructed to characterise instrumented sharp indentation. From these functions and elasto-plastic finite

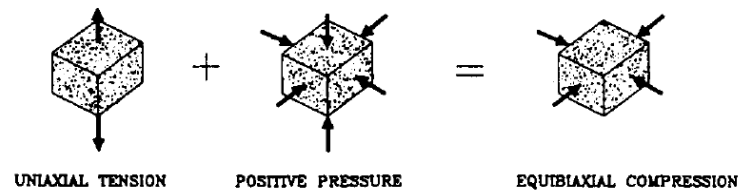
element computations, analytical expressions were derived to relate indentation data to elasto-plastic properties. As shown in Figure 2.15 (a), the forward algorithms allow the calculation of the indentation response for a given set of elasto-plastic properties, whereas the reverse algorithms enable the extraction of elasto-plastic properties from a given set of indentation data Figure 2.15 (b). Comprehensive sensitivity analyses were carried out for both forward and reverse algorithms, and the computational results showed good agreement with experimental data for two aluminium alloys 6061-T6511 and 7075-T651 aluminium. A representative plastic strain was identified as a strain level which allows for the construction of a dimensionless description of indentation loading response, independent of strain hardening exponent  $n$ . The proposed reverse analysis provides a unique solution of the reduced modulus  $E^*$ , a representative stress  $\sigma_r$ , and the hardness  $H$ . With this information, values of  $\sigma_y$  and  $n$  can be determined for the majority of cases considered in the work, provided that the assumption of power law hardening adequately represents the full uniaxial stress–strain response. A major drawback for the approach lies in the poor sensitivity to variation of testing parameters. The predicted plastic properties are very strongly influenced by even small variations in the parameters extracted from instrumented indentation experiments (*Dao et al., 2001*).

Figure 2.16 shows a typical inverse modelling approach using an interactive method (*Meuwissen et al., 1998*). This process involves interactively changing the material parameters in the FE models until the predicted result or results match the experimental results. In this approach, optimisation algorithm could be coupled with the finite element method in order to find the optimal values for a set of target material parameters. A user defined objective function serves to measure the optimality of the parameters. Finally, an optimal fit of the simulated data to the experimental is reached. This approach has been used for different materials including metals, polymeric foam and bio-materials (*Kauer 2001; Bolzon et al., 2004; Gérard et al., 2005; Hendriks et al., 2006; Ren et al., 2006*). As shown in Figure 2.16 the FE modelling is repeated with changing material parameters until an optimum combination of material properties is found. This approach required re-running the FE models during the optimisation process, which can take a large amount of time to reach the optimal solution with increased the computational cost.

Kauer (2001) applied this method with suction tests to determine the linear material parameter of the human skin. In this work, the experimental data is the pressure displacement data. The parameters in FE models of the suction test were varied until a close match between the experimental results and numerical was reached. Gerard et al (2005) employed similar iterative optimal method with indentation experiments characterizing the mechanical behaviour of the human tongue. To determine the constitutive law from this indentation experiment, i.e. the global relationship that can be assumed between strain and stress inside the body, an optimization algorithm based on an “analysis by synthesis” strategy was elaborated. It consists of (1) assuming a given constitutive law, (2) building a finite element analysis (FEA) of the indentation experiment, (3) comparing the simulations provided by this FEA with the indentation measurements, (4) using this comparison to propose a change of the constitutive law that should bring the FEA simulations and the measurements closer, and (5) starting again with (2) up to the point where the comparison carried out in (3) gives satisfactory results (*Gérard et al., 2005*). Ren et al (2006) used a parametric approach to determine Young’s modulus of silicone rubber from *in vivo* surface testing. The approach is shown in Figure 2.17, which involved a two-staged approach using rough range data first and then refining the material. This method could effectively reduce the amount of computational work required but the approach has to be based on a good pre-knowledge of the materials.



(a) Deformation modes of various experimental tests for defining material parameters (*ABAQUS User Manual 6.11*).



(a)

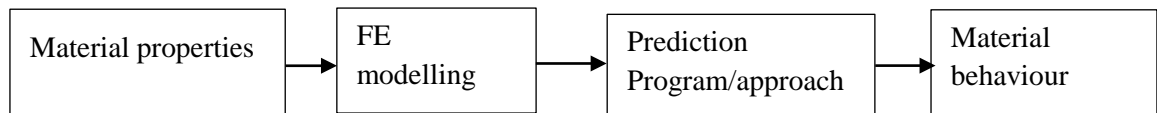


(b)

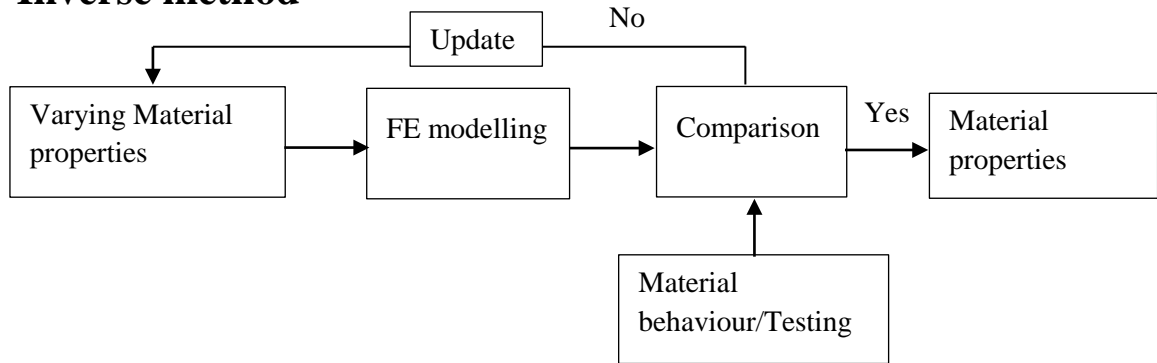
(b) Equivalence of stress states shown by superposition of hydrostatic pressure  
*(Charlton, 1993)*

**Figure 2.13** Different stress strain conditions and equivalent stress state by combining different testing modes.

### Direct method

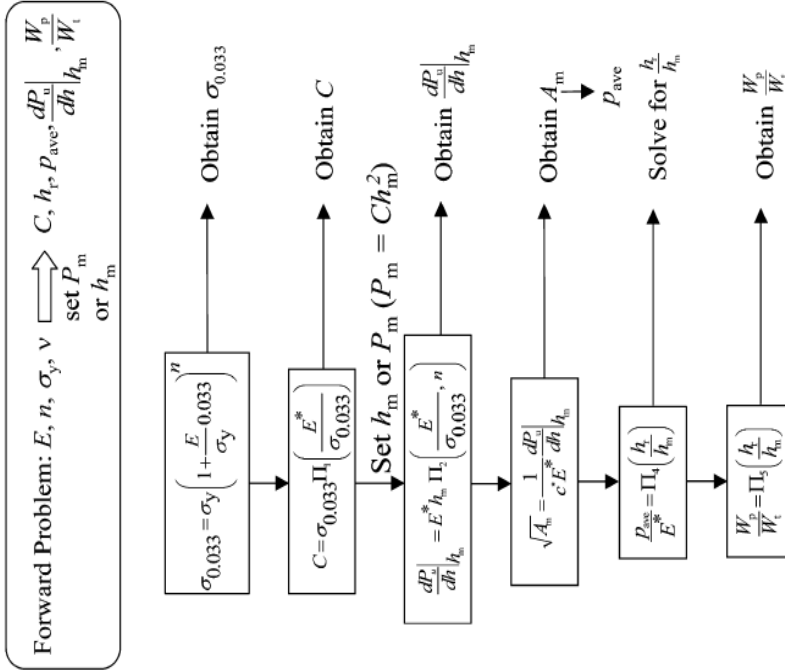


### Inverse method



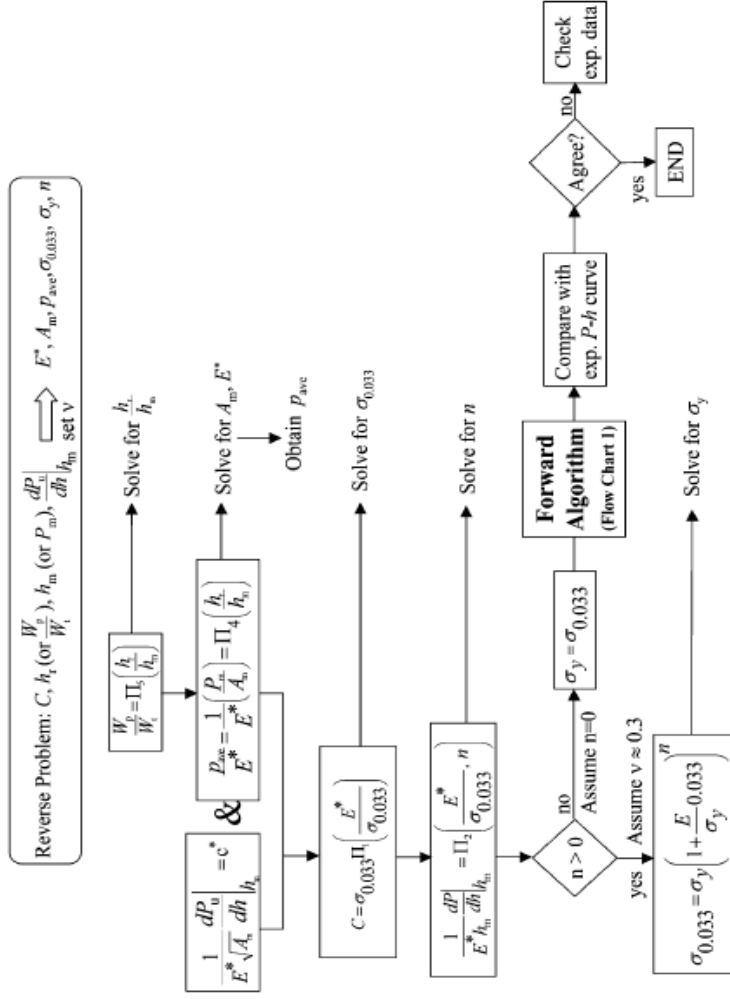
**Figure 2.14** Combined experimental and numerical method to estimate material properties or predict material behaviour.

Flow Chart 1: Forward analysis algorithms



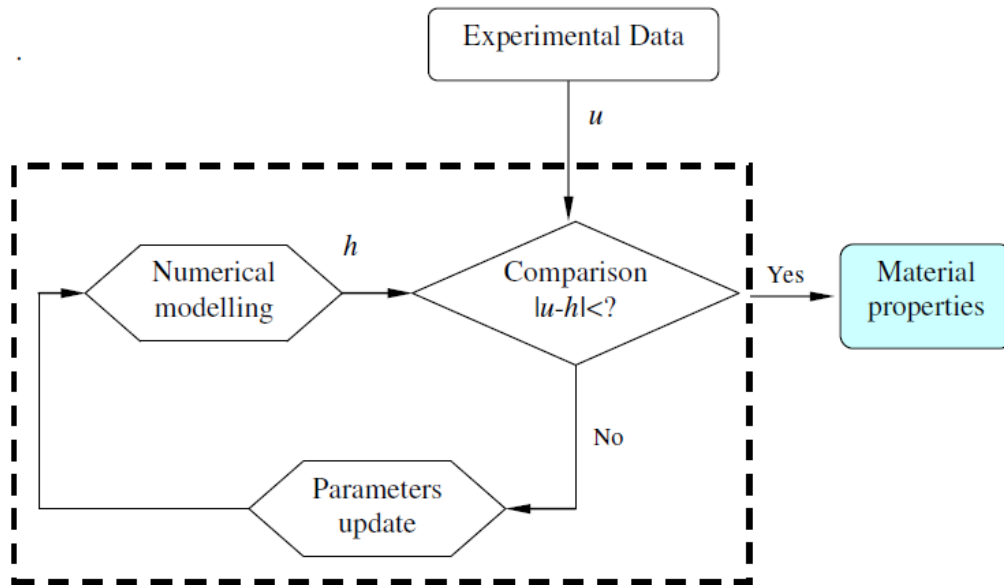
(a) Forward process

Flow Chart 2: Reverse analysis algorithms



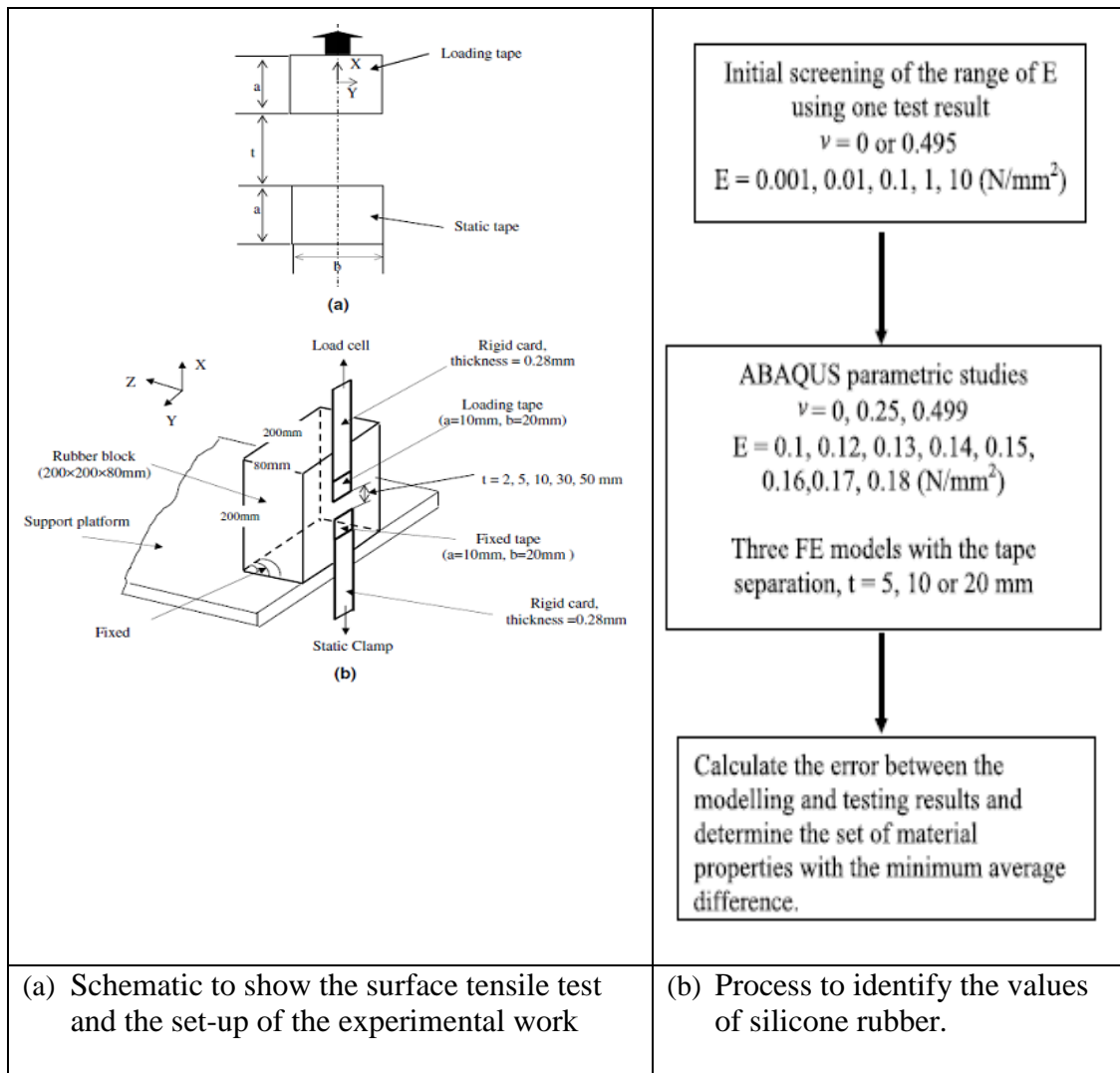
(b) Reverse process

Figure 2.15 Flow chart showing typical procedures in forward (a) and reverse (b) method (Dao et al., 2001).



**Figure 2.16** Block diagram of the mixed numerical-experimental method ( $u$  denotes the observation of experiments.  $h$  the output of the numerical/finite-element modelling (Meuwissen *et al.*, 1998).





**Figure 2.17** Use of parametric studies in inverse materials properties identification of rubber block based on surface tension tests (*Ren et al., 2006*).

## 2.8 Artificial Neural Network (ANN)

Artificial neural network (ANN) is a system that can process input information to its interconnected neurons and learn from trial and error. Feed forward ANNs are one type of ANN that consists of input layer, hidden layers and output layer. In application, the complexity of the underlying problem determines the number of hidden layers and neurons. In order to use ANN for prediction purposes, firstly, the neural network should be trained by processing input datasets and then, following a proper training algorithm, a fully trained neural network model could provide a rather accurate output when new input data is presented to it. Each ANN consists of three main components, namely, learning law, network architecture and activation function. The form of these components depends on the type of underlying problems (*Ali et al., 2010*). There are some main advantages of ANN method. Firstly, a major advantage of the use of neural networks for data modelling is that they are able to fit complex nonlinear models and these models do not have to be specified in advance. Secondly, it is possible to train a neural network to perform a particular function by adjusting the values of connections (weights) between elements. Thirdly, neural networks are composed of elements operating in parallel, which allows increased speed of calculation compared to slower sequential processing. Fourthly, neural networks have the ability to detect all possible interactions between predictor variables: the hidden layer of a neural network gives it the power to detect interactions or interrelationships between all of the input variables. There are also some disadvantages of ANN method limiting its applications. ANN operates as black boxes. The rules of operation in neural networks are completely unknown.

The performance of an ANN depends on many issues and factors. Some key factors commonly evaluated in ANNs for engineering problem included choice of number of neurons, choice of the activation function, over fitting, early stopping, partition of the data, etc. (*Su, 2014*). The number of neurons directly influences the performance and the demand on computing resources of an ANN system. The rule for proper selection of neuron number is that the number of neurons should be sufficient in producing results of acceptable accuracy in the meantime avoid over fitting. If the network is over trained, even though the accuracy of the training may increase but the overall accuracy of the ANN will decrease in particular for predicting untrained data. If the complexity of the network is too high for the problem being considered (e.g.

unnecessarily using too many neurons), the ANN system will learn all the details of the training patterns, potentially including the noise, which doesn't reflect the nature of the material or system. With an over-trained system, the ANN will try to match/find output values from the trained data rather than trying to interpolate to a new output values. An effective way to avoid over training is to determine the optimum number of neurons (normally through trials) and partition of the data (*Meng and Lin, 2008*).

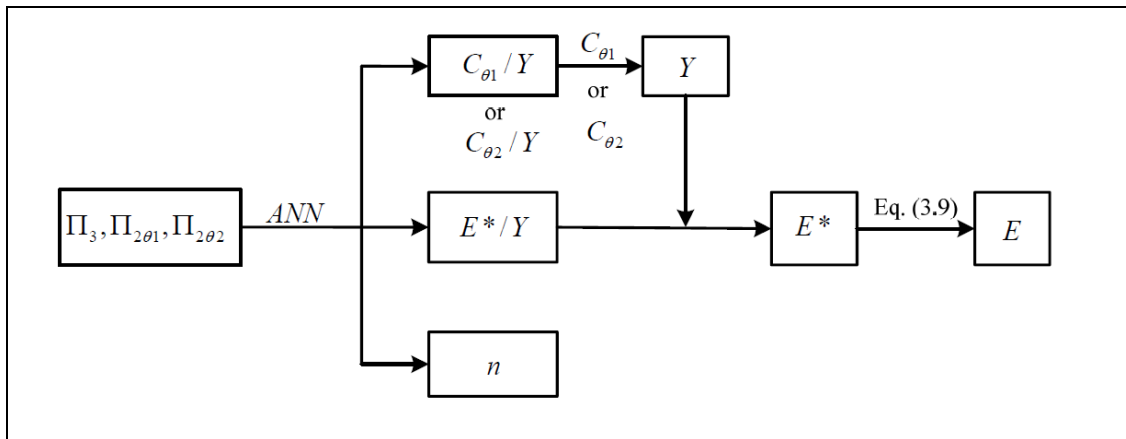
So far many researchers used ANN techniques to solve complex nonlinear relationships associated with indentation testing. A combined mechanical property evaluation methodology with automated ball indentation (ABI) simulation and ANN analysis is evolved to evaluate the mechanical properties for Carbon Manganese Steel (SA-333 Grade-6) and Stainless Steel (SS-304LN) (*Sharma et al., 2011*). Sinha (2013) used ANN techniques and genetic algorithm to research optimization of mechanical property and shape recovery behaviour of Ti (~49 at.%) Ni alloy. An ANN model was used in prediction of abrasion of rubber composites, which was composed of abrasion and six mechanical properties (shore A hardness, stress at 100%, stress at 300%, tensile strength, elongation at break and tear strength) of styrene-butadiene (SBR) based rubber (*Wang et al., 2013*). Yas (2014) employed neural networks and imperialist competitive algorithm to optimise the volume fraction of three-parameter functionally graded beams.

The use of ANN in materials property estimation could be a complex process, in many cases, the program or structure of ANN has to be designed to suit the problem, which could be deciding what input to use or what will be used as output if the physical parameters/properties could not directly be used. Some specific data process has to be implemented. For example, the main measurement result in indentation is force-indentation depth curves, but the parameter describing P-h curves is not necessary linked mathematically to the property parameters. Harsono (2009) used a single neural network approach (Figure 2.18(a)) to study the prediction of yield stress and work hardening coefficients based on a single indenter approach, while the input is the surface ratio between work done and total energy ( $W_R/W_t$ ) and the ratio of the curvature ratio of two different indenter angles ( $C_1/C_2$ ). The comparison between the

ANN predictions is listed in Table 2.4 in comparison with the target value. The yield strength shows a good agreement but the work hardening coefficients showed a very high deviation. This shows that ANN can be used to predict the materials properties but could not necessarily achieve a high accuracy for all the material parameters. This does not imply that program is not useful but to highlight the fact that when developing ANN, the goal should be to try to achieve the best rather than purely to produce accurate number on limited cases. Recently, Budiarsa (2013) has applied a similar surface fitting approach to predict the P-h curves of elastic and plastic properties and used it to predict the Rockwell hardness values with known properties. In another recent work, Su (2014) used ANN method to predict the nonlinear hyperelastic properties of EVA (Ethylene-vinyl acetate) foam. As shown in Figure 2.18(b), in the work, the input is the P-h curves of EVA foams; the outcome is nonlinear parameters of hyperfoam models. In both cases, the work has used full P-h curves. It is of interest to explore the feasibility of using such an approach to predict the shore hardness or material properties.

**Table 2.4** Comparison of the predicted material properties obtained from ANNs algorithm with inputs for various combinations of three-sided pyramidal indenter tips (Harsono, 2009).

	Al6061	Al7075
$E^*$ [GPa]		
Actual	70.2	73.4
ANN	56.5	75.7
[% deviation]	[-19.52]	[+3.13]
Oliver and Pharr Method (1992)	85.0	86.2
[% deviation]	[+21.1]	[+17.4]
$Y$ [MPa]		
Actual	284.0	500.0
ANN	283	498
[% deviation]	[-0.35]	[-0.40]
$n$		
Actual	0.080	0.122
ANN	0.0957	0.0944
[% deviation]	[+19.63]	[-22.62]



(a) Flow chart of proposed ANN based on a single ANN model.

$$\left. \frac{C}{Y} \right|_{\theta_1} = \Pi_{1\theta_1} \left( \frac{E^*}{Y}, n \right)$$

$$\left. \frac{C}{Y} \right|_{\theta_2} = \Pi_{1\theta_2} \left( \frac{E^*}{Y}, n \right)$$

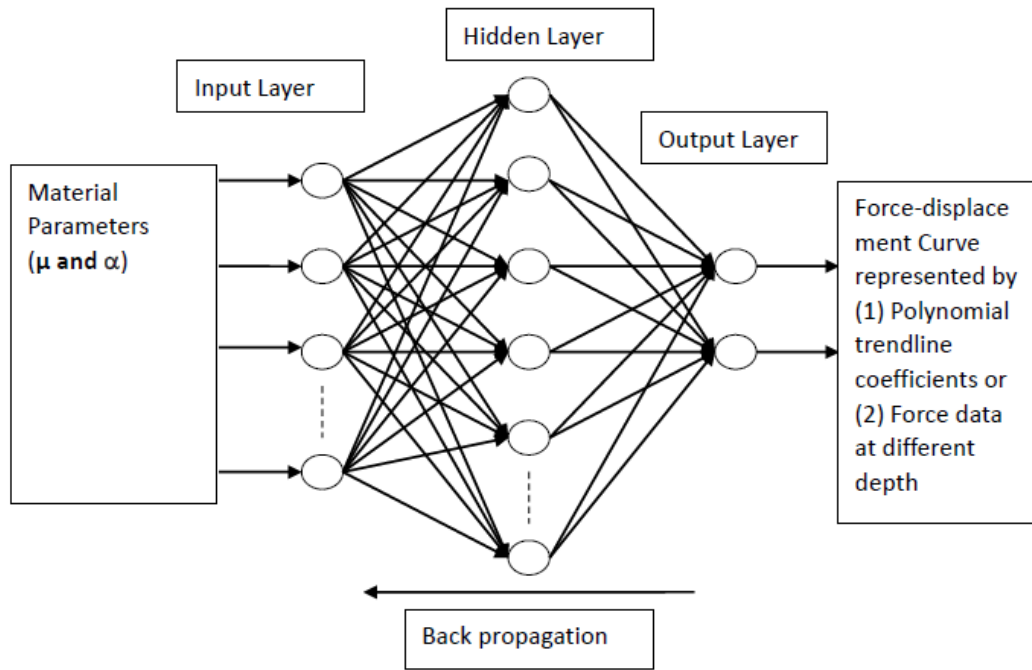
$$\left. \frac{W_R}{W_T} \right|_{\theta_1} = \Pi_{2\theta_1} \left( \frac{E^*}{Y}, n \right)$$

$$\left. \frac{W_R}{W_T} \right|_{\theta_2} = \Pi_{2\theta_2} \left( \frac{E^*}{Y}, n \right)$$

$$\frac{C_{\theta_1}}{C_{\theta_2}} = \frac{\Pi_{1\theta_1}}{\Pi_{1\theta_2}} = \Pi_3$$

(b) Surface function ( $\Pi$ ) used in the ANN inverse program.

**Figure 2.18** (a) A single ANN system used in predicting plastic properties based on conical indentation (a) and the equations (b) (Harsono, 2009).



**Figure 2.18 (b)** Feed-forward neural network with back propagation algorithm for predicting the indentation force-displacement data based on material parameters ( $\mu$  and  $\alpha$ ) (Su, 2014).

**CHAPTER THREE**  
**RESEARCH PLAN AND**  
**EXPERIMENTS**

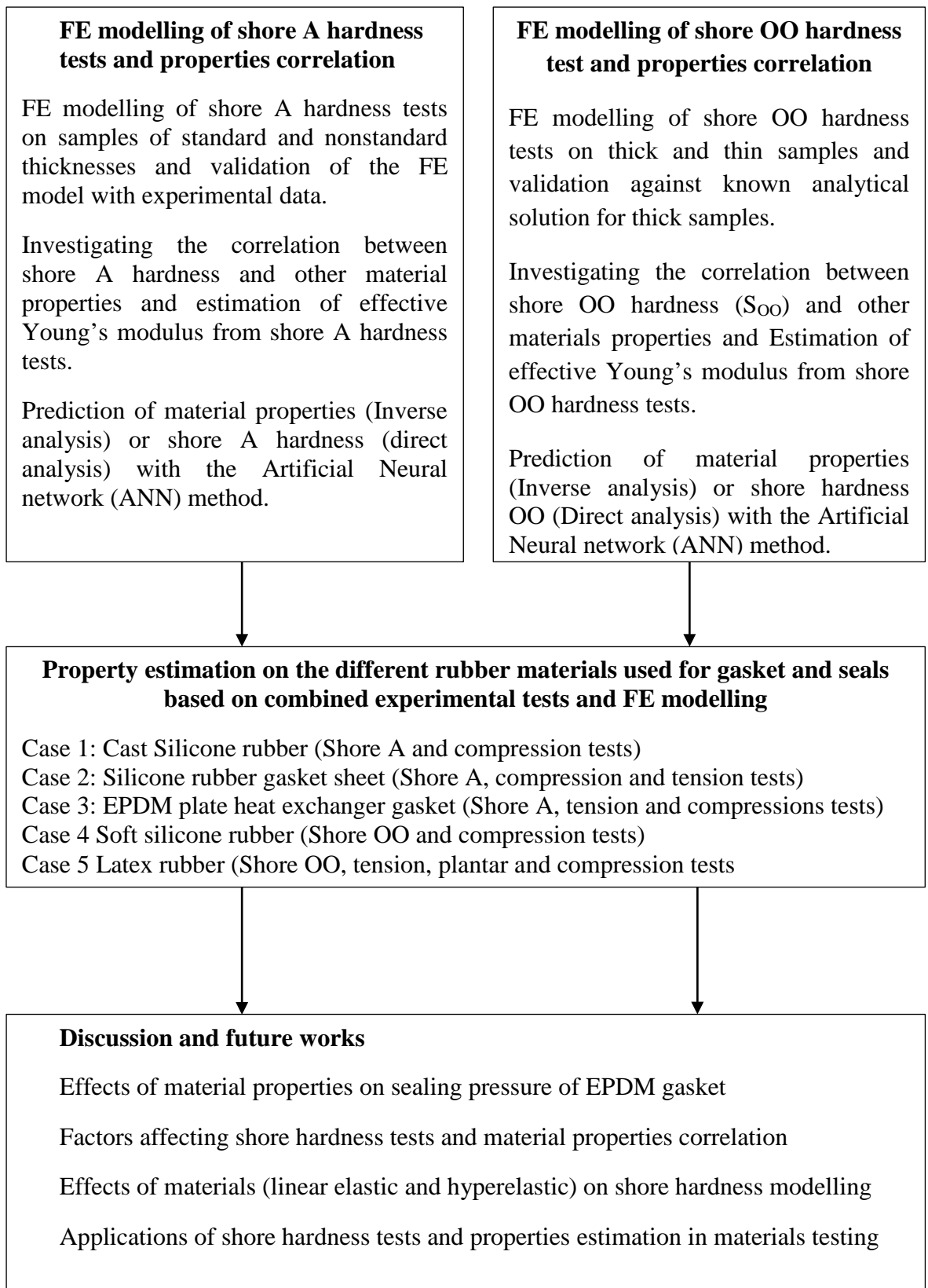


### **3.1 Introduction**

Figure 3.1 is a flow chart showing the main modelling and testing work of this project. In the first two parts, FE models of shore A and shore OO hardness are developed and used to establish the relationship between hardness and Young's modulus ( $E$ ) for samples with standard and nonstandard thicknesses over different hardness ranges. Shore A hardness is mainly for relatively hard rubbers and shore OO hardness is for relatively soft materials. The numerical models developed are then used to produce comprehensive data to assess the feasibility of using ANN to predict the  $E$  values from hardness in inverse analysis or predict hardness from known material properties. In the next part, the FE model and the hardness-properties chart for sample of different thicknesses are combined with experimental tests to estimate the Young's modulus of several gasket rubber materials (five cases). The predicted properties are used to simulate different type of mechanical tests of the corresponding samples. This work on several different rubber materials in different forms is mainly to assess the level of accuracy and limitation of the material property identification approach based on shore hardness tests. In the discussion section, the effects of material properties on the sealing performance of a gasket are illustrated using an EPDM gasket for a plate heat exchanger as an example. The main factors affecting shore hardness simulation and application is discussed supported by additional testing and FE modelling data. In combined experimental and numerical work, a range of tests have been used and corresponding FE models are developed, some of which are summarised in Table 3.1. Further details of the key testing facilities and materials are to be presented in the next few sections.

**Table 3.1** List of main tests and materials.

<b>Main tests</b>	
i. Shore A hardness test ii. Shore OO hardness test iii. Uniaxial tensile test iv. Planar test v. Uniaxial compression test vi. Indentation bending test	
<b>Main Materials</b>	<b>Tests and FE models</b>
Hard silicone rubber of different thicknesses (Made in the lab)	Shore A hardness test, Compression test
Thin silicone rubber gasket sheet (1.5mm)	Shore A hardness test, Compression test, Tensile test
EPDM gasket of complex cross-section for plate heat exchanger	Shore A hardness test, Compression test, Tensile test
Soft silicone rubber of different thicknesses (Made in the lab)	Shore OO hardness test, Compression test
Latex rubber sheet of different thicknesses (Made in the lab)	Shore OO hardness test, Tensile test, Planar test
Other Materials associated with the work: PTFE envelope gasket	Tests and FE model: Tensile test, indentation bending tests



**Figure 3.1** Flow chart to show the main research work in FE modelling and testing.

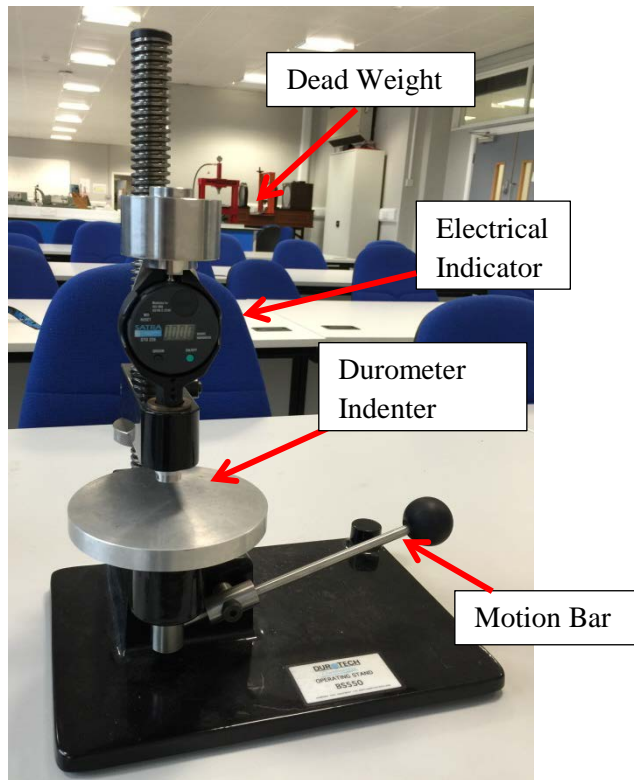
## **3.2 Testing facilities**

### **Shore Hardness Tester**

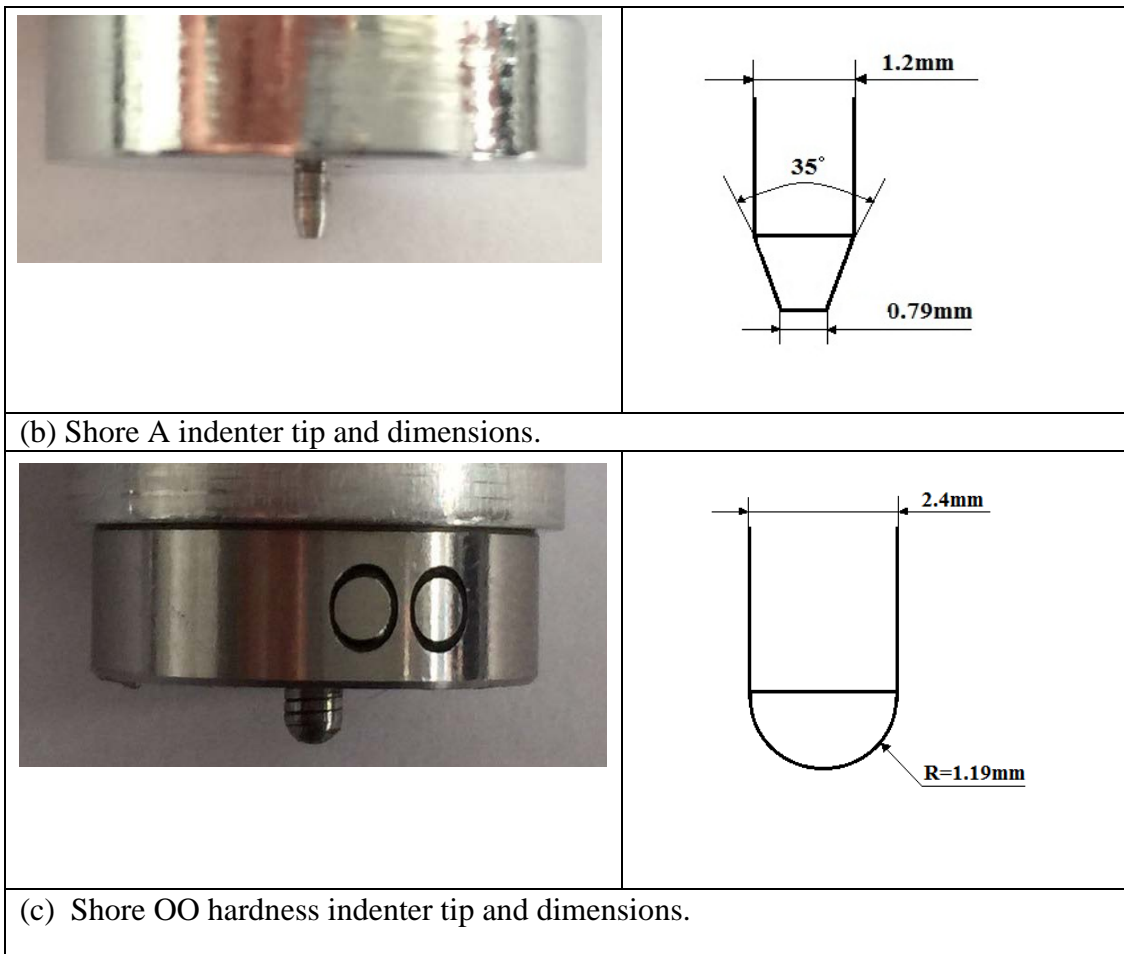
Figure 3.2 shows the Durometer shore hardness test machine (Hampden Test Equipment Ltd.). A DUROTECH Operating Standard BS550 was used to measure the shore A and shore OO hardness of the sample by monitoring either the hardness values or the spring deflection from the electrical indicator. The indenter and the dimensions of the shore A and shore OO hardness tester are shown in Figure 3.2 (b) & (c), respectively. During a measurement, a dead weight is used on the top of the Durometer indenter, 1 kg for shore A hardness and 400 g for shore OO hardness for balancing the contact. The main indentation load is controlled by the spring. In the hardness tests, each sample of the rubber materials was tested by at least six times, the final result was calculated by the average values of the tests. For some samples, cross examination by different operators were also conducted to ensure the consistency of the data. In addition, in the early stage of the project, the test data of the main machine used was crossed compared with another handheld shore hardness tester, and results showed a good agreement.

### **Tensile and compression testing machine**

Figure 3.3 shows the uniaxial tensile and compression test machine. The uniaxial tensile and compression tests and planar tests were performed on this test machine (model: Tinius Olsen, H50KS). Different load cells have been used when performing different tests on different materials. The displacements and the reaction forces were recorded. The machine is also equipped with a laser extensometer and environmental chamber. Specific rigs are available in different types of compression and indentation bending tests.



(a) Durometer shore hardness indentation test machine



**Figure 3.2** Durometer shore hardness indentation test machine (a) and the indenters (shore A (b) and shore OO (c)).



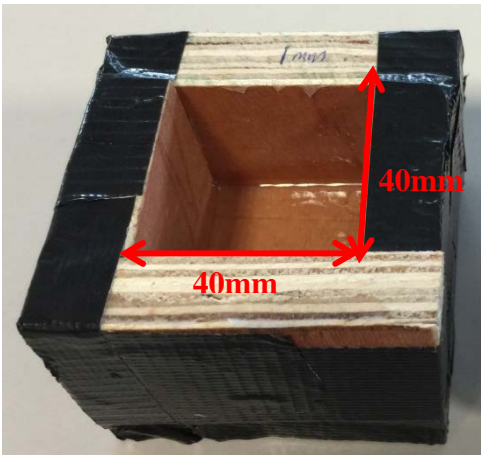


**Figure 3.3** Tensile and compression tests machine.

### 3.3 Materials

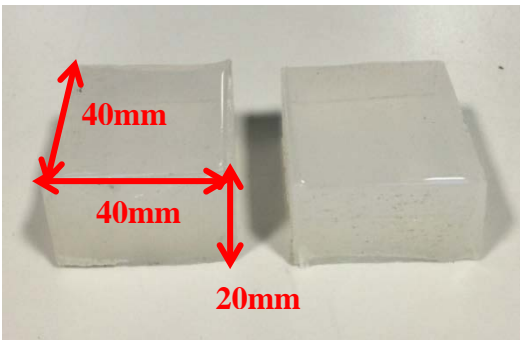
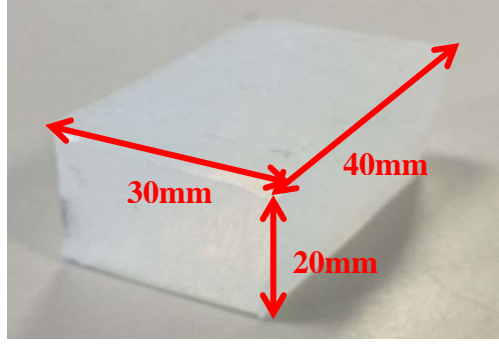
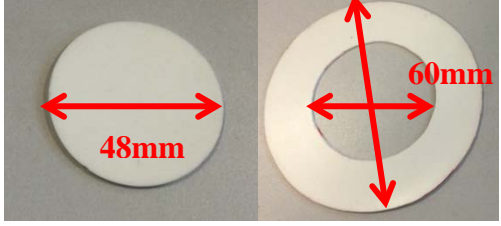

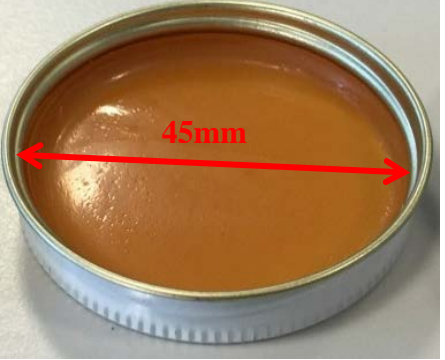
Figure 3.4 shows the equipment used to cast silicone rubber samples including a vacuum casting machine and oven used for curing and the mould. The vacuum casting machine was used for de-gassing to remove the air from the mixture of the silicone solvent and the curing agent. The oven was for the curing process at a temperature of 40°C. Both pieces of equipment were manufactured by MCP Group Ltd. (UK). A wood mould is used to cast silicone rubber samples of different thicknesses after mixing and degassing.

Figure 3.5 shows the materials used in this work. Figure 3.5 (a) is a silicone rubber sample cast in the laboratory using the facilities shown in Figure 3.4 for shore A test. Samples of different thicknesses (1-20mm) have been made. Figure 3.5 (b) shows round and ring samples cut from the same batch of thin silicone rubber gasket sheets (200mm×200mm×1.5mm) purchased from Fast Gaskets & Parts Limited. Both types of samples were used in shore A and compression tests. Tensile tests were also conducted on the sample. The sample has also been used in assessing the effect of lubricant on the hardness tests results. Figure 3.5 (c) shows an EPDM gasket embedded in a corrugated stainless steel heat exchanger plate. The gasket has an irregular cross section shape which offers a good case to evaluate the use of shore hardness in characterising gaskets in practical situations. A range of tests were performed on the material including shore A, tension/compression under different supporting/fixing conditions. Figure 3.5 (d) is another silicone rubber cast in the lab used for assessing shore OO hardness tests. It is much softer by using a different ratio of resin and hardeners from the hard silicone rubber used for shore A (Figure 3.5(a)). Compression test was conducted on this soft silicone rubber to assess the property estimation from shore OO hardness. Figure 3.5 (e) is a latex rubber sheet in the sample holder. Samples of different thickness (1-3mm) have been used. Data from a range of tests have been used to characterise the materials including shore OO, tensile, planar and shear test. No thick sample has been made for latex rubber due to the difficulties in the casting process associated with extensive shrinking and porosity of thick samples.

 <p>A vertical white machine with a blue door. The door has a window showing a white cup inside. Above the door, the text "5/01 VACUUM CASTING SYSTEM" is visible. To the right of the door are several control buttons and a gauge.</p>	 <p>A white rectangular oven with a black handle on the left side. At the bottom front, there is a red control panel with a power switch, a white dial, and a red dial.</p>
<p>(a) Vacuum casting machine.</p>	<p>(b) Heating/curing oven.</p>
 <p>A rectangular wooden mould with black tape on the sides. Red arrows indicate the dimensions: 40mm in width and 40mm in height. The word "1cm" is written on the top edge.</p>	
<p>(c) Wood mould for cast silicone rubber samples.</p>	

**Figure 3.4** Equipment and tools used in Silicone rubber casting and curing.



	
<p>(a) Cast silicone rubber (hard for shore A tests).</p>	<p>(b) Cast silicone rubber (Soft for shore OO tests)</p>
	
<p>(c) Gasket silicone rubber sheet (for shore A tests)</p>	<p>(d) EPDM heat exchanger gasket (for shore A tests)</p>
	
<p>(e) Latex rubber (Soft for shore OO tests).</p>	

**Figure 3.5** Different types of rubber samples used in the work.

### **3.4 FE modelling program**

The FE modelling is performed using ABAQUS (version 6.11) with subroutine functions. Main numerical works include modelling of shore A and shore OO hardness tests as well as compression and tensile tests. When simulating shore hardness tests on softer materials with a lower Young's Modulus, a re-meshing program is developed to cope with the excessive element distortion. The process involves firstly developing an FE model in ABAQUS CAE to generate a replay file (.rpy file). The RPY file is coded in Python (a general purpose, high level programming and scripting language available for various platforms). The ABAQUS .rpy file records the operational procedures and key input parameters, which could then be modified (e.g. dimensions or material properties) and re-run the model (ABAQUS Scripting User's Manual). In the re-meshing program for shore hardness FE model, "Part2DGeomFrom2DMesh" operation is used to build a new geometry from a deformed model by controlling the feature angles. The ABAQUS "map solution" function is used to transfer key state variables, such as stresses and strain, into the new model. Details of the operation could be found in ABAQUS Users Analysis Manual (V6.11). This is an effective approach for two dimensional models as in the case for shore hardness FE model (axial symmetric model).

**CHAPTER FOUR**  
**FE MODELLING, RESULTS AND**  
**ANALYSIS**

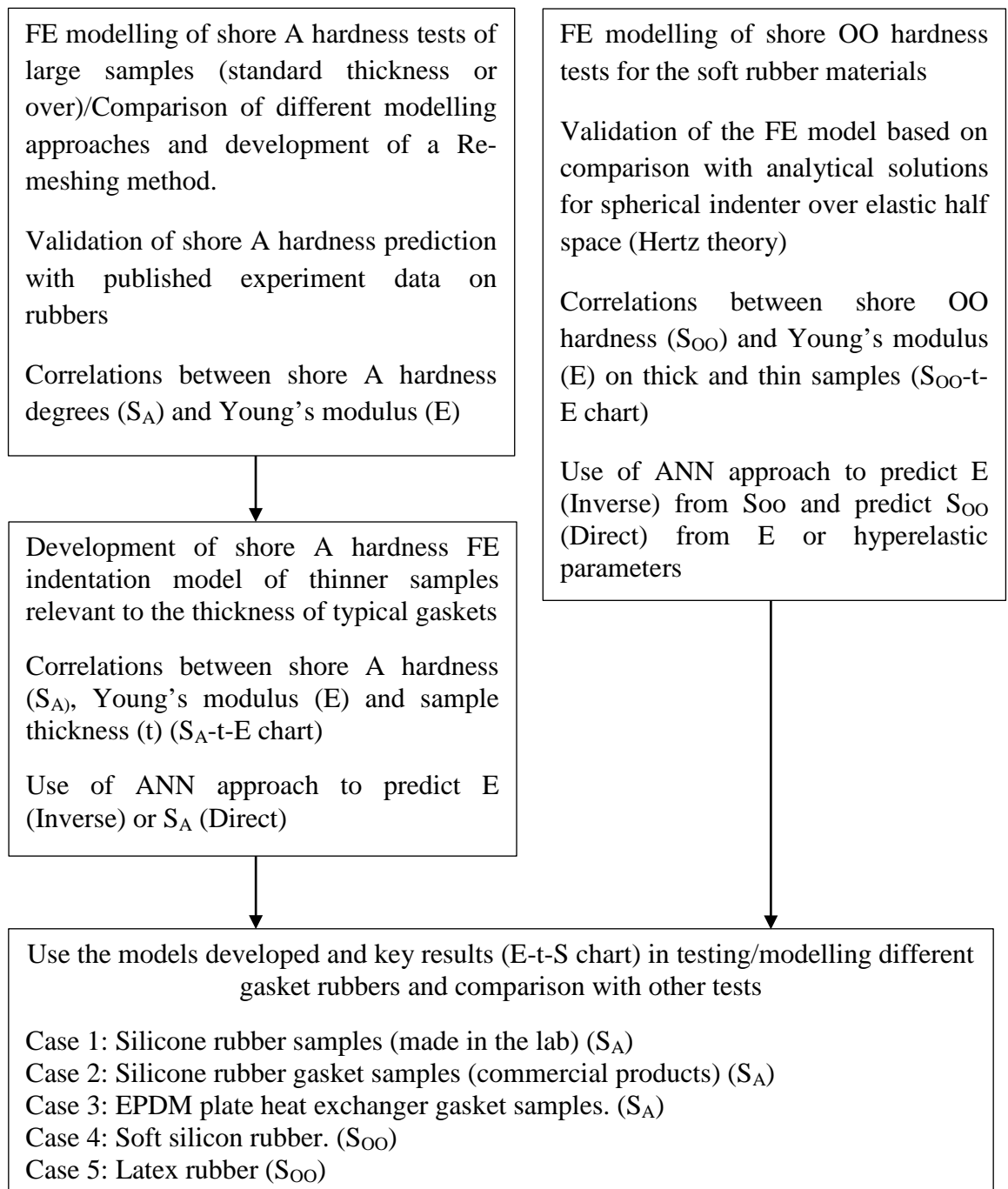
## 4.1 Introduction

Figure 4.1 is a flow chart showing the main research works including the development of FE modelling programs for shore A and shore OO hardness tests, evaluation, use of the FE model in establishing the hardness-property relationships for samples with standard and nonstandard thickness and their applications in characterising the properties of typical gasket materials. The data is also used in developing an ANN program to inversely predict the E values from shore A and shore OO hardnesses (designated as  $S_A$  and  $S_{OO}$ ), or directly estimate  $S_A$  or  $S_{OO}$  for situations where the material properties are known.

One major part of the work is the development of FE modelling of shore A hardness test and correlation between  $S_A$  and E values for samples of standard thickness and thinner samples for relatively hard rubber materials. As listed in the figure, firstly, an FE indentation model of shore A hardness test is developed and the FE results are evaluated by comparing the results with published experimental test data on rubber materials. Different modelling approaches have been systematically assessed including the standard and explicit analysis, and a re-meshing method. The suitability of each approach is assessed based on whether or not the approach is able to produce consistent modelling results over a wide range of elastic modulus, thickness and different level of element deformation as the shore A hardness is force controlled. The FE model is validated against the published data on rubber materials, and the validated model is used to establish the correlation between shore A hardness ( $S_A$ ) and the Young's modulus (E) for standard thickness ( $t=6$ ) and thinner samples. In the studies, the thickness used is relevant to the typical gasket/seals.

Another part of the work is focused on the modelling of shore OO hardness test with a spherical indenter for relatively softer materials, as shore A hardness is not suitable for softer rubber. In the work, a FE model of shore OO hardness is firstly developed and validated against a known analytical solution for a thick sample (Elastic half space). Using the validated FE model, the correlation between the shore OO hardness and the Young's modulus for samples of different thicknesses is determined. In another part, the use of ANN material property estimation and shore hardness

prediction is also explored for both shore A and shore OO hardness. In the direct program, the program is used to predict shore hardness based on known material properties and thickness. In the inverse modelling approach, the material property is estimated from known shore hardness values and sample thickness using the ANN method. As shown in the figure, the program developed and the key results are used to characterise some typical gasket materials of different types, thickness and structures. Case 1 used silicone rubber samples made in the laboratory. Case 2 is a thin silicone rubber gasket commonly used for pipelines. Case 3 is EPDM gasket samples for a plate heat exchanger. Case 4 is a soft silicone rubber made with different harder/acceleration for shore OO hardness tests. Case 5 is a latex rubber with known linear elastic and hyperelastic parameters. In all cases, systematic hardness tests are performed, then the E values are predicted from the E-t-S<sub>A</sub> (Case 1-3) or E-t-S<sub>OO</sub> (Case 4-5) charts. The level of accuracy/feasibility of the method is assessed by simulating tests under different conditions using the properties estimated.



**Figure 4.1** Flow chart showing the main research work in developing the FE modelling program and its applications in testing rubbers.

## 4.2 FE modelling of shore A hardness tests of linear elastic materials with standard sample thicknesses (over 6mm)

### 4.2.1 FE model

Figures 4.2 (a&b) show the structure and mesh of a 2-D axial-symmetric model of shore A hardness tests. The shore A indenter was modelled as an analytically rigid body. The indenter material, hardened steel, is a lot stiffer and stronger than the rubber materials to be tested. The indenter is of symmetrical nature, an axial-symmetric model could effectively reduce the demand on computation resources. The element used is CAX3, which is Continuum, Axisymmetric, 3-node element. (*ABAQUS 6.11 Manuals*). As shown in the model, finer meshes have been applied around the indenter to improve the accuracy. The thickness and the width of the model are 6 mm and 12 mm (According to the ASTM D2240-05), respectively. The supporting platform was modelled as an analytically rigid plate, as normally a metal plate is used which is a lot stiffer than the rubber materials being tested. The bottom plate is fixed in all directions in the model using an Encastre condition. Contact has been defined between the indenter surface and material surface, the bottom material surface and the plate with a friction coefficient of 0.1. This is commonly used in rubber-metal contact situation (*Dirikolu et al., 2004*). The effect of the coefficients of friction has been studied over a potential range; the results are to be discussed in Chapter 5. The mesh in the regions directly under the indenter tip was refined with high mesh density in order to obtain accurate results in the initial FE model. Different analysis approach has been explored in the preliminary works including both standard and explicit analysis. A re-meshing program is developed to cope with the large deformation when a softer material (lower E values) is being tested. Elastic properties are used rather than hyperelastic models, in order to establish a simple and practical approach to be used especially in gaskets or seals, which is normally under relatively low strain level. The Poisson's ratio is set to be 0.495 as rubber is incompressible. The suitability of the linear elastic and hyperelastic models in modelling shore A and OO hardness tests have been systematically studied and some results are to be presented in the discussion chapter.

Figures 4.2 (c&d) show the typical displacement fields under the indenter and the force-displacement curve. The procedure to determine the displacement point (at

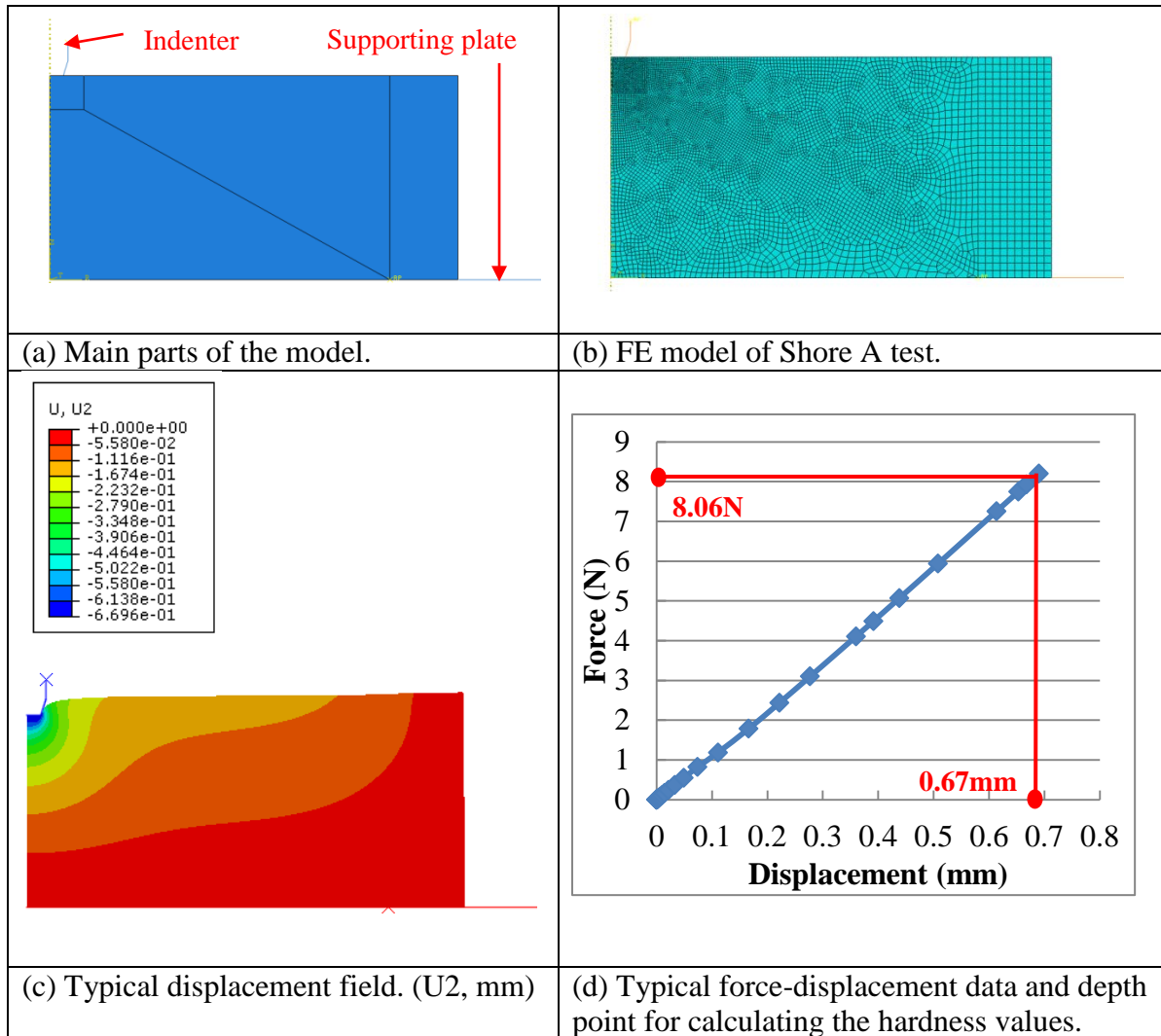
$P=8.06\text{N}$ ) for calculating the shore A hardness value (shore A hardness reading) is illustrated in Figure 4.2(d). The shore A hardness is calculated following equation (Johannes *et al.*, 2006):

$$S_A=100-40*h \quad (4.1)$$

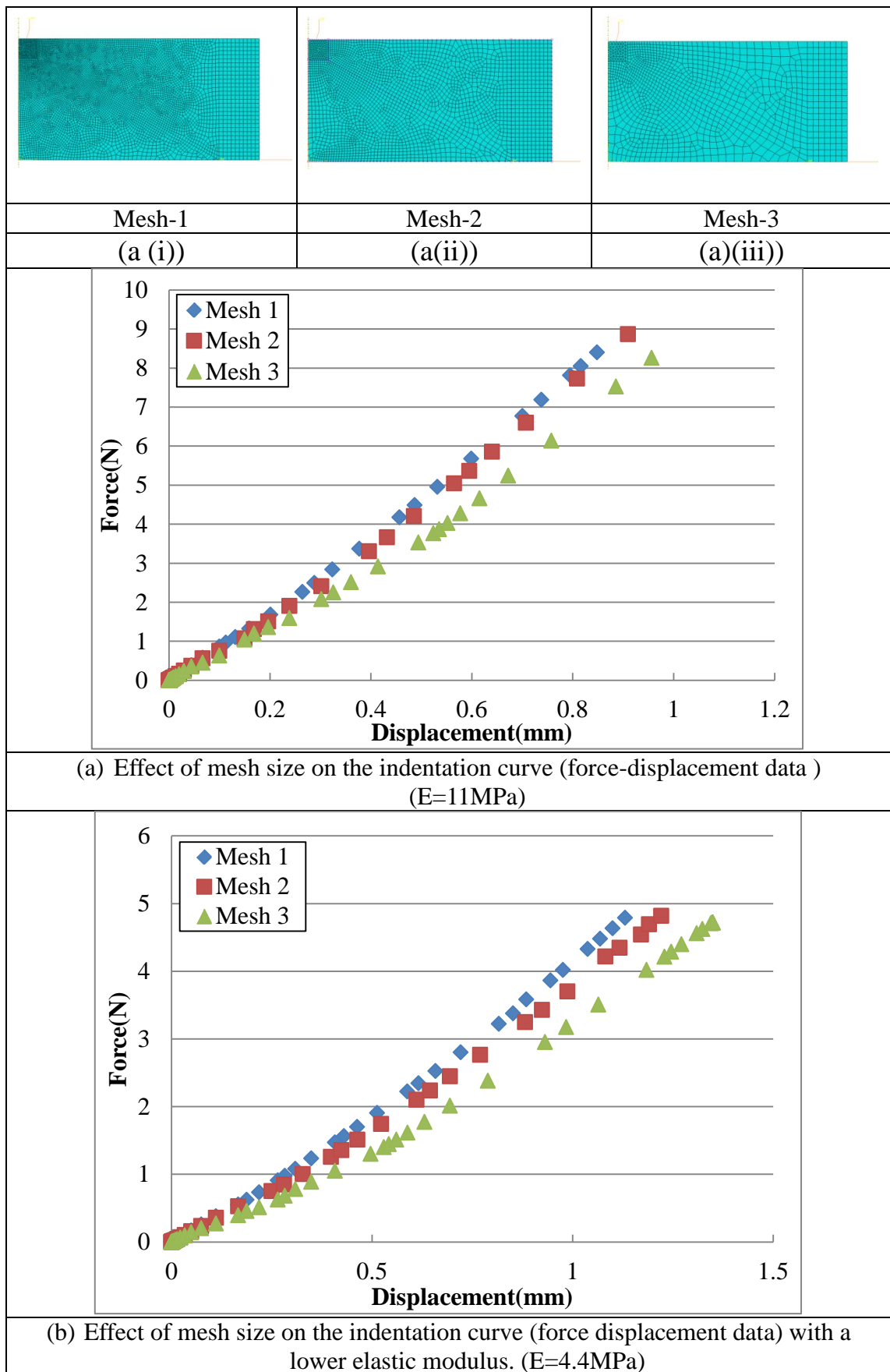
where  $S_A$  is the shore A hardness and  $h$  is the indentation depth at an indentation force of 8.06N.

As the hardness is defined by the displacement at a fixed load, the maximum deformation/displacement is dependent on the material properties (i.e. Young's modulus), so it is the extent of deformation/distortion of the elements. The meshes in the model were generated with pertinent symmetry consideration to reduce the calculation size with different mesh density for different regions. The potential influence of all these factors on the accuracy of the modelling process needs to be investigated. This was assessed by varying the meshing scheme (i.e. mesh density) in the FE models, and then comparing the P-h (force-displacement) curves. Figure 4.3 shows the different mesh sizes used in the shore A hardness FE indentation model and the P-h curves of the different meshing approaches. There are four main parts in the FE model as shown in Figure 4.2(a). The edges of the square region underneath the indenter are modelled with uniform element size, which is changed in the mesh sensitivity tests (i.e. 0.05, 0.1 and 0.15 mm designated as mesh1, 2 and 3). As shown in the force displacement data (Figure 4.3(b)), the results became insensitive to the mesh density, and therefore mesh size-0.1 mm was set as the suitable mesh density. For the data with a lower E value, the P-h curves show (Figure 4.3(c)) a similar situation for the element sizes. A mesh size of 0.1 mm is sufficiently accurate for both E values. In addition, the indentation curves for lower Young's modulus values cannot reach the force for the shore A hardness (8.06N). A similar case was observed even when the mesh sizes were further reduced. When the Young's modulus is low, the deformation of the material becomes much larger/more intense causing extensive distortion of the elements. Even though the modelling approach works for higher E values, a new approach has to be developed to be able to produce consistent and comparable results. A viable approach is by using the re-meshing method.





**Figure 4.2** FE model of shore A hardness test: Structure of the model and meshes (a&b), typical displacement field (c) and force-displacement curve (d) showing the procedure to determine the shore A hardness by using the displacement at a force of 8.06N.

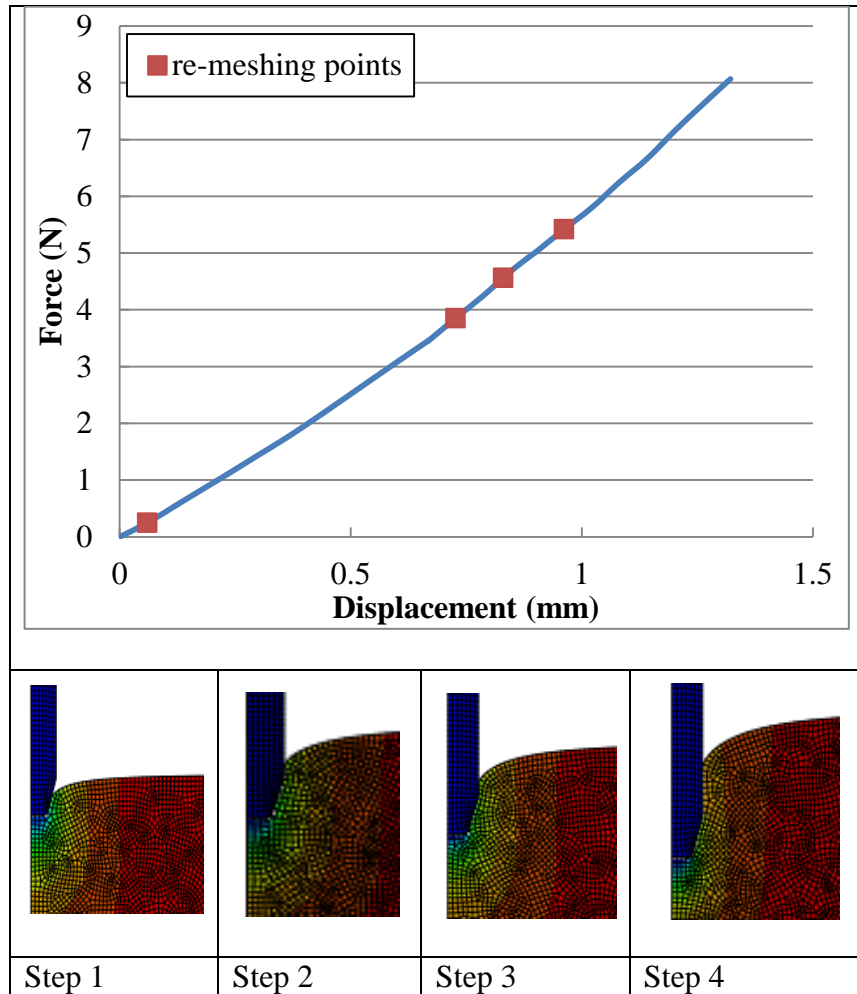


**Figure 4.3** Effect of mesh density on the indentation curves with different Young's modulus. (Sample thickness=6mm). The mesh size for the square region underneath the indenter is set at 0.05, 0.1 and 0.15 for mesh 1, 2 and 3, respectively).

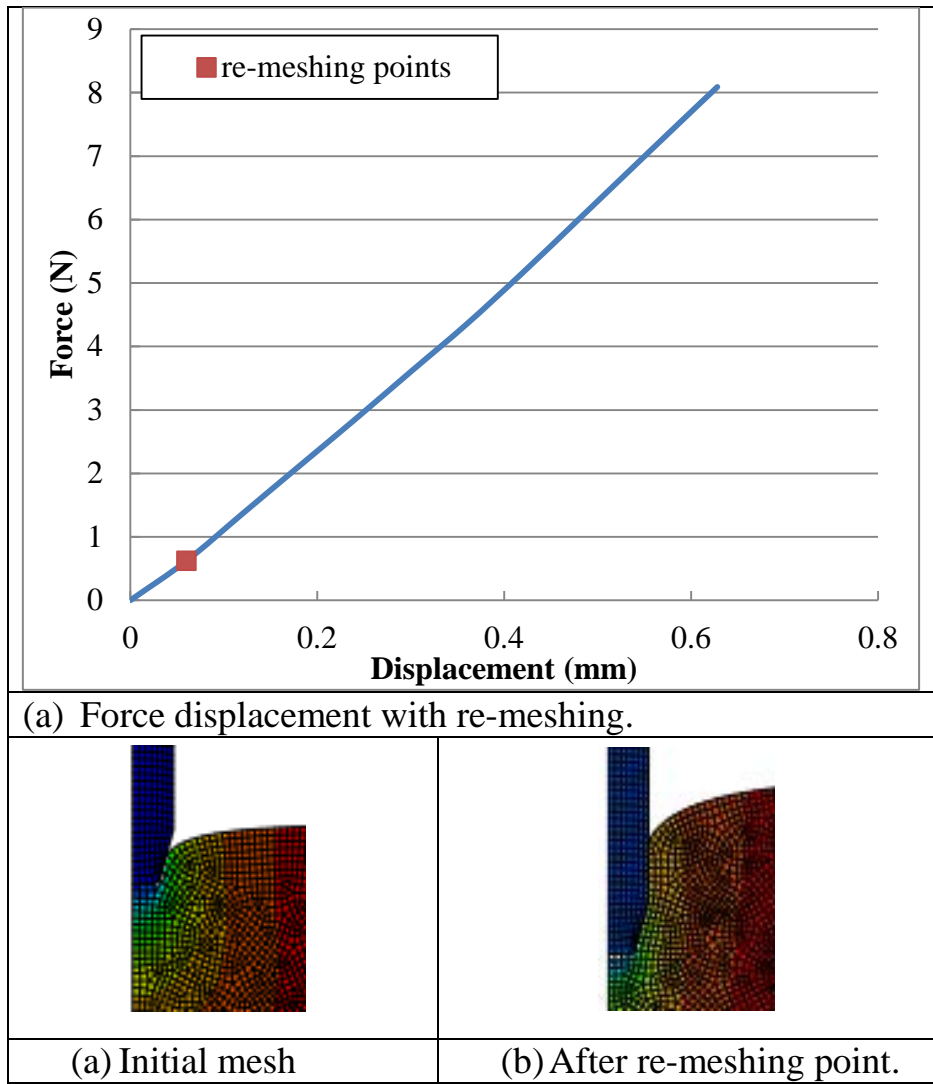
#### **4.2.2 Re-meshing method used in the FE model of shore A hardness test**

As shown in section 4.2.1, for the models with higher elastic material properties, the standard static model of shore A hardness test was capable of reaching 8.06 N required to estimate the shore A hardness. However, when the model was used on materials with lower elastic material properties ( $E \leq 10$  MPa), it was unable to reach the full force (8.06N) for the shore A hardness test. A procedure with re-meshing method has been developed for solving this issue. In this process, a normal standard static FE model was built first then submitted for simulation. If the model (with the assigned properties) is aborted due to excessive element distortion before reaching the specified displacement which covers the force of 8.06 N, a new model is automatically re-built based on the deformed geometry of the previous model and the results from the old model are transferred to the new model, as predefined data to run a new simulation. The model is re-meshed as the geometry is changed as the position of the indenter and geometry of the sample has changed, all part instances are re-assembled. The material properties, step settings, interaction settings and boundary conditions are not changed and continue from the original model. The model with re-meshing method was created using the Python programming, which is a subroutine function of ABAQUS 6.11.

Figures 4.4&4.5 show some typical re-meshed models of the region underneath the indenter over multiple steps for materials of high/low elastic modulus. In the case of lower E values (Figure 4.4), there are four steps of re-meshing during the simulation. The mesh element was initially set to 12,000 elements in the first step. In the second step the mesh element was changed to 14,549 elements. In the third step the mesh element was changed to 14,648 elements. In the fourth step the mesh element was changed to 14,743 elements. In the case of higher elastic properties as shown in Figure 4.5, there are only two steps during the simulation. The mesh element was initially set to 12,000 elements in the first step. In the second step the number of elements was changed to 14,592.



**Figure 4.4** Re-meshing points and deformation fields illustrating the working process of the re-meshing program. ( $E=4.4\text{MPa}$ )

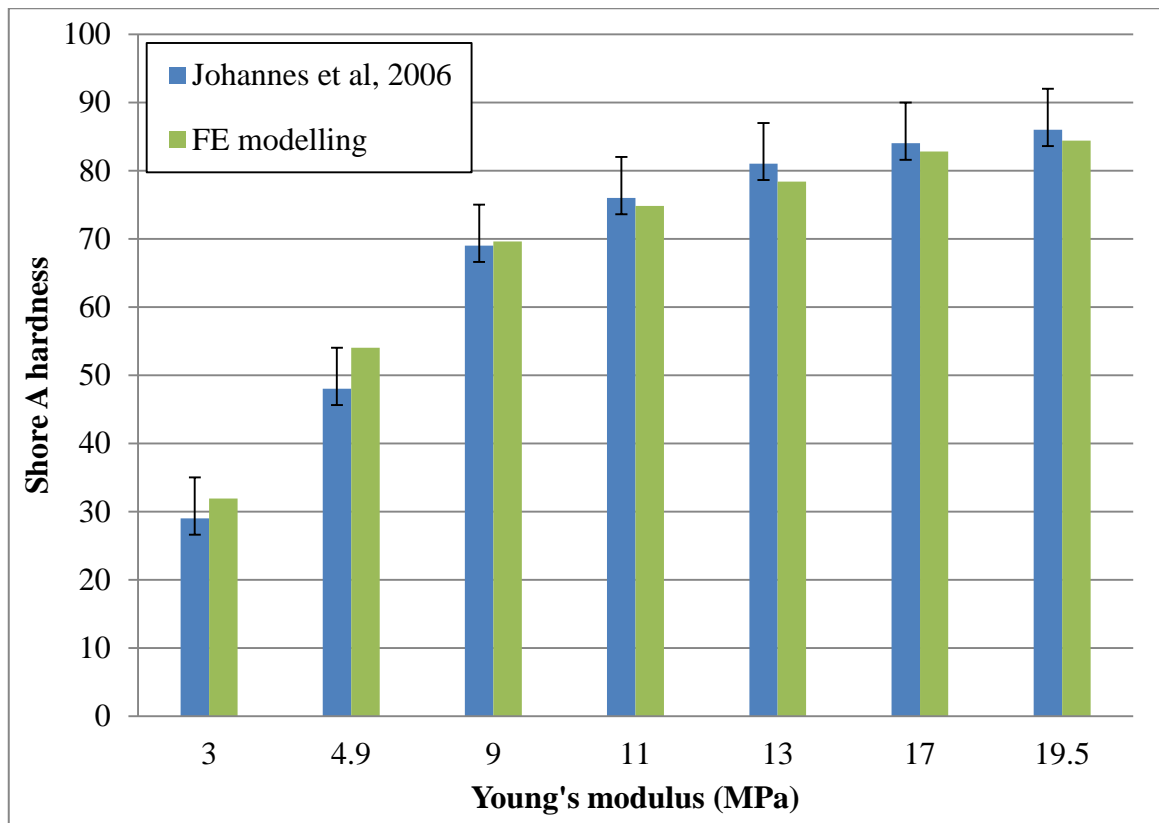


**Figure 4.5** FE force displacement data ( $E=11\text{MPa}$ ) with re-meshing point to show that for a higher Young's modulus, less/no re-meshing is required as the depth is much lower to reach the force for the shore A hardness.

#### **4.2.3 Shore A hardness ( $S_A$ ) for samples with standard thickness ( $t$ ) over different Young's modulus ( $E$ ) and comparison with published data on rubbers**

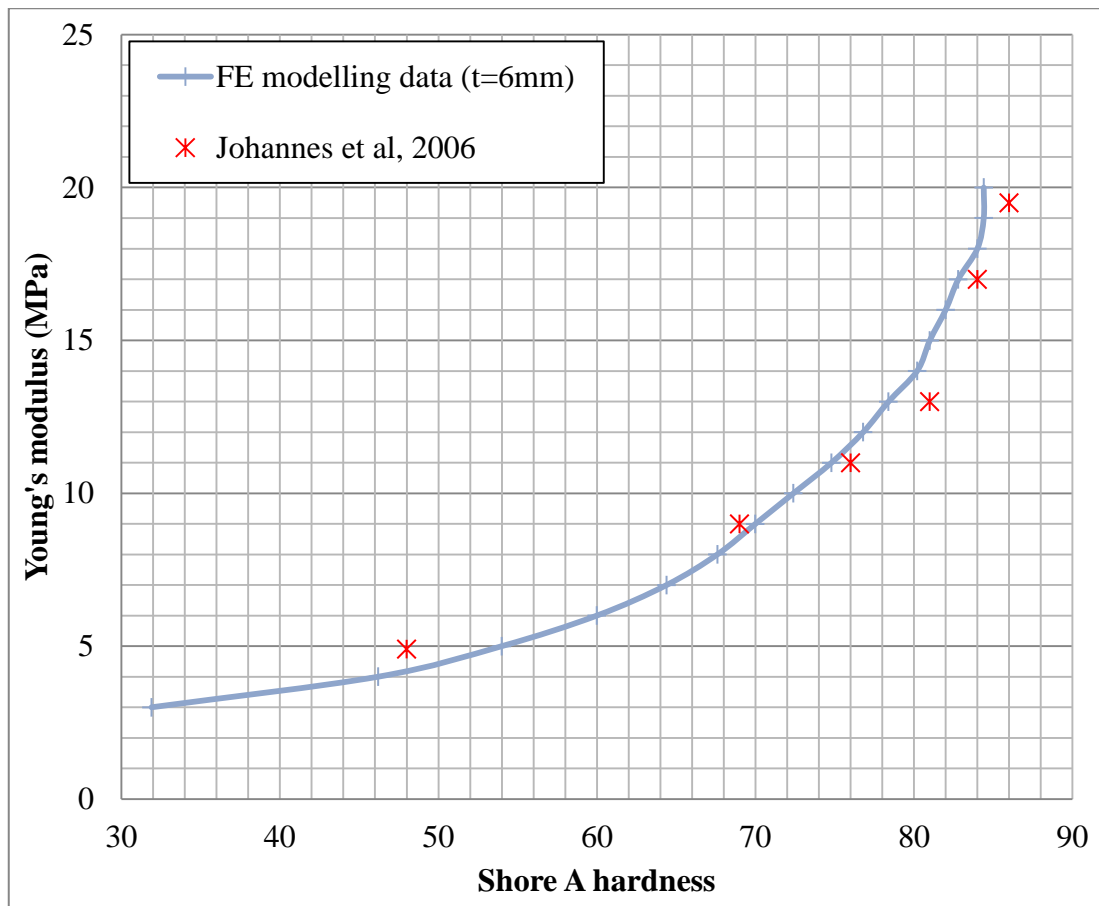
Compared to standard tests such as tension or compression tests, the shore A hardness is influenced by many factors. The main focus of this work is to develop a practical method for characterising rubber materials commonly used for seals or gaskets with sufficient accuracy for this application field. The FE model is firstly validated against published data on rubbers to improve the robustness of the approach. Figure 4.6 is a bar chart showing the comparison between FE predicted shore A hardness values with Young's modulus in this work and the data from a published paper (*Johannes et al., 2006*). All the experimental data was directly depicted from the paper based on the shore hardness and compression tests on various rubber materials. In the work, compression tests were used to determine the  $E$  values of the rubbers used in the shore hardness tests and all the samples are standard samples (6 mm thick). The experimental test data from the published papers included hardness data and Young's modulus of six rubber materials, which provided this work with a systematic dataset to assess the accuracy of the FE modelling approaches over a modulus range relevant to gaskets. As shown in the figure, all the numerical data is in a good agreement with the experimental data. In some cases, the numerical and experimental data are very close. The error bars represents the maximum difference (within 10 %) in depicting the hardness values from the figure on the paper. These data show that the shore A hardness simulation is sufficiently accurate. Figure 4.7 plots shore A hardness values versus Young's modulus for samples with a standard thickness. The data from the published papers is also presented. Both sets show a similar trend with the shore A hardness increasing with the Young's modulus. There is more significant increase with shore A hardness at relatively lower  $E$  values. At the higher end, the change of shore A hardness becomes less significant with increasing  $E$  values. This feature could have direct implications on the selection of gasket/seal materials or the development of new materials, as it may cause the sealing stress/force to follow a different trend from the hardness (which is commonly used as the indicator for sealing performance). This is to be analysed in the discussion chapter. Based on the data, it could be seen that there is a clear link between  $S_A$  and  $E$ , when  $E$  is between 3 and 15 MPa. Within this range it is reasonable to estimate the  $E$  values from the shore A hardness. Outside of this range, such a practice may cause inconsistency either under or overestimating the  $E$  values. Given that the shore A hardness test is force controlled rather than based on the P-h

curve, the deformation state of the material when reaching the full load at 8.06 N is the most relevant characteristic for shore A hardness. Figure 4.8 compares the vertical displacement profile for cases with higher or lower elastic modulus at different depth before reaching the load of 8.06 N; Figure 4.8 (a-c) are for  $E=4.4$  MPa, Figure 4.8 (d-f) are for  $E=11$  MPa, the displacement is much lower than that with  $E=4.4$  MPa. However, there is no significant influence in the displacement distribution from the base plate, which suggests that a thickness of 6 mm is sufficient to avoid severe sample size effects. However, in some cases, such as gaskets, samples with a thickness of 6 mm or over are not readily available. It is essential to extend the established modelling program to thinner samples.

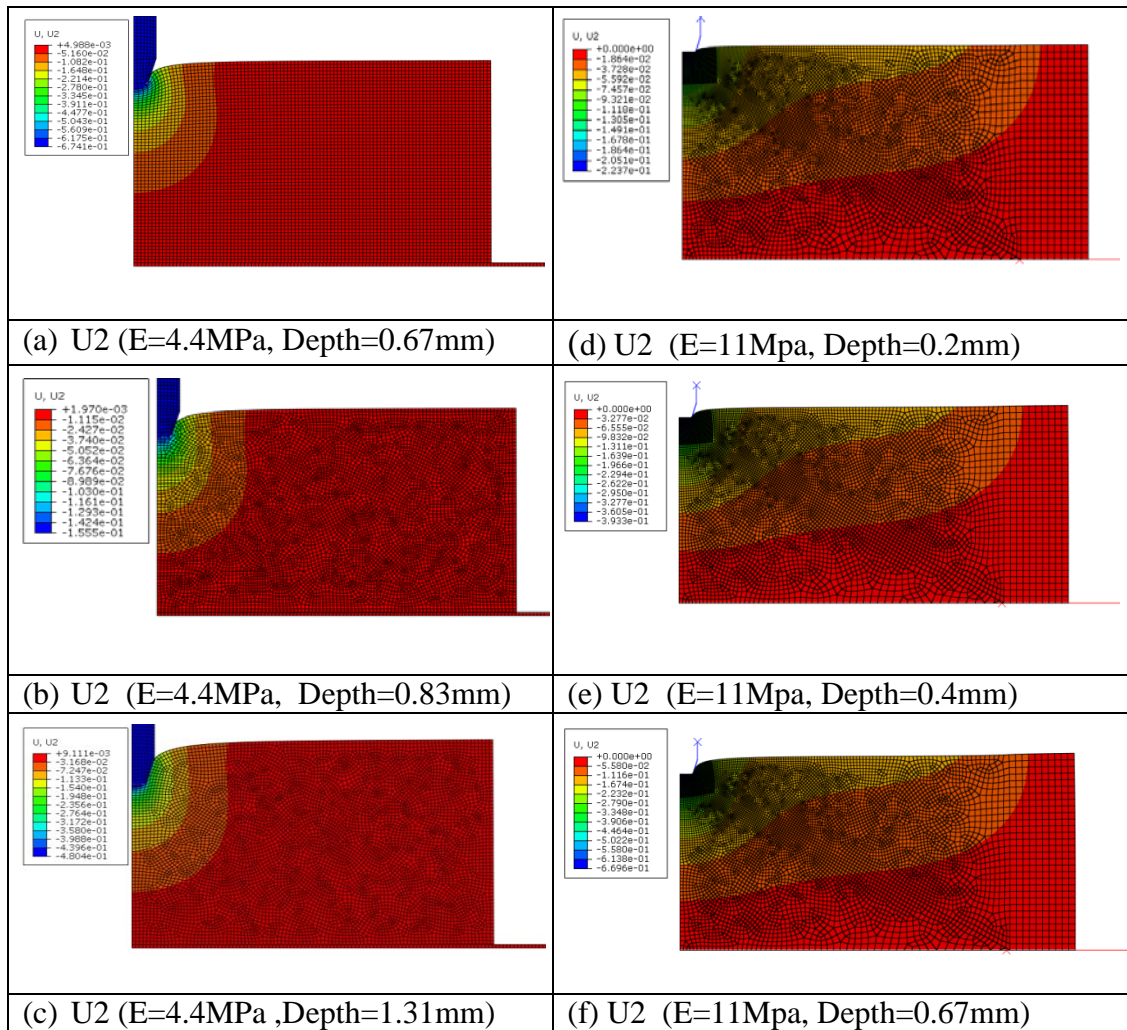


**Figure 4.6** Comparison between FE predicted shore A hardness values with different Young's modulus and experimental data from published paper on rubbers (*Johannes et al., 2006*). (The error bar represents maximum difference in depicting the data from the paper).





**Figure 4.7** Correlations between shore A hardness values and Young's modulus. (Sample thickness=6mm).



**Figure 4.8** Vertical displacement (U2) distributions with a low Young's modulus (E=4.4MPa) and a higher Young's modulus in shore A hardness on sample of standard thickness.

### 4.3 FE modelling of shore A hardness tests of thinner samples (finite thickness samples)

The shore A hardness test presented in the previous section is applicable to relatively thick samples (6 mm or over). However, most gasket or seal rubbers are relatively thin. The FE modelling program is transferred to thinner samples aiming to establish a method to estimate the elastic properties of the materials from shore hardness tests of nonstandard specimens. This would allow the onsite measurement of material properties and enhance the use of indentation as a convenient way of testing rubber based gasket. Figure 4.9 shows a typical FE model of shore A hardness test on a thinner sample with a thickness of 2 mm. The FE program is developed in a way that the thickness of the sample can be easily changed by entering the thickness data in the .rpy program (a python program). Other thicknesses studied included 1 mm, 2 mm, 3 mm, 4 mm and 5 mm, this range is sufficient to cover typical thicknesses for gaskets and seals. A thin gasket offers significant advantages as it can increase the strain and pressure within a small displacement. However, a thinner gasket may put high demand on issues such as flatness of the part surfaces (*Flitney, 2011*). Similar to the previous indentation FE model for a thick specimen, the indenter was modelled as an analytically rigid body. The axisymmetric element CAX3 (an axisymmetric element) is used and finer meshes have been applied around the indenter to improve the accuracy. The width of the model was kept at 12 mm. (According to the ASTM D2240-05). The bottom supporting plate was modelled as an analytically rigid body as it is much stiffer and stronger than the rubber material being tested. The bottom plate was fixed in all degrees of freedom. Contact has been defined between the indenter surface and material surface using penalty method with a friction coefficient of 0.1. Mesh size for the region underneath the indenter used in the initial model is 0.1 mm and a re-meshing rule is applied.

Figure 4.10 shows typical force-displacement curve for  $E=4.4$  MPa and  $E=11$  MPa for a sample thickness of 2 mm. In the FE model for  $E=11$  MPa, no re-meshing is triggered to reach the force (8.06 N) for shore A hardness. In the FE model for  $E=4.4$  MPa, the re-meshing process had four steps to achieve the force of 8.06 N and the main steps are shown in the Figure 4.10 (b). The mesh was initially set to 2266 elements in the first step. In the second step the number of element was automatically changed to 2299. In the third step the mesh continued to change to 2311 elements. In

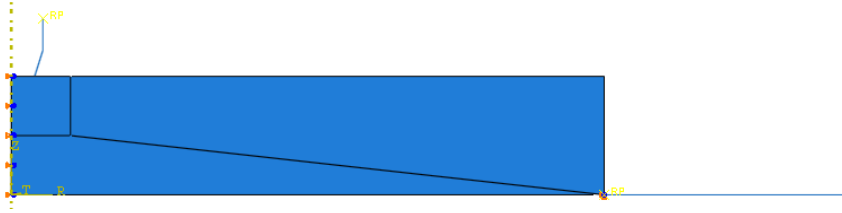
the fourth step the mesh was changed to 2349 elements finally. As illustrated in Figure 4.10(a), the shore hardness value is determined based on the indentation depth at which the indentation forces reaches 8.06 N.

Figure 4.11 shows the domain of parameters with varying sample thickness and properties. The range of thickness and property values is relevant to the typical gasket used in industries. As shown in the figure, the thickness range between 1 mm-5 mm and the Young's modulus range between 3-20 MPa. There are 90 models in total. This detailed systematic study will map out the effects of thickness and material properties, it will also provide a detailed dataset in developing ANN programs to predict hardness values based on thickness and elastic properties (to be presented in section 4.6). Figure 4.12 shows the procedure to process the P-h curve for each combination of thickness and properties. The process involves using curve fitting of P-h data, then calculates corresponding displacement for an indentation load of 8.06 N, then determines the shore hardness values, which is a function of both the intrinsic material properties (in this case, E values) and sample thickness.

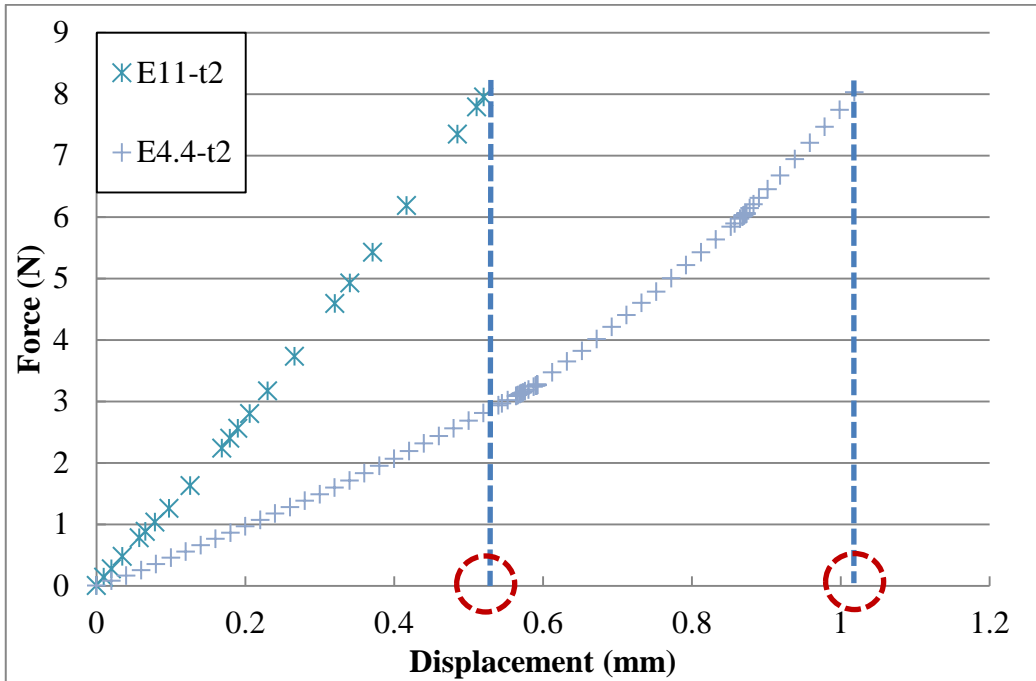
Figure 4.13 shows typical P-h curves for different sample thicknesses with  $E=11$  MPa. As shown in the figure, the initial part of the curves for  $t=3, 4, 5$  and  $6$  mm are very close, then the indentation force is getting different. At the load point for shore A hardness, the displacement is slightly different among these four thicknesses. This suggests that the shore A hardness value will show only a small difference in this range. Also shown in the figure, the P-h curves for  $t=1$  and  $2$ mm are significantly different from the data for other thicknesses. The shore A hardness data is further plotted in Figure 4.14. As the thickness gets thinner, the apparent shore hardness reading increases, but the change of  $S_A$  for different E values is different. Materials with higher E values are less sensitive to the thickness change, while the  $S_A$  of a material with lower E values are more sensitive to the thickness change.

Figure 4.15 is a chart plotting the shore A hardnesses and E values for different thicknesses. As shown in the figure, when the E value is high, the effect of thickness is less significant. The hardness between  $t=1$  mm and  $t=6$  mm is less than 10 % for

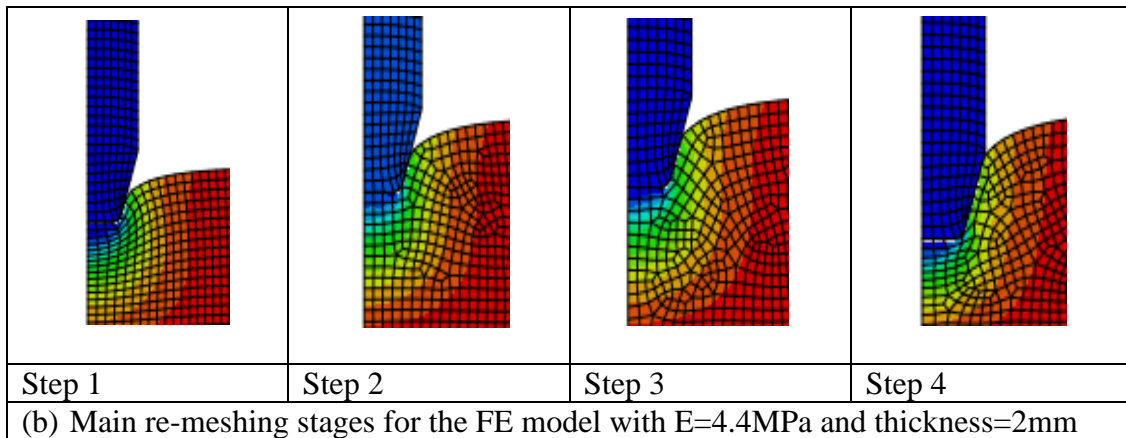
$E=20$  MPa. At medium level of  $E$  values ( $E=10$  MPa), the difference between  $t=1$  mm and  $t=6$  mm is around 15 %; When the material is softer, e.g.  $E=3$  MPa, the hardness difference between thin and thick samples is much more significant. At  $t=1$  mm,  $S_A$  is  $\sim 68$ ; while for  $t=6$  mm,  $S_A$  is 32,  $S_A$  is increased almost 100 %. This Elastic modulus-thickness-Shore hardness chart (designated as  $E$ - $t$ - $S_A$  chart) would provide a tool to predict the  $E$  values from samples of different thickness rather than rely on the availability of standard samples with a thickness of 6mm or over. This made it possible to predict the  $E$  values inversely from shore hardness values. This could be very important for testing rubber materials either in materials development and characterisation of rubber product such as gaskets/seals. Some typical cases are to be presented in the next section.



**Figure 4.9** Typical FE model of the shore A hardness test on a thinner (non-standard thickness) sample.

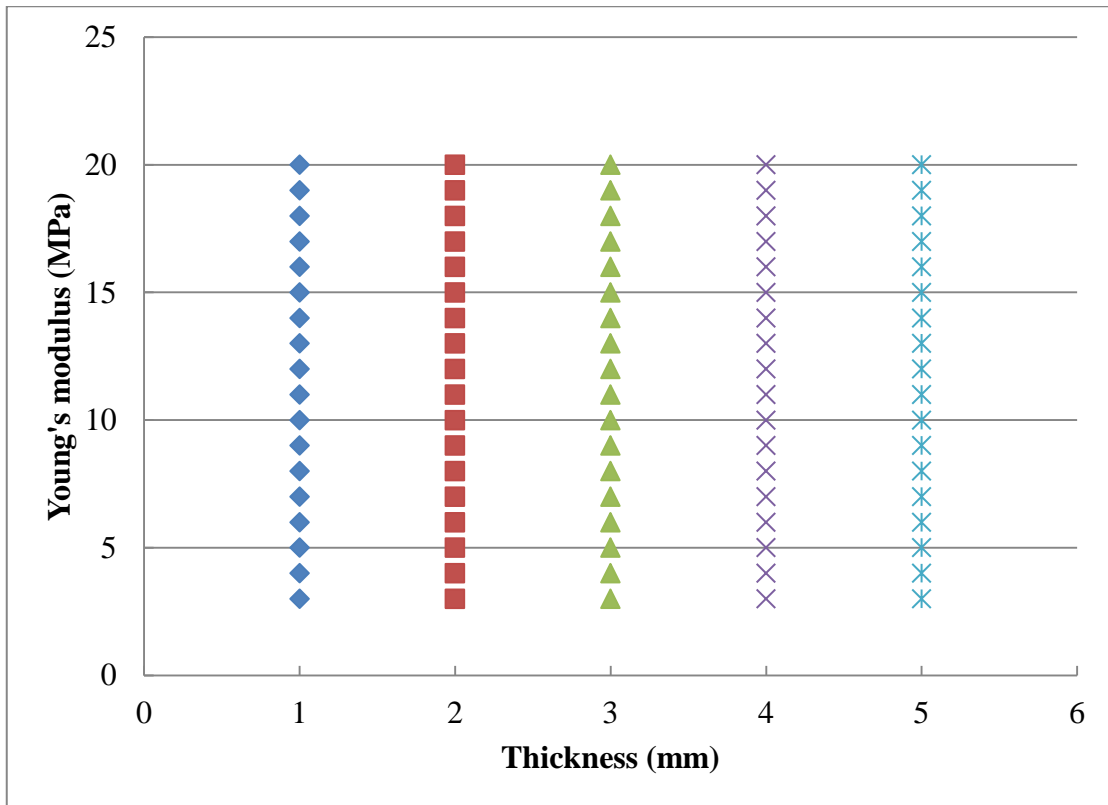


(a) P-h curves in different E values

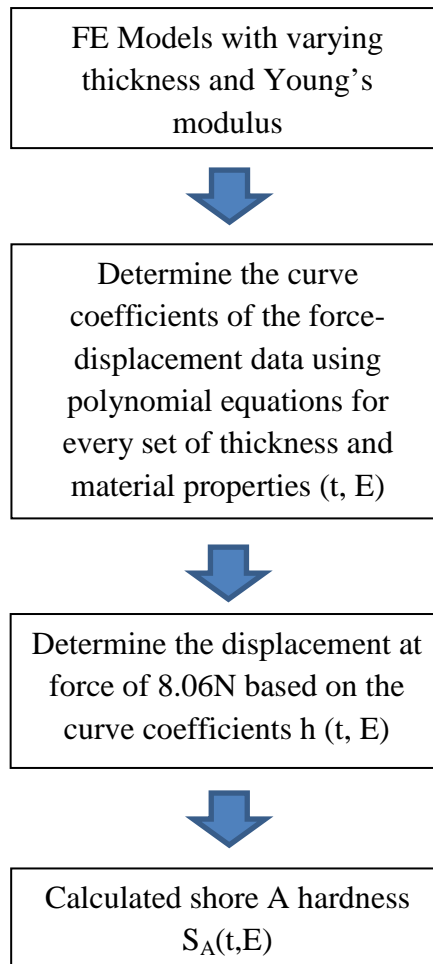


(b) Main re-meshing stages for the FE model with  $E=4.4\text{MPa}$  and thickness=2mm

**Figure 4.10** Typical P-h curve and re-meshing stages for thinner samples ( $t=2\text{mm}$ ) with different E values. The point in the red circle represents the displacement point used to calculate the shore hardness values for the corresponding E values and thicknesses.

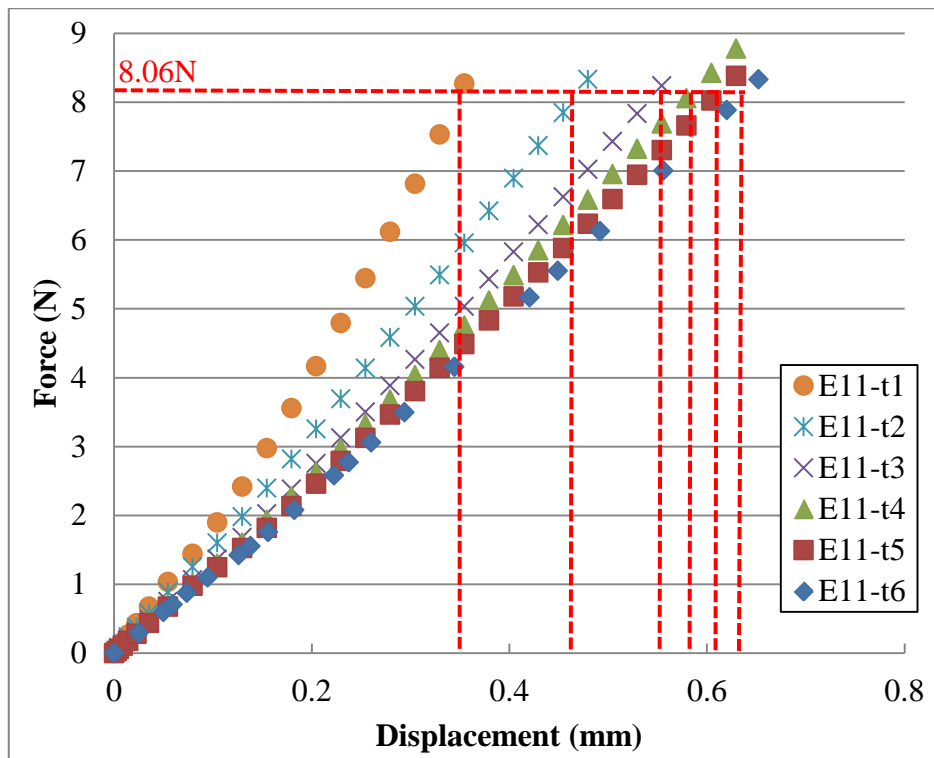


**Figure 4.11** Simulation domains showing the range of thicknesses and properties varied in the FE model to produce data for establishing the correlation between shore A hardness and Young's modulus for thinner samples. The range of Young's modulus (3-20 MPa) is defined based on the properties range of gasket rubbers. The FE modelling results are also used for providing data to ANN in direct and inverse analysis of shore hardness.

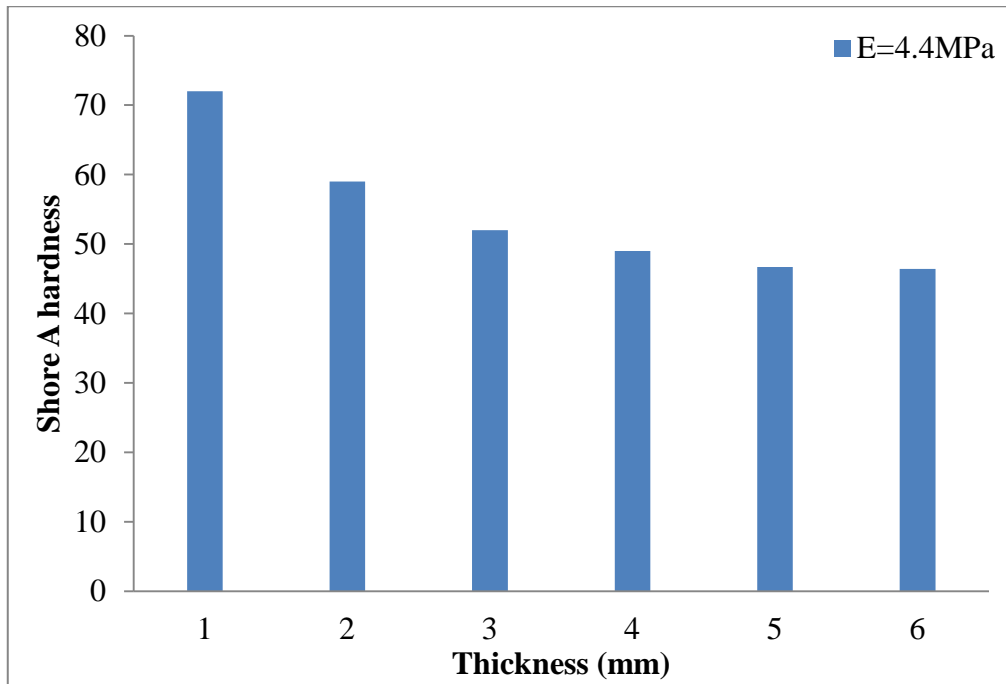


**Figure 4.12** Main data processing procedures to determine the shore A hardness value ( $S_A$ ) for different combinations of sample thickness ( $t$ ) and materials properties ( $E$ ).

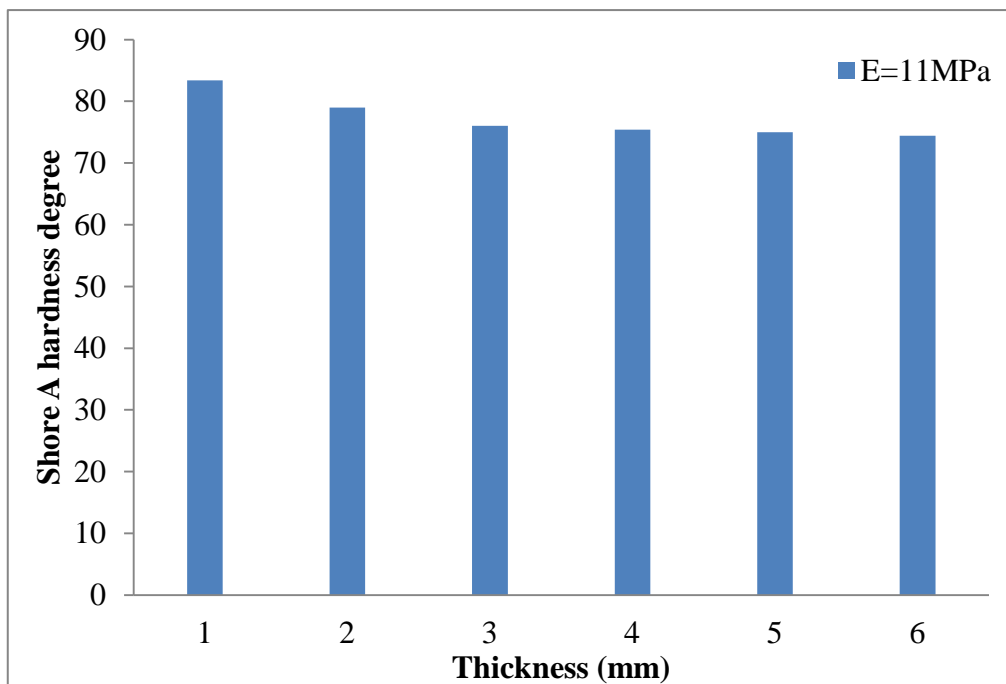




**Figure 4.13** Indentation P-h curves of samples with different thicknesses ( $E=11\text{MPa}$ ).

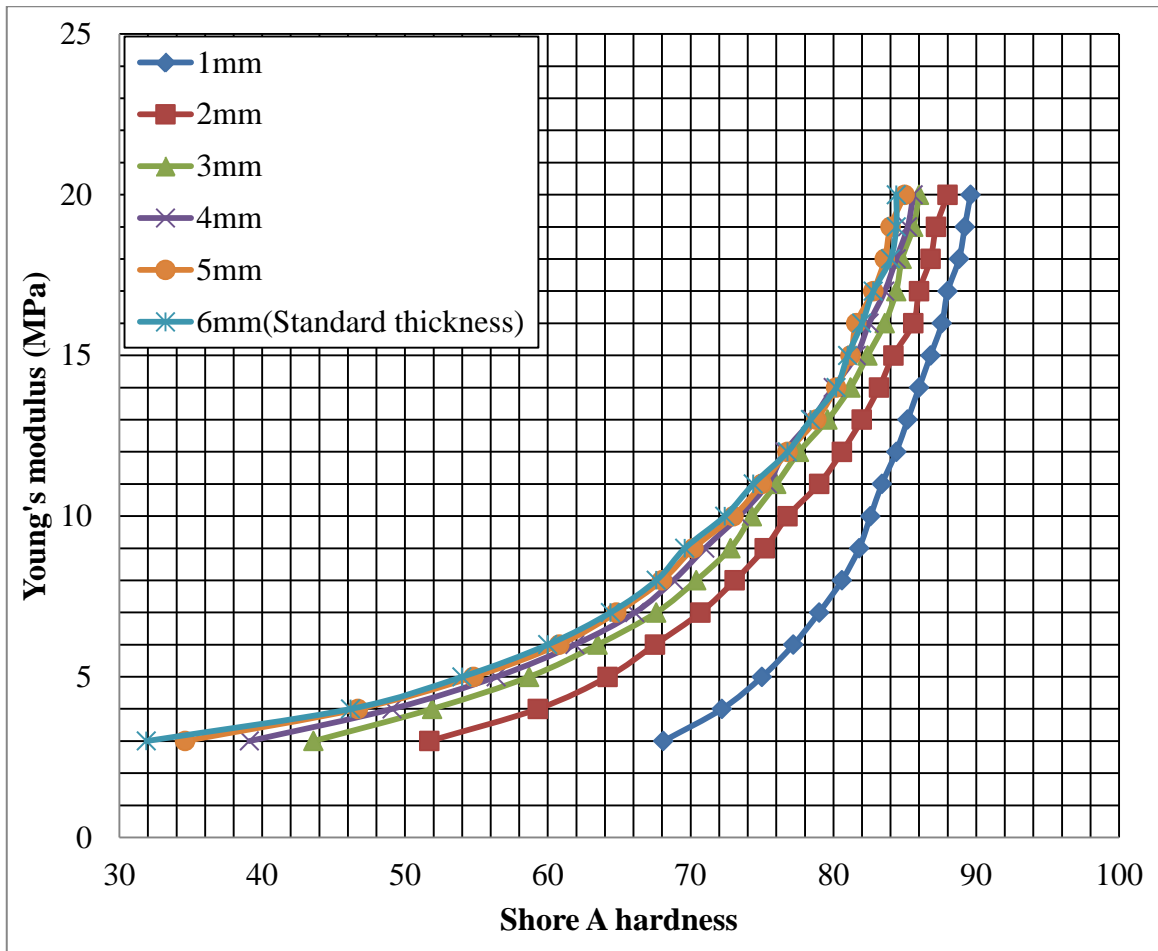


(a) Typical  $S_A$  showing the effect of sample thickness for relatively soft rubber ( $E=4.4\text{MPa}$ ).



(b) Typical  $S_A$  showing the effect of sample thickness for relatively stiffer rubber ( $E=11\text{MPa}$ ).

**Figure 4.14** Bar chart to show the change of apparent shore A hardness ( $S_A$ ) with the sample thickness.



**Figure 4.15** Correlations of shore A hardness values with Young's modulus and sample thicknesses.

#### **4.4 Use of the relationship between elastic modulus, thickness and shore A hardness in the testing and modelling of rubber and gaskets**

This section presents the procedure and brief results using the relationship between  $E$ ,  $t$  and  $S_A$  ( $E$ - $t$ - $S_A$  chart) developed. As explained in section 4.3, this chart could be used as a tool to predict the  $S_A$  values from the  $E$  and thickness, more usefully, to estimate the  $E$  values from shore A hardness values on a sample with known thickness. In addition, the work also assesses some potential issues associated with shore A hardness testing on a gasket, such as potential anisotropic properties, influence of shape and size of the sample. In each case, shore hardness is performed on the materials, and then the  $E$  value is determined from the  $E$ - $t$ - $S_A$  chart. The  $E$  value is then used in FE models simulating compression/tension testing of non-standard samples/conditions. This will provide an effective way to assess the accuracy of predicted  $E$  values by comparing the FE results (based on the predicted  $E$  value) and the experimental test data of the same material. Three cases are presented for shore A hardness tests. Case-1 is silicone rubber samples with different thickness made in the lab. Shore A hardness is able to test the material on different planes and on samples of different thicknesses. In this case, the predicted  $E$  value is assessed by using the  $E$  value in the FE model of compression test. In the second case (Case-2), a commercially available silicone gasket material ( $t=1.5$  mm) is used. The shore A hardness and  $E$  value are determined, then the  $E$  value is used in an FE model simulating the tensile tests of long strip sample and compression tests of multi-layered set-up. In the third case (Case-3), an EPDM gasket (with an irregular cross-section shape) for plate heat exchanger is tested. The hardness and  $E$  value are determined, and then the  $E$  value is used as input to FE model simulating the tensile and compression tests (flat plate) of the gasket. Another configuration is also presented where the gasket is compressed within a grooved gasket plate. This will provide a comprehensive program to evaluate the accuracy and limitation of using the  $E$ - $t$ - $S_A$  chart in estimating the material properties. It also set a base for simulation/estimating the force and sealing pressure required in gasketed plate heat exchanger (the results are to be presented in the discussion chapter).

#### **4.4.1 Case 1: Testing and modelling of cast silicone rubber samples with different thicknesses**

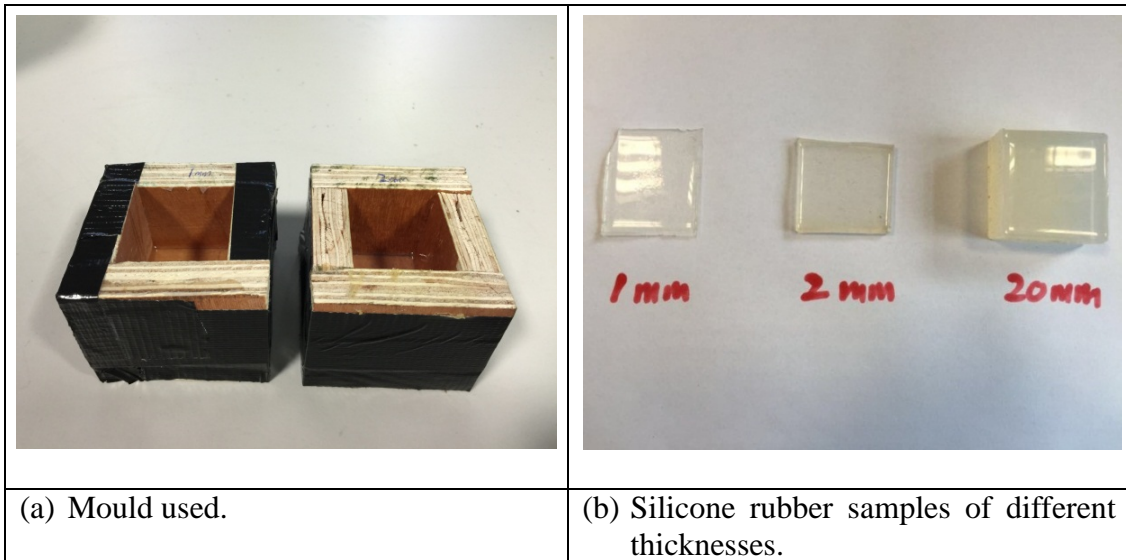
Figure 4.16 shows the mould used to make silicone rubber samples of different thicknesses. The thickness of the thick sample is 20 mm and the width of the sample is 40 mm. The thicknesses of the two thinner samples are 1 mm and 2 mm, respectively, and the width of the samples is 40 mm. All of the samples were made by a material system of T-4 base silicone solvent and silastic T4 curing agent using vacuum casting and curing system (See Chapter 3 for detailed procedure).

To assess the potential anisotropic properties, shore A hardness tests have been performed on the different planes of the thick sample as schematically shown in Figure 4.17(a). This can be conveniently tested with the shore A hardness tester, which is a significant advantage. In each case, at least 6 tests were tested by at least two operators, the error bars represent the standard deviation of the six tests. Evident from the comparison of shore A hardness values between three planes, the material is close to isotropic.

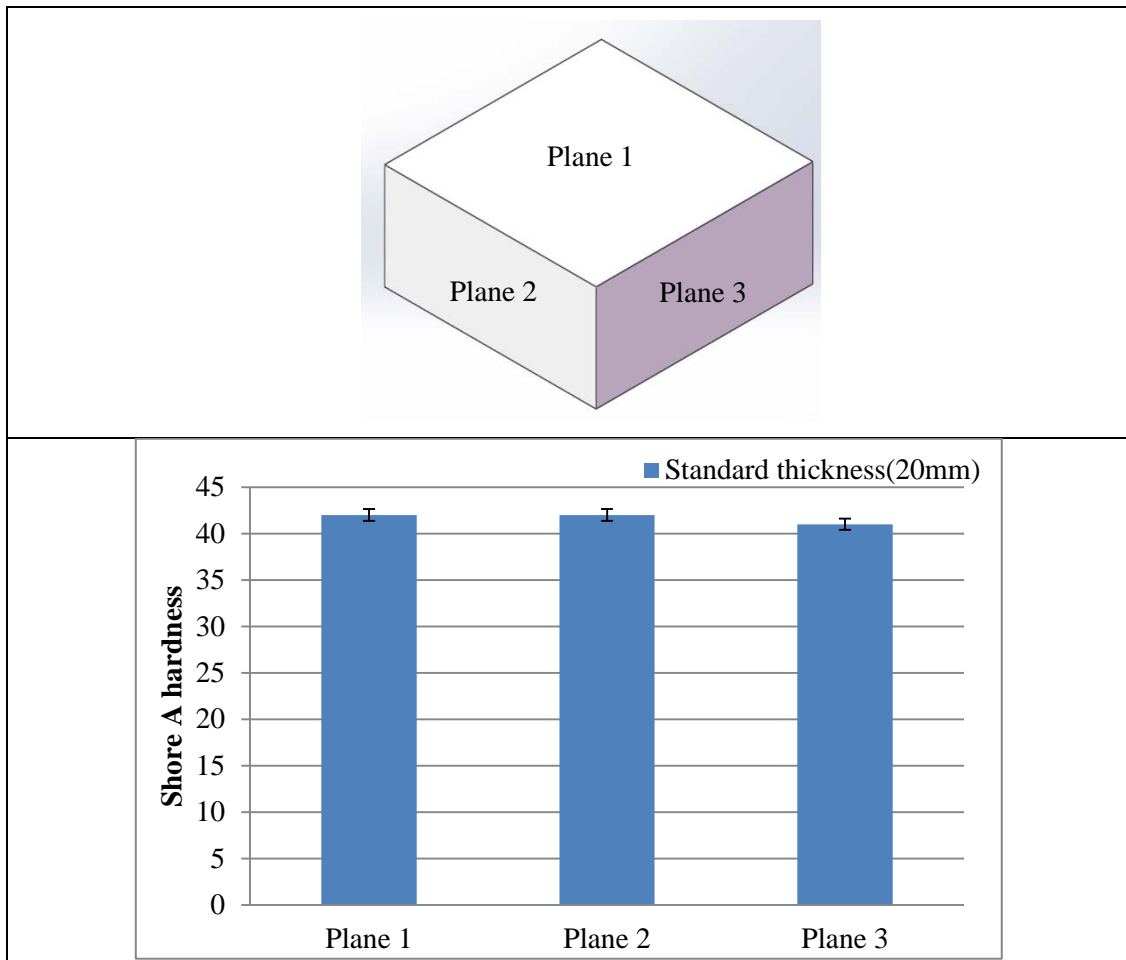
Figure 4.17 (b) shows the comparison of shore A hardness test data for the silicone rubber sample with different thicknesses. As shown in the bar chart, the hardness values of the samples are significantly different. The shore A hardness readings for the 1 mm and 2 mm thick samples are much higher than that of the 20mm thick sample. Figure 4.18 compares the predicted elastic modulus of the samples based on the E-t-S<sub>A</sub> chart. There are some differences between the E values, but in general they are within a similar range.

Figure 4.19 shows the comparison between the experimental data and the FE modelling results of the thick silicone rubber sample under uniaxial compression test. The uniaxial compression test was performed on a tensile/compression machine (Figure 4.19 (a)). Two flat plates were used to compress the sample, one flat plate was the support plate which is fixed at the bottom position, another flat plate was used to compress vertically, which is attached to the load cell to record the force and the displacement (as introduced in Chapter 3). The compression test of the silicone

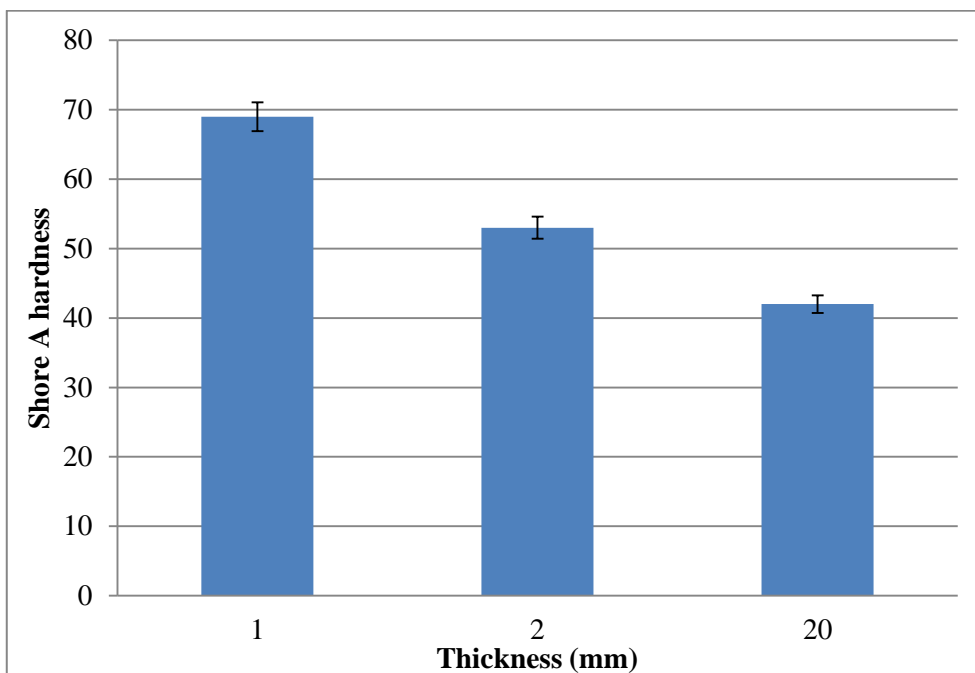
rubber was simulated by a 3D model as shown in Figure 4.19 (b). The element type used is 6-node linear triangular prism element type (C3D6), the width and thickness of the sample model is 40 mm and 20 mm, the same as the thick sample shown in Figure 4.17. The bottom plate is fixed by all degrees of freedom and a displacement is applied to the top plate moving down onto the sample. The material properties used are the averaged elastic modulus from the estimation based on the shore A hardness (Figure 4.18). As shown in Figure 4.19 (c), the force-displacement data from the FE simulation and the compressions tests showed a reasonable trend. The match between test and FE data is very good at lower displacement (in this case before 0.8 mm), then the difference becomes more significant, the maximum difference is within 12 %. This result suggests that estimating E values from shore A hardness values is a feasible approach for silicone rubber.



**Figure 4.16** Case one: silicone rubber samples of different thicknesses made in the lab.

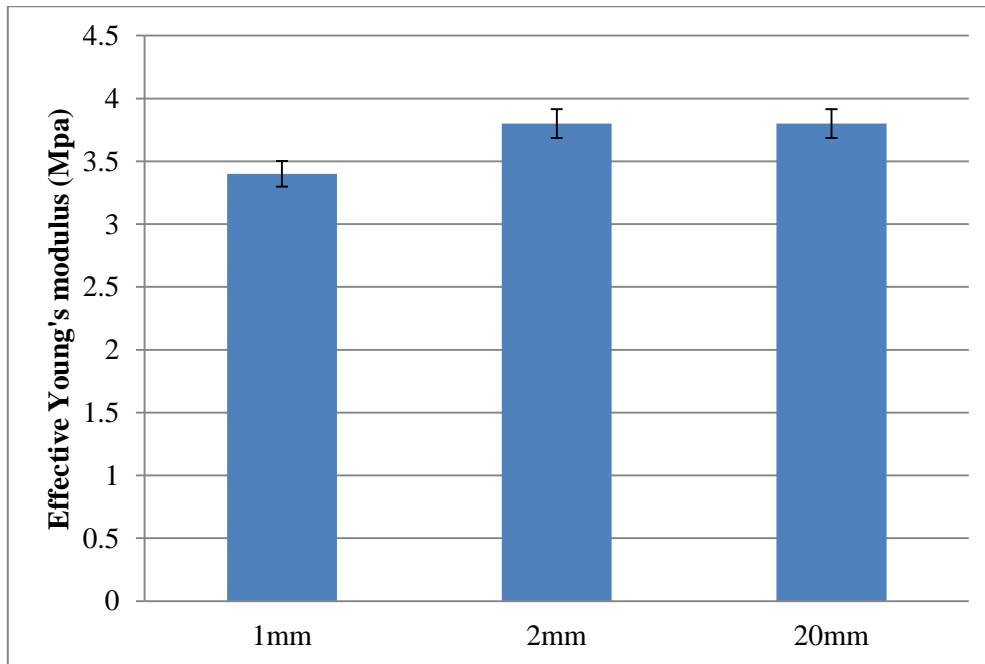


**Figure 4.17 (a)** Comparison of shore A hardness values tested on the three planes of the thick silicone rubber sample.

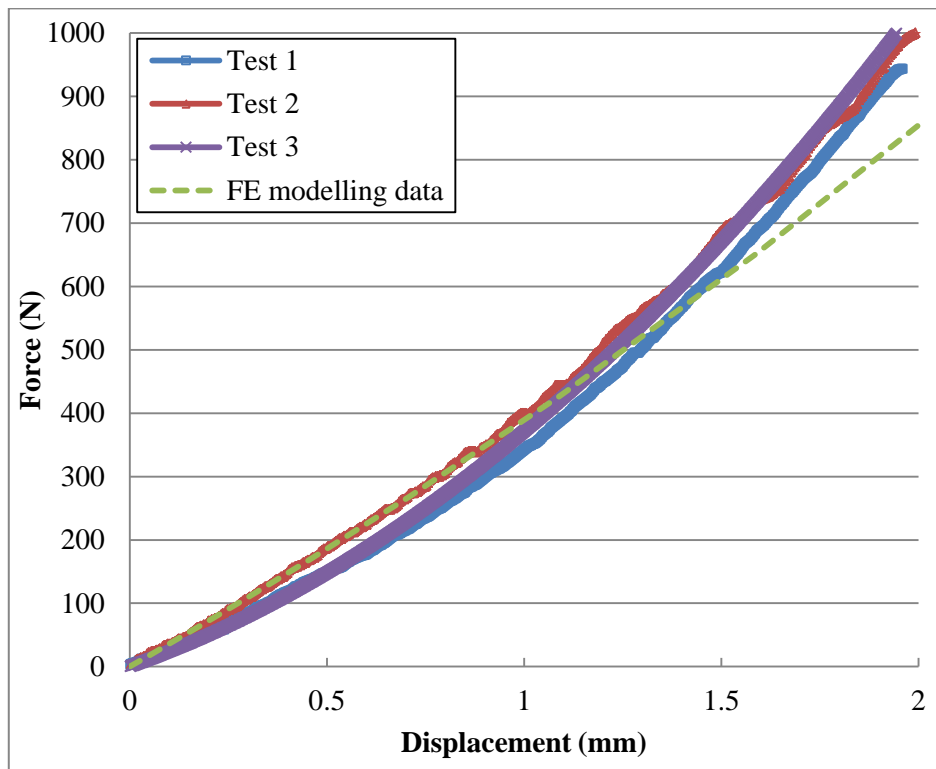
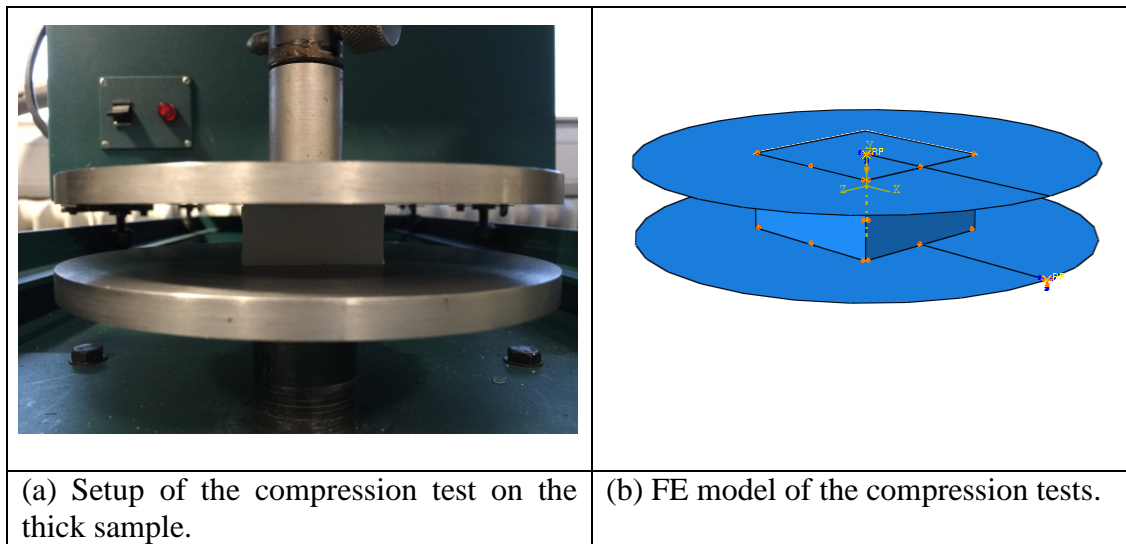


**Figure 4.17 (b)** Shore A hardness values/readings of silicone rubber sample with different thicknesses.





**Figure 4.18** Bar chart showing the predicted elastic modulus from shore hardness tests of sample with different thickness based on the E-thickness-shore A hardness chart.



(c) Comparison of the experimental force displacement curve and FE prediction using the material properties inversely estimated based on the shore A hardness tests.

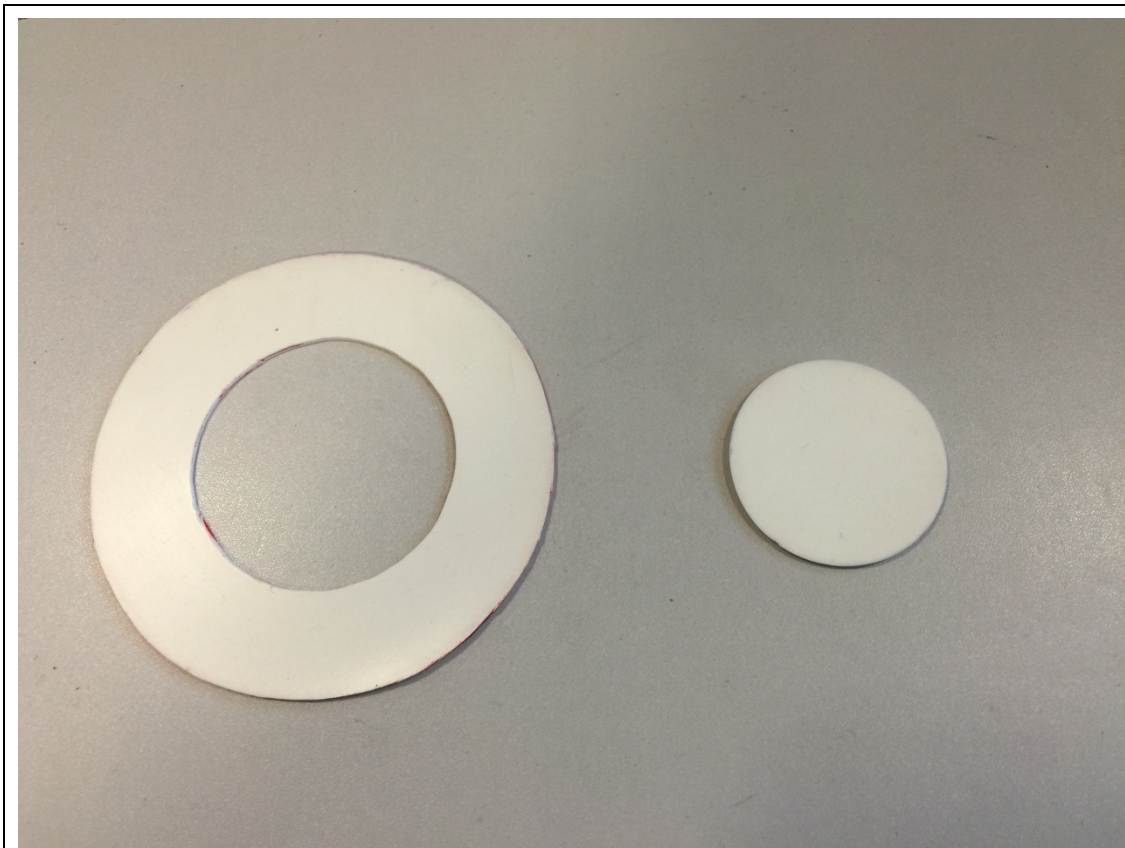
**Figure 4.19** The experimental setup and FE modelling results of compression test of the thick silicone rubber sample.

#### 4.4.2 Case 2: Testing and modelling of thin silicone rubber gasket sheet

The material in this case is a commercially available silicone rubber gasket sheet with a thickness of 1.5mm. It can be used for a range of applications including pipeline gaskets. Figure 4.20 shows typical round and ring shaped samples cut from the gasket sheet. The diameter of the round sample is 48 mm. The inner diameter and outer diameter of the ring sample is 60 mm and 110 mm, respectively, which can be fit into an enveloped gasket with PTFE cover. This is a typical case where no thicker sample is attainable, so the tests have to be done with a thin sample. If the intrinsic elastic properties can be obtained from shore A hardness tests from nonstandard thickness and shape, then it would make it easier for materials identification, comparison or selection process.

For thin samples, uncertainty associated with friction effect becomes a major concern that needs to be investigated. In this work, Shore hardness tests have been conducted under normal dry condition and different lubricated conditions as a comparison (in other words, as a way to estimate potential maximum error range). The tests consist of investigating the friction effect of the round type silicone gasket samples and the ring type silicone gasket samples. Three frictional conditions are designed including dry sample bottom surface and the contact plate (i); use of silicone based lubricant (ii); use of non-silicone based lubricant (iii). Figure 4.21 shows the shore hardness data under different lubrication conditions. As shown in the figure, in both the round and ring samples, the use of lubricant showed some limited influence on the shore A hardness values. The hardness value with lubricant is about 6 % (maximum) lower. The hardness data for the round and ring sample are comparable, with the hardness of the ring sample being slightly lower. This may be due to the fact that the width of the ring is slightly narrower, which is a situation unavoidable in real tests of gaskets. The data shows that this uncertainty with position is within 5 %. To assess the accuracy of the E values predicted, tensile tests have been performed on a thin long strip samples; compression tests of the round samples and the ring sample have been also been performed. The FE model using the estimated E value was developed to simulate these tests. Given the compression is based on non-standard thin specimen and measurement of the strain is difficult, this modelling approach offers a much better way to assess the work by directly comparing the force displacement data obtained from the test and FE modelling.

Figure 4.22 (a&b) shows the uniaxial compression tests of the round type silicone rubber gasket sample and the ring type silicone gasket sample. The uniaxial compression tests of both samples (3 rubber layers in each case) were conducted on the tensile/compression machine. The compression test of the round type silicone gasket sample was simulated in full scale in the FE model, while only a quarter of the ring sample was modelled using plane symmetric conditions. The element type used is C3D6 in both cases. The diameter of the round sample is 48 mm and the thickness of the sample model is 4.5 mm in total (equivalent of 3 layers of rubber sheet). The inner diameter and outer diameter of the ring sample model is 60 mm and 110 mm respectively. The thickness of the sample model was 4.5 mm, the same as 3 layers of the gasket sheet. In the FE model, the bottom plate is fixed in all degrees of freedom, and a displacement is applied to the top plate to simulate the compression. The material property used was inversely estimated from the shore A hardnesses. As there is no 1.5 mm thickness on the E-t-S<sub>A</sub>, the E value is determined through interpolation of the E values for the shore A hardness value, i.e. plots a curve for E vs. t (t1, 2, 3, 4, 5 mm) for data with the same S<sub>A</sub>. Then the E value for t=1.5 mm can be determined from the curve. Figure 4.23 (a) shows the comparison between the experimental test data and FE modelling results of tensile test. A 3D FE model of the uniaxial tensile test was built mimicking the tensile tests of a strip cut from the gasket sheet. The width and the length of the test sample are 20 mm and 160 mm, respectively. The dimension of the part to be clamped/pulled is 15 mm on both sides. The force displacement data is directly used for comparing experimental and FE data rather than stress-strain curves. In the FE model, the element type used is C3D8R, an 8-node linear brick, reduced integration, hourglass control element. As shown in the figure, the experimental data and the FE model showed a good agreement in particular in the lower displacement part. Figure 4.23 (b-c) shows the comparison of the experimental force-displacement data and the FE modelling results of the round type silicone rubber gasket samples and the ring type silicone rubber gasket samples in the compression tests. In both cases, the FE results showed a reasonable agreement with the tests data. The maximum error is within 10 %. Even though the overall shape of the curve is different it shows that the E value estimated is sufficient to represent the material behaviour for gasket applications under relatively simple loading and small deformation.



(a) Round and Ring samples of silicone rubber gasket used in shore hardness and compression tests.



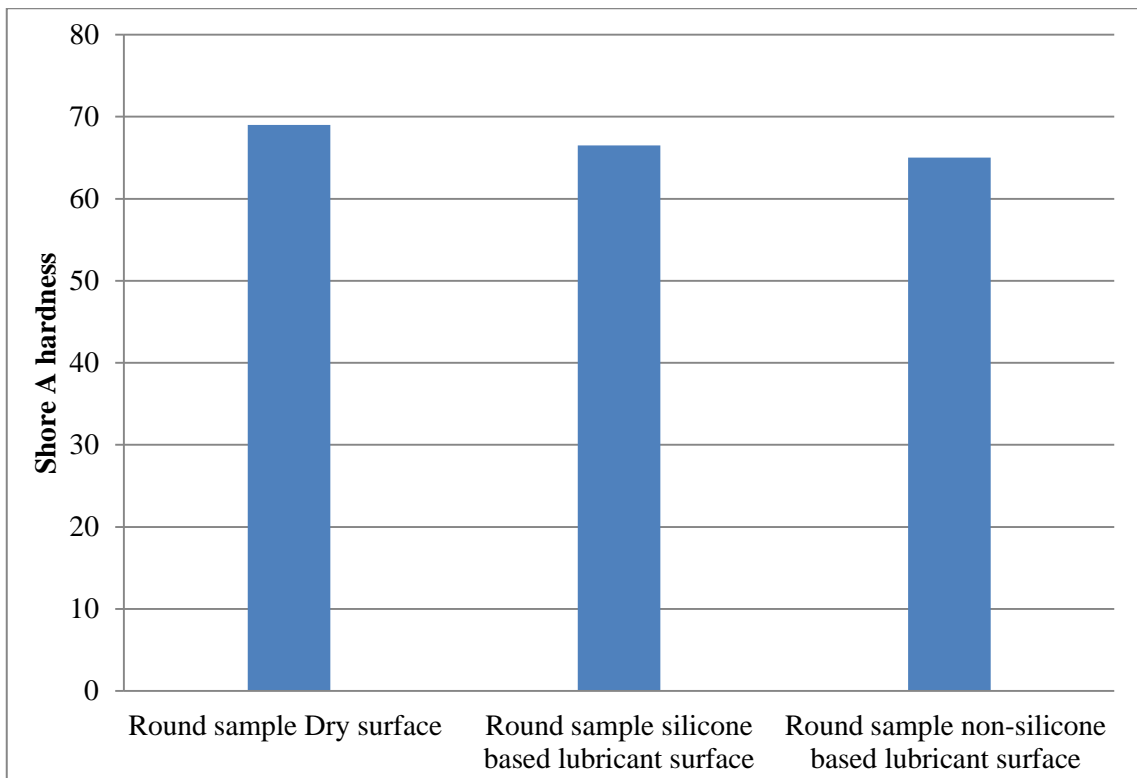
Testing position



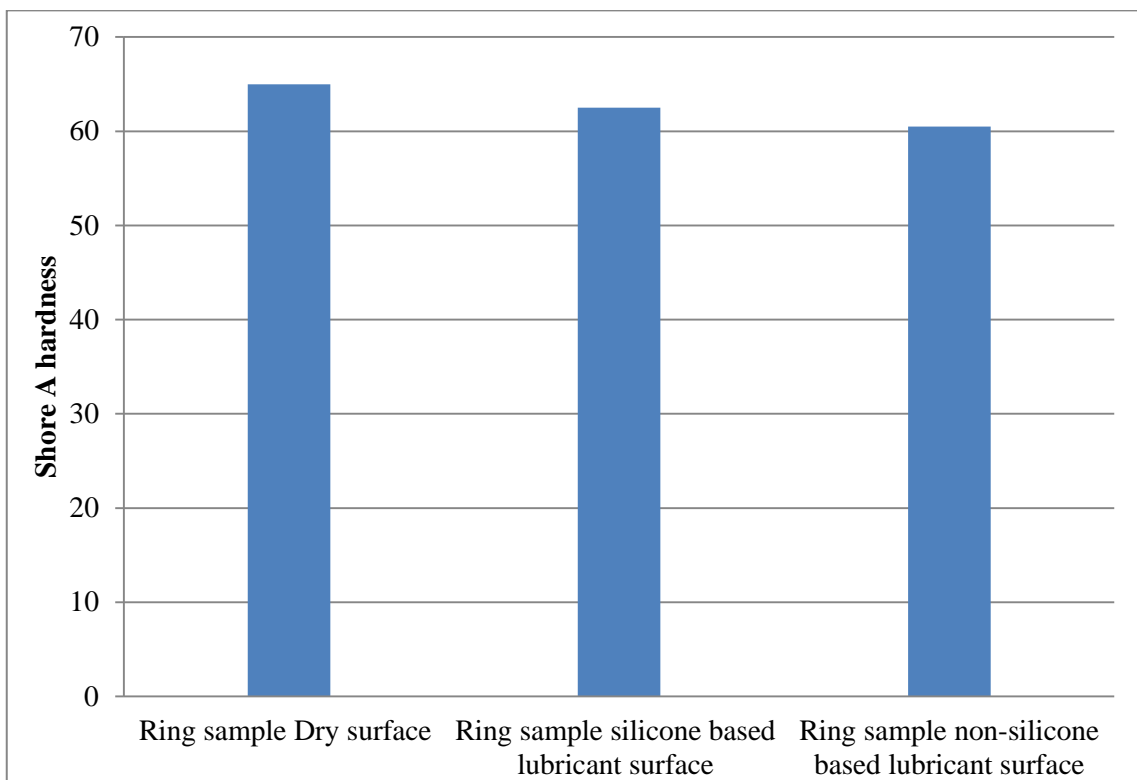
Testing position

(b) Testing position on the round sample and ring samples.

**Figure 4.20** Silicone rubber samples cut into different shapes from a commercially available gasket sheet and the shore hardness test procedure (Case 2).

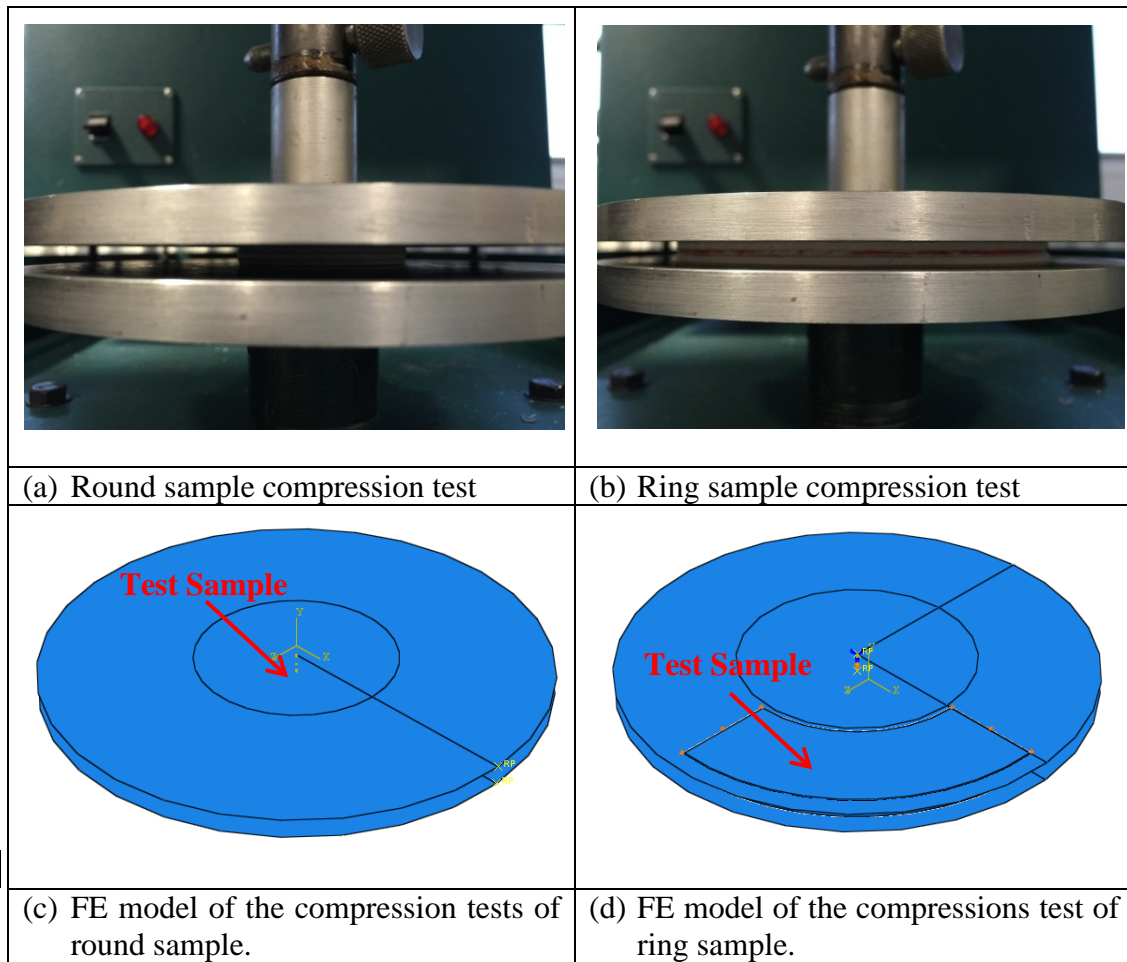


(a) Round sample

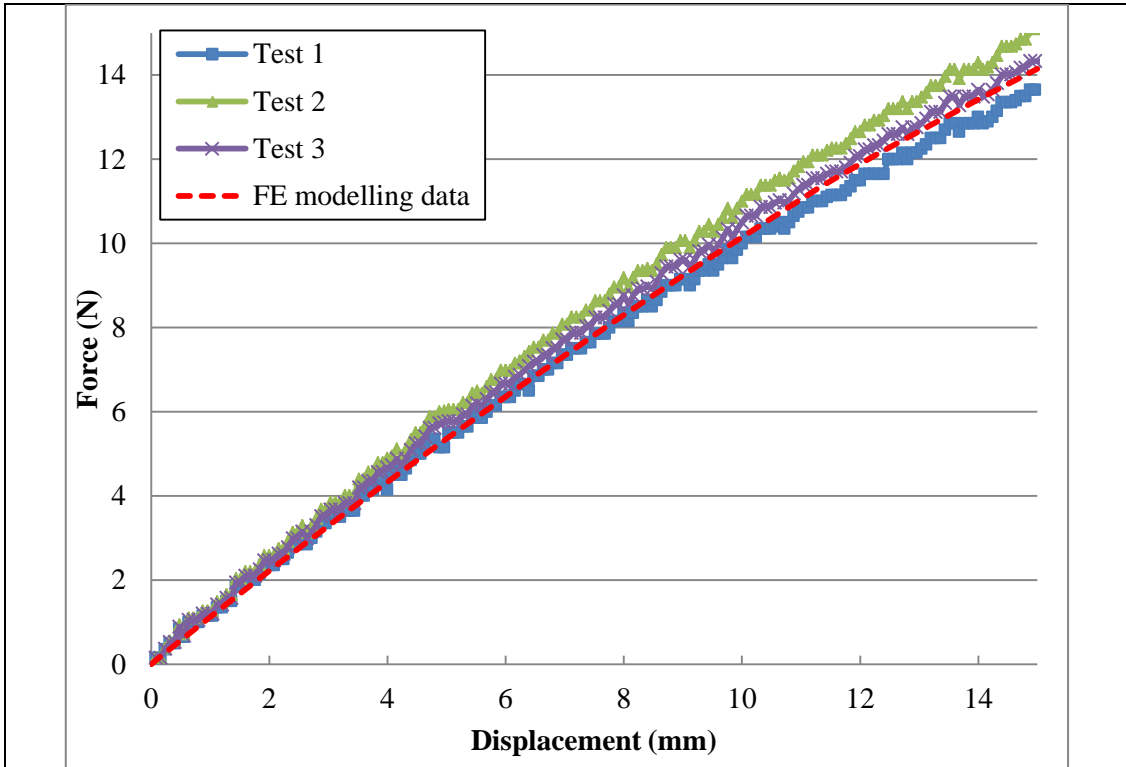


(b) Ring sample

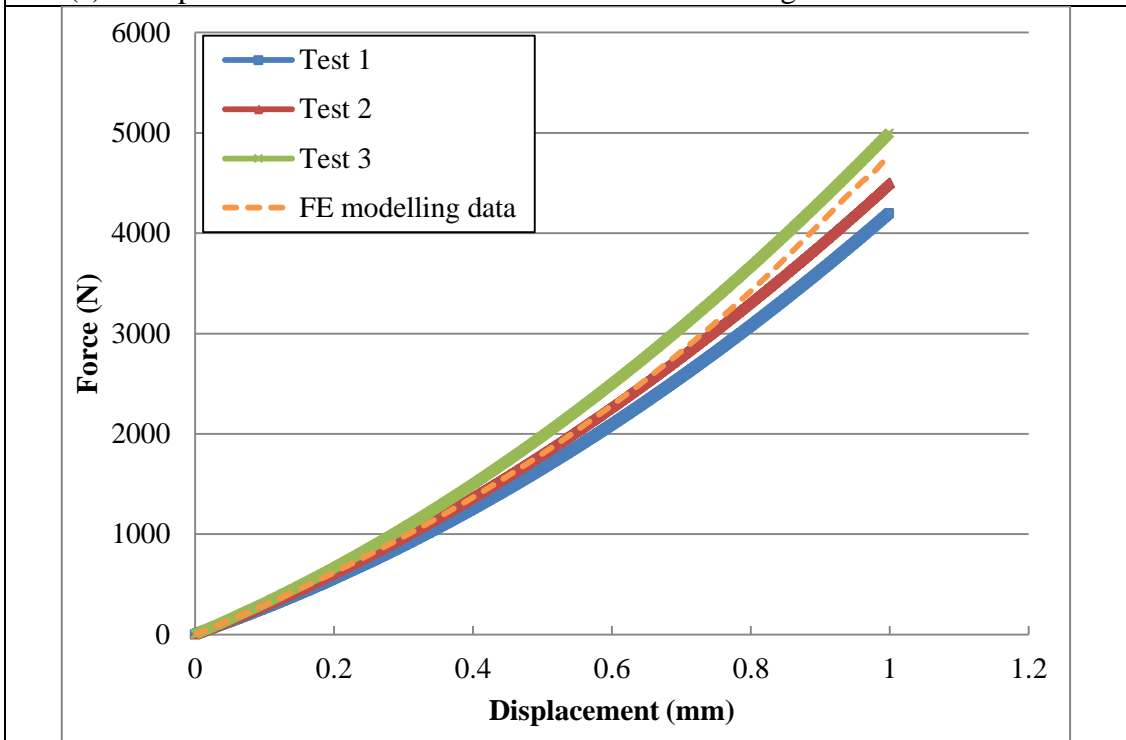
**Figure 4.21** Bar charts showing the shore A hardness of silicone rubber sheet measured with different sample shapes and lubricant conditions.



**Figure 4.22** Uniaxial compression tests of the round (a) and the ring silicone rubber gasket sample (b) and FE models simulating the tests (c & d).

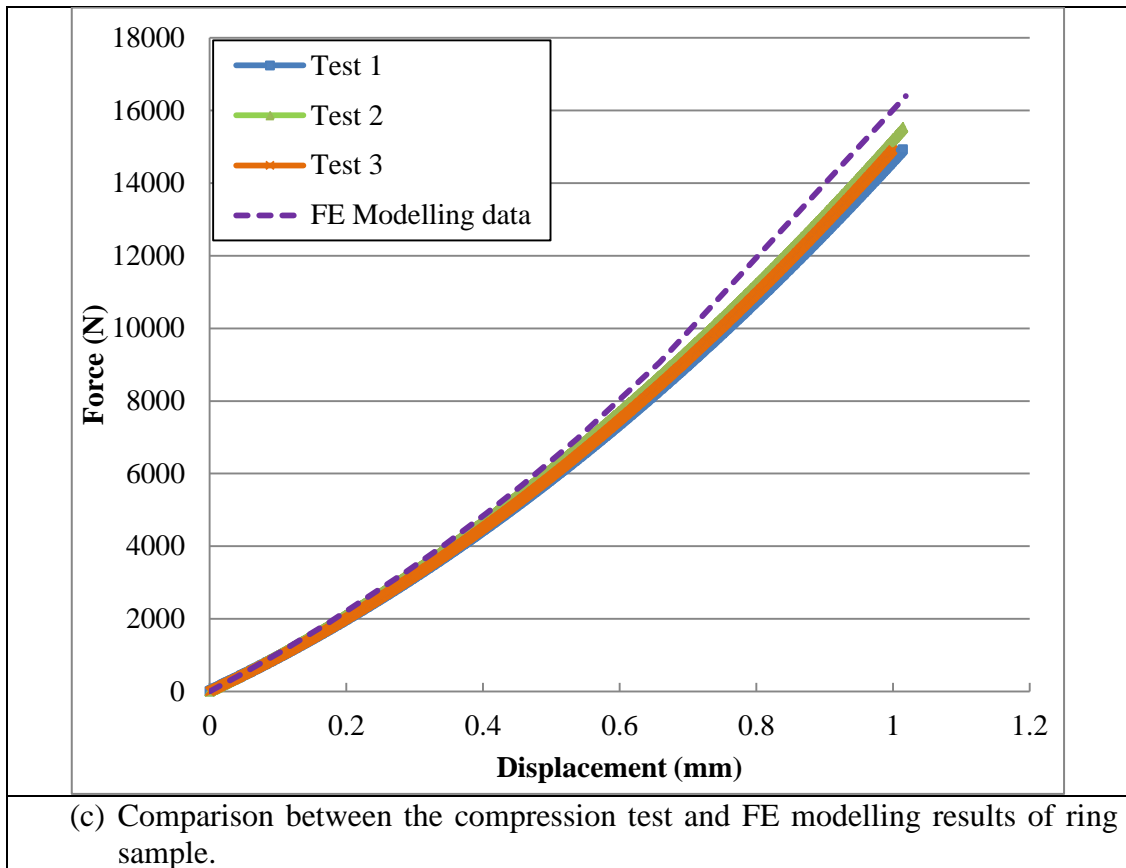


(a) Comparison of the tensile test data and FE modelling results.



(b) Comparison between the compression test and FE modelling results of round sample.



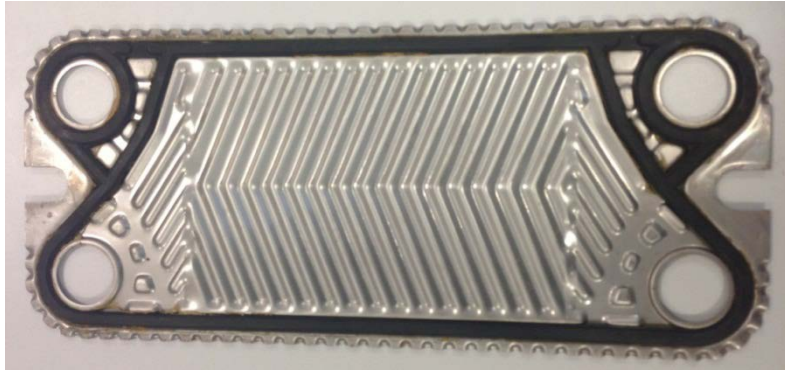


**Figure 4.23** Comparison of the experimental data and the FE modelling results of the round and ring samples of the silicone rubber gasket sample under different loading conditions.

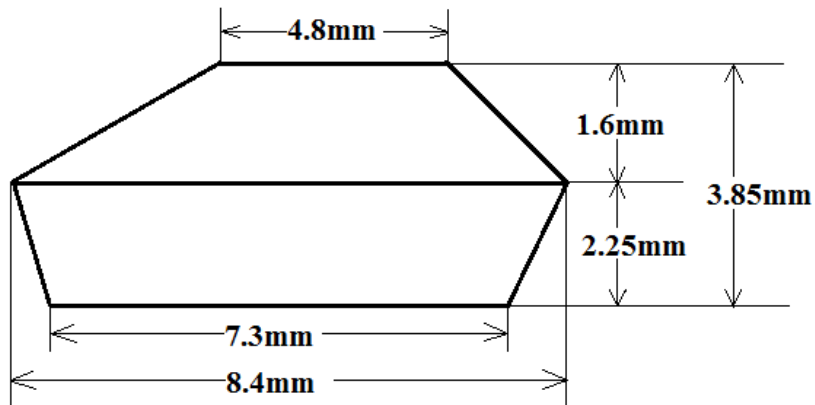
#### 4.4.3 Case 3: Testing and modelling of an EPDM plate heat exchanger gasket

Case 3 is a gasket for a plate heat exchanger, the gasket is made of an EPDM rubber. It was cut from a full gasket shown in Figure 4.24 (a). In service condition, the gasket is used in-between corrugated metal plate in the heat exchanger (PHE) for preventing leakage of the media from the channels between the plates to the surrounding atmosphere (*Schröder, 2014*). EPDM is one of the most widely used materials, other candidate materials include Viton rubber and NBR rubber. The working temperature of EPDM rubber is  $-50^{\circ}\text{C}\sim 150^{\circ}\text{C}$ . The compression set ratios of EPDM rubber, Viton rubber and NBR rubber are 30 %, 35 % and 25 %, respectively (*Chinese National Standard of Plate Heat Exchanger, NB/T 47004-2009*). Figure 4.24(b) shows the cross sectional shape and dimension of the gasket. Detailed examination has been performed, the shape of the cross-section at different location of the whole gasket is similar. The shape of the gasket is specially designed to maximise the sealing performance, which depends on the pressure of the inner edge of the gasket under compression. Some further details will be shown in the discussion chapter investigating the effects of materials properties on the sealing pressure. Given the irregular shape of the gasket, a shore hardness test is more difficult to perform than on a large specimen, as the guard of the indenter is not fully supported by the small surface area of the gasket. Figure 4.25 shows the different testing positions for the shore hardness tests evaluated in this work. Position-1 refers to tests conducted on the top surface of the gasket; position-2 refers to shore hardness tests on the bottom surface, either on the machine test or manually holding the hardness tester. The hardness values are plotted in Figure 4.25(b), which confirms that the shore hardness values are comparable under different testing positions. Shore A hardness tests have been tried on the cross section area of the gasket, which results in a similar value as the data tested on the top and bottom surfaces. These findings suggest that the material can be treated as an isotropic material in the FE model. To assess the accuracy of the E value predicted from the shore A hardness, a range of tests have been performed on the gasket specimen, as schematically shown in Figure 4.26 including a uniaxial tensile test, uniaxial unconstrained compression test on a flat plate and uniaxial constrained compression test with sample in the groove of the heat exchanger plate. All of the experimental tests were performed with a tensile test machine (Tinius Olsen H50KS Benchtop Tester, see Chapter 3). In the uniaxial tensile test, the sample was clamped to the fixtures, one of which is

pulled upward, while the other one is fixed. The deformation of the rubber gasket specimen was monitored by the crosshead movement as well as a laser extensometer. In the compression tests, there were two different setups; one was an unconstrained compression test with a flat supporting plate; the other one was a constrained compression test with the sample sitting in the groove of the PHE plate. Figure 4.27 shows the FE models of the compression tests. In the FE models, the geometry of the gasket was modelled using 3D deformable elements, C3D10H, which is a 10-node quadratic tetrahedron, hybrid, constant pressure element. The supporting plate is modelled as a 3D analytic rigid body. The displacement applied is in the range of 25 % of the total thickness of the gasket. The elastic modulus used is 12 MPa which was inversely estimated from the E-t-S<sub>A</sub> chart. Figure 4.28 shows the comparison between experimental test data and FE modelling results of the EPDM gasket sample in uniaxial tensile test (a); unconstrained compression test (b) and compression tests in the grooved heat exchanger plate (c). In all cases, the FE data showed a good agreement with the tests data. This suggests that the E values estimated from the shore A hardness tests are reasonably accurate.

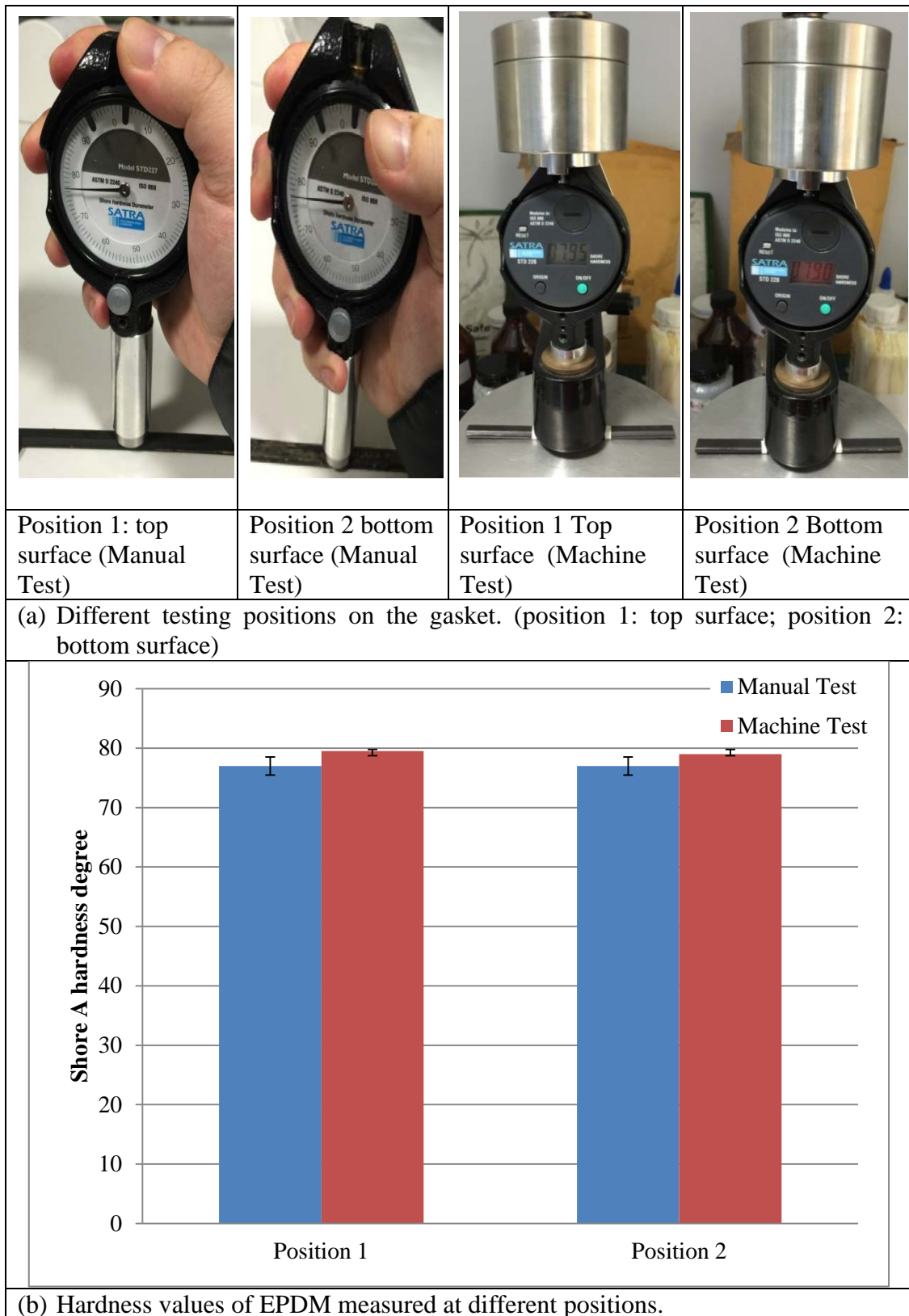


(a) Heat exchanger gasket.

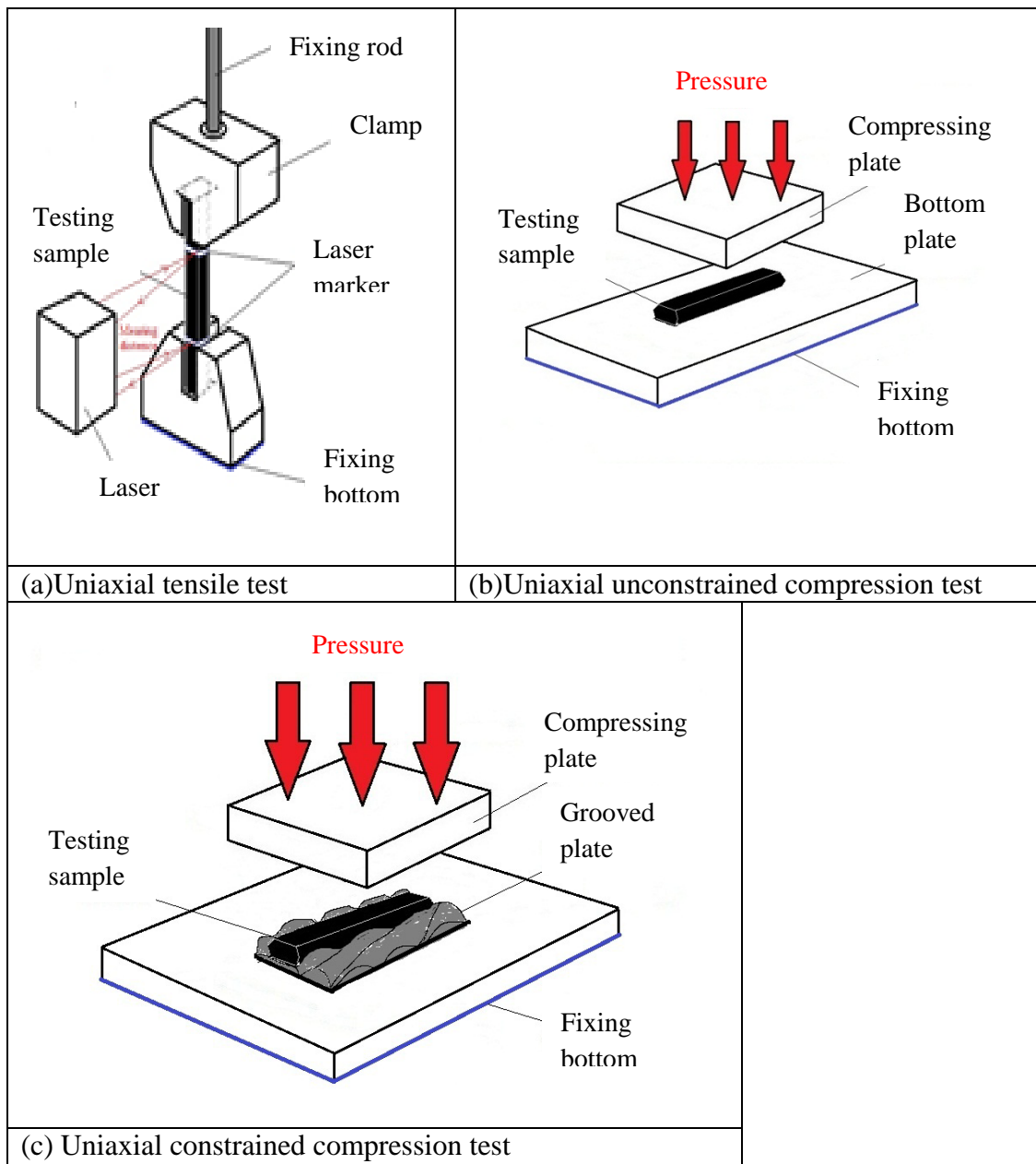


(b) Cross section shape and dimensions.

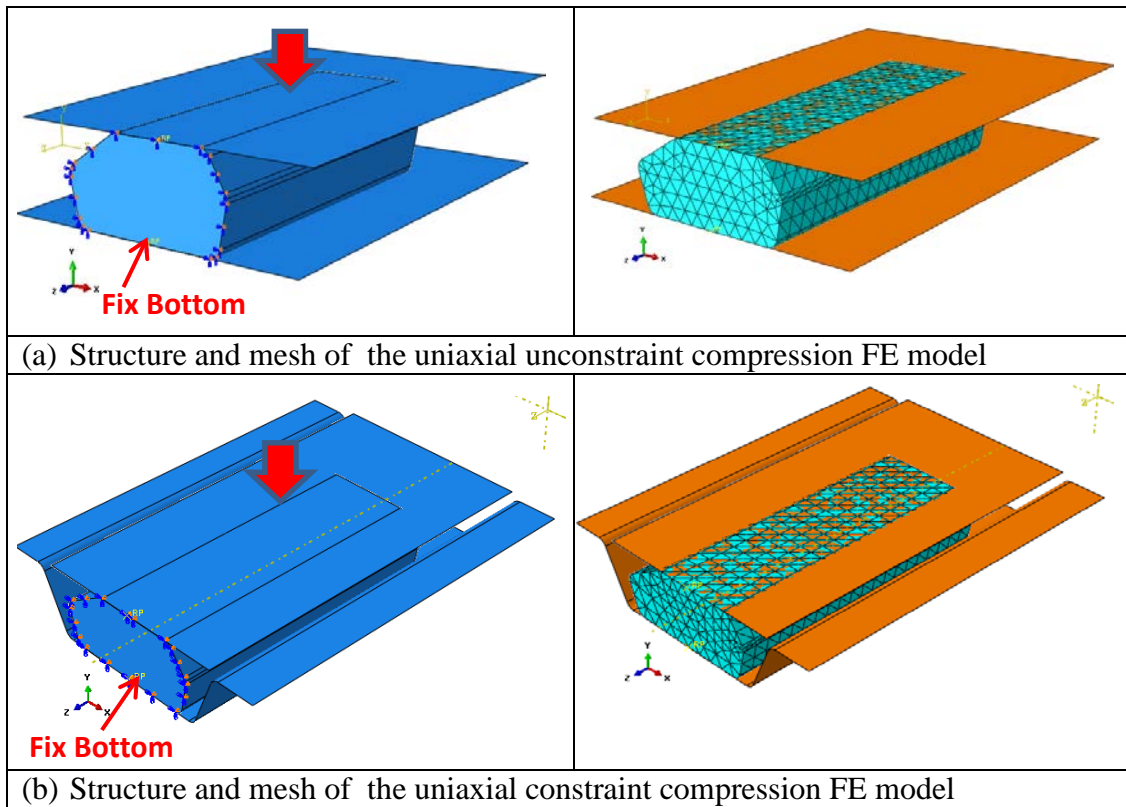
**Figure 4.24** EPDM plate heat exchanger gasket samples and the cross-section shape. The cross section shape is the same at different locations.



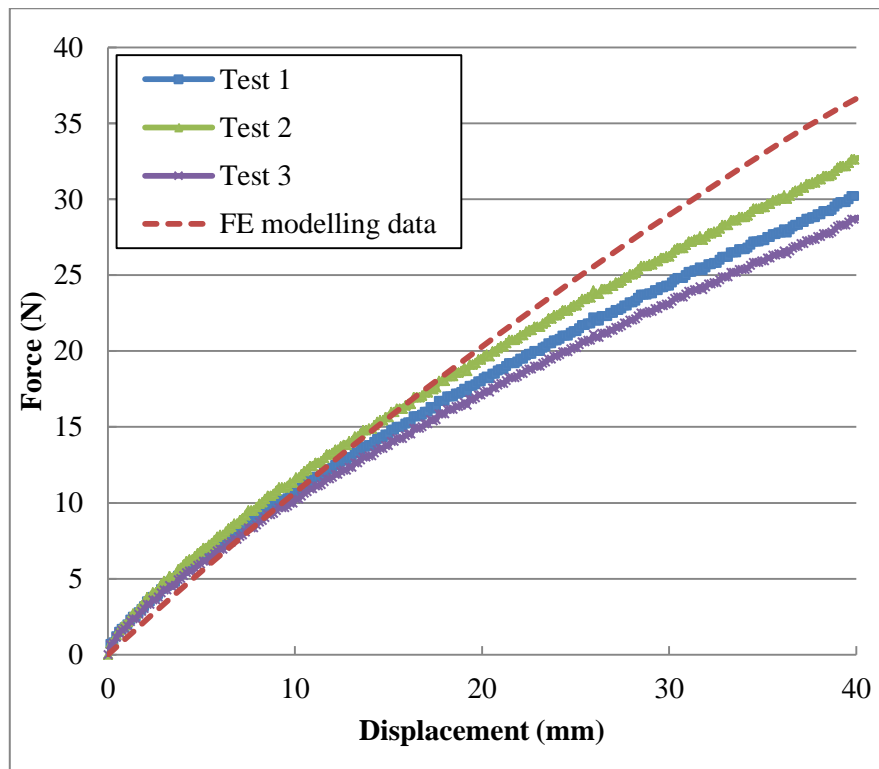
**Figure 4.25** Shore A hardness tests conducted on different planes of the EPDM plate heat exchanger gasket.



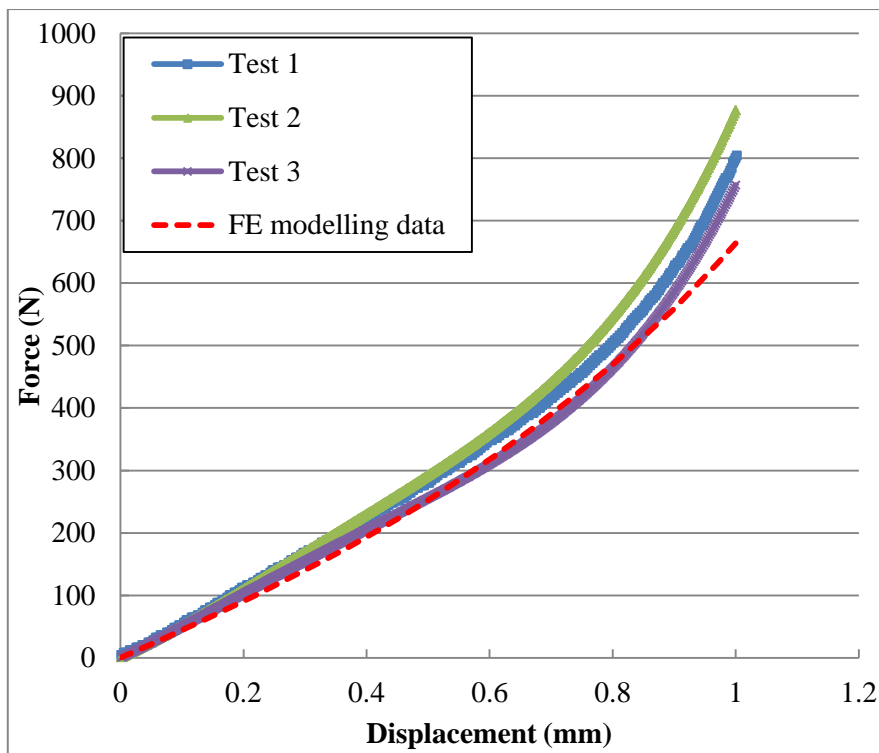
**Figure 4.26** Uniaxial tensile test, uniaxial unconstrained compression test and uniaxial constrained compression test of the EPDM gasket sample.



**Figure 4.27** FE models of the uniaxial unconstrained compression test and uniaxial constrained compression test of the EPDM plate heat exchanger gasket sample.

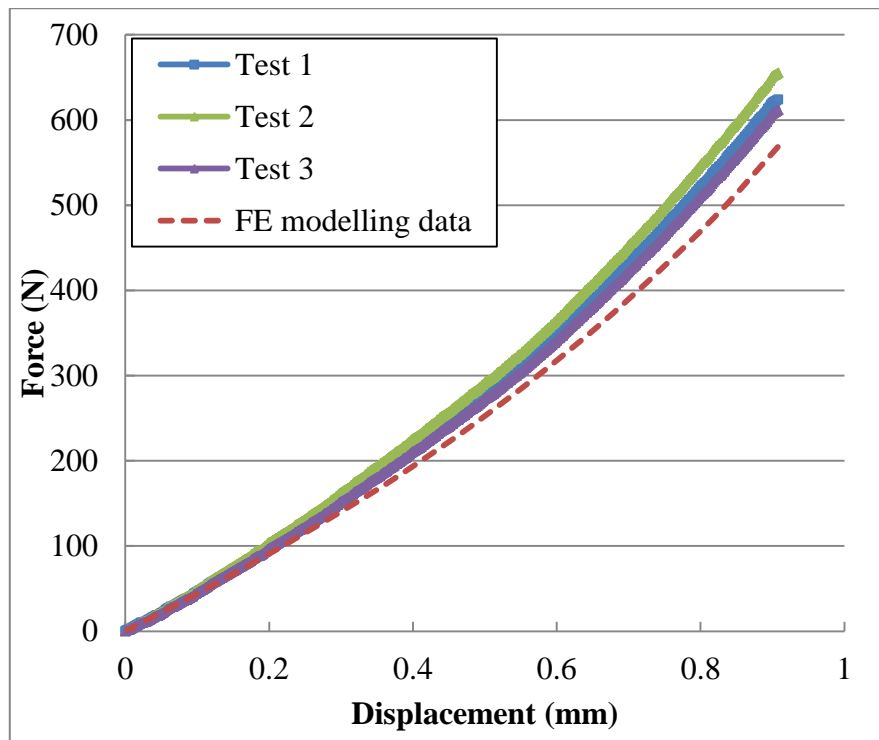


(a) Comparison between the experimental test and FE prediction of the tensile test.



(b) Comparison between the experimental test and the FE modelling results of uniaxial unconstrained compression test.





(c) Comparison between the experimental test and FE modelling results in uniaxial constrained compression test (the sample was in the heat exchanger plate).

**Figure 4.28** Comparison of the experimental test and FE modelling results of EPDM gasket under different loading conditions.

## 4.5 FE modelling of shore OO hardness tests with a spherical indenter on soft rubber materials

### 4.5.1 FE modelling of shore OO hardness tests

From the work presented in the last section, it is a viable way of estimating the E values from the shore A hardness values. However, it is known that shore A is not suitable for soft rubber (*Guide to UV light curing technology, Dymax Corporation*), normally it is used when shore A hardness of the material is between 20-90 (*ASTM D2240-05*). Based on trials with FE modelling, when the shore A hardness value is lower than 30, the change of shore A hardness is not very sensitive to variation in the E values. This made shore A hardness not suitable for characterising soft rubbers. When the shore A hardness value is lower than 30, the material group involved is more likely to be a gel, which is not the material group focus of this work. In addition, in preliminary works, when the rubber is too soft the shore A indenter could puncture/penetrate the material. One potential approach for soft rubber is to use a blunt indenter, such as spherical indenter which may potentially avoid these problems. One suitable option within the shore hardness system is shore OO hardness. With spherical indentation, most of the published works in inverse property identification were based on data from continuous indentation, it is important to evaluate the feasibility of such a process based on a single indentation value (e.g. shore OO hardness values) on thick and thin samples. This is particularly important as many soft rubbers are used in a form of thin structures rather than a bulk block form.

Figure 4.29 (a) shows the close up view of the shore OO indenter tip and key dimensions. The shore OO hardness indenter is a spherical indenter with a radius of 1.19 mm. Figure 4.29 (b) shows the FE model of shore OO hardness test on a sample with a standard thickness (6 mm). Similar to the previous indentation FE model of shore A hardness, the indenter (hardened steel) is much stiffer than the samples. The element type, CAX3 (an axisymmetric element), is used with finer meshes being applied around the indenter to improve the modelling accuracy and efficiency. In the initial FE model, the width of the model was set as 12 mm, the thickness is 6 mm (*ASTM D2240-05*). Contact is defined between the supporting platform and sample similar to the situation commonly encountered in a real test. The platform is

modelled as an analytically rigid body. In the model, the bottom plate was fixed in all directions using the Encastre condition. The friction coefficient is set as 0.1. This is commonly used in rubber and metal surface contact (*Bensia et al., 2012*). Detailed work on sensitivity of friction is to be discussed in a later section. Mesh size effects have been performed to assess the effect of the element sizes on the force-displacement data, the final mesh size for the region underneath the indenter is 0.1mm. The results of the mesh sensitivity tests are not shown to preserve clarity and avoid repeatability.

Figure 4.30 shows the FE modelling results of force displacement data in comparison with the prediction of a known analytical solution, which is valid for large samples (elastic half space). The equation is as the following (*Johnson, 1985*):

$$F = \frac{4ER^{1/2}h^{3/2}}{3(1-\nu^2)} \quad (4.2)$$

where  $E$  and  $\nu$  are the Young's modulus and Poisson's ratio of the indented material, respectively, and  $R$  is the radius of the rigid indenter.  $h$  is the resulting indentation depth and  $F$  is the applied force on the rigid indenter. As shown in the figure, the trend of the FE modelling results is in a good agreement with data based on the analytic solution. The FE modelling results and the analytical solutions were very close until the displacement of 0.5 mm. After the displacement of 0.5 mm, the indentation force of the FE modelling results is slightly higher than the forces of the spherical analytic solution. The difference between both data was within 5 %. Similar agreement could be observed with other material properties. This shows the FE result is sufficient and accurate. Figure 4.31 shows a typical displacement field underneath the indenter and force-displacement curve. As shown in the figure, the indentation depth corresponds to the force for shore OO hardness (1.1 N) is determined from the P-h curve. The shore OO hardness is then calculated following equation (*Johannes et al., 2006*):

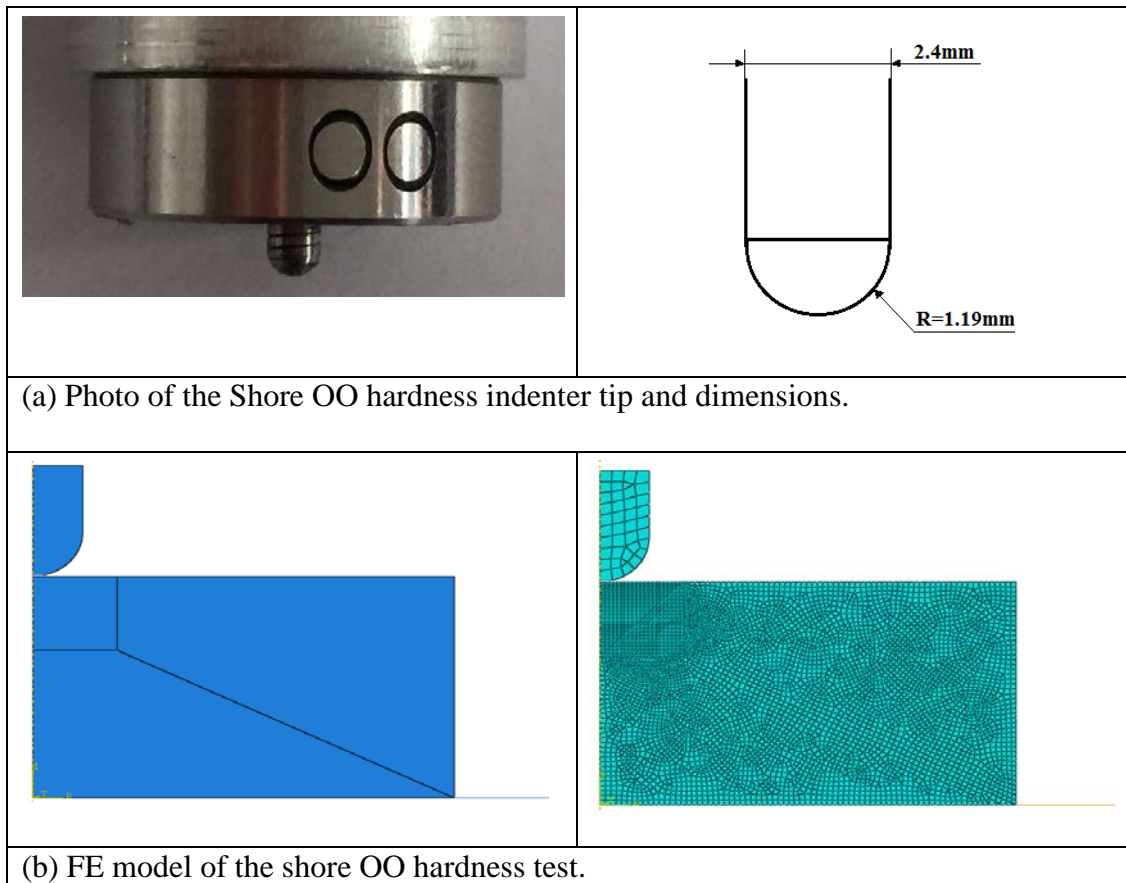
$$S_{OO} = 100 - 40 * h \quad (4.3)$$

where  $S_{OO}$  is shore OO hardness and  $h$  is the indentation depth at force of 1.1 N.

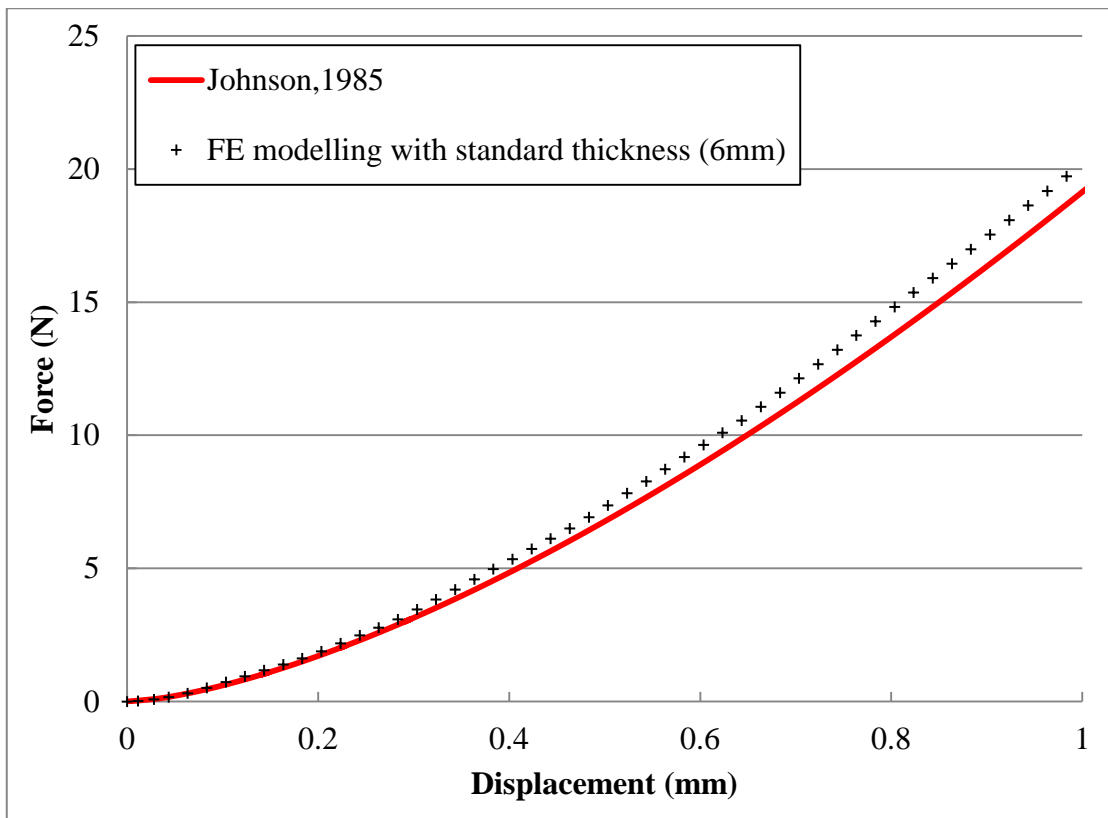
Figure 4.32 shows the correlations of shore OO hardness values and Young's modulus for a thick sample (6mm in thickness) in comparison with results predicted based on the analytical solution for spherical indentation. In the parametric FE studies, the Young's modulus range was varied from 1 MPa to 10 MPa, the corresponding range of the shore OO hardness value is between 70 and 94. This is a range commonly used in industries for rubber related products (*Hardness for Rubber Rollers, Imperial rubber products Inc.*). As shown in the figure, the shore OO hardness increased with the Young's modulus. When the E value is over 8 MPa, the shore OO hardness changes at very small scale with increasing E values. This suggests that the shore OO tests will not be very sensitive to the intrinsic materials property change after 8 MPa. This might be the reason why different shore hardness tests have to be designed in order to avoid this limitation. At lower E values, the error between the shore OO FE modelling results and the spherical analytical solutions was 4 % for most of the material property range, the minimum error between the shore OO FE modelling results and the spherical analytical solutions was 1 %. This suggests that E value can be correlated to shore OO hardness for thick samples with a standard thickness (6 mm or over). The FE model of shore OO hardness is extended to thinner samples of different thickness, where the analytical solution becomes invalid. Figure 4.33 shows the correlations between apparent shore OO hardness values (this represents the reading of the hardness tester) for samples with different thicknesses against the Young's modulus in the FE models. The sample thickness includes 1, 2, 3, 4, 5 and 6 mm. In each case, a new FE model is developed with a corresponding sample thickness. Details of the modelling process and associated mesh sensitivity tests are not shown to preserve clarity.

The figure (Figure 4.33) shows several important observations of the thickness effects. Firstly, similar to the case for thick sample as shown in Figure 4.32, in all the thicknesses, the effect of E is more significant when E is between 1-8 MPa than the cases when E is over 8 MPa. Secondly, at higher E values, the effect of thickness is much less significant. At E=10MPa, the shore OO hardness value for 1 mm and 6 mm is 95 and 94 respectively, representing only a 1 % difference. However, at the end for softer rubbers, with E=2 MPa, the difference in hardness is much more significant. The shore OO hardness value for t=1 mm is 88.6, about 8 % harder than the hardness for t=6 mm. Thirdly, at higher E value, the shore OO hardness for thickness

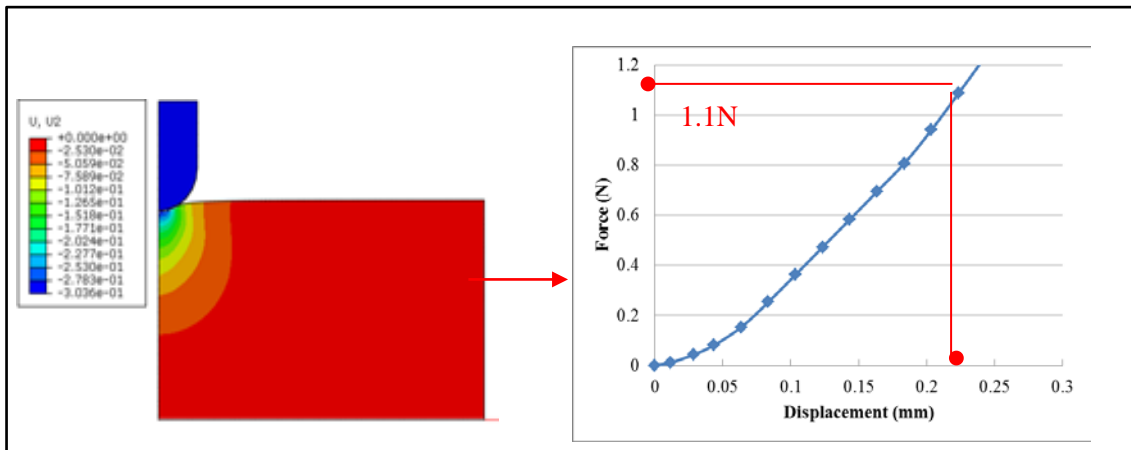
of 3, 4, 5, and 6 mm is almost identical. In other words, thickness will not have a significant effect at this material property range and a thin sample can be used depending on the availability. This could be a significant advantage in a situation where a thick sample is not available or when making a thick sample is more costly in terms of materials cost with expensive materials. On the other side, the less significant influence of thickness means that the testing results will be relatively robust when there is uncertainty with the thickness for hard samples. But for soft materials, any uncertainty of the thickness may directly influence the shore OO hardness results. These data clearly show that there is a link between E value and the shore OO hardness, which can be used to determine E values of a material based on the shore OO hardness values from samples of different thicknesses. This Young's modulus-thickness-shore OO hardness chart (E-t-S<sub>OO</sub> chart) is to be assessed in the next two case studies. One is on a soft silicone rubber, one is a latex rubber, and both materials are made in the laboratory.



**Figure 4.29** FE model of the shore OO hardness test on samples of standard thickness.

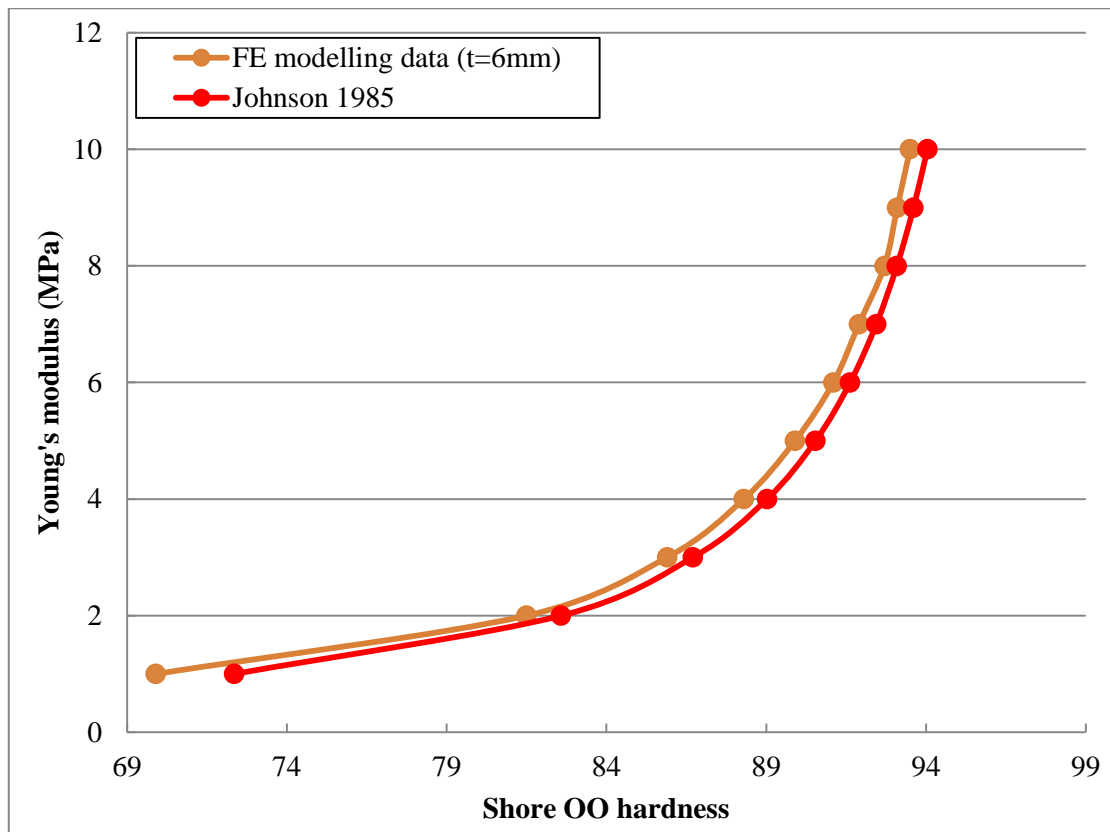


**Figure 4.30** Comparison between P-h curves of shore OO indentation from FE modelling and the analytical solutions.

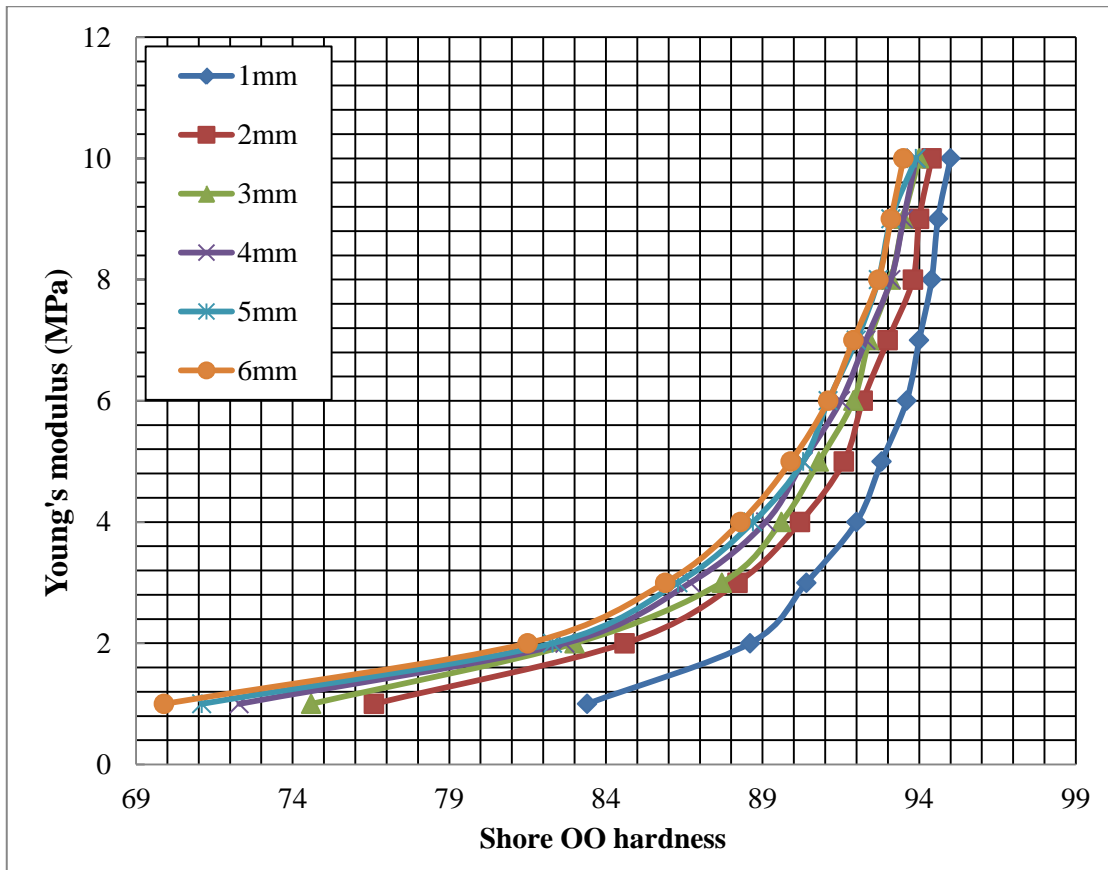


**Figure 4.31** Typical force-displacement curve with a shore OO indenter and the procedure to determine the displacement point corresponding to the load for shore OO hardness ( $E=5\text{MPa}$ ).





**Figure 4.32** Correlation of shore OO hardness values and Young's modulus based on FE data and analytical solution for spherical indentation of thick samples (*Johnson, 1985*) (t=6mm).

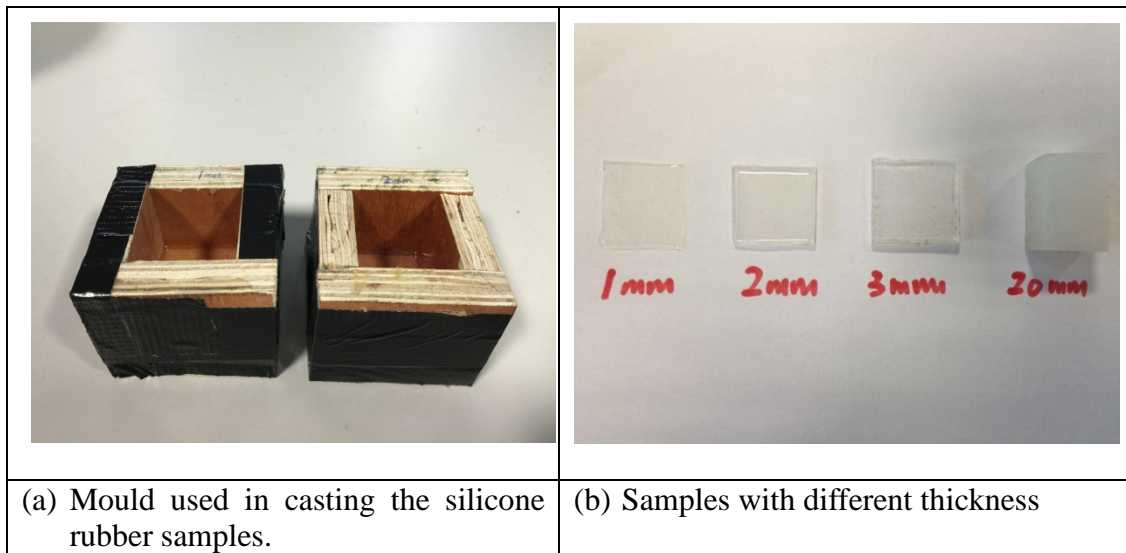


**Figure 4.33** Correlation of shore OO hardness values and Young's modulus based on FE data on samples of different thicknesses.

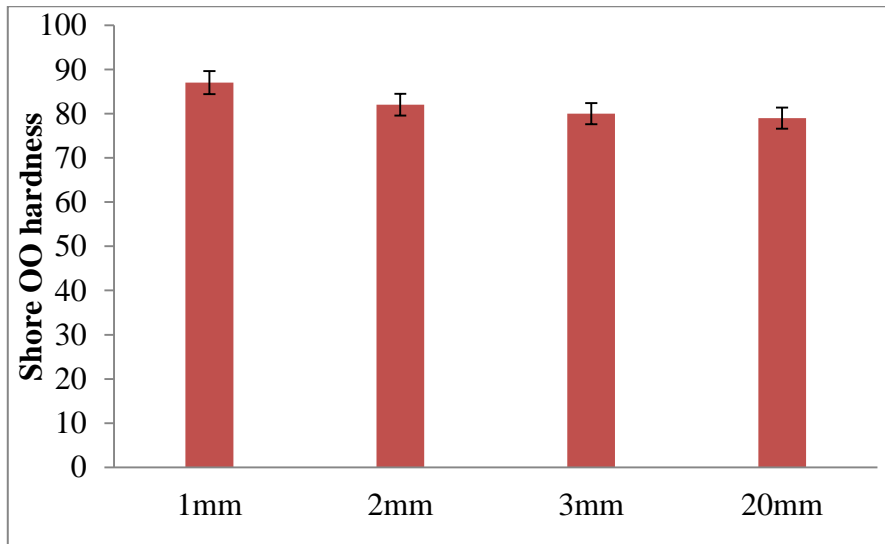
#### 4.5.2 Application of shore OO hardness–E relationship on silicone rubber

To assess correlation between the shore OO hardness and material properties, a softer silicone rubber sample has been made in the laboratory. The work used the same resin system (as in the case 1 for shore A hardness) but different ratio between part A and Part B of the resin. The thickness of the samples is 1, 2, 3 and 20 mm, respectively. The thicker sample is later used in the compression tests of the same material to assess the accuracy and limitation of the E value estimation. Figure 4.34 shows the mould used and samples produced. Figure 4.35 plots the hardness values for all the samples. Each data is the average of more than 6 tests and the error bars represent the standard deviation. As shown in the figure, the shore OO hardness values are much higher for the thin sample than the thick sample. Based on these hardness values, the E values are evaluated using the E-t-S<sub>OO</sub> chart (Figure 4.33). Figure 4.36 plots the predicted E values based on the shore hardness values for the soft silicone rubber samples with different thicknesses. There are some variations of the E values, but in general the E values from different samples fall within a similar range. The average Young's modulus could effectively be used to represent the properties of the material.

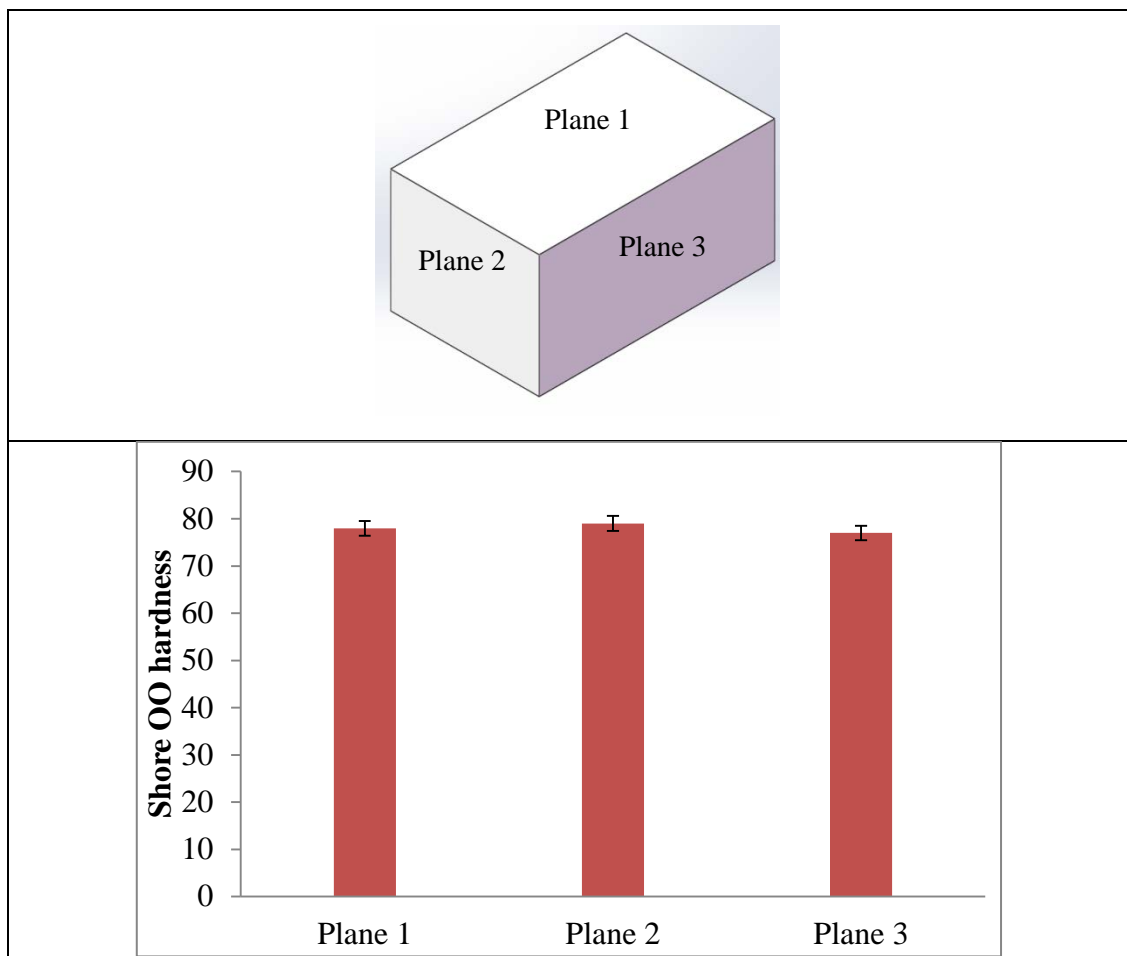
To assess the accuracy of the prediction of Elastic modulus, compression tests on the thick sample have been performed. Given this is a nonstandard sample from which it is difficult to derive the stress strain curve directly, a FE model has been developed mimicking the compression test. In the FE model, the averaged Young's modulus from the shore hardness tests is used (Figure 4.36). Figure 4.37 shows the comparison of the experimental data and FE modelling results of the compression test. As shown in the figure, the FE predicted compression force displacement curve is in a reasonable agreement with the test data, which suggests that the E value predicted is reasonable and accurate.



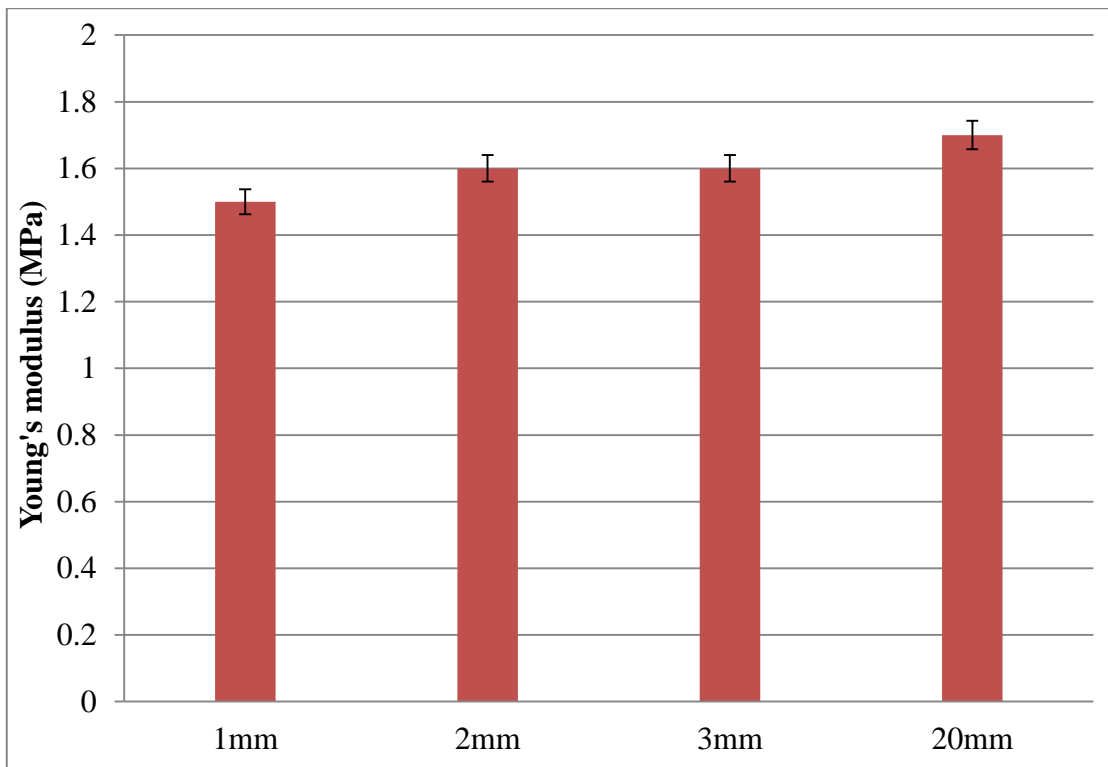
**Figure 3.34** Soft silicone rubber samples with different thicknesses.



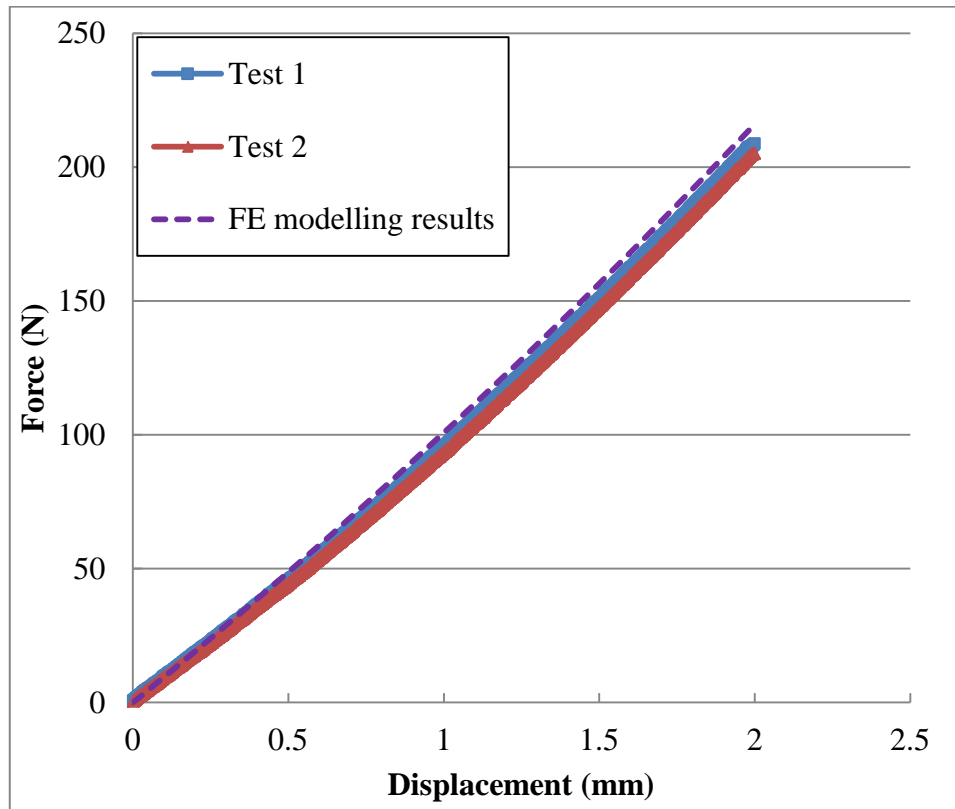
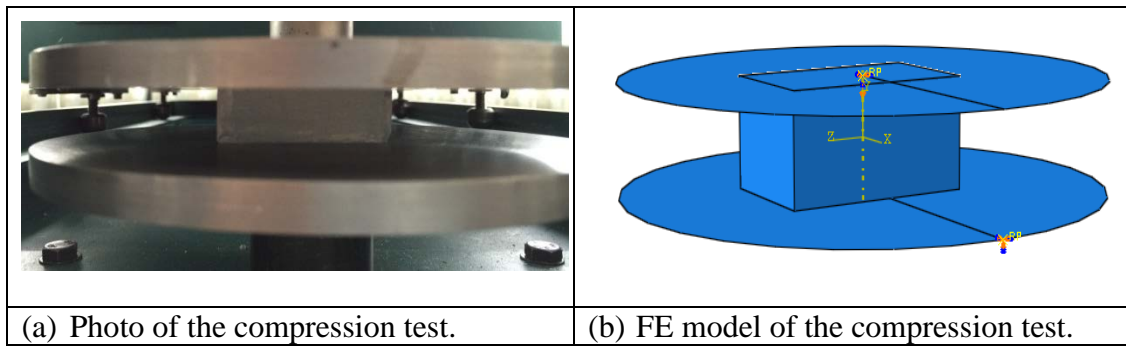
**Figure 4.35 (a)** Measured hardness values of silicone rubber of different thickness.



**Figure 35 (b)** Measured hardness values of soft silicone rubber when tested on different planes of the thick sample.



**Figure 4.36** Predicted E values based on the shore hardness of silicone rubber with different thickness.



(c) Experimental and FE data of compression tests.

**Figure 4.37** Comparison of the experimental compression test and FE modelling results based on the elastic properties predicted from shore OO hardness tests. ( $E=1.6\text{MPa}$ , averaged based on the data in Figure 4.36).

### 4.5.3 Shore OO hardness tests of latex rubber and properties estimation

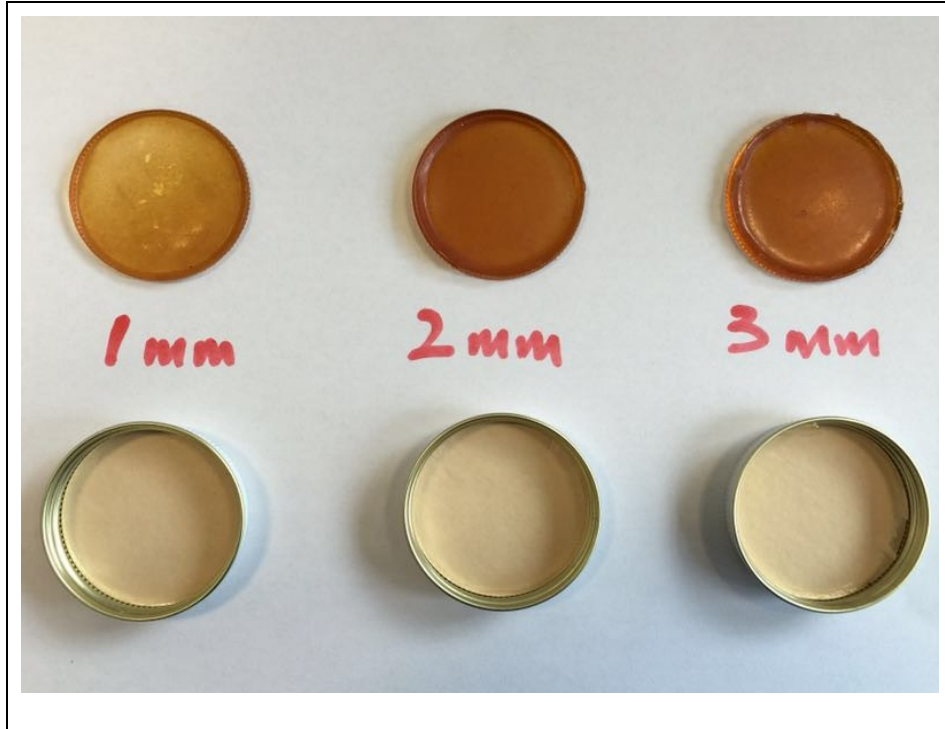
Another case to assess the validity and the accuracy of the estimated E values from shores OO hardness to be presented is on a latex rubber. Latex rubber is widely used in many applications from medical to food industries. They are much softer than rubbers such as EPDM. The latex rubber tested in this part has been used in other projects, so the Young's modulus and nonlinear hyperelastic properties are known, including the uniaxial and planar tests, which are used to derive the parameters different strain energy functions such as the Mooney Rivlin and Ogden models. This will provide an opportunity to assess the accuracy of the E value estimated from the shore OO hardness. It also provides a case to assess comparatively the prediction of shores OO from both linear elastic and hyperelastic properties based on the test data of the same sample.

Figure 4.38 shows the samples of different thicknesses for shore OO hardness tests. The three thicknesses used are 1, 2 and 3 mm. Due to the large contraction in volume associated with latex rubber in the moulding process, it is difficult to produce thicker samples. Trials in making thicker samples resulted in an uneven top surface. The measured hardness values of the three latex rubber samples are shown in Figure 4.39. The error bars represent the standard deviations of at least six tests. It shows that there is a slight difference between the thin and thick samples, but the hardness values are in a reasonably close range. The Young's modulus is estimated based on the shore OO hardness values, the results are plotted in Figure 4.40. It clearly shows that the estimated E values are in a reasonable range of the Young's modulus from the uniaxial tensile tests (1.25MPa). Figure 4.41 shows the comparison between the FE predicted hardness values of different thickness samples with the estimated E value, original shore hardness data and FE prediction based on nonlinear hyperelastic properties from combination of shear (planar) and tension tests (Ogden hyperelastic model) (Aw, 2015). The hyperelastic strain energy model chosen is the 1st order Ogden model in the FE model simulation.

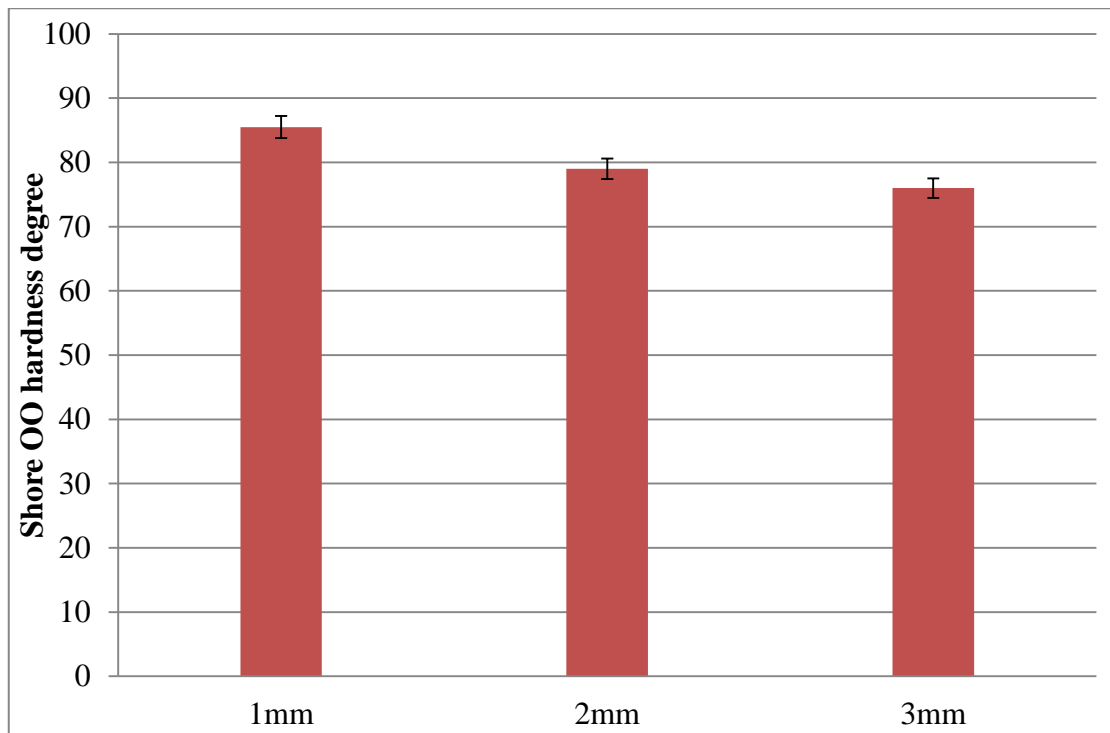
$$W_O(\lambda_1, \lambda_2) = \sum_{p=1}^N \frac{\mu_p}{\alpha_p} (\lambda_1^\alpha + \lambda_2^\alpha + \lambda_1^{-\alpha} \lambda_2^{-\alpha} - 3) \quad (4.4)$$



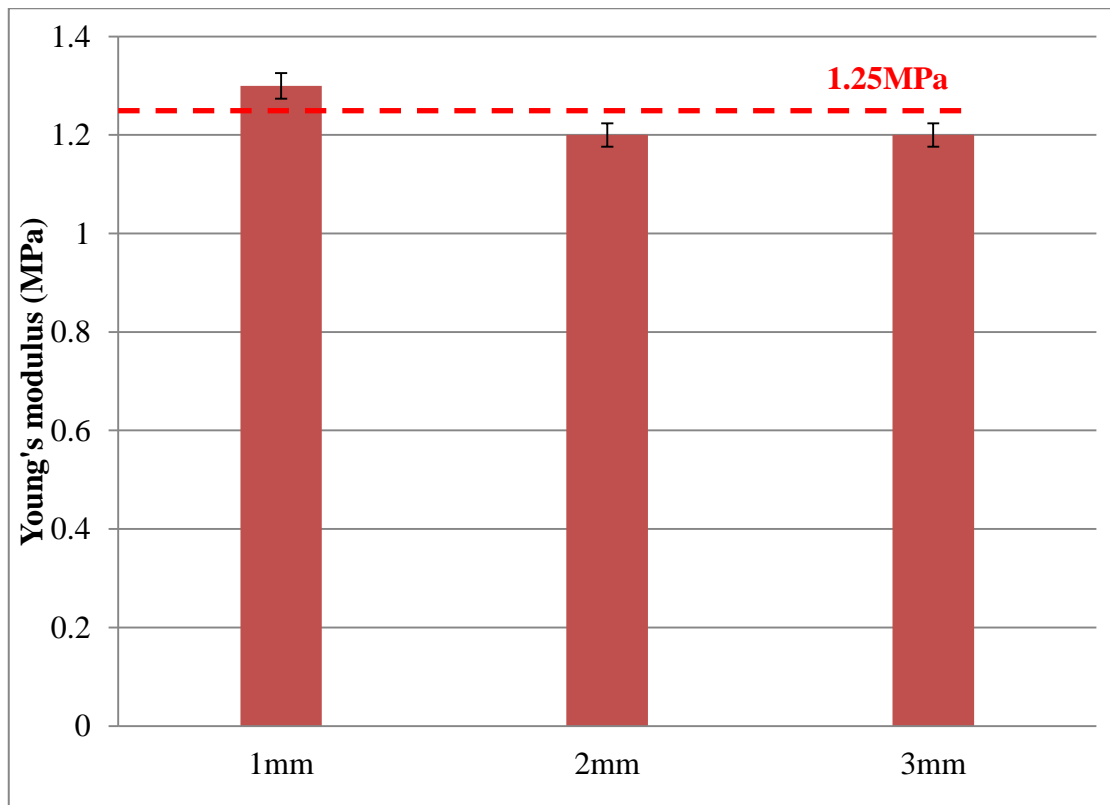
Where  $N$  is the model's order and  $\mu_p, \alpha_p$  are material parameters to be determined experimentally.  $\lambda_1^\alpha, \lambda_2^\alpha$  are the deviatoric principal stretches (*Ogden, 1972*). There are many hyperelastic models suitable to predict the shore OO hardness. The Ogden model is chosen that it may provide a mean to inversely predict the hyperelastic properties, while other models (e.g. Mooney Rivlin model) are known to suffer from non-uniqueness (*Aw, 2015*). As shown in the figure, the FE predicted shore hardness values based on the estimated  $E$  value is comparable to the prediction based on complex hyperelastic model for all sample thickness. This suggests that the elastic model based on Young's modulus is sufficiently accurate in modelling the shore OO hardness tests. This is linked to the way that the shore OO hardness is defined and the operative range of hyperelastic models. This is to be further analysed in the discussion in chapter 5.



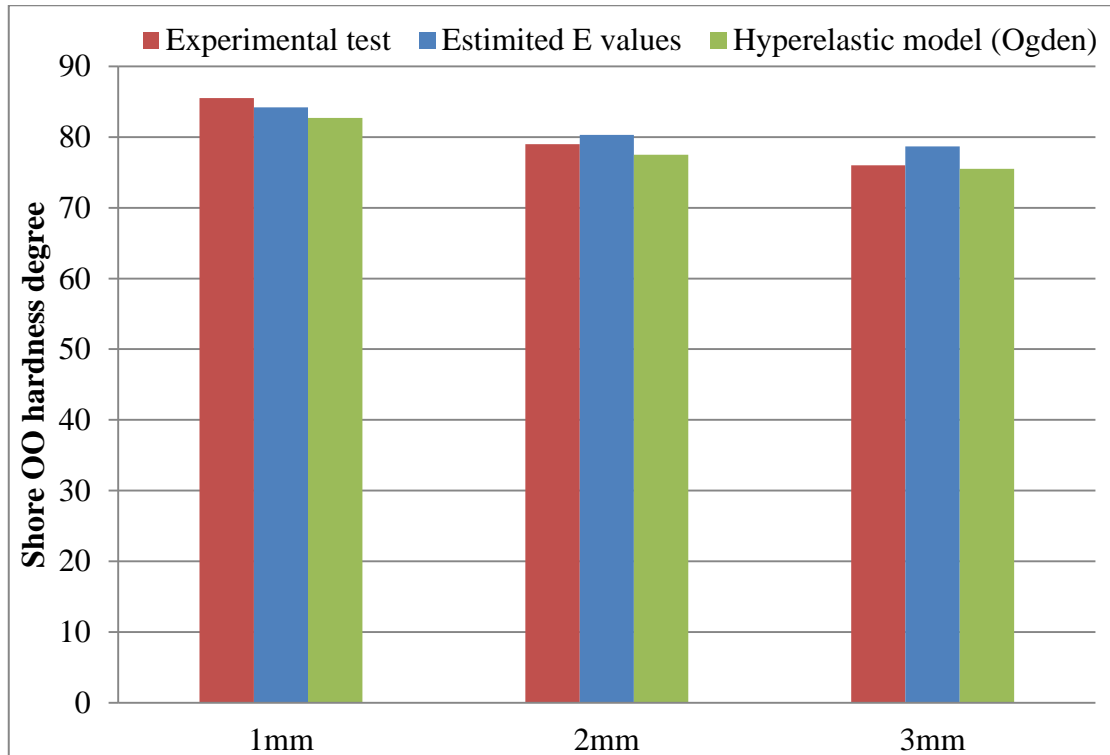
**Figure 4.38** Photos of the latex rubber samples of different thickness for the shore OO hardness tests.



**Figure 4.39** Measured hardness values of latex samples of different thicknesses.



**Figure 4.40** Predicted E values for latex samples of different thicknesses.



**Figure 4.41** Comparison between the FE predicted hardness values of different thickness samples with the estimated E values, testing data and FE prediction based on nonlinear hyperelastic properties from combination of shear (planar) and tension tests (Ogden model).

#### **4.6 Use of ANN to estimate material properties in inverse analysis and predict shore hardness through direct analysis**

From the work presented in the last few sections, the FE models developed have been successfully used in establishing the correlation between the shore hardness and linear elastic properties in both hard and soft rubbers relevant to gasket applications. The case studies show that the approach is a suitable method to estimate the Young's modulus with sufficient accuracy for these applications. In practical cases, rubber products may be supplied by all thicknesses with unknown properties, a guess or interpolation has to be made to be able to use the Elastic modulus, thickness and shore hardness chart. An automatic program to directly give the values will be of practical benefit. One potential approach is to explore the use of ANN based approach to evaluate its effectiveness/feasibility in (1) estimating materials properties from shore hardness tests; (2) predicting the shore hardness if the material properties and thickness are known. For an ANN program, the key is to be able to provide sufficient data to train evaluate and test the program, this might be difficult to purely rely on experimental data as it will be costly in terms of materials and time. But with the validated FE models developed, much more data can be produced to train and evaluate the ANN. This section will briefly present some key results.

Figure 4.42 (a) shows the proposed feed-forward neural network with back propagation algorithm for estimating the elastic material properties (E) from shore hardness data. The shore A & shore OO hardness value for six different sample thicknesses are used as the input training data. The corresponding linear elastic moduli are used as the output values. Two hidden layers are used, layer 1 uses the tan-sigmoid transfer function (TANSIG) and layer 2 uses the linear transfer function (PURELIN). The number of neurons is optimised by comparing the error of predicted and target values in the training. The accuracy is to be checked in following three stages. (1) Firstly the accuracy of the program in predicting data used in the training, then (2) the accuracy of the program in predicting data (generated from additional FE models) not used in the training. (3) Then the program is used in predicting E values based the shore hardnesses in real tests with realistic sample dimensions.

The performance and validation of ANN in certain way depends on the quality and density of the data. Table 4.1 lists the training and output data used for the ANN for

shore A hardness. As shown in the table, the Young's modulus is ranged from 3 to 20 MPa, the thickness is ranged from 1 mm to 6 mm (similar to the data range in Figure 4.15). There are 108 points in total for the training and output data. The last additional 20 data points are randomly picked, to be used as evaluation data with Young's modulus between 4, 6, 8, 10 and 12 MPa and the sample thickness from 1.5 mm to 4.5 mm. For each material property set, the numerically predicted force-displacement data were fitted with polynomial curve fitting, the curve coefficient is then used to calculate the displacement at the specific force for shore hardness test. Thus the corresponding shore hardness, sample thickness and E values is established and systematically used in ANN.

**Table 4.1** Training and output data for the ANN shore A hardness tests.

Training and output data															
No.	E	t	S <sub>A</sub>	No.	E	t	S <sub>A</sub>	No.	E	t	S <sub>A</sub>	No.	E	t	S <sub>A</sub>
1	3	6	31.9	40	6	4	61.9	79	9	2	75.2	118	12	2.5	80
2	4	6	46.2	41	7	4	66.4	80	10	2	76.6	119	4	3.5	48.3
3	5	6	54	42	8	4	68.8	81	11	2	79	120	6	3.5	61.5
4	6	6	60	43	9	4	70.8	82	12	2	80.6	121	8	3.5	69.2
5	7	6	64.4	44	10	4	73.2	83	13	2	82	122	10	3.5	74.4
6	8	6	67.6	45	11	4	74	84	14	2	83.2	123	12	3.5	77
7	9	6	69.6	46	12	4	76.6	85	15	2	84.2	124	4	4.5	45.1
8	10	6	72.4	47	13	4	78.5	86	16	2	85.6	125	6	4.5	60
9	11	6	74.8	48	14	4	80	87	17	2	86	126	8	4.5	68.3
10	12	6	76.8	49	15	4	81.6	88	18	2	86.8	127	10	4.5	73.1
11	13	6	78.4	50	16	4	82.5	89	19	2	87.2	128	12	4.5	76.8
12	14	6	80.2	51	17	4	83.6	90	20	2	88				
13	15	6	81	52	18	4	84.4	91	3	1	68.1				
14	16	6	82	53	19	4	85.2	92	4	1	72.2				
15	17	6	82.8	54	20	4	85.6	93	5	1	75				
16	18	6	84	55	3	3	43.6	94	6	1	77.2				
17	19	6	84.4	56	4	3	51.9	95	7	1	79				
18	20	6	84.6	57	5	3	58.7	96	8	1	80.6				
19	3	5	34.6	58	6	3	63.5	97	9	1	81.8				
20	4	5	46.7	59	7	3	67.6	98	10	1	82.6				
21	5	5	54.8	60	8	3	70.4	99	11	1	83.4				
22	6	5	60.8	61	9	3	72.8	100	12	1	84.4				
23	7	5	64.8	62	10	3	73.6	101	13	1	85.2				
24	8	5	68	63	11	3	75	102	14	1	86				
25	9	5	70.2	64	12	3	77.6	103	15	1	86.8				
26	10	5	72.8	65	13	3	79.6	104	16	1	87.6				
27	11	5	75.2	66	14	3	81.2	105	17	1	88				
28	12	5	76.8	67	15	3	82.4	106	18	1	88.8				

29	13	5	78.8	68	16	3	83.6	107	19	1	89.2				
30	14	5	80.2	69	17	3	84.4	108	20	1	89.6				
31	15	5	81.2	70	18	3	84.8	109	4	1.5	62.5				
32	16	5	81.6	71	19	3	85.6	110	6	1.5	70.6				
33	17	5	82.8	72	20	3	86	111	8	1.5	75.8				
34	18	5	83.6	73	3	2	51.7	112	10	1.5	79				
35	19	5	84	74	4	2	59.3	113	12	1.5	83.6				
36	20	5	85	75	5	2	64.2	114	4	2.5	53.2				
37	3	4	39.1	76	6	2	67.5	115	6	2.5	64.5				
38	4	4	49.1	77	7	2	70.7	116	8	2.5	71.3				
39	5	4	56.4	78	8	2	73.1	117	10	2.5	76				

E = Young's modulus (MPa), t = sample thickness (mm), S<sub>A</sub> = shore A hardness.

Figure 4.43 shows the influences of the number of neurons on the prediction accuracy of the ANN program in the training process when it is used to inversely predict material properties from the shore A hardness. The relative error for the predicted parameter (in this case, Young's modulus) is calculated using the following equation:

$$Relative\ error(E) = ABS\left(\frac{E_{Predict} - E_{Target}}{E_{Target}}\right) \quad (4.5)$$

where  $E_{Predict}$  is ANN predicted data of Young's modulus,  $E_{Target}$  is the corresponding original target data.  $ABS$  represents the absolute value function. As shown in the figure, when 5 neurons are used in the ANN program, the maximum relative error is within 8 %, which is slightly higher than the case of 10 neurons. Further increasing the number of neuron (for example 20), the maximum error becomes much higher. This suggests that it is reasonable to use 10 neurons in the ANN program to inversely predict the Young's modulus from shore harnesses.

Figure 4.44 (a) shows the relative errors of inversely predicted Young's modulus using training data as the input data. In all of the 108 data points, the maximum relative error is 10%, this indicates the overall accuracy of the predicted Young's modulus. Figure 4.44 (b) shows the relative errors when using data that has not been included in the training data. In all 20 data points, the maximum error could be as high as 18 %. It suggests that ANN could predict the E values to a certain level of accuracy, but the error range is relatively high. There are 5 data points with error over 10% among the 20 data points tested. Figure 4.45 shows predicted E values of rubber samples based on the experimental data for the three cases (Case 1, Case 2 and Case 3)



presented in Section 4.4. In all cases, the ANN prediction and the estimated E values directly from the shore hardness are within a similar range, but in some cases, the maximum error is about 15 %.

Table 4.2 shows the training and output data of the ANN shore OO hardness tests. As shown in the table, the Young's modulus is ranged from 1 to 10 MPa, with a thickness of 1-6mm (the same as in Figure 4.33). There are 60 points in total used for the training and output data. The last additional 20 data points are randomly picked, to be used as evaluation data with Young's modulus between 2, 4, 6, 8 and 10 MPa and the sample thickness from 1.5 mm to 4.5 mm. These data points are used for evaluating the accuracy of the ANN developed as data not used in the training.

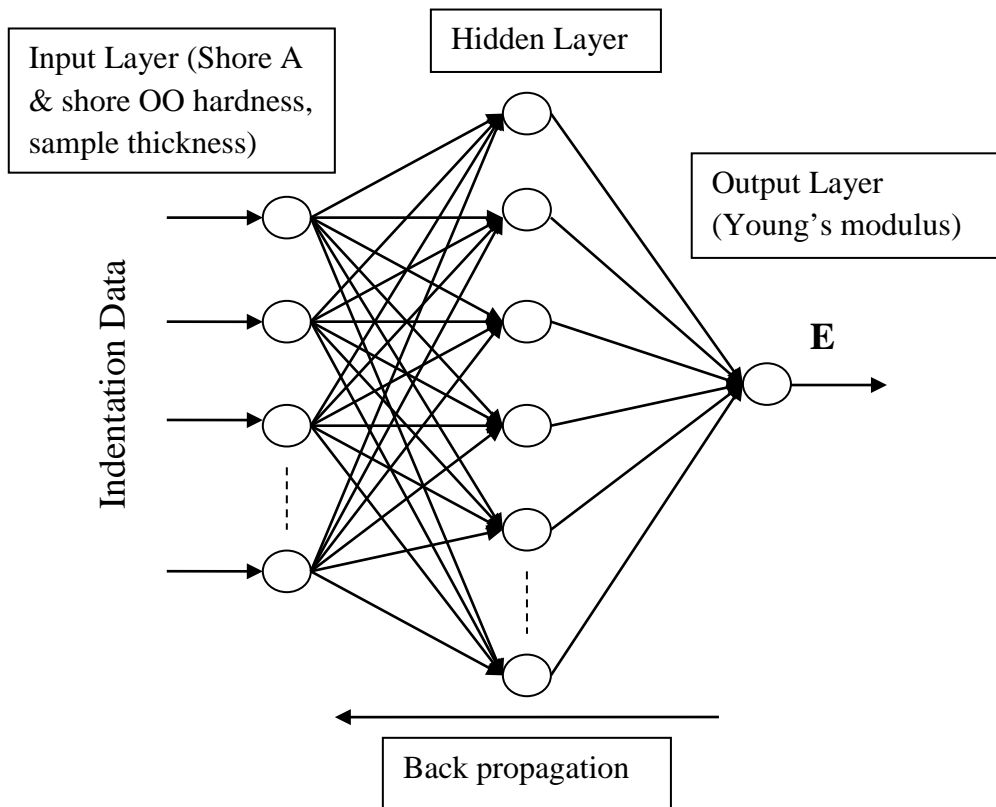
**Table 4.2** Training and output data for the ANN shore OO hardness tests.

Training and output data											
No.	E	t	Soo	No.	E	t	Soo	No.	E	t	Soo
1	1	1	83.4	40	10	4	93.9	79	8	4.5	93.2
2	2	1	88.6	41	1	5	71.1	80	10	4.5	94
3	3	1	90.4	42	2	5	82.3				
4	4	1	92	43	3	5	86.3				
5	5	1	92.8	44	4	5	88.7				
6	6	1	93.6	45	5	5	90.3				
7	7	1	94	46	6	5	91.1				
8	8	1	94.4	47	7	5	92				
9	9	1	94.6	48	8	5	92.7				
10	10	1	95	49	9	5	93.1				
11	1	2	76.6	50	10	5	93.9				
12	2	2	84.6	51	1	6	69.9				
13	3	2	88.2	52	2	6	81.5				
14	4	2	90.2	53	3	6	85.9				
15	5	2	91.6	54	4	6	88.3				
16	6	2	92.2	55	5	6	89.9				
17	7	2	93	56	6	6	91.1				
18	8	2	93.8	57	7	6	91.9				
19	9	2	94	58	8	6	92.7				
20	10	2	94.4	59	9	6	93.1				
21	1	3	74.6	60	10	6	93.5				
22	2	3	83	61	2	1.5	86.4				
23	3	3	87.7	62	4	1.5	90.8				
24	4	3	89.6	63	6	1.5	92.8				

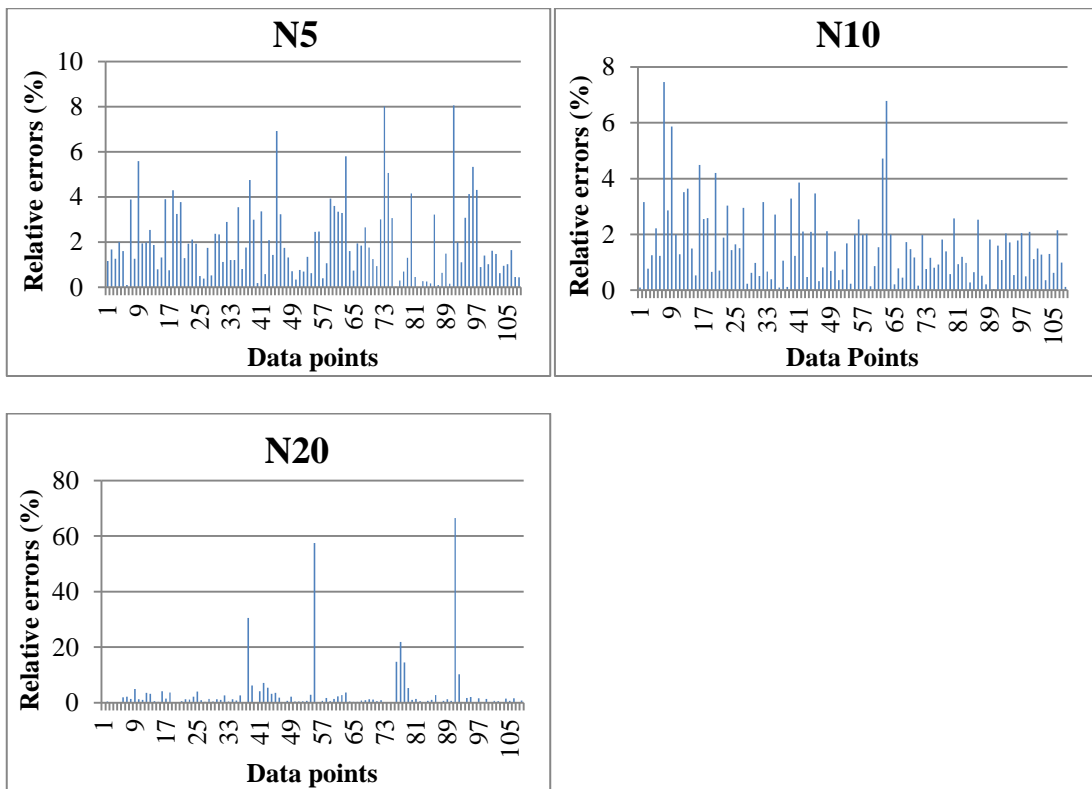
25	5	3	90.8	64	8	1.5	94				
26	6	3	91.9	65	10	1.5	94.8				
27	7	3	92.4	66	2	2.5	84.8				
28	8	3	93.1	67	4	2.5	89.6				
29	9	3	93.5	68	6	2.5	92				
30	10	3	94	69	8	2.5	93.4				
31	1	4	72.3	70	10	2.5	94.4				
32	2	4	82.7	71	2	3.5	84				
33	3	4	86.7	72	4	3.5	89.6				
34	4	4	89.1	73	6	3.5	92				
35	5	4	90.3	74	8	3.5	93.2				
36	6	4	91.5	75	10	3.5	94				
37	7	4	92.3	76	2	4.5	82.8				
38	8	4	93.1	77	4	4.5	89.4				
39	9	4	93.5	78	6	4.5	91.6				

E = Young's modulus (MPa), t = sample thickness (mm), Soo = shore OO hardness.

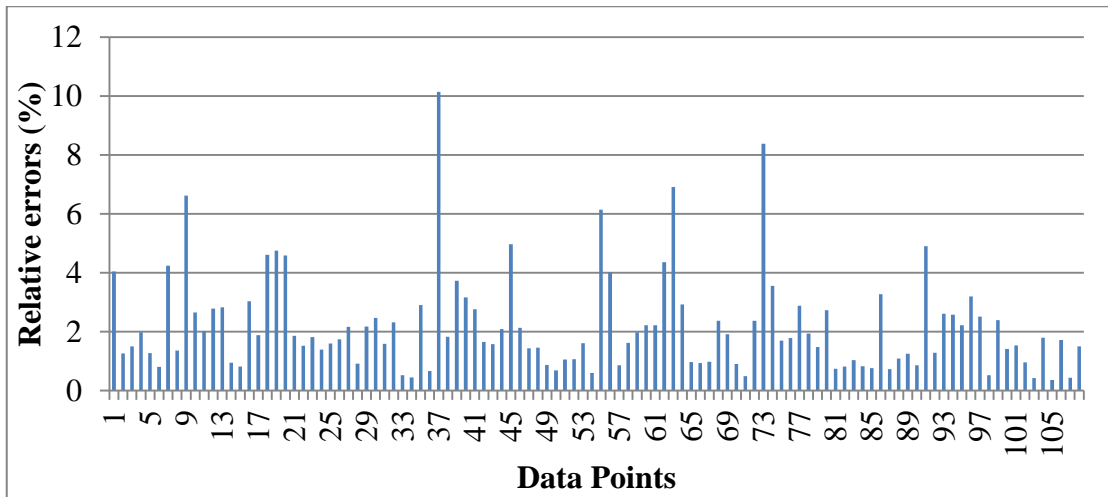
Figure 4.46 shows the relative errors of ANN predicted Young's modulus using the training data and non-training data as the input data for shore OO hardness. In the case of trained data as shown in Figure 4.46 (a), the maximum relative error is 10 % among all of the data points. In the case of using data not included in the training data (Figure 4.46 (b)), the maximum error is less than 13 %. This is slightly better than the case for shore A hardness, but here are still several data with errors close to 10%. Figure 4.47 shows the prediction of E values of rubber materials based on the experimental tests, E-t-S<sub>OO</sub> chart and the ANN approach. The data (Young's modulus) for the experimental test was inversely estimated/determined based on the chart of the shore OO hardness, the sample thickness and the effective Young's modulus (Figure 4.33). The data labelled as ANN values are predicted from ANN program. As shown in the figure, the E values obtained through these two approaches are within a reasonable range, with the variation within 15 %. Similar to the case of shore A, a higher difference is observed in the thicker samples, this is a reasonable trend. With the thickness increase, the shore hardness is not changing with the thickness of the sample significantly, or not changing at all beyond certain thickness range, this made it difficult for ANN to distinguish the difference among the data. This is a clear limitation of the ANN approach.



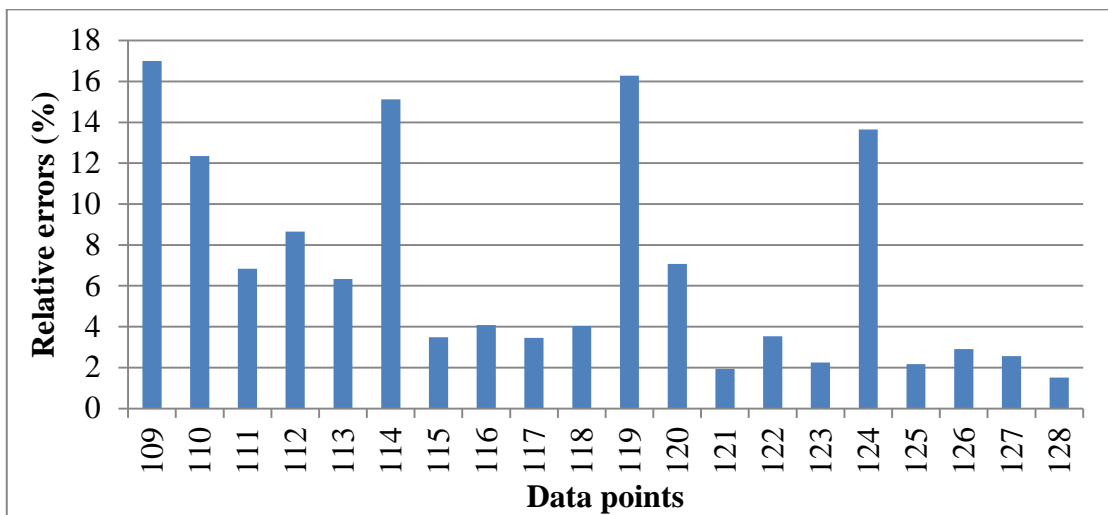
**Figure 4.42** Proposed feed-forward neural network with back propagation Algorithm for estimating the elastic material properties (E) based on shore hardness data.



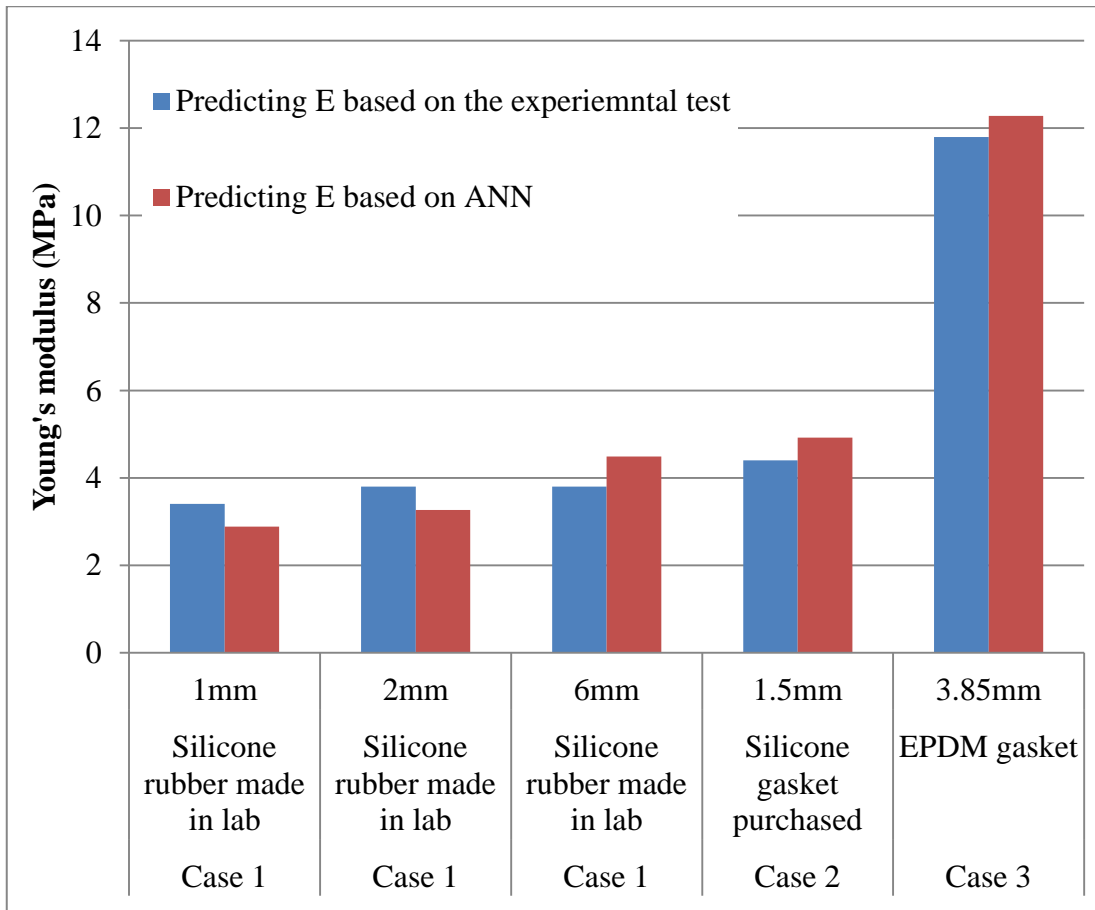
**Figure 4.43** Effects of the number of neuron on the relative error of predicted E values in ANN training.



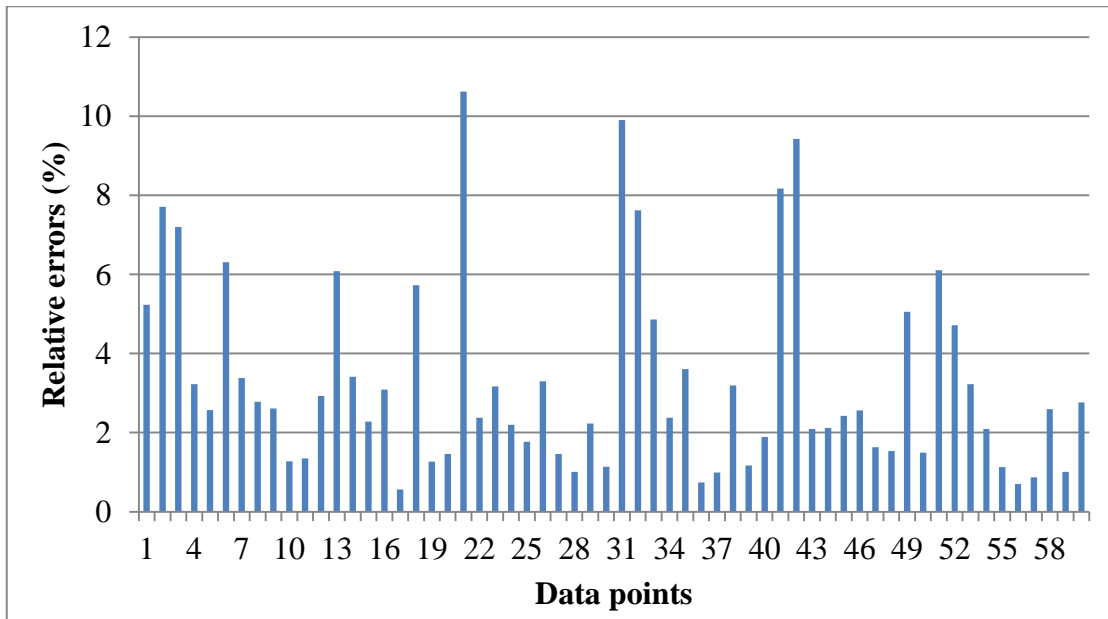
**Figure 4.44 (a)** The relative error of ANN predicted E values using training data as the target. (Shore A). (Detailed properties for each data points could be found in Table 4.1).



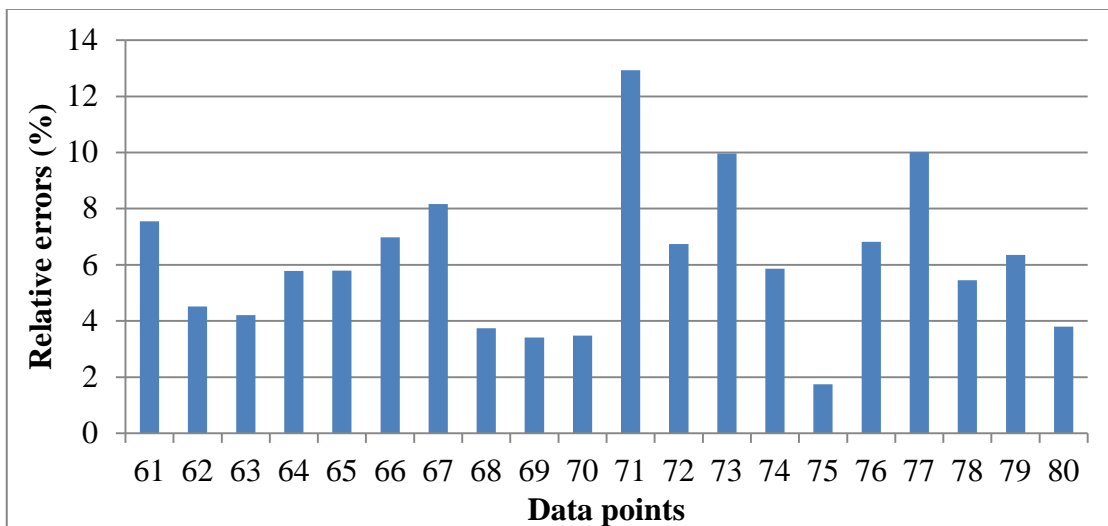
**Figure 4.44 (b)** The relative error of ANN predicted E values based on data not used in the training. (Shore A). (Detailed properties for each data point could be found in Table 4.1).



**Figure 4.45** Predicted E values of different rubbers based on the shore hardness for case1, 2 and 3 (Shore A).

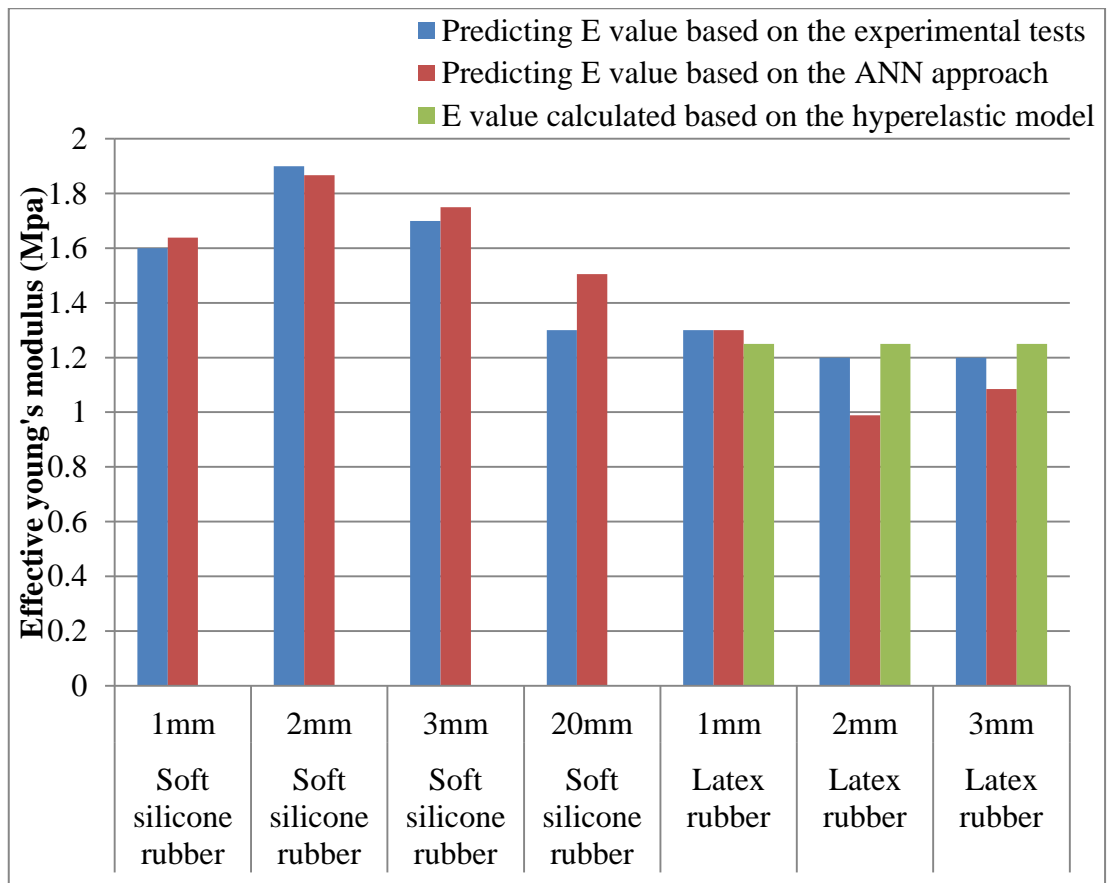


(a) The relative error of ANN predicted E values using training data as the target. (Shore OO). (Detailed properties for each data point could be found in Table 4.2).



(b) The relative error of ANN predicted E values using data not used in the training as the target. (Shore OO) ((Detailed properties for each data point could be found in Table 4.2).

**Figure 4.46** The relative error of ANN predicted E values based on shore OO hardness data.



**Figure 4.47** Comparison of predicted E values based on experimental data (shore OO) through different approaches.



#### 4.7 Prediction of Shore hardness using ANN for thick and thin samples

In this section, the results of predicting the shore hardness from known material properties and sample thickness are presented. The ANN structure and procedure is similar to those presented in the previous section. Shore hardness is an indicator of the properties of a material as well as an indentation resistance of a layered system (soft layer on a rigid base). In many case, thin rubber sheet are used on a rigid/stiffer base (*Pinarbasi, 2009*). A direct analysis to predict the shores hardness of samples of different thicknesses not only can tell the indentation stiffness, it can also be linked to perception of softness/comforts, etc. (*Chandler, 1999; Darmanis et al., 2006*).

Figure 4.48 shows the ANN structure, the inputs are the materials properties and dimensions (thickness of the layer). The output is shore A hardness or shore OO hardness. In this direct analysis, the input of the training data is thickness and E, as in in Table 4.1. There are two hidden layers, layer 1 uses the tan-sigmoid transfer function (TANSIG) and layer 2 uses the linear transfer function (PURELIN). The relative error of shore hardness is calculated using the following equation:

$$Relative\ error(SH) = ABS\left(\frac{SH_{Predict} - SH_{Target}}{SH_{Target}}\right) \quad (4.6)$$

where  $SH_{Predict}$  is ANN predicted data of shore hardness,  $SH_{Target}$  is the corresponding target data. *ABS* represents the absolute value function.

Figure 4.49 shows the effect of the number of neurons on the prediction accuracy of the ANN program in estimating shore A hardness from the E values and sample thickness. When the neuron number used is 5 in the ANN program, the maximum relative error is as high as 20 %. When 10 neurons are used, the maximum error is much better (within 1.5 %). If the ANN program is using 20 neurons, the maximum error becomes slightly higher than the case for neuron number of 10. This suggests that it is reasonable to use neuron number of 10 in the ANN program. Figure 4.50 (a) shows the relative errors of ANN predicted shore A hardness using the training data as the input. In all of the 108 data points, the maximum error is 2 %. Figure 4.50 (b) shows the relative errors of the prediction when using data which has not been used in the training. Among all the 20 data points, the maximum error is less than 6 %. These

data show that the prediction accuracy of shore hardness is much better than that when predicting the E values using ANN.

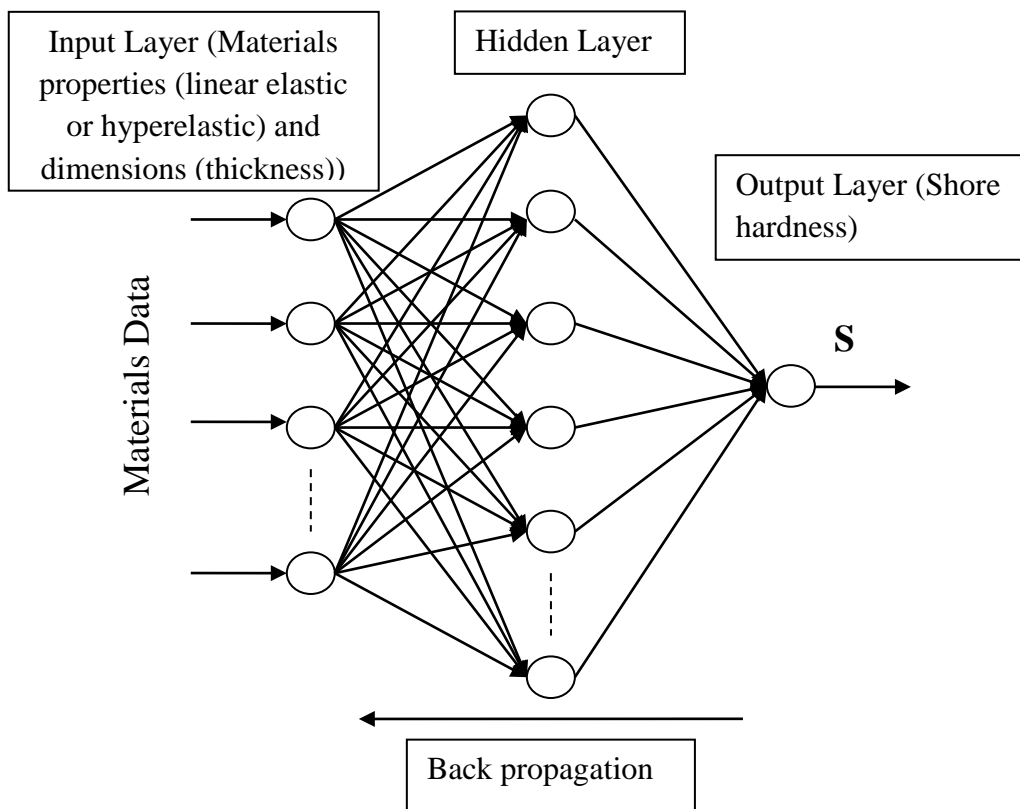
Figure 4.51(a) shows the relative errors of ANN predicted shore OO hardness using the training data as the input. In all the 60 data points, the maximum error is less than 2 %. Figure 4.51(b) shows the relative errors using data which has not been used in the training. In all the 20 data points, the maximum error is also less than 2%. This again shows that the accuracy of the prediction for shore OO hardness is much better than that when predicting the E values using ANN. The work has been extended to using hyperelastic properties in predict the shore OO hardness. A typical example when using 1<sup>st</sup> order Ogden model with shore OO is shown in Figure 4.52. The nonlinear parameters are mu ( $\mu$ ) and alpha ( $\alpha$ ) in the Ogden model.

$$W_o(\lambda_1, \lambda_2) = \sum_{p=1}^N \frac{\mu_p}{\alpha_p} (\lambda_1^\alpha + \lambda_2^\alpha + \lambda_1^{-\alpha} \lambda_2^{-\alpha} - 3) \quad (4.7)$$

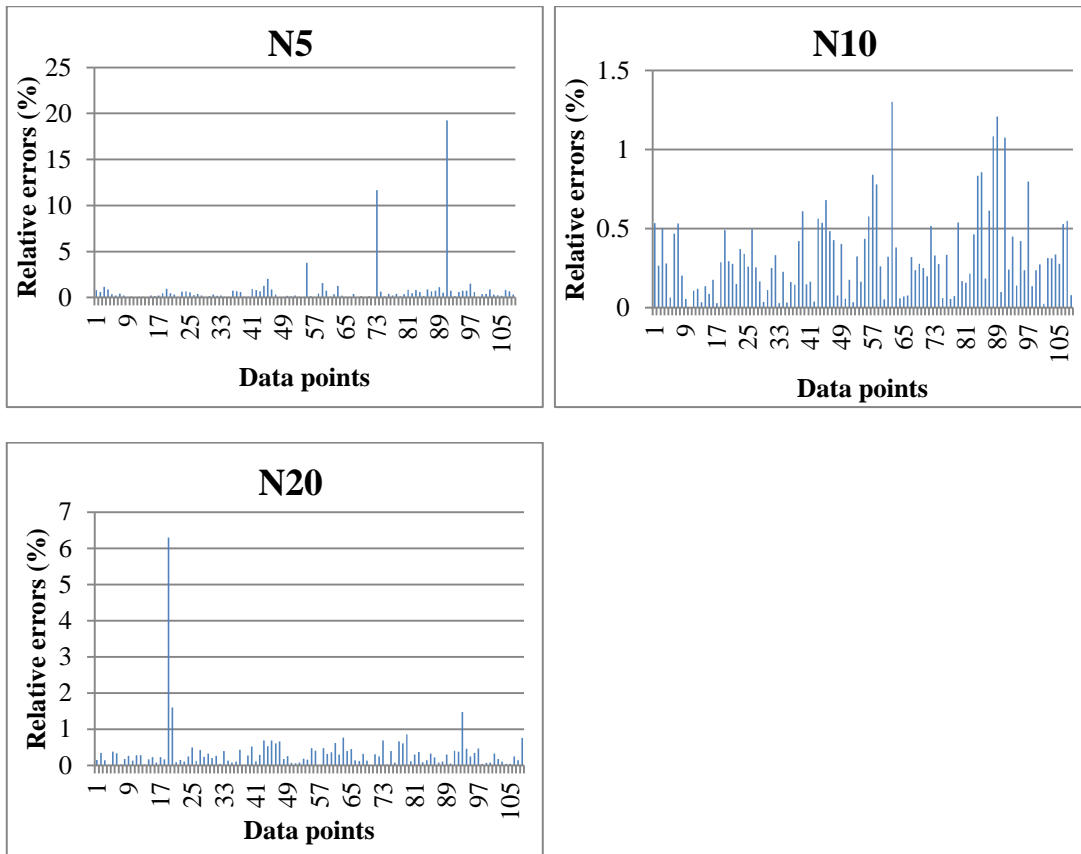
where N is the model's order,  $\mu_p$ ,  $\alpha_p$  are material parameters to be determined experimentally.  $\lambda_1^\alpha$ ,  $\lambda_2^\alpha$  are the deviatoric principal stretches (*Ogden, 1972*). The process to generate data for the ANN using hyperelastic data is much more complicated than that using a single Young's modulus as there are three inputs.

ABAQUS parametric studies is used to generate a simulation space with parameter  $\mu$  in a range of 0.3-1.9, and parameter  $\alpha$  in a range of 0.5-3.3 with a thickness of 1, 3 or 6mm. There are total 216 data points used for the training and evaluation. Additional 54 data points were produced using the same FE parametric study program to generate data with the parameter between  $\mu$  (0.3 to 1.9) and  $\alpha$  (0.1, 3.7). The sample thickness used a range from 1, 3 and 6 mm. These data points are used for the testing the ANN accuracy as data not used in the training. Figure 4.52 (a) shows the relative errors of ANN predicted shore OO hardness based on the nonlinear material parameters using the training data as the input. In all of 216 data points, the maximum error is less than 1 %. It indicates the high accuracy of using ANN to predict shore OO hardness with known nonlinear material parameters and the sample thickness. Figure 4.52 (b) shows relative errors in predicted shore OO hardness when using data which has not been used in the training. In all 54 data points, the maximum error is less than 1 %. These results clearly show that ANN would perform much better in

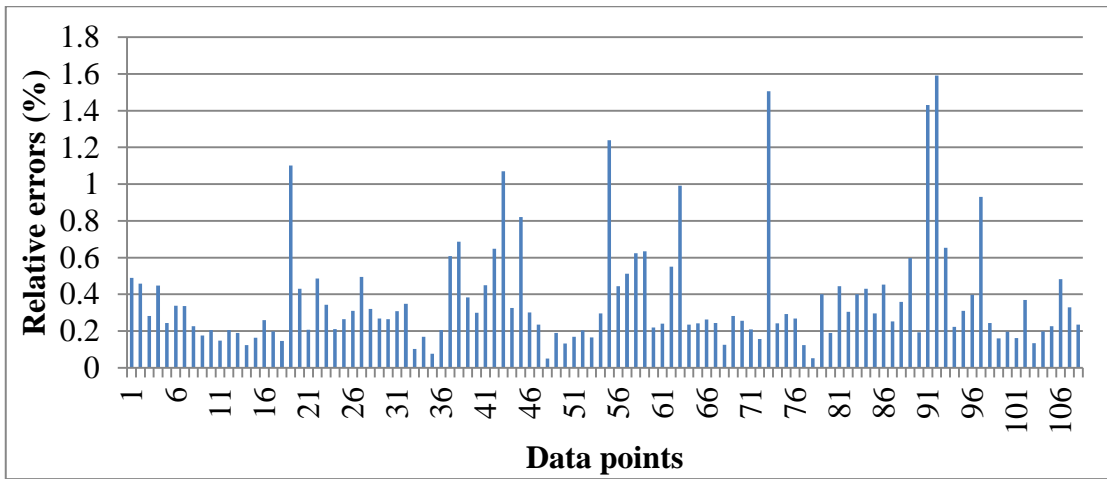
predicting shore hardness values when the thickness and the material properties are known. The properties could be either Young's modulus or nonlinear hyperelastic parameters.



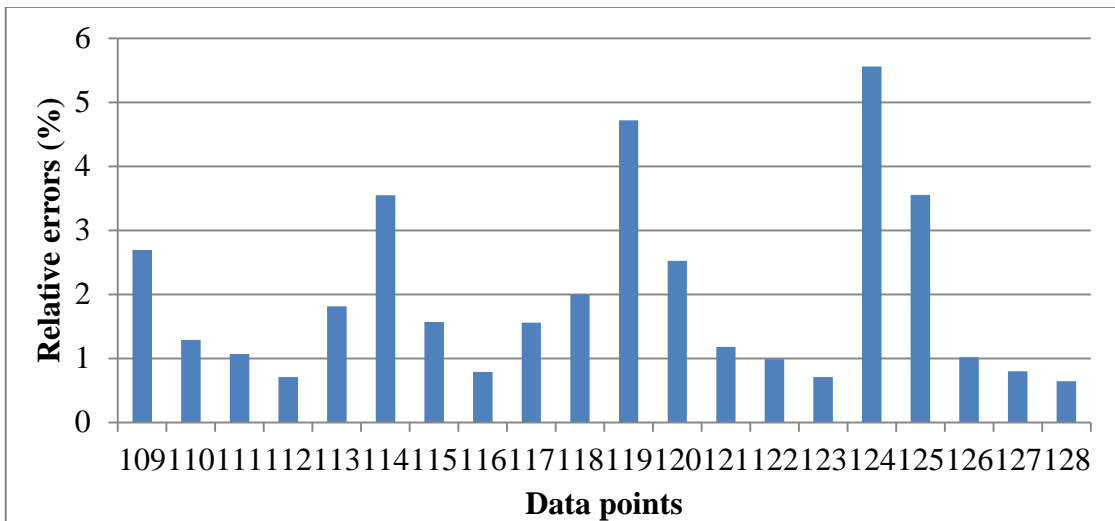
**Figure 4.48** Proposed feed-forward neural network with back propagation Algorithm for estimating the Shore hardness from known material properties and sample dimensions.



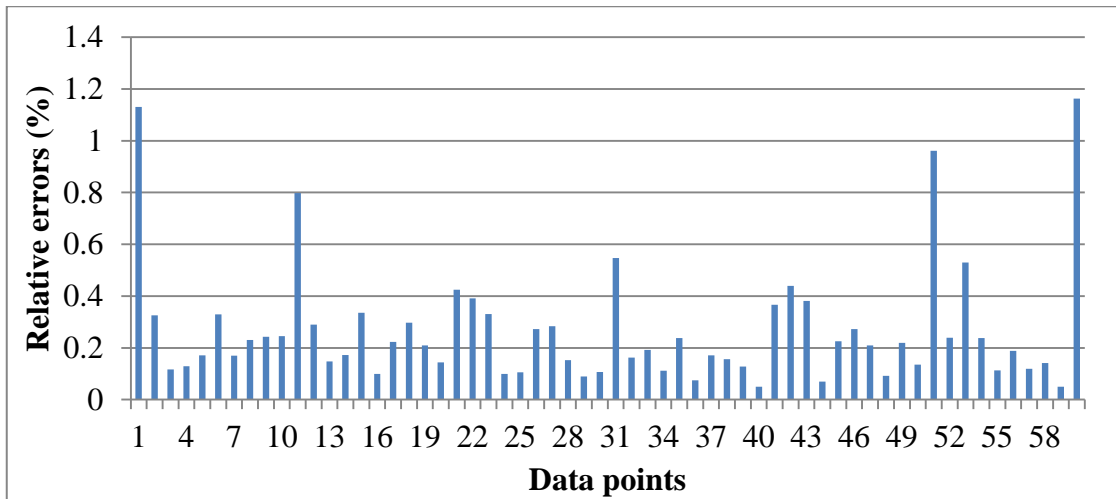
**Figure 4.49** Effects of the number of neuron on the relative error of predicted shore A hardness (Direct ANN program).



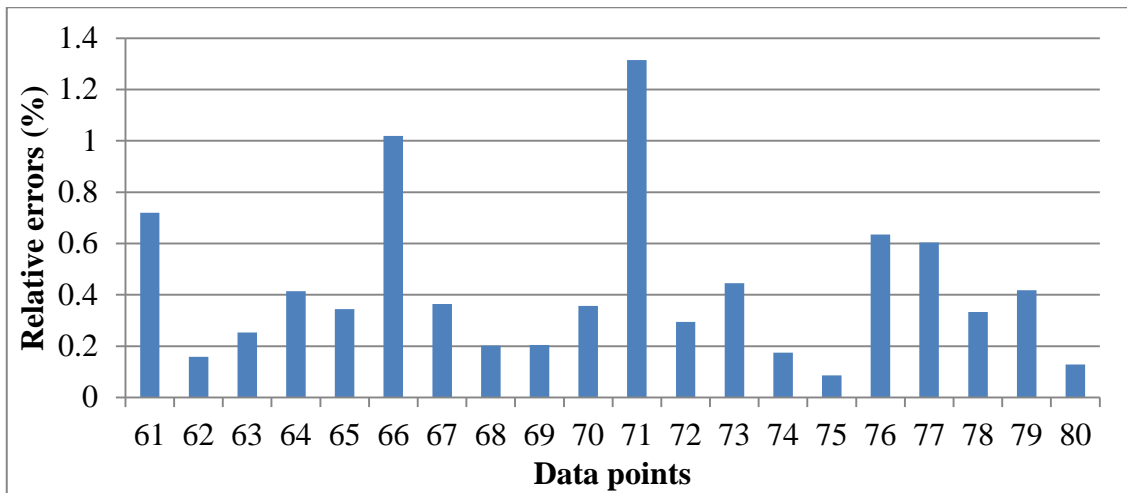
**Figure 4.50 (a)** Relative error in predicted shore A hardness using the training data as input (direct predict shore A hardness) (neuron number =10).



**Figure 4.50 (b)** Relative error in predicted shore A hardness using data not used in the training as input (direct predict shore A hardness) (neuron number =10).

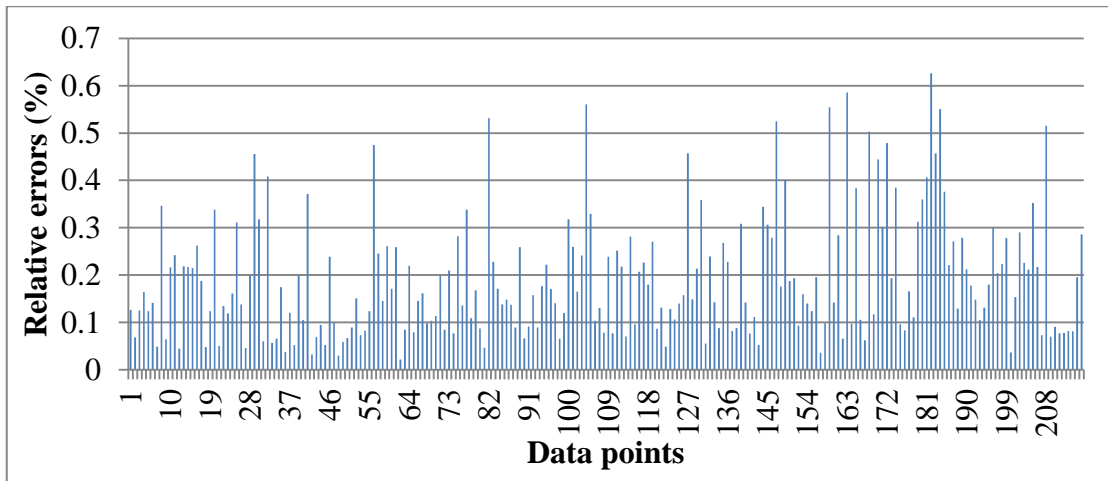


(a) Relative error in predicted shore OO hardness using the training data as the input data (direct predict shore OO hardness) (neuron number =10).

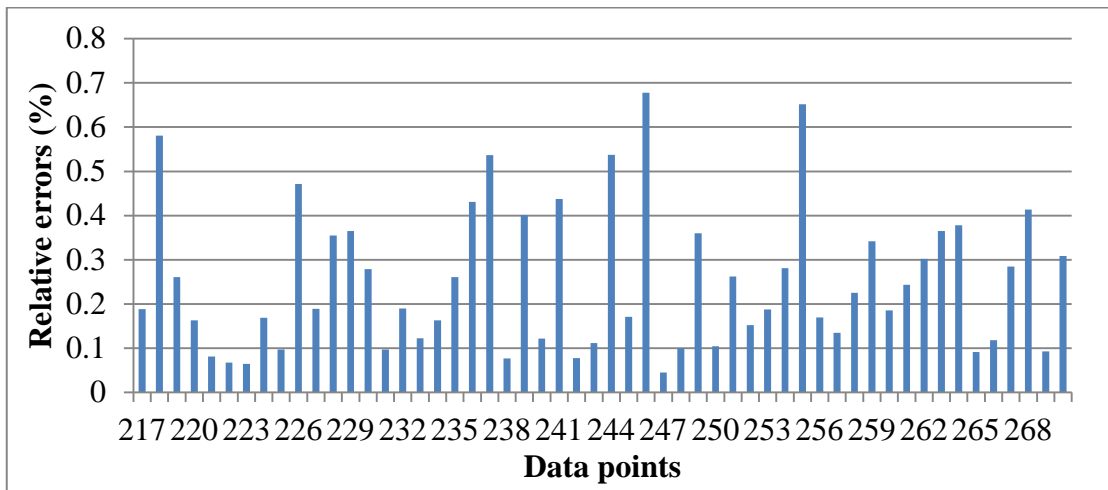


(b) Relative error in predicted shore OO hardness using data not used in the training data as input (neuron number =10)

**Figure 4.51** Typical results showing the accuracy of the ANN in predicting Shore OO hardness from E values and sample thicknesses.



(a) Relative error in ANN predicted shore OO hardness from nonlinear hyperelastic parameters and sample thickness using the training data as the input data (direct prediction of shore OO, neuron number =10)



(b) Relative error in ANN predicted shore OO hardness from nonlinear hyperelastic parameters and sample thickness using data not used the training as the input data. (direct prediction of shore OO, neuron number =10)

**Figure 4.52** Typical ANN results showing the accuracy in predicting Shore OO hardness from nonlinear hyperelastic parameters (Ogden strain energy function) and thicknesses.



# CHAPTER FIVE

## DISCUSSION

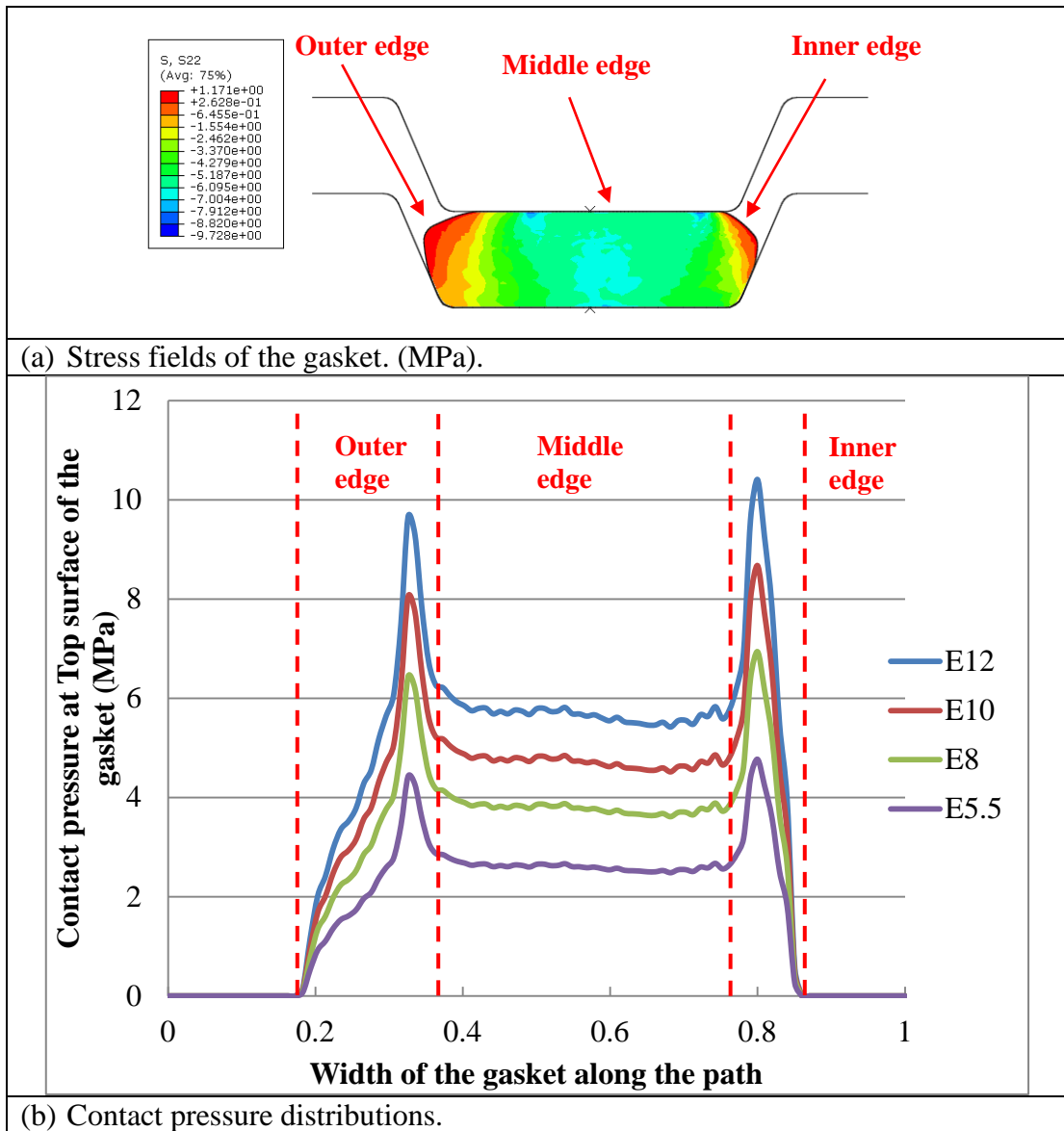
## 5.1 Applications of indentation and characterize the material properties

Shore hardness testing is a very important material testing method for softer materials (in comparison with metal and ceramics) such as plastics and rubbers. Due to the nature of the testing methods, it is a challenging task to link the hardness to constitutive material properties (such as Young's Modulus or hyperelastic material parameters). For metals and plastic where the material properties are controlled by elastic-plastic properties, the material model is relatively simple, the stress strain curves can be described by a power law relationship with a clear elastic and plastic region (*Luo et al., 2007; Callister et al., 2012*). As shown in Section 2.2.2, Shore hardness has a complex system with different indenter shapes and loading range. This made it difficult or impossible to develop a property link that is applicable to all materials and material models. For practical applications, it would be a more effective way to focus on some specific shore hardness type and situation where the materials, loading condition and acceptable level of accuracy are better understood. This work focused on the use of shore A and shore OO hardness on rubber materials with a particular application on gasket or seals, which are known to be mainly under compression load in service with a relatively low strain level. Shore A hardness is widely used in rubber materials ranged from pencil rubber to gasket and tyres. Published works on shore OO hardness is relatively limited compared to shore A hardness, however, its application is becoming increasingly significant with new developments of rubber for areas such as medical, and food processing (*Li et al., 2013*). One advantage of spherical based indentation is that it did not damage the sample. Most of the cases (Chapter 4, cases 1-5) reported in this work are based on gasket materials, but some of the key finding could be applicable/relevant to other areas.

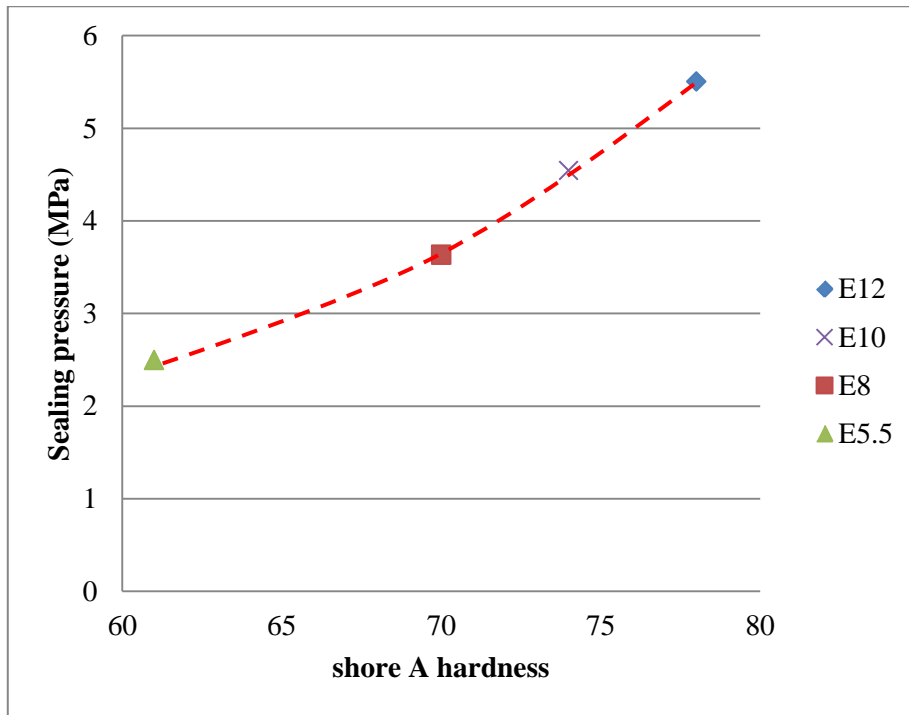
As presented in Chapter 4, detailed FE models have been developed to simulate shore A and shore OO hardness. In the FE of shore A hardness, a re-meshing program has to be developed to cope with the larger deformation when a relatively soft material is involved. In the FE model for shore OO hardness, adaptive meshing is used which is sufficient as the indentation load is relatively low and the contact between a spherical indenter and the sample is smoother. In both cases, an FE model was developed first to simulate thick samples (sample close to or thicker than the standard thickness of 6mm). This approach has provided a meaning to assess the

accuracy of the FE model where experimental data or analytical solutions are available. The shore A hardness data was compared to published data on rubber with corresponding shore hardness and Young's modulus data and shows a good agreement. The shore A hardness and Elastic Modulus correlation established has also been compared to the published data from other sources (*Milani et al., 2012*). These data are not presented in the result section as the detailed source of the property was not entirely clear. In the case of the shore OO hardness tests, the FE data was compared to the analytical solutions. Both cases showed the FE model is reasonably accurate. The validated modelling approach was then transferred to thinner samples. This has proven to be an effective approach evident from the agreement with experiment data for different conditions through the five material case-studies. As shown in the results in section 4.4, the data between E, thickness and shore hardness established could be effectively used in estimating the Young's modulus. The three case studies for shore A hardness and two cases studied for shore OO hardness all showed reasonable agreement with the experimental data. The approach using compression/tension tests of nonstandard shape has been effective to compare the results rather than purely based on property data or stress strain curves, as it offers a situation close to the condition when a gasket is being assembled. A range of different conditions were selected either purposely or rigorously to assess the approach or limited by the availability of samples, but all showed that the Young's modulus predicted is within a reasonable accuracy, at least for gasket applications. There is always a limitation for work in estimating material properties from tests such as indentation. The accuracy range depends on the material properties used and the application targeted. For metal material, where the material model is elastic plastic, the prediction of yield stress and Young's modulus could be relatively close, for example, the data in Table 2.4 (*Harsono, 2009*). The error of the predicted E value was about 15 %. But the error in work hardening coefficient was as high as 20 %. In addition, there is also a problem with non-uniqueness when two parameters are jointly used (*Budiarsa, 2013*). Rubber is known to have hyperelastic properties, but the results reported in this thesis have focused on the Young's modulus, since for gaskets and seals (flat surface based), Young's modulus would be sufficient to respect the materials. One advantage of using E values lies in that it's simple and there is no issue with non-uniqueness given the Poisson's ratio for rubber is close to 0.5. As presented in results of ANN prediction, the works on hyperelastic models show that it can be used to predict the shore hardness, but estimating the hyperelastic

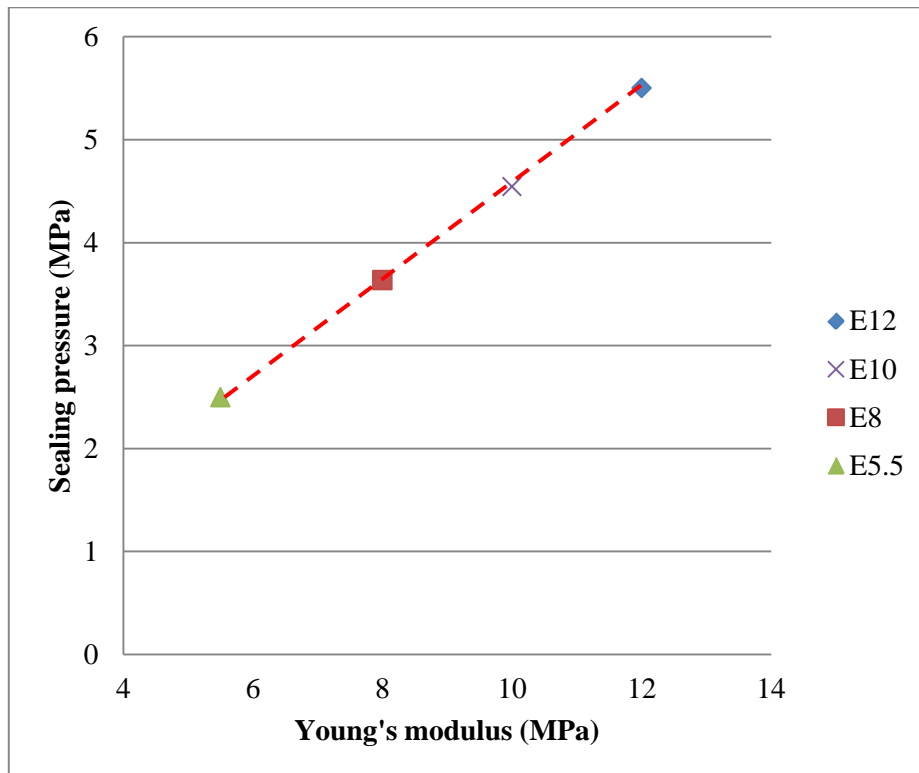
parameters from shore hardness is difficult. Some details are to be presented in a later section. Materials selection is an important part for gasket design. The FE modelling based approach is becoming increasingly important for the design of systems involving the use of gaskets or seals. Despite the wide use of shore hardness in rubber materials, shore hardness cannot be directly used as input material properties, so it is very useful if the E value can be estimated. A general rule in gasket is that the thinner, the better, as it can strain the materials with a small displacement. Therefore, many gasket or seal materials are supplied in a thinner form rather than the standard 6 mm thickness specified for shore hardness tests. As shown by the application cases, the work established would allow direct estimation of the E values from these non-standard samples as well as thick samples. In some case it is not possible to have access to thick samples. For example, as in Case 3, the EPDM gasket sample has a complex cross-sectional shape. This type of plate heat exchanger is widely used in chemical, pharmaceutical and heating supplying industries (*Sadik et al., 2002*). The gasket needs to provide a seal between the chevron stainless steel plates and reduce the leakage of the media (*Vishal, 2013*). The gasket material selection is critical to obtain an optimal sealing performance. A gasket is evaluated based on its seal ability, and a gasket is said to be performing if it provides a low leakage rate under the applied load, during the service life (*Arghavani et al., 2001*). With the correlation between shore hardness and E values, the FE model has been developed to simulate the effects of material properties on the sealing force, which can provide quantitative data for materials selection or new material design. Some typical results are illustrated in modelling the deformation of an EPDM gasket compressed within the heat exchanger plates (Figure 5.1). Figure 5.1(a) shows the deformed shape of the gasket with a displacement of 25 % of the original height in a plane strain model. The length used in the model is the overall load bearing length of the gasket. As shown in Figure 5.1(b), the contact pressure is directly influenced by the E values. The sealing force is defined as pressure at the inner edge in contact with the medium (*Lorenz et al., 2009*). Figure 5.2(a) shows the effects of shore hardness on the change of contact pressure of the gasket. Obviously the relationship between the shore A hardness and the sealing pressure is nonlinear. Figure 5.2(b) shows the effects of Young's modulus on the change of contact pressure of the gasket, it clearly shows that the relation between the pressure and E value curve is close to linear. This linear relationship would potentially make comparing materials much easier.



**Figure 5.1** FE modelling of gasket contact pressure in a plate heat exchanger plate and effects of material properties on the sealing pressure.



(a) Sealing force vs. shore A hardness.



(b) Sealing pressure vs. Elastic modulus of the materials.

**Figure 5.2** Effects of hardness and Elastic modulus on the sealing force.

## 5.2 Effect of different indenter shape and sample thickness on the indentation resistance and deformation of the material

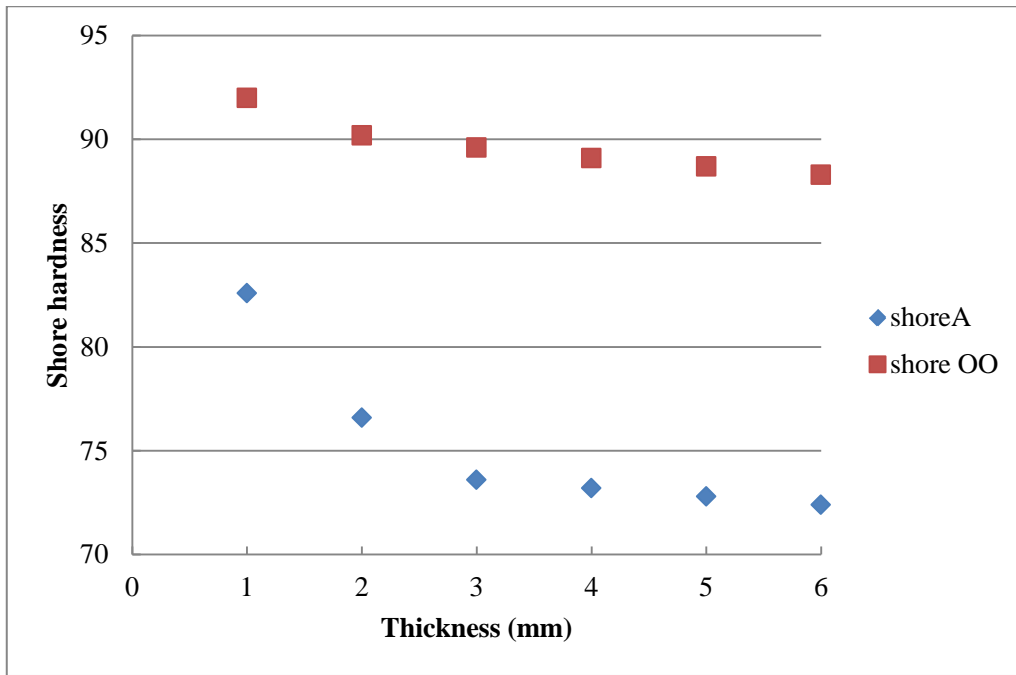
In the shore A and shore OO hardness the indentation system, the indenter tips are different. Shore A hardness indenter tip is a combination of cone and flat end. Shore OO hardness indenter is a typical spherical indenter. Shore A hardness is suitable for harder samples with the Young's modulus ranged typically from 3 MPa to 15 MPa. When the Young's modulus is over 15 MPa, there is no big difference among the shore A hardness values with increasing Young's modulus. This is consistent in the fact that, for hard rubber (*Durometer Hardness Scales – General Reference Guide*), shore A is mostly suitable for shore hardness between 20-90. For harder rubbers with even higher E values, shore D hardness is required which uses a cone indenter with a tiny round tip. For soft rubber, the shore A hardness indentation is not suitable because the indentation force of shore A hardness value required is 8.06 N, a very large indentation depth is required for soft materials to reach this load, which may cause uncertainty with the test results.

Shore OO hardness is suitable for softer materials, the material properties range studied in this work is from 1 MPa to 6 MPa, which is representative for softer rubber materials such as latex, silicone rubber. The material group with lower hardness is more likely belonging to gels rather than rubber. When the Young's modulus is higher than 6 MPa, there is no significant difference in the shore OO hardness values. It is of less importance to investigate the link between E values and SH<sub>OO</sub> as shore OO hardness becomes insensitive to the increase of E values. For hard rubber, the shore OO hardness indentation is not suitable because the indentation force of shore OO hardness required is only 1.1 N. The indentation depth is too small to be accurately detected by the displacement of the spring. When testing samples of different thickness, shore A hardness indentation test has given consistent and repeatable results, however, with sample lower than  $t < 1$  mm, the tests become unreliable due to the effects of the support plate. In addition, the shore A indenter may damage the sample if the sample is too thin. This is not a major concern for shore OO hardness, there is no damage in the shore OO hardness test with the thin samples. As the sample thickness decreases, the interaction between the base and the sample and its contribution to the indentation resistance increases. Figure 5.3 shows the change of the shore hardness values with the sample thickness for shore A and

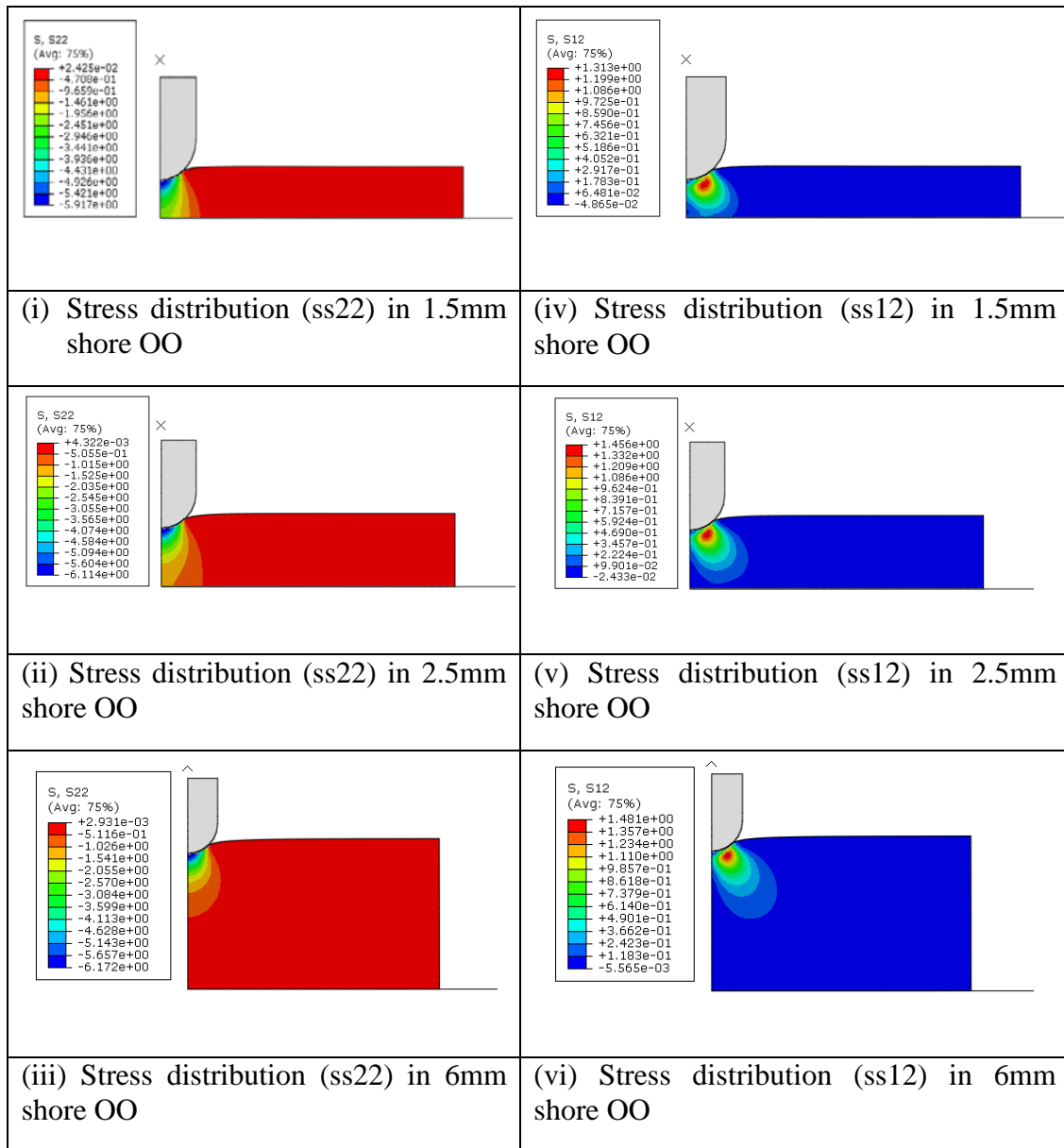
shore OO hardness. In both cases, the curve showed a clear smooth change of hardness against the thickness. The influence of thickness on shore A hardness becomes less significant when the sample becomes thicker.

With the use of thin samples, it has made it possible to extend the use of shore A or shore OO hardness. For example, when the sample is thinner, then it is easier to reach the load for shore A hardness when the E value is lower than the normal working range, so shore A hardness can be used. Similarly shore OO hardness can be used to tests the softer materials than its normal range, due to the effect of the hard base, the displacement required becomes lower to reach the required load. Figure 5.4 shows the stress distributions under the indentation of different thicknesses. In both shore OO hardness in Figure 5.4 (a) and shore A hardness in Figure 5.4 (b), the distribution of the normal and shear stresses changes with the sample thickness. As the sample is getting thinner, the pattern change with normal stress is much more significant than the shear stress. This suggests that the compression loading becoming more dominant when the sample is thinner. This is a situation closer the loading condition of a gasket.

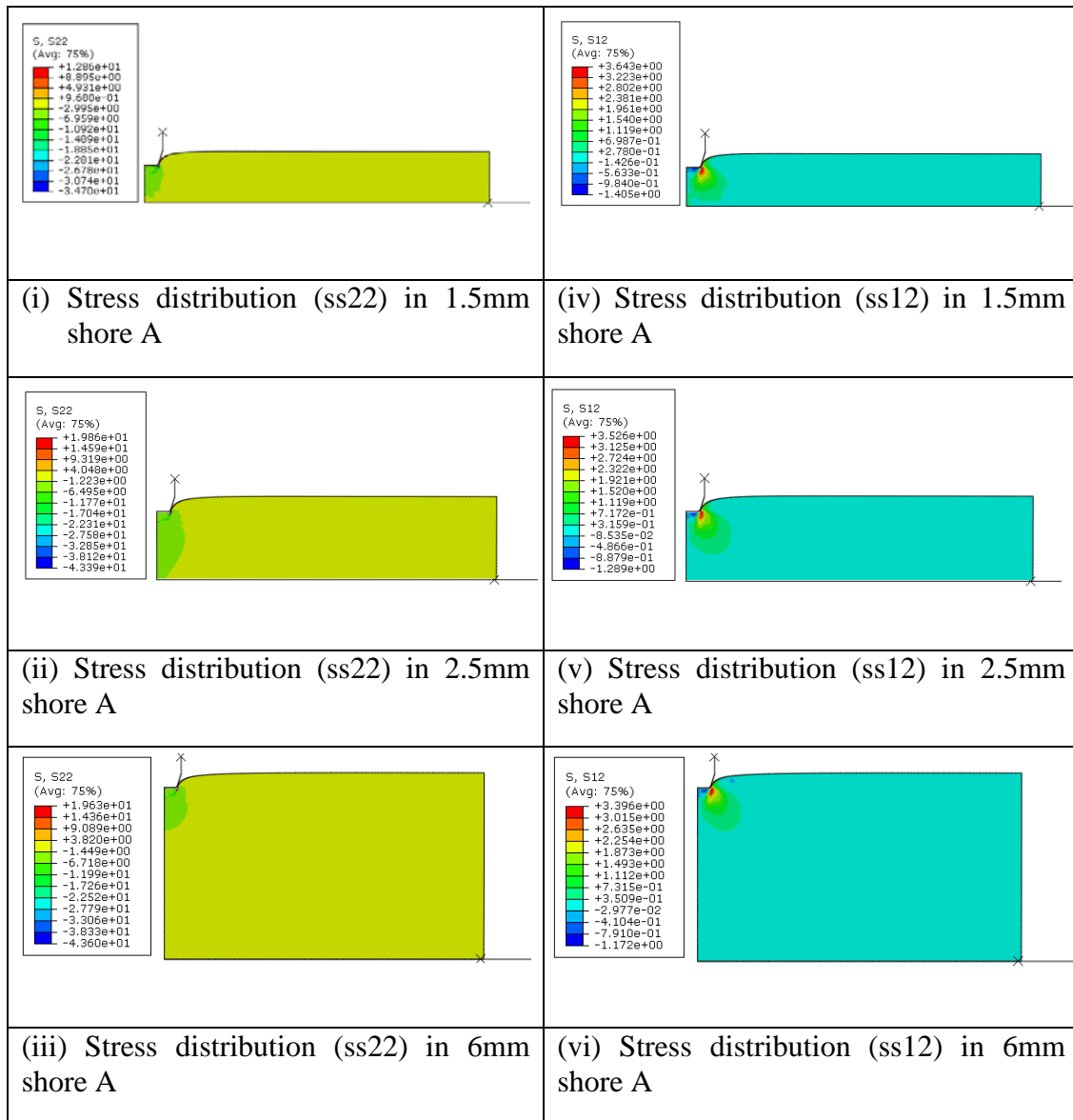




**Figure 5.3** Change of shore hardness with sample thickness. (E=10MPa).



**Figure 5.4 (a)** Indentation stress distributions (MPa) for shore OO indenter on samples of different thicknesses.



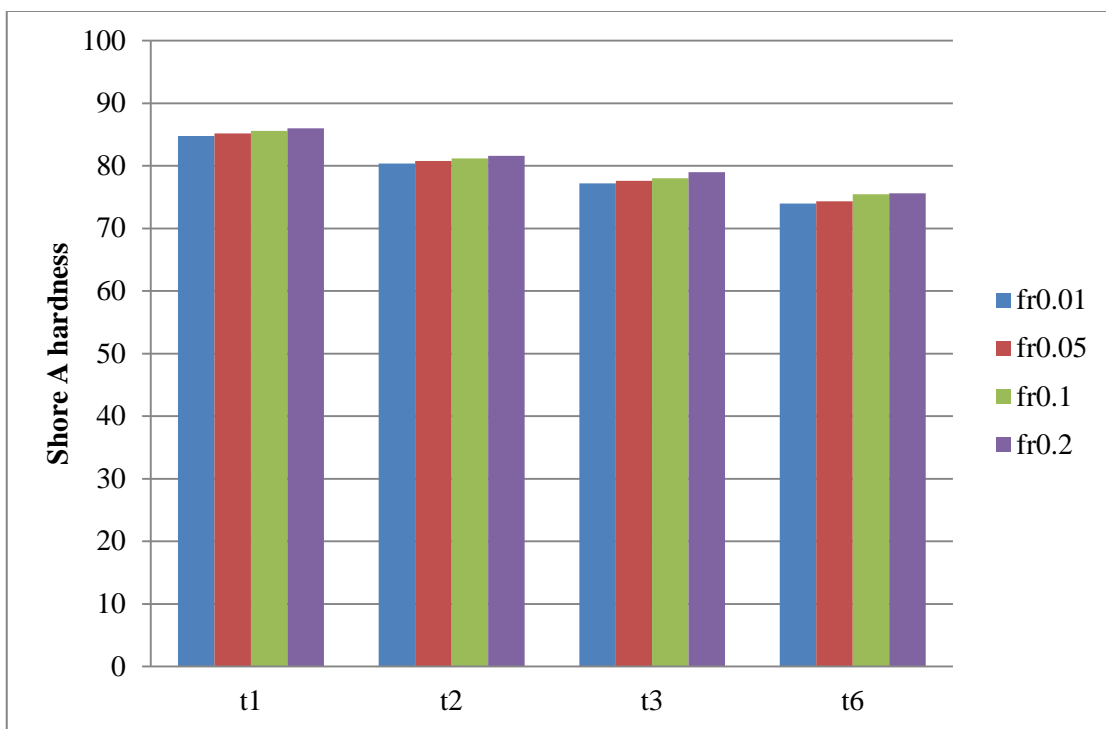
**Figure 5.4 (b)** Indentation stress distributions (MPa) for shore A indentation on samples of different thicknesses.

### 5.3 Factors affect the indentation process and shore hardness measurements

There are many factors which may affect indentation process regarding to shore hardness, for example, whether it is using the frame to support the sample or manually holding the machine; variation of measurement style of the operator, alignment of the indenter, surface of the support plate, friction effects, and temperatures (*Mohamed et al., 2003*). All these may influence the shore hardness results. Several of these have been assessed in this work to ensure the consistency of the results. Most of the test data has been cross checked by different operators in this work, the variation is with ~3 % between different persons. Tests have been conducted to compare the case of a properly supported base underneath the sample and the case of the manual tests. The variation of effect is within 3-5 % as far as the sample surface is reasonably flat. As shown in Figure 4.17, tests on the hard silicone rubber made at three planes showed comparable hardness values, which suggest that there is no significant anisotropy in hardness/properties. Given shore hardness has a guarding plate, it has worked well to avoid misalignment. A trial has also been made by deliberately introducing an inclining angle, but no major influences on the shore hardness value was observed, as the guard plate will ensure a reasonable balanced position. This is a clear advantage for shore hardness, which probably has contributed to its wide application despite the fact that there is no universal link with constitutive material properties over all the shore hardness scales. The link with E value for certain group material (as the results established in the work for gasket rubbers) would probably further enhance its use linking shore hardness with CAE modelling and products development.

Friction effect is a critical factor which may affect the results in the shore A and shore OO hardness tests. There are two parts of friction effect. One is the interface between the indenter and the sample, the other is the effect of friction between the sample and the supporting base. In order to assess the possible effects of the friction condition at the sample-supporting plate interface, tests have been performed on a dry surface and lubricated surfaces. As shown in Figure 4.21, the average difference in shore hardness from tests with different lubrication conditions for the round type silicone gasket samples was about 5.7 %. The average error of the friction effect on the ring type silicone gasket samples was 4.6%. Similar level of lubricant effects on shore hardness has also been observed in other samples. The lubricated situation

evaluated in this work represents an extreme situation in real tests, in real gasket assembly process, most of cases are on dry surface, so it is reasonable to conclude that the error due to uncertainty of friction should be relatively low even with thin samples. In the FE models, the friction coefficient used is based on typical data between rubbers and metal etc. (Deladi, 2006). As the sample thickness decreased, the friction effect may become more uncertain. This is assessed by running models with different coefficients. Some typical results of predicted shore hardness are shown in Figure 5.5. The data showed that the effects of friction on the shore hardness prediction are not significant for these applications within the property range for this work.

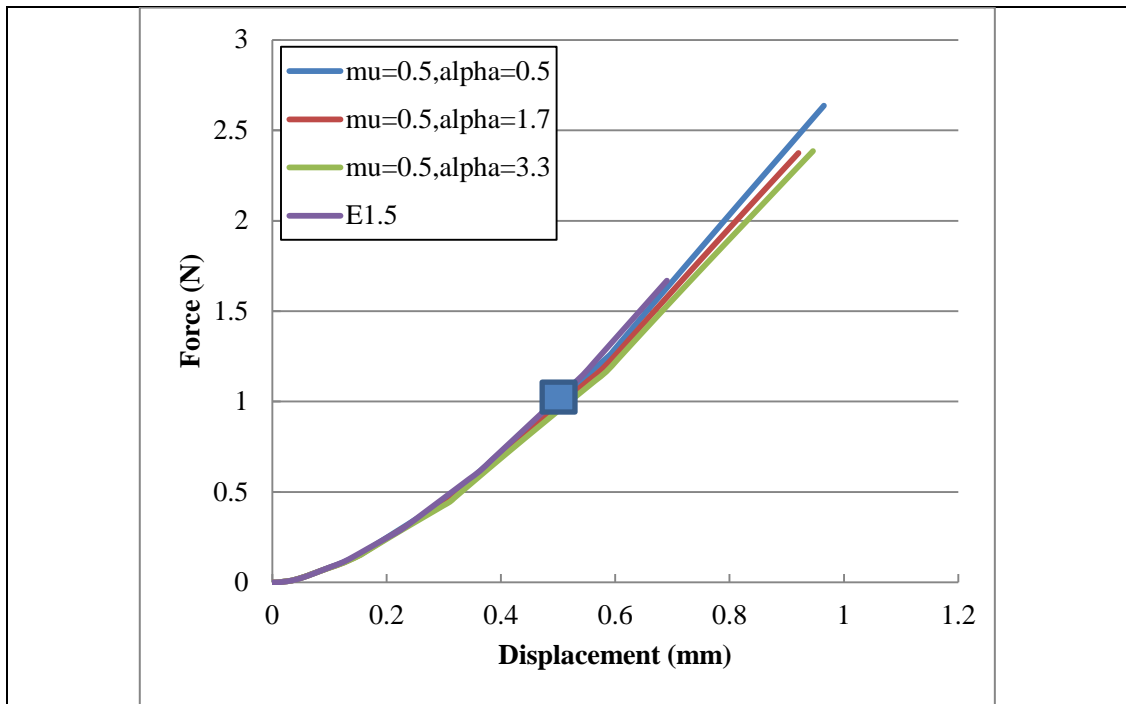


**Figure 5.5** Evaluation of the effect of friction on the predicted shore A values ( $E=11\text{MPa}$ ) using FE model.

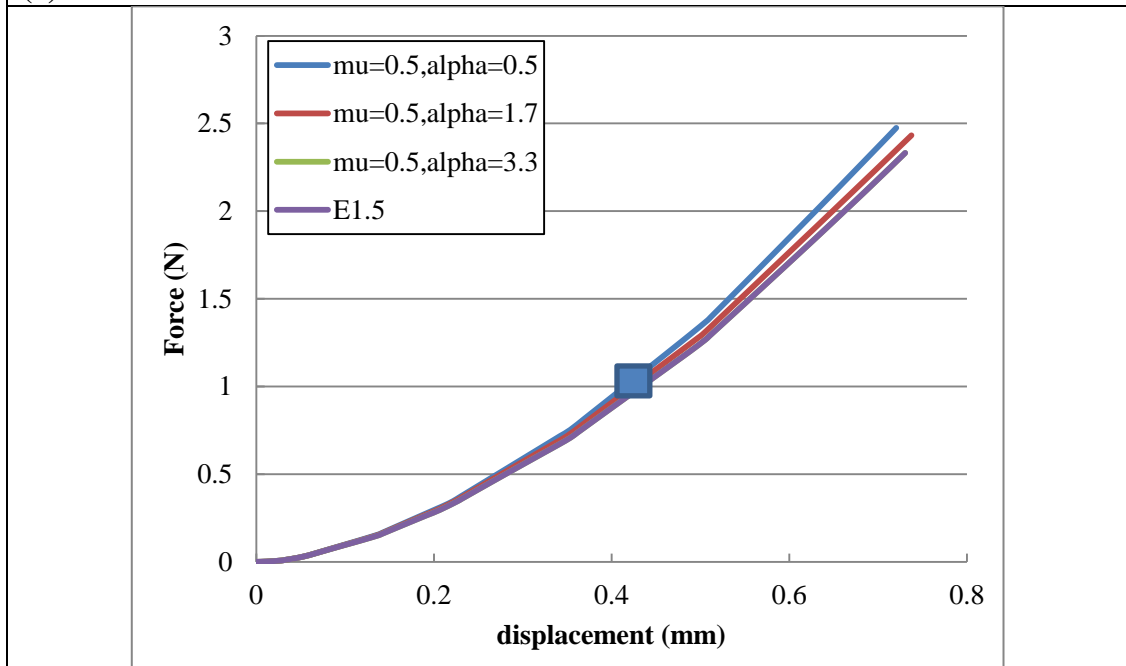
#### 5.4 Effects of choice of linear and nonlinear hyperelastic properties on shore hardness modelling

Rubber has a very complex mechanical behaviour even under simple loading condition such as tension, compression, and shear. Under indentation process, the boundary condition is not well defined, which made it even more important to select the right type of material models for different applications. Both linear elastic (represented by the Young's modulus and Poisson's ratio) and hyperelastic models are widely used (*Gracia et al., 2010*). For shore hardness simulation, the work presented has been mainly focused on using linear elastic model within the property range for gasket rubber. In all the cases, the predicted E values showed a reasonable agreement with testing data. For several materials, the Young's modulus predicted from hardness tests on samples of different thickness were within a reasonable range and no systematic influence of the sample thickness is observed. From the latex rubber data, non-linear material properties can also be used to predict the shore OO hardness, it naturally opened up a possibility extract to the hyperelastic properties from the shore OO hardness. Systematic trials using the ANN have been performed to inversely predict the hyperelastic parameters from shore hardness. The results show that it is not possible to robustly/uniquely predict both parameters for the Ogden model. This is found to be associated with the different effect of the Ogden parameter  $\mu$  and  $\alpha$  on the force displacement curve. Some typical results are briefly presented here. Figure 5.6 shows the comparison of the FE force-displacement curves of the shore OO indentation model with different linear and nonlinear properties. The nonlinear properties are selected from the simulation space which is used to generate the ANN approach. There are two main observations. Firstly, it is clearly shown that the displacement of the indenter at the point corresponding to the force for shore OO hardness (as labelled on the curve) is comparable between the model with a single material property of Young's modulus and hyperelastic model. Secondly, at the higher displacement, the curves for the same ' $\mu$ ' and ' $\alpha$ ' start to show some difference. This suggests that it is not possible to inversely predict these parameters from hardness tests as within the displacement range of the shore OO tests, there is very limited difference between forces for these different hyperelastic parameters. The compression FE models with different nonlinear and linear material properties of rubbers are also tried and the results are similar to the comparison of the shore OO FE indentation models, where different combination of hyperelastic properties resulted in comparable force displacement data.

A similar concept of evaluation on the choice of materials models and potential inverse modelling has also been applied to shore A hardness using a set of well-established materials tests data (*ABAQUS Benchmarks Manual 6.11*). The material data included uniaxial tests, biaxial and simple shear tests. All the data was input into the FE model, and then different strain energy functions are used as well as a linear elastic model with a single Young's modulus. Figure 5.7 shows the comparison of the force-displacement data with the linear elastic material properties (Young's modulus) and the nonlinear material properties in the thin (2mm) and thick (6mm) samples. The force corresponding to the load for shore A hardness test are labelled on the figures. In both cases, the displacement at 8.06N for the linear elastic material properties and nonlinear material properties are very close, this suggests that the shore hardness values will be comparable. In other words, the use of linear elastic property (Young's modulus) is sufficient for modelling shore A hardness. A major advantage of using E value lies in the fact that it is much easier to measure than hyperelastic parameters, which has to be based on a combination of the different tests (as explained in section 2.7). This also shows that during the shore indentation, the compression deformation is the dominating condition as it has a flat tip. The use of E values also made it easier to compare materials or the same material at different conditions, for example, when testing the temperature effects, where complex shear test (essential to predict the nonlinear parameters) is not possible. It will also make the material development much easier as the hardness and E values can be directly estimated. The work may also be used to characterise some complex gasket such as an enveloped gasket, in which a rubber based core is enclosed in plastic (PTFE). Other works in this project showed that the elastic and plastic properties of PTFE sheet can be inversely predicted using miniature puncture tests. This combined with shore hardness tests method on the rubber core in work, would make the measurement and modelling envelope gasket much easier.



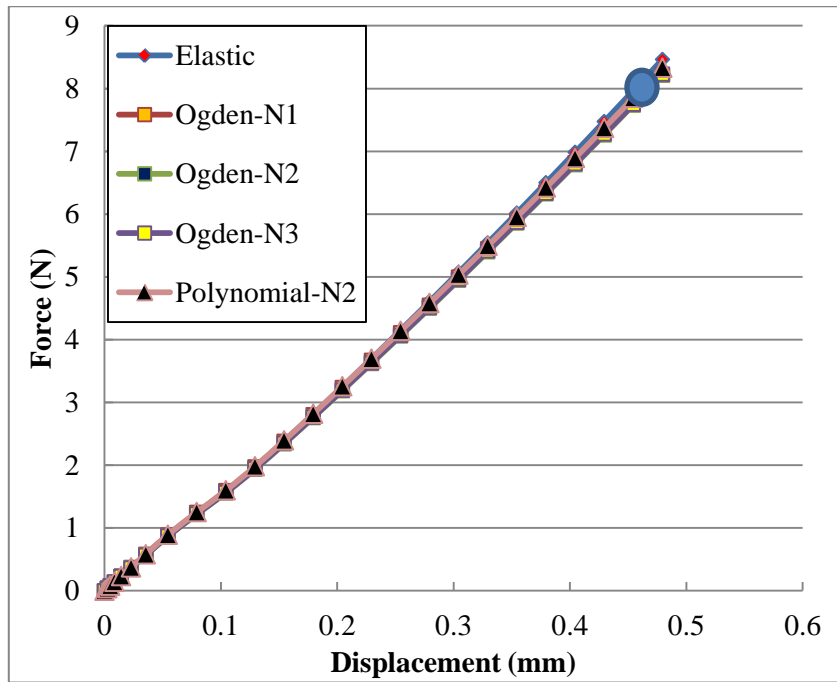
**(a)  $t=6\text{mm}$**



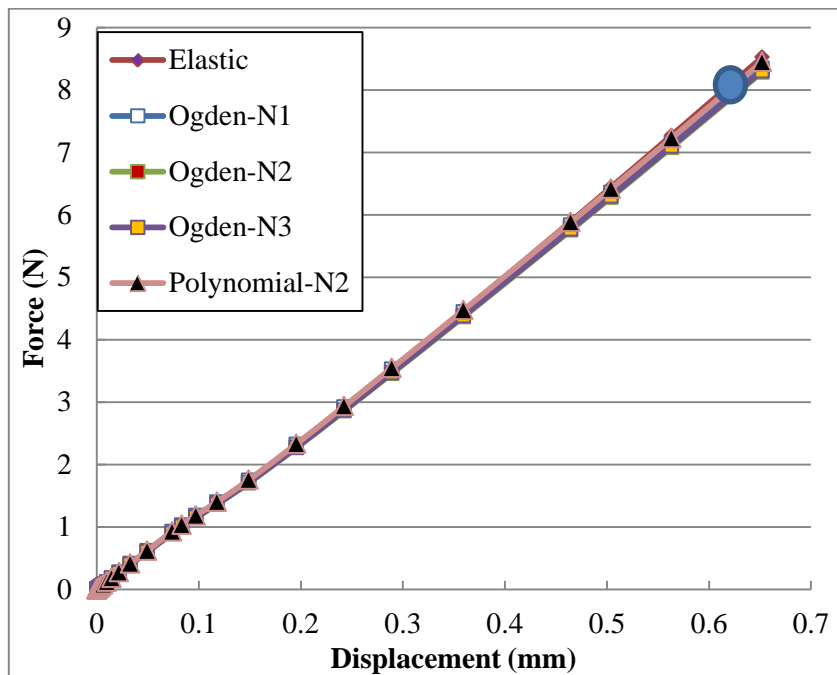
**(b)  $t=2\text{mm}$**

**Figure 5.6** Typical force–displacement curves with same Ogden parameter ‘ $\mu$ ’ but different parameter ‘ $\alpha$ ’. This material property result in the same shore OO hardness as labelled at the force point for shore OO hardness.





(a) Numerical force-displacement curves of shore A test of a rubber material using linear elastic and different hyperelastic parameters. ( $t=2\text{mm}$ )



(b) Numerical force-displacement curves of shore A test of a rubber material modelled with linear elastic and different hyperelastic models. ( $t=6\text{mm}$ )

**Figure 5.7** FE modelling results of shore A hardness with different strain energy functions and models based on the testing data set on the same material. It shows the shore A hardness is the same when using linear or hyperelastic models.

CHAPTER SIX  
CONCLUSIONS AND FUTURE  
WORKS

## 6.1 Summary and Conclusions

In this work, the shore hardness testing of rubber materials principally used for gasket applications and correlation between shore hardness and linear elastic and hyperelastic properties have been systematically investigated. A detailed FE model of the shore A hardness test has been developed with re-meshing functions in order to cope with excessive elements distortion when simulating softer materials, which enabled FE simulation over a range of E values. The model is used in modelling shore A hardness on samples with standard thickness (over 6 mm) and the result is validated against published data. FE models of thin samples are then developed and successfully used to predict the shore hardness of thinner samples over a range of properties relevant to gasket applications. A chart linking shore hardness, Young's modulus and samples thickness is established and used to analyse shore hardness of three cases including silicone rubber made in the lab with different thicknesses, thin silicone rubber gasket and an EPDM gasket for plate heat exchangers. In all of the cases, the estimated E values based on shore hardness tests are able to predict the deformation of the material including tensile and compression under different conditions. In the shore OO hardness modelling, the numerical results are shown to be in a good agreement with analytical solutions for spherical indenters. The shore hardness, thickness and E value chart established are used to evaluate the properties of a soft silicone rubber and latex rubber. In both case, the E values predicted from tests on samples of different thickness is able to predict the experimental data of tension and compression tests. In the case of latex rubber, the predicted material property is also in agreement with hyperelastic properties from combined tensile and planar tests.

Based on the FE model developed, extensive data over a larger spectrum of material properties are developed and used in developing an ANN program for inverse estimation of material properties from shore hardness and direct prediction of shore hardness from known material properties. The results show that the E values can be predicted from shore hardness tests with an accuracy within 10 % for both shore A and shore OO hardness tests. The prediction for data used in the training is much better than the prediction of data not used in the ANN training. However, the program is not able to predict the hyperelastic properties. In the direct analysis, the ANN is able to predict the shore hardness values accurately (within 5 % error) from

the linear elastic properties (i.e. Young's modulus) and sample thickness or hyperelastic parameters and thickness. The effect of indenter shapes, testing conditions and choice of linear or hyperelastic models was established and discussed, which will provide a detailed understanding to further enhance the use of shore hardness tests as a quick and effective way in testing rubber materials.

## **6.2 Recommendations for further works**

This work has established a framework in studying shore hardness tests on rubber materials including modelling and the factors affecting the tests. The work can be extended into the following areas:

1. Use of shore hardness in investigating temperature effects on materials. Gasket is used in different temperatures, which directly influences the load bearing capacity and creep behaviour. From the preliminary work, shore hardness can be used conveniently to test the shore hardness at a higher temperature. Currently, a new project is looking at testing materials at higher temperatures.

2. Use of the hardness–E relation to study the effect of composition or curing time on the property changes. With the link between hardness and E values, it is possible to quantify the change of material properties with time. At the moment all the rubbers are cured for a long time, which is time consuming and not cost-effective.

3. Extend the work to shore D hardness tests. This work has been focused on the properties range related to rubber gaskets and seals. The program developed can be extended to shore D hardness tests, which is applicable to the rubber materials used in tyres and shoe soles. A new project considering the shore hardness and cycle pedal pin interaction is going to use the program developed to simulate shore D hardness tests.

## References

- Abbasi, A. A., Sayyaadi, H., and Vossoughi, G. R., 2011, Sensitivity analysis of mouse embryos in needle injection experiment using artificial neural network. *International Conference on Future Information Technology*, **13**, 304-309.
- ABAQUS User's Manual, version 6.11, Hibbitt, Karlsson & Sorensen.Inc.
- ABAQUS Benchmarks Manual 6.11 (3.1 Elasticity – 3.1.4 Fitting of rubber test data).
- Ali, A., Hosseini, M., and Sahari, B. B., 2010. A review of constitutive models for rubber-like materials. *American Journal of Engineering and Applied Sciences*, **3(1)**, 232.
- Alnawafleh, M. A. and Al-Ghathian, F. M. 2005. Dynamical properties analysis of frictional winding mechanism with bobbin elastic support. *American Journal of Applied Sciences*, **2(4)**, 828.
- Arghavani, J., Derenne, M., and Marchand, L., 2001. Fuzzy logic application in gasket selection and sealing performance. *Advanced Manufacturing Technology*, **18**, 67-78.
- Armstrong, R.W., 2013. Elastic, plastic, cracking aspects of the hardness of materials. *Journal of Modern Physics B.*, **27**, 11-21.
- ASTM F36: Test Method for Compressibility and Recovery of Gasket Materials.
- ASTM F38: Test Methods for Creep Relaxation of a Gasket Material.
- ASTM D395 Standard Test Methods for Rubber Property – Compression Set.
- ASTM D-2240 Standard Test Method for Rubber Property – Durometer Hardness.
- Atkin, R. J., and Fox, N., 1980. *An Introduction to the Theory of Elasticity*. Prentice Hall Press.
- Austrell P. E., 1997, *Modelling of Elasticity and Damping for Filled Elastomers*, Report TVSM-1009, Lund University, Sweden.
- Aw J., 2015. Development of New Inverse Modelling Methods for Predict the Nonlinear Hyperelastic Parameters from Indentation Bending Tests. *PhD Thesis*, Liverpool John Moores University, UK.
- Brown, R., 2005. *Physical Testing of Rubber*, 4<sup>th</sup> Edition, Springer Press.
- Bolzon, G., Maier, G., and Panico, M., 2004, Material model calibration by indentation, imprint mapping and inverse analysis. *International Journal of Solids and Structures*, **41**, 2957-2975.
- Bensia, M., Babic, B., Grbovic, A. and Stefanovic, Z., 2012. Computer-Aided Modelling of the Rubber-Pad Forming Process. *Materials and Technology*, **46**, 503-510.
- Budiarsa, N., 2013, Development of FE and Representative Stress Based Method for P-h Curves and Hardness Prediction for Vickers and Spherical Indenter. *PhD Thesis*, Liverpool John Moores University, UK.
- Callister, W., and David G. R., 2012. *Fundamentals of Materials Science and Engineering: An Integrated Approach*. John Wiley & Sons Press.
- Chandler, H., 1999. *Introduction to Hardness Testing* (2<sup>nd</sup> Edition), ASTM International Press.
- Chandrasekaran, C., 2009. Rubber Seals for Fluid and Hydraulic System. *Plastics Design Library*, William Andrew Press.
- Charlton, D. J., Yang, J., and Teh, K. K., 1994. A Review of Methods to Characterize Rubber Elastic Behavior for Use in Finite Element Analysis. *Rubber Chemistry and Technology*, **67(3)**, 481-503.
- Chung D.D.L., 2001. Materials for thermal conduction. *Applied Thermal Engineering*, **21**, 1593-1605.

- Ciesielski, A., 1999. *An Introduction to Rubber Technology*, (Report) RAPRA Technology Limited.
- Currie A.R., 1998. *The Use of Asbestos Free Materials on Static Sealing on Pumps*. (Report) Flexitallic Ltd.
- Curtis, A., 2011. *Martins Rubber: An introduction to gaskets*, <http://www.soooperarticles.com>. (accessed 29<sup>th</sup> May 2015)
- Czernik, D., 1996. *Gasket: Design, Selection, and Testing, Mechanical Engineering*, McGraw Hill Professional.
- Dao, M., Chollacoop, N., Van Vliet, K. J., Venkatesh, T. A. and Suresh, S., 2001. Computational modelling of the forward and reverse problems in instrumented sharp indentation. *Acta Materialia*, **49(19)**, 3899-3918.
- Darmanis, S., Athanasios, P., Apostolos, P., Emmanuel, A., Dionisios, V., and Konstantinos, K., 2006. Static indentation test for neocartilage surface hardness in repair of periosteal articular cartilage defects. *Acta Orthopaedic Belgica*, **72**, 621-632.
- Datta, R. N., and Flexsys, B. V., 2002. *Rubber Curing Systems*, Chemtec Publishing.
- Deladi, E. L., 2006. Static friction in rubber-metal contacts with application to rubber pad forming processes. *PhD Thesis*, University of Twente. The Netherlands.
- Dimitriadis, E. K., Horkay, F., Maresca, J., Kachar, B. and Chadwick, R. S., 2002. Determination of elastic moduli of thin layers of soft material using the atomic force microscope. *Biophysical Journal*, **82(5)**, 2798-2810.
- Dirikolu, Husnu, M., and Esra, A., 2004. Computer aided modelling of flexible forming process. *Journal of Materials Processing Technology*, **148**, 376-381.
- “DuroMatters! Basic Durometer Testing Information”. [www.ccsi-inc.com/t-durometer-testing.htm](http://www.ccsi-inc.com/t-durometer-testing.htm) (accessed 29th May 2015).
- “Durometer Hardness Scales – General Reference Guide”, 2008, (Report) Paramount Industries Inc.
- “Durometer Hardness Handbook”, Instron Company, 2004.
- Farine, M., 2013. Instrumented indentation of soft materials and biological tissues. *PhD Thesis*, Eidgenössische Technische, Zürich.
- “Flanges, Gaskets & Bolts, Technology”, (Report) Flowstar Inc. <http://www.flowstarvalveshop.com/flanges-gaskets-bolts/> (accessed 29th May 2015).
- Flitney, R. K., 2011. *Seals and Sealing Handbook, Technology & Engineering*, Elsevier Press.
- “Gasket Type and Material Overview”, (Report) Seal-mart Company.
- Gent, A. N., 2001. *Engineering with Rubber: How to Design Rubber Components*, Hanser Verlag.
- Gérard, J. M., Jacques, O., Vincent, L., Pascal, P., and Yohan, P., 2005, Non-linear elastic properties of the lingual and facial tissues assessed by indentation technique Application to the biomechanics of speech production. *Medical Engineering & Physics*. **27**, 884–892.
- González, L., Valentín, J. L., Fernández-Torres, A., Rodríguez, A. and Marcos-Fernández, A., 2005. Effect of the network topology on the tensile strength of natural rubber vulcanizate at elevated temperature. *Journal of Applied Polymer Science*, **98(3)**, 1219–1223.
- Gracia, L.A., Liarte, E., Pelegay, J.L., and Calvo, B., 2010. Finite element simulation of the hyperelastic behaviour of an industrial rubber: Application to design of rubber components, *Finite elements in Analysis and Design*, **46**, 357-368.
- Groover, M. P., 2010. *Fundamentals of Modern Manufacturing: Materials, Processes, and Systems* (4<sup>th</sup> Edition), John Wiley & Sons.
- Guan, H., Yang, F., and Wang, Q., 2011. Study on evaluation index system of rubber materials for sealing. *Material and Design*, **32**, 2404-2412.
- “Guide to UV light curing technology”, (Report) Dymax Corporation, 2012.

- “Hardness for Rubber Rollers”, (Report) Imperial rubber products Inc., 2012.
- Harsono, E. D. Y., 2009. Material Characterization via simulated indentation test including effect of friction. *PhD thesis*, National University of Singapore.
- Hasha, B., 2010. “What gasket properties are most important, and how do I use them?”, Fluid Sealing Association Publication, USA.
- Hay, J., 2009. Introduction to Instrumented Indentation Testing. *Nanomechanical Characterization of Materials by Nanoindentation Series*, Society for Experimental Mechanics.
- Hendriks, F. M., Brokken, D., Oomens, C. W. J., Bader, D. L. and Baaijens, F. P. T., 2006, The relative contributions of different skin layers to the mechanical behaviour of human skin in vivo using suction experiments. *Medical Engineering & Physics*, **28**, 259-266.
- Hu, F. and Olusanya, A., 1997. *Measurement of Creep and Stress Relaxation in Rubber and Rubber Type Materials*. NPL Report CMMT(B)158.
- Johansson, B., and Oscar J., 2006. *Verification of FE-Model for Gasket Compression*, (Report) Alfa Laval Lund AB, Sweden.
- Johannes, K., and Studer, M., 2006, Determining the modulus of elasticity in compression *via* the shore A hardness. Carl Hanser Verlag, Munich, Germany.
- Jiménez-Piqué, E., Gaillard, Y., and Anglada, M., 2007. Instrumented indentation of layered ceramic materials. *Key Engineering Materials*, **333**, 107-116.
- Johnson, K. L., and Kenneth L. J., 1985. *Contact Mechanics*. Cambridge University Press.
- Johnson, P. S., 2001. *Rubber Processing: An Introduction*. Hanser Verlag, Germany.
- Kauer, M., 2001, Inverse finite element characterization of soft tissue with aspiration experiments. *PhD Thesis*, Swiss Federal Institute of Technology.
- Kelly, K., 2007. Application of advanced computer-aided engineering (CAE) methods for quality and durability of fuel cell components. (Report) *DOE Hydrogen Program, Advanced Engineering Solutions*, Castle Rock, Co.
- Kim, B., Yang, H., Chun, M., and Park, Y., 2014. Shore Hardness and Tensile Bond Strength of Long-term Soft Denture Lining Materials. *J Prosthet Dent.*, **112(5)**, 1289-97.
- Kong, X., Yang, Q., Li, B., Rothwell, G., English, R., and Ren, X. J., 2008, Numerical study of strengths of spot-welded joints of steel. *Materials and Design*, **29**, 1554-1561.
- Lattimer A., 2012. An introduction to gasket selection and installation, (Report) European Sealing Association.
- Li, C., Liu, Y., Zeng, Q. and Ao, N., 2013. Preparation and antimicrobial activity of quaternary phosphonium modified epoxidized natural rubber, *Material Letters*, **93**, 145-148.
- Lorenz, B., and Persson, B. N. J., 2009. Leak-rate of seals: comparison of theory with experiment, *Europhysics Letters*, **86(4)**, 52-54.
- Luo, J. and Lin, J., 2007. A study on the determination of plastic properties of metals by instrumented indentation using two sharp indenters. *International Journal of Solids and Structures*, **44**, 5803-5817.
- Mahaling, R. N., Kumar, S., Rath, T. and Das, C. K., 2007. Effects of rubber—filler interaction on the developments of physical, mechanical, and interfacial properties of Vamac—Silica Nano-composites. *Journal of Elastomers and Plastics*, **39(3)**, 253-268.
- Mainardi F. and Spada G., 2011. Creep, relaxation and viscosity properties for basic fractional models in rheology. *The European Physical Journal*, **193(1)**, 133-160.



- Meng Y and Lin B, 2008, A feed-forward artificial neural network for prediction of the aquatic ecotoxicity of alcohol ethoxylate, *Ecotoxicology and Environmental Safety*, **71**, 172–186.
- Meuwissen, M.H.H., Oomens, C.W.J., Baaijens, F.P.T., Petterson, R. and Janssen, J.D., 1998, Determination of the elasto-plastic properties of aluminum using a mixed numerical-experimental method, *Journal of Materials Processing Technology*. **75**, 204–211.
- Milani, G., and Federico, M., 2013. Two-step model to maximize mechanical performance of extruded EPDM weather-strips. *Society of Plastics Engineers Journal* (online), **1**, 1-4.
- Modan, R. Y. and Desai, R. N., 2013. Effect of resin content in EPDM/Low-Density polyethylene blends on their mechanical properties. *International Journal of Engineering Science and Innovative Technology (IJESIT)*, **2(2)**, 187-196.
- Mohamed, M. I. and Aggag, G. A., 2003. Uncertainty evaluation of shore hardness testers. *Measurement*, **33**, 251-257.
- Mooney M., 1940. A theory of large elastic deformation. *Journal of Applied Physics*, **11(9)**, 582-592.
- Morgans, R., S. Lackovic, and Cobbold, P., 1999. Understanding the IRHD and Shore Methods used in Rubber Hardness Testing. *American Chemical Society Publication*, Florida.
- Naik, V. R. and Matawala, V. K., 2003. Experimental investigation of single phase chevron type gasket plate heat exchanger. *International Journal of Engineering and Advanced Technology*, **2(4)**, 362-369.
- Nelson, N. Rino, N. Siva Prasad, and A. S. Sekhar, 2015. Effect of thermal loading on sealing behavior of single and twin gasketed flange joints. *Proceedings of the Institution of Mechanical Engineers, Part E: Journal of Process Mechanical Engineering* (online 2<sup>nd</sup> March).
- Obidiegwu, M. U. and Ogbobe, O., 2012. Mechanical and flammability properties of low density polyethylene/kola nitida wood fibre composites. *Academic Research International*, **2(3)**, 230-238.
- Ogden, R. W., 1972. Large deformation isotropic elasticity-on the correlation of theory and experiment for incompressible rubber-like solids. *Proceedings of the Royal Society of London. A. Mathematical and Physical Sciences*, **326**, 565-584.
- Persson, B. N. J., 2006. Contact mechanics for randomly rough surfaces. *Surface Science Reports*, **61(4)**, 201-227.
- Petr, B., Ctvrtlik, R. and Stranyancke, M., 2010. Potential Utilisation for nanotesters. *Chem. Listy* **104**, 295-298.
- Petre, M. T., Erdemir, A., and Cavanagh, P. R., 2007, Determination of elastomeric *Biomechanics and Biomedical Engineering*. **9(4)**, 231-242.
- Pinarbasi, S. 2009. Compressive behavior of rubber-based seismic isolation bearings. *International Earthquake Symposium*, Kocaeli, Turkey.
- Pinarbasi, S. and Akyuz, U., 2004, Investigation of Compressive Stiffness of Elastomeric Bearings. *6<sup>th</sup> International Congress on Advances in Civil Engineering*, Istanbul, Turkey
- “Preparation of synthetic polyisoprene latex and its use in coagulant dipping”. (Report) Kraton Inc. (2014).
- Rahul N. and Matt T., 2006. *Measuring Hardness and More through Nanoindentation*. (Report) Fischer Technology, Inc.
- Rajasekar, R., Heinrich, G., Das, A., and Das, C. K., 2009. Development of SBR-nanoclay composites with epoxidized natural rubber as compatibilizer. *Journal of Nanotechnology*. **May**, 1-5.

Ren, X. J., Hooper, R. M., Griffiths, C. and Henshall, L. J., 2002, Indentation size effect (ISE) in single crystal MgO. *Philosophical Magazine A*, **82(10)**, 2113-2120.

Ren, X. J., Li, B., Gu, Y. D., English, R., and Rothwell, G., 2009. Characterisation of nonlinear material parameters of foams based on indentation tests. *Material and Design*, **30**, 2708-2714.

Ren, X. J., Smith, C. W., Evans, K. E., Dooling, P., Burgess, A., Wiechers, J., and Zahlan, N., 2006, Experimental and numerical investigations of the deformation of soft materials under tangential loading. *International Journal of Solids and Structure*. **43**, 2364-2377.

Sabrenal, H. E., 2010. Influences of accelerators on the structures & properties of nitrile butadiene rubber. *Modern Applied Science*, **4(4)**, 47-61.

Sadik, K., Liu H., and Pramuanjaroenkij A., 2002. *Heat Exchangers: Selection, Rating, and Thermal Design*, CRC Press.

Santangelo, P. G. and Roland, C. M., 2003. Role of strain crystallization in the fatigue resistance of double network elastomers. *Rubber chemistry and technology*, **76(4)**, 892-898.

Saunders, E. A. D., 1988. *Heat Exchangers: Selection, Design and Construction*. Longman, London.

Schaefer, R. J., 2009. *Mechanical Properties of Rubber*, McGraw Hill Press.

Schröder, E., Klaus N., Fabian N., and Vetter, C., 2014. Study on heat transfer in heat exchangers for a new supercritical organic ranking cycle. *Heat Transfer Engineering*, **35**, 1505-1519.

“Sealing Technology – BAT guidance notes”. (Report) European Sealing Association (ESA), 2009.

Serope K. and Steven R. S., 2006. *Mechanical Behaviour Testing and Manufacturing Properties of Materials* (5<sup>th</sup> Edition), Pearson Education Inc. Press,

Shah, K. P., 2008. Gaskets – Materials and Types, *Practical Maintenance*, June, <https://practicalmaintenance.wordpress.com>.

Shanks, R. A. and Kong I., 2013. General purpose elastomers: structure, chemistry, physics and performance. *Advanced Structured Materials*, **11**, 11-45.

Sharma, K., Vivek, B., Vaze, K. K., and Ghosh, A. K. , 2011. Numerical simulation with finite element and artificial neural network of ball indentation for mechanical property estimation. *Indian Academy of Sciences*, **36(2)**, 181-192.

“Shore (Durometer) Hardness Testing of Plastics”, MatWeb (<http://www.matweb.com/reference/shore-hardness.aspx>). (accessed 29<sup>th</sup> May 2015)

“Shore Durometer Conversion Chart”, (Report) Seal & Design Inc.

Sidwell, J. A., and Martin, J. F., 2000. Rubbers in contact with food. (Report) RAPRA Technology Limited.

Sinha, A., Dey, S. S., Chattopadhyay, P. P., and Datta, S., 2013. Optimization of mechanical property and shape recovery behaviour of Ti-(~ 49at.%) Ni alloy using artificial neural network and genetic algorithm. *Materials & Design*, **46**, 227-234.

Sohn, M. S., Kim, K. S., Hong, S. H., and Kim, J. K., 2002. Dynamic mechanical properties of particle-reinforced EPDM composites. *Journal of Applied Polymer Science*, **87(10)**, 1595–1601.

Steinetz, B. M., 2006. Seal Technology, *Mechanical Engineers’ Handbook: Materials and Mechanical* (3<sup>rd</sup> Edition), John Wiley & Sons.

Su, X. X., 2014, Indentation Curve Prediction and Inverse Material Parameters Identification of Hyperfoam Materials Based on Intelligent ANN Method. *PhD Thesis*, Liverpool John Moores University.

Sun, X., 2007. The Devulcanization of Unfilled and Carbon Black Filled Isoprene Rubber Vulcanizates by High Power Ultrasound. PhD Thesis, University of Akron.

- Suzuki, N., Ito, M., and Ono, S., 2005. Effects of rubber/filler interactions on the structural development and mechanical properties of NBR/silica composites. *Journal of applied polymer science*, **95(1)**, 74-81.
- Swift, H., 1952. Plastic instability under plane stress. *Journal of the Mechanics and Physics of Solids*, **1(1)**, 1-18.
- Tarawneh, F. M. M, and Muafag, S., 2005, Friction forces in O-ring Sealing, *Americal Journal of Applied Sciences*, **2(3)**, 626-632.
- “The Stiffness of Rubber”, University of Cambridge. Website source: <http://www.doitpoms.ac.uk/tlplib/stiffness-of-rubber/printall.php>. (accessed 29<sup>th</sup> May 2015)
- Thibeau, R., 2004, Selecting conductive Form-in-Place gaskets, (Report) Laird Technologies.
- VanLandingham, M. R., 2003. Review of Instrumented Indentation. *Journal of Research of National Institute of Standards and Technology*. **108(4)**, 249-265.
- Wang, B., Ma, J. H., and Wu, Y. P., 2013. Application of artificial neural network in prediction of abrasion of rubber composites. *Material and Design*, **49**, 802-807.
- Wang, L., Manglik, R. M., and Sundén, B., 2007. Plate Heat Exchangers: Design, Applications and Performance, WIT press.
- Weiss, J. A. and Gardiner, J. C., 2001. Computational modelling of ligament mechanics. *Critical Reviews in Biomedical Engineering*, **29(3)**. 303-371.
- “White paper – Nonlinear finite element analysis of elastomers”, MSC Software Corporation.
- Yas, M. H., Kamarian, S., and Poursaghar, A., 2013. Applications of imperialist competitive algorithm and neural networks to optimise the volume fraction of three-parameter functionally graded beams. *Journal of Experimental & Theoretical Artificial Intelligence*, **26(1)**, 1-12.